ettc 2022

European Test and Telemetry Conference

Conference Proceedings

10 -12 May 2022 in Nuremberg, Germany
In cooperation with SENSOR+TEST 2022

Proceedings

European Test and Telemetry Conference – ettc2022

10 -12 May 2022, Nuremberg Germany

The European Test and Telemetry Conference – ettc2022 is organized by the European Society of Telemetry.

The European Society of Telemetry
Arbeitskreis Telemetry e.V.
Rudolf-Diesel-Straße 29a
82216 Gernlinden (Germany)
Tel.: +49 (0)8142-284582-0, Fax: +49 (0)8142-284582-2
info@telemetry-europe.org
www.telemetry-europe.org

This volume covers the proceedings of the European Test and Telemetry Conference – ettc2022, and contains the manuscripts of the lectures.

The authors are responsible for form and content of the papers.

AMA Service GmbH accepts no responsibility for the correctness and completeness of the details and the consideration of private rights of third parties.

Publisher:
AMA Service GmbH
Von-Münchhausen-Str.49 • 31515 Wunstorf / Germany
Tel. +49 5033 9639-0 • Fax +49 5033 9639-20
info@ama-service.com
www.ama-service.com / www.sensor-test.com / www.ama-science.org

ISBN 978-3-9819376-6-4

Dear Telemetry Friends,

On behalf of the European Society of Telemetry, it is a great pleasure for me to present to you the proceedings of the European Test and Telemetry Conference 2022.

After two years of excessive usage of digital communication tools like Gmeet, WebEx, Zoom, Teams, Skype, etc, it is time to meet in person again!

The way we prepare and analyse tests has evolved, as well as the way we perform and conduct those tests. However, we all concluded that the face-to-face exchange could not be replaced by any digital event. ettc2022 is the first in –person telemetry event since the outbreak of the pandemic in 2020.

We are more than happy that ettc20022 welcomes so many participants.

Following the education and training missions of the European Society of Telemetry, ettc2022 features a fee Short Course on IP Telemetry, held by Silvus Technologies and friendly sponsored by ATCOM Télémétrie.

The exhibition of ettc2022 displays more than 30 companies, a third of them new to the show. The conference presents a dense technical program of more than 40 high quality papers, merged in these Conference Proceedings. As always, you can find the latest and most promising methods here but also hardware and software ideas for the telemetry solutions of tomorrow.

With the best possible exchange within the testing community in mind, the 33rd Symposium of the Society of Flight Test Engineers, European Chapter, takes place in parallel to ettc2022 this year. The instrumentation specialists meet their internal customers, the test engineers can dive in the telemetry technologies, and both can attend to the presentations of the others.

The ultimate success of the conference remains entirely dependent upon your continued patronage. So thank you very much for supporting ettc2022 again in presence in Nuremberg!

Many thanks also to our loyal sponsors, Safran Data Systems and Airbus.

We are always seeking ways to improve the European Test and Telemetry Conferences. Please contact us with ideas, critiques, suggestions, and join us on www.telemetry-europe.org.We are looking forward to meeting you!

Renaud Urli
President of the European Society of Telemetry

1. Networks & Data acquisition

Chair: Philipp Wager, Airbus Defence and Space GmbH, Manching (Germany)

2. Data Acquisition

Chair: Regine Pattermann, umlaut SE, Aachen (Germany)

3. Time-Space Position Technologies

Chair: Valentin Belaud, Safran Data Systems, Courtaboeuf Cedex (France)

4. Sensors

Chair: Murat Imay, Deutsche Aircraft GmbH, Wessling (Germany)

5. Imaging & Video

Chair: Patrick Quinn, Curtiss-Wright, Dublin (Ireland)

6. Data Management Standards

Chair: Didier Schott, ArianeGroup, Verneuil sur Seine (France)

7. Data Management

Chair: Pedro Rubio, Airbus Defence and Space, Getafe (Spain)

DATA SYSTEMS

SAFRAN


airbus.com
SMALL
JOURNEYS
DEMAND
A
BIG CHANGE
Reimagining transport through the power of innovation, the fully electric CityAirbus NextGen is designed to connect people. With an 80km operational range, this four-seat vertical take-off and landing aircraft offers new options for community journeys, while zero emissions help keep the world a beautiful place.
AIRBUS

DOI 10.5162/ettc2022/1.1

Implementing Tmns Data on Demand

Rocco Docimo, Ben Kupferschmidt, Kathy Rodittis
Curtiss-Wright, 15 Terry Dr, Newtown, PA, 18940, USA
rdocimo@curtisswright.com, bkupferschmidt@curtisswright.com,
krodittis@curtisswright.com

Abstract
The Telemetry Network Standard (TmNS) was released as part of the 2017 version of the IRIG-106 standards. Traditionally, serial streaming telemetry data has been sent on a unidirectional link from the test article to the ground. The TmNS standard offers a new approach to acquiring flight test instrumentation (FTI) data that changes this paradigm by allowing the use of bi-directional data links. These bi-directional links allow for commands and requests to come from the ground back to the aircraft. This offers a new capability to the flight test community to request data on demand from the flight test recorder.

One of the longest-standing problems with traditional telemetry has been data dropouts. These gaps in the flight test data can occur at any point in a test flight, and they can prevent the ground controllers from knowing if a test was successfully completed. TmNS offers a solution to this problem by allowing the ground to request a PCM backfill to re-send the section of the data that was lost. This paper explores a fully functional demonstration system that Curtiss-Wright has created to show an end-to-end PCM backfill operation using a TmNS compliant recorder, two TmNS radios, and the IADS real-time visualization and analysis software.

Key words: TmNS, Data On Demand, PCM Backfill, Transceiver

Introduction
Pulse code modulation (PCM) telemetry has been the foundation of the flight test industry for over 50 years. PCM telemetry, however, has imperfect RF performance, resulting in flawed real-time data on the ground. This inadequate data still facilitates much-needed real-time data services, such as safety of flight, but limits the amount of data analysis tasks that can be performed in real-time.

Over the years, many technological methodologies have been used to either identify or limit the frequency of the data dropouts caused by PCM RF telemetry. Some key examples are:

1. Checksum/CRC checks
   a. Efficient at detecting bit errors, so bad data is not processed
   b. Provides no ability to correct for those errors
2. Forward error correction
   a. Variety of different algorithms, each with their advantages and tradeoffs
   b. Generally, incurs a high amount of overhead on a bitstream

In this paper, a system is presented showing how to achieve near-perfect data quality on the ground in a real-time operational scenario. This system uses approaches defined in the IRIG-106 Telemetry Network Standard (TmNS) set of standards, namely PCM backfill, using commercial off-the-shelf (COTS) hardware and software supplied by Curtiss-Wright, all of which are available today.

System Architecture
The demonstration system consists of several Curtiss-Wright products:

MnACQ-2600 – A data acquisition unit (DAU) that outputs a TmNS compliant Ethernet stream of data and a PCM output. The data contained in the TmNS Ethernet Stream and the IRIG-106 Chapter 4 PCM output is the same.

NSW-12GT-1 – A network switch capable of statically and dynamically routing data from multiple network elements.

nREC-4000S-3 – A TmNS compliant recorder that can respond to data on-demand requests from other hardware/software for actively recording TmNS data files.

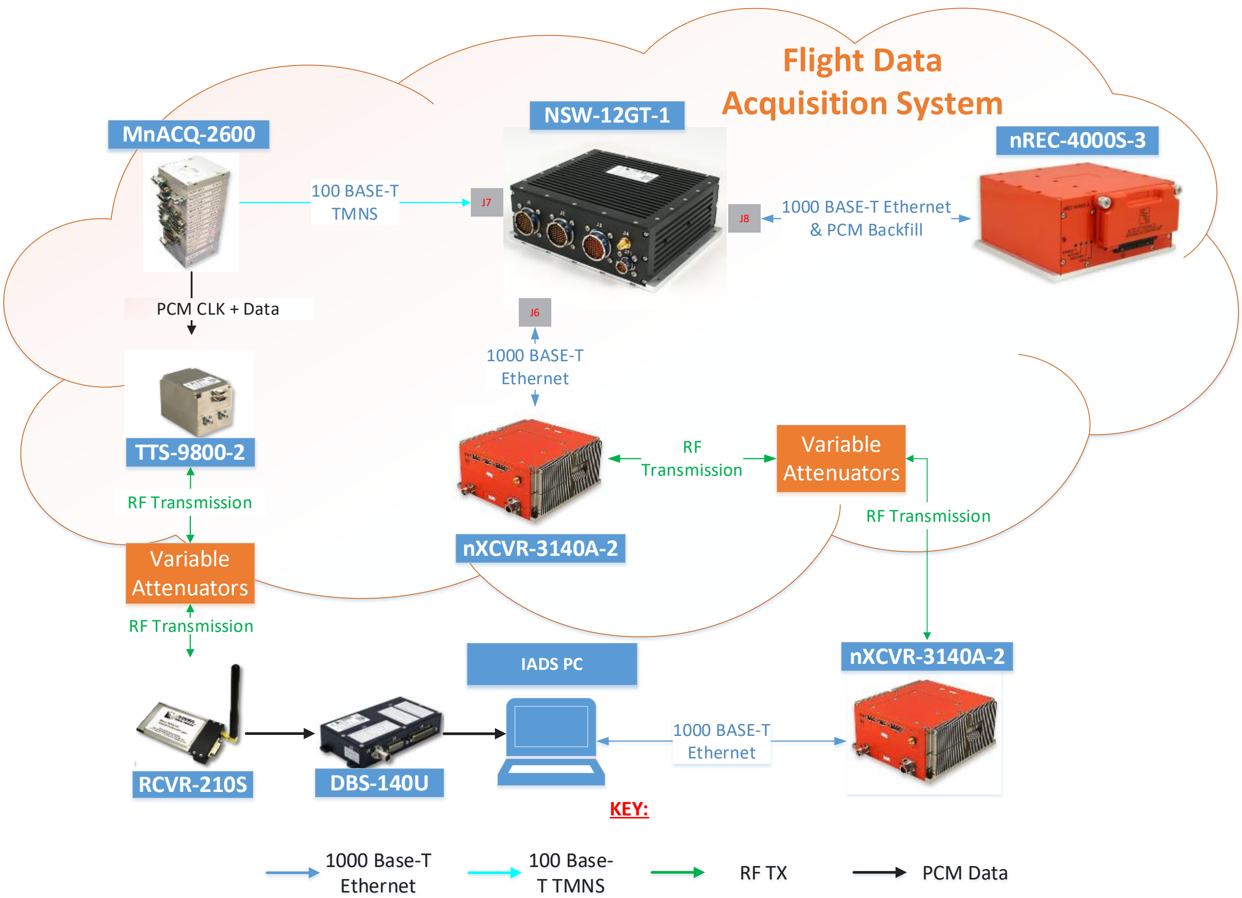

Fig. 1. System Architecture Diagram

nXCVR-3140A-2 – A TmNS compliant radio, allowing bi-directional communication between ground and air installations.

TTS-9800-2 – An IRIG-106 Chapter 2 compliant PCM transmitter with tri-band support for S, L, and C RF frequency bands.

RCVR-210S – A receiver/bit sync module that can demodulate RF transmitted PCM data and recover the bit clock.

DBS-140U – A 40 Mbps USB 2.0 Bit Sync/Decom that parses an IRIG-106 Chapter 4 PCM stream and passes the data to ground station software for display and analysis.

IADS – Industry-leading ground station software to process and display a variety of different flight test inputs.

Variable Attenuator – An RF attenuator that can vary the amount of RF attenuation.

System Theory of Operation
In this system, the data originates at the MnACQ-2600 and follows two paths: the Ethernet recording path and the IRIG-106 Chapter 4 PCM transmission path. The Ethernet recording path is where the MnACQ-2600 outputs IRIG-106 Chapter 24 TmNS packets, routed through the 12-port switch, to the nREC-4000S-3, which is actively recording the data, as if a flight test is occurring.

The IRIG-106 Chapter 4 PCM transmission path takes the same data payload in the IRIG-106 Chapter 24 TmNS packets and outputs that data as an IRIG-106 Chapter 4 PCM output. The IRIG-106 Chapter 4 PCM output is connected to the TTS-9800-2, which modulates the data in L-band, S-band, or C-band with an SOQPSK modulation. In a typical flight test application, the TTS-9800-2's RF output would be wired to an antenna for RF transmission over variable distances during the flight test to be received at a ground station.

To demonstrate the system at the ITC 2021 show, the TTS-9800-2 will transmit the IRIG-106 Chapter 4 PCM data. We will then use RF coaxial cabling and multiple attenuators to simulate the distance between the transmitting and receiving antennas. This will also lower the overall power level to an acceptable level for the RCVR-210S receiver. A variable attenuator is also included in the multiple attenuators to have the ability to degrade the RF power level from a functional power level to a marginal power level to a non-functional level.

The RCVR-210S receives the RF coaxial cable after the attenuation and de-modulates and bit-syncs the signal to recover the clock and data and input it to the DBS-140U decom.

The DBS-140U will receive the recovered clock and data signals and decom the IRIG-106 Chapter 4 PCM minor/major frames. This consists of checking for a Sync Pattern every X number of bits and, if applicable, a Sub-Frame ID (SFID) at a particular word location in the PCM minor frame. If, for some reason, the Sync Pattern is not found every X number of bits or an incorrect SFID is found, the frame will be discarded and the decom will enter a search mode, where it checks for the Sync Pattern anywhere in the data stream. Once a match is found, it will check the match by advancing X number of bits and verifying that the Sync Pattern is found in the expected location. Once this happens, the decom will enter a lock state and begin passing frames to the software once again.

IADS will then receive the PCM frames and extract parameter data for viewing in real-time displays, such as strip charts.

To facilitate a bi-directional connection from the ground PC to the airborne recorder, the system contains a pair of nXCVR-3140A-2 transceivers. These transceivers are capable of wirelessly transmitting and receiving Ethernet packets. One of the nXCVR-3140-2 transceivers, which we will refer to as the ground transceiver, is connected to an Ethernet port on the PC that is running IADS. In a real-world system, this transceiver would connect wirelessly to the airborne transceiver on board the test vehicle, but in the demonstration system, the ground nXCVR-3140A-2's RF connection is passed through attenuators to simulate transmission distances and attenuate the RF power. The other end of the RF connection connects to the airborne nXCVR-3140A-2. The airborne nXCVR-3140A-2 has an Ethernet connection to the NSW-12GT-1, allowing Ethernet packets to flow to and from the airborne network.

The nXCVR-3140A-2 transceivers differ from traditional PCM transmitters in the following key ways:

1. The nXCVR-3140A-2 transceivers transmit Ethernet packets, whereas the TTS-9800-2 transmitter transmits a PCM bitstream.
2. The nXCVR-3140A-2 transceivers can transmit data to and from the ground, creating a bi-directional link from the air to the ground. Traditional PCM transmitters can only telemeter data from air to the ground. The ground does not have a way to communicate back to the air.
3. Multiple nXCVR-3140A-2s can use the same RF spectrum to transmit data. This is done via a shared schedule between groups of nXCVR-3140A-2s, which allocate transmit and receive time for each transceiver.
4. The nXCVR-3140A-2s utilize burst mode SOQPSK modulation, which is a modulation scheme that is only present when data needs to be transmitted. Traditional PCM telemetry does not use burst mode modulation schemes, so conventional transmitters cannot transmit on the same RF spectrum.

It is important to note that there is no data flowing through the nXCVR-3140A-2 links for this demonstration. The bidirectional link will be utilized only when needed by the IADS software to fill in missing data.

We will use adjustable attenuation on the RF links in order to simulate data dropouts. At baseline, with little attenuation between the TTS-9800-2 transmitter and the RF receiver, IADS will be able to process and display parameters with no data loss. The processed parameters are displayed as normally done with traditional PCM telemetry. To simulate the RF dropouts from normal over the air PCM telemetry, we will raise the attenuation between the TTS-9800-2 transmitter and RF receiver. This will result in a state of marginal performance where good PCM frames will be passed to IADS along with a mixture of missing frames and/or frames with bit errors.

The IADS software has the responsibility of doing the following tasks in this scenario:

1. Detecting problematic PCM frames:
    a. Missing PCM frames.
    b. PCM frames with bit errors.

2. Sending low latency TmNS data requests to the nREC-4000S-3 when it detects erroneous or missing frames.
3. Receiving the requested frames from the nREC-4000S-3.
4. Replacing the missing or bad PCM frames in the PCM telemetry stream with the nREC-4000S-3 frames.
5. Processing the new PCM telemetry stream with the "PCM backfill" frames to make an error-free data presentation of all parameters in the PCM telemetry.

Detection and Retrieval of Problematic PCM Frames

There are several requirements that the PCM telemetry frame must meet to allow IADS to detect problematic PCM frames. For a major frame with multiple minor frames, a SFID is necessary. Combined with the Sync Pattern, a SFID allows IADS to uniquely identify each PCM minor frame. This also provides IADS with the ability to identify missing PCM minor frames by detecting cases where the SFID value skips one or more expected values. However, this will not allow IADS to detect larger chunks of missing data, such as multiple missing major frames.

To detect larger chunks of missing data, the PCM frame must include an embedded 48-bit IRIG time stamp that resolves time since the beginning of the current year with microsecond resolution. Since PCM telemetry is a synchronous continuous bitstream, every minor frame represents a fixed amount of time. In the event where multiple major frames are missing, it is possible to calculate how many frames are missing from the following information:

1. By knowing the length of the PCM telemetry frame in bits and combining this with the stream's bit rate, we can calculate the time per minor frame.
2. The start time for the TmNS data request is set by storing the last good timestamp that was received before a series of bad/missing PCM frames. The end time for the TmNS data request is set by the most recently received PCM frame's time or, in the case where the programmable timeout period of bad/missing PCM frames is met, the current time in the decom. The subtraction of the end time from the beginning time gives us the amount of time without PCM telemetry.
3. By dividing the amount of time without PCM telemetry by the known PCM telemetry frame time, we can arrive at the number of minor frames missing from the time interval.

So far, we have only addressed how to detect missing PCM frames of varying sizes in a real-time PCM telemetry stream coming from a decom. We have not addressed how to detect bit errors in the individual PCM frames. Bit errors are a common scenario in PCM RF transmission. It should be noted that bit errors present in either the SFID or the Sync Pattern are expected to be dropped at the DBS-140U decom, as they will not pass the frame check sequence. This means that errors in the SFID or Sync Pattern will appear to IADS as a time gap rather than a bit error. Bit errors that occur within the PCM frame data, but otherwise have good SFID and Sync patterns, are not detectable via the DBS-140U decom.

To detect the case where bit errors are present in a PCM frame without errors in both SFID and Sync pattern, a 16-bit CRC is calculated by the MnACQ-2600 and inserted into the data in every minor frame. This CRC is calculated between each pair of CRC samples, and the resulting calculated CRC value is inserted into the PCM data. When IADS receives the PCM telemetry data, it will calculate the CRC value on the received PCM frame and compare it to the CRC value stored in the PCM frame. If the CRC values are the same, no bit errors have occurred in the PCM frame, and IADS can safely assume all bits are correct in the frame. If the CRC values are different, IADS knows that one or more bit errors have occurred in the minor frame and should be thrown away.

Please note that, in a 16 bit CRC, there is a 1 in 65536, or roughly 0.0015%, chance that a frame with a bit error in it will have the same calculated CRC value as the original calculated CRC value from the MnACQ-2600. This risk is deemed acceptable for this demonstration system. If this risk does not meet operational requirements, longer CRCs (such as 32-bit or 64-bit) could be implemented in the hardware and IADS to mitigate this risk.

DOI 10.5162/ettc2022/1.1

	Word 1	Word 2	Word 3	Word 4	Word 5	Word 6	Word 7	Word 8	Word 9	Wor
Frame 1	SFID (0000)	High Time	Low Time	Micro Time						
Frame 2	SFID (0001)	High Time	Low Time	Micro Time						
Frame 3	SFID (0002)	High Time	Low Time	Micro Time						
Frame 4	SFID (0003)	High Time	Low Time	Micro Time						
Frame 5	SFID (0004)	High Time	Low Time	Micro Time						
Frame 6	SFID (0005)	High Time	Low Time	Micro Time						
Frame 7	SFID (0006)	High Time	Low Time	Micro Time						
Frame 8	SFID (0007)	High Time	Low Time	Micro Time						
Frame 9	SFID (0008)	High Time	Low Time	Micro Time						
Frame 10	SFID (0009)	High Time	Low Time	Micro Time						
Frame 11	SFID (000A)	High Time	Low Time	Micro Time						
Frame 12	SFID (000B)	High Time	Low Time	Micro Time						
Frame 13	SFID (000C)	High Time	Low Time	Micro Time						
Frame 14	SFID (000D)	High Time	Low Time	Micro Time						
Frame 15	SFID (000E)	High Time	Low Time	Micro Time						
Frame 16	SFID (000F)	High Time	Low Time	Micro Time						

Fig. 2. Sample PCM Format With SFID, Time Words, and CRC

When IADS detects a missing or bad CRC frame, it is thrown away, and the time of the bad or missing frame is calculated from the last good frame's time and saved in memory. IADS will then wait until it receives an error-free frame or a timeout period has expired. At that point, IADS will determine the end time for the event.

In TmNS, each data channel is identified by a unique ID called the Measurement Definition ID, which is formed at the TmNS Data source, the MnACQ-2600 in this demonstration. IADS will create a TmNS data request, which requests a stream of TmNS data identified by the channel's MDID and the start and stop times for the missing PCM telemetry frames. The TmNS data request is then sent via Ethernet, through the ground nXCVR-3140A-2 to the airborne nXCVR-3140A-2, then through the NSW-12GT to the nREC-4000S-3.

The nREC-4000S-3 is anticipated to be in an active recording session, recording data from the MnACQ-2600 (and in a practical application, many other DAUs) when the TmNS data request is received. The nREC-4000S-3 parses the TmNS data request and searches all recordings, including the active recording, for the specific stream's MDID identifier as well as start and end times of interests.

Once the nREC-4000S-3 finds the data of interest from the TmNS data request, it streams a TmNS data response back to the IADS PC through the transceiver network. The IADS PC then receives and parses the TmNS data response from the nREC-4000S-3. IADS will then fill in the bad and missing frames with the error-free frames from the nREC-4000S-3. The now error-free data can then be updated in every real-time display in IADS, such as the strip chart.

The result of this system is an error-free data presentation of the PCM telemetry. This is made possible by utilizing the unique TmNS capabilities of the nXCVR-3140A-2 and nREC-4000S-3 hardware, integrated with the IADS real-time telemetry software.

As an example, Figure 3 shows two IADS strip chart displays of the same parameter from a PCM telemetry stream. The left strip chart is experiencing RF disturbances and has errors in the data, while the right strip chart has been corrected using the PCM backfill process, and it shows perfect sine wave data.

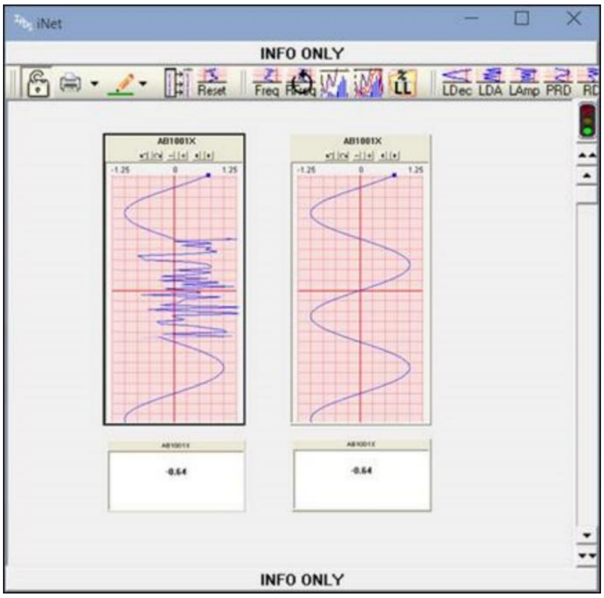

Fig. 3. PCM strip chart example of a parameter with and without the PCM backfill functionality

Additional System Considerations

A cost of this error-free data presentation using this PCM backfill process will be some amount of additional latency in all PCM telemetry data. IADS needs to reserve extra time to detect, formulate, send the TmNS data request, receive the TmNS data response from the aircraft with the missing/bad PCM telemetry frames, and fill them into the original PCM stream before IADS sends the PCM telemetry data to the screen for the analysts to view.

This latency will be variable, based on several different factors:

1. Size of the PCM telemetry minor frame.
   a. Larger minor frames will take longer to transmit to the ground if errors are found in them.

2. Length of IADS timeout period before requesting TmNS frames.
   a. If several PCM frames are erroneous in a row, IADS will keep track of a maximum wait time or number of frames before sending the TmNS data request.
   b. This maximum wait time will also add to latency. The latency that is added is a tradeoff between the transceiver bandwidth utilization and the available processor power on the nREC-4000S-3.
3. The overall schedule of the nXCVR-3140A-2 network.
   a. The schedule of the nXCVR-3140A-2 network defines how often each nXCVR-3140A-2 in the entire RF network has an available time slice to transmit data.
   b. A "worst-case" latency can be calculated based on the transmit and receive schedules of the overall nXCVR-3140A-2 network.
4. The time between receiving the TmNS data request and transmitting the TmNS data response from the nREC-4000S-3.
   a. This is a processer dependent operation and could be variable based on several factors of the nREC-4000S-3, including:
      i. How many files are on the nREC-4000S-3
      ii. How much data is stored on the media
      iii. How large or small the TmNS data request for data is
      iv. How large or small the TmNS data response is (this will be related to the size of the TmNS data request)

This variable latency will drive a configurable latency model in IADS. The user can select how long to delay the PCM telemetry data before sending the data to a display. For this demonstration, the latency will be determined empirically. It is predicted not to exceed 150 milliseconds.

It is also possible that the nXCVR-3140A-2 will have an RF transmission issue, similar to those found in the original PCM telemetry. Some factors which mitigate this potential issue are:

1. The nXCVR-3140A-2 link is only utilized when there is a problem receiving RF PCM telemetry, leaving its predicted utilization far less than that of the RF PCM telemetry.
   a. Less utilization leaves fewer opportunities for issues in the transmission and receiving of this data to occur.
2. Robust RF performance with 20 Watts of RF power and a -86 dBm typical receiver sensitivity.
3. The nXCVR-3140A-2 transmits RF MAC frames, which consist of LDPC code blocks, which the receiving nXCVR-3140A-2 can automatically correct.
4. IADS can build a similar detection and re-request process if there are issues with receiving the TmNS data response frames from the nREC-4000S-3 through the nXCVR-3140A-2 radio links at the expense of additional latency.

Overall Benefits of Pcm Backfill Model

Once a well-understood and acceptable end-to-end latency model is in place between IADS and the rest of the ground/airborne network, data anomalies from traditional RF PCM telemetry can be significantly reduced or eliminated entirely. This enhancement is envisioned to provide significant value to control rooms viewing the real-time PCM RF telemetry and, thus, to flight test programs.

By utilizing a "request and backfill data only when needed" model of PCM backfill and the nXCVR-3140A-2's burst mode SOQPSK modulation, enhanced data quality can be achieved with a spectrum efficient approach using a primary PCM RF link along with limited utilization of the nXCVR-3140A-2's bi-directional RF network.

Because of the nXCVR-3140A-2's burst mode SOQPSK modulation, many nXCVR-3140A-2s can utilize the same spectrum and "take turns" when to transmit/receive data via their schedules. Also, because this service is envisioned to be used only in the infrequent cases when needed, multiple flight test programs and multiple control rooms can utilize a single ground network to communicate with a network of airborne nXCVR-3140A-2s on multiple aircraft. This saves bandwidth and cost compared to each flight test program having its own airborne and ground hardware. Since all the nXCVR-3140A-2 in the RF network need to be programmed with the same schedule, this will drive the need for enhanced inter-program communication and management. However, with this cost comes a benefit for all flight test programs: enhanced data quality with a shared ground service model, reducing cost and improving data quality with minimal additional spectrum consumed.

This better data quality can allow more analysis tasks that need high data quality to happen in real-time in the control rooms. Previously, these tasks could only be done via the flight recordings. An example of this would be a power spectral density (PSD) analysis, which relies on a Fast Fourier Transform (FFT) as a primary mathematical computation of the analysis. When an FFT computation has incorrect or missing samples in its data set, the data result becomes skewed/incorrect. However, with the added confidence of perfect data and the combination of IADS real-time archival and retrieval capabilities, it is possible to produce near real-time PSD plots that can be trusted to make decisions. Decisions like whether a given test point is passed or potentially if it needs to be re-flown while the aircraft is still in-flight.

This also can drive flight test programs to use their PCM bandwidth differently than they do today. Generally, the telemetered PCM format contains a subset of the data that is collected by the onboard instrumentation system due to RF spectrum bandwidth limitations. Thanks to the PCM backfill feature, it is possible to guarantee excellent data quality over the telemetry link. This means that the flight test engineers can skew the data included in the PCM format towards analysis-based tasks and reduce the amount of purely informational data.

The ultimate result of this feature will hopefully be the ability to accomplish more test points per flight while simultaneously shrinking the amount of time required for data processing of flight test data. It allows the end-users to have a trusted set of data available to start data analysis while the aircraft is still in the air.

Conclusion

Increased performance in flight test programs is best achieved by finding ways to move the industry forward through technological innovation, enhanced system integration, and feature-rich functionality exceeding ordinary operational requirements.

Curtiss-Wright believes that the PCM backfill capability that is made possible by our implementation of the TmNS standard across our product line will help to further this goal by moving the industry forward. It will empower engineers to walk away with “clean” data without having to re-fly “noisy” test points or wait for post-flight data processing. Most important, PCM data backfill is the gateway to many other future innovations thanks to the unique abilities that the TmNS transceivers provide for low latency, spectrum efficient, Ethernet-based communication with airborne instrumentation networks while in flight.

In partnership with the IRIG-106 TmNS standards, Curtiss-Wright believes that this will lead to an increase in the number of test points that are successfully accomplished in a single mission. This will reduce flight test schedules and enable the flight test industry to do more in less time than ever before. All stakeholders in a flight test program will benefit from this. PCM backfill is only the beginning of the added value created from the integration activity of making the ground and air systems operate as one.

References

[1] Telemetry Standard, Range Commanders Council Document IRIG-106-19, Chapters 4, 21, 22, 23, 24, 25, 26, 27, and 28, July 2019.

DOI 10.5162/ettc2022/1.2

T-7A Distributed Test: Remote Testing of Prototype Aircraft

Rebecca A. Aronoff
United States Air Force Test Center
Edwards AFB, CA 93523, USA
rebecca.aronoff@us.af.mil

Abstract

The T-7A is the new jet trainer aircraft for the United States Air Force. The prototype T-7A test aircraft were flown based out of a contractor test facility 2,800 km away from the Air Force test team. The combined government and contractor test team established distributed test operations that enabled engineers to monitor real-time flight test missions with telemetered data and communication in control rooms at both the contractor location and the remote government location. This paper describes the setup and capabilities of the network connection; the events used to establish distributed test operations; the concept of operations across multiple organizations; technical, organizational, and contractual challenges encountered and lessons learned; and planned future growth of this capability.

Key words: distributed test operations, remote test, real-time telemetered data, experimental flight test, T-7A Advanced Pilot Trainer

Background

The T-7A Advanced Pilot Trainer is the United States Air Force's new jet trainer aircraft. It will replace the T-38 as the primary aircraft for Undergraduate Pilot Training and Introduction to Fighter Fundamentals Pilot Training. The T-7A is a clean-sheet design aircraft with a single engine, tandem cockpit, and digital flight control system.

Test flights of the T-7A were flown by contractor test pilots, with a ground-based control room of engineers that monitored real-time data telemetered from the test aircraft and controlled the flow of test events. The engineers in the control room were led by a test conductor who communicated directly with the aircrew, while groups of specialized discipline engineers monitored specific aircraft parameters. The software used to display the real-time telemetered data was the Interactive Analysis and Display System (IADS). IADS allowed the team to design specialized displays and analysis windows to optimize data monitoring.

The initial T-7A testing was conducted on two prototype aircraft at the contractor test facility in St. Louis, Missouri, USA. The lead developmental test organization was a government test team with the Air Force Test Center, located 2,800 km away at Edwards Air Force Base (AFB), California, USA. Future T-7A testing will occur both in St. Louis and at Edwards AFB, with simultaneous testing planned for aircraft at each test location. The test team consisted of government personnel based out of Edwards AFB and contractor personnel based out of St. Louis.

To minimize travel for control room personnel, the combined test team established Distributed Test Operations (DTO). DTO refers to the streaming of real-time aircraft test data and audio from a primary test site to a remote test site. DTO was used to connect test control rooms in St. Louis and at Edwards AFB to each other, enabling the rooms to operate virtually as a single control room. In this construct, it was imperceptible to the airborne test aircrew that there were multiple control rooms, versus the standard single control room. The control room located at the same facility as the aircraft was defined as the primary control room, and the control room at the other test site was defined as the remote control room. Figure 1 shows a test conductor in the remote control room during a T-7A DTO mission.

Fig 1. Remote Control Room during DTO.

DOI 10.5162/ettc2022/1.2

The establishment of T-7A DTO involved both technological developments and organizational agreements to align processes, techniques, and procedures between the government and contractor organizations.

Equipment Installation and Setup

The Defense Research and Engineering Network (DREN) was used to connect the contractor and government test sites. The DREN was a high-performance secure network owned by the United States Department of Defense, with service delivery points at various sites across the country. The DREN had data transfer speeds of up to 100 Gbps.

Prior to the establishment of T-7A DTO, some infrastructure updates were required. DREN delivery points already existed at Edwards AFB and near the contractor facility in St. Louis. The T-7A team sponsored the DREN installation to the contractor facility and installed the equipment required to send the mission data and communication over the DREN. This equipment included an access gateway that interfaced with the existing telemetry and communication systems; a network Ethernet switch that received information from two video encoders (for outgoing DTO), sent information to two video decoders (for incoming DTO), connected to the access gateway, and sent information to an encryptor/decryptor; and an encryptor/decryptor that encrypted outgoing data to the DREN and decrypted incoming data from the DREN. A diagram of the setup on one side of the DREN is shown below in Figure 2; the setup was mirrored on the opposite site of the DREN. The hardware installation for the T-7A DTO effort was completed in March 2020.

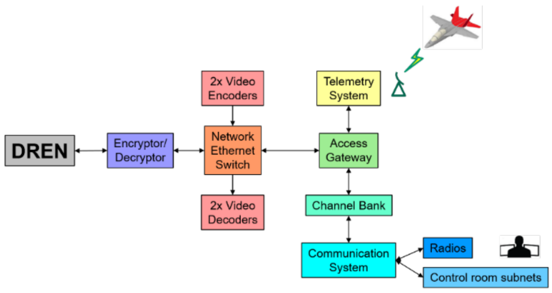

Fig. 2. Equipment Setup for DTO.

Capabilities

During DTO, both control rooms received real-time information including: aircraft telemetered data, “hot mic” audio from the test pilots, two-way communication capability to the other control room, radio capability to the test aircraft, and live video feeds from ground stations.

Aircraft telemetered data allowed engineers in the control room to monitor aircraft parameters real-time. Hundreds of aircraft parameters were available, and discipline engineers used IADS displays to view the data relevant to their specialty. Many of these data parameters were required to monitor aircraft safety and evaluate test maneuvers. Examples of these data parameters included aircraft airspeed, pitch rate, control surface positions, engine temperature, etc.

“Hot mic” provided a one-way live audio feed from the cockpit to the control room. This allowed the aircrew to ask questions and provide comments to the control room without physically keying a microphone or radio switch.

The inter-room communication system between the two control rooms (not transmittable to the aircrew) included a “room net” with all control room participants at both locations, as well as “subnets” for subgroups of control room personnel. It was possible to use up to 24 subnets at a time, although typical missions used only five subnets. Subnets were divided up by flight test discipline (flying qualities, propulsion, subsystems, loads, etc.) to enable each discipline to speak to their counterparts in both control rooms about test point maneuvers and data quality.

Live video feeds from ground stations permitted the control room team to view the aircraft during ground operations, taxi, takeoff, and landing.

The bandwidth connection on the DREN between St. Louis and Edwards AFB was 100 Mbps. A telemetry stream of T-7A flight data was 5 Mbps, and two telemetry streams were sent across the DREN for DTO missions (one primary stream and one backup stream). The communication (radios and inter-room communication) was 1.5 Mbps. Live video was approximately 1 Mbps; only one live video stream was typically used, but the team maintained the capability to send/receive two video streams per mission. Thus, the maximum bandwidth used for a T-7A DTO mission was ~13.5 Mbps. If two DTO missions were conducted simultaneously (such as one from each test location), ~27 Mbps would be used. Thus, even at maximum expected bandwidth demand, T-7A DTO would only use about 27/100 Mbps of bandwidth; therefore, DREN bandwidth was not a limiting factor for DTO missions.

DTO Establishment and Events

Prior to conducting the first live flight test mission using DTO, a data playback event was completed as buildup. During this playback

DOI 10.5162/ettc2022/1.2

event, simulated real-time aircraft data and audio, live video, and control room communications were sent from the control room in St. Louis to a control room at Edwards AFB. While the data was a playback file, the software in the control room, IADS, treated the data as live aircraft data. Issues (discussed below) discovered during this event were investigated and corrected prior to the first live T-7A DTO flight test event, which was conducted on 30 April 2020.

As of the publication of paper (April 2022), 56 real-time DTO missions have been conducted. All of these live missions were conducted with the primary control room and aircraft in St. Louis, and the remote control room at Edwards AFB. Flight test with an aircraft at Edwards AFB is scheduled to begin in July 2022.

As risk reduction for DTO missions with Edwards AFB as the primary test site, data playback tests were conducted from a control room at Edwards AFB to a control room in St. Louis. The first test involved sending simulated live aircraft data and real live video from a control room at Edwards AFB to a control room in St. Louis. The second test evaluated the potential for simultaneous DTO missions at both test locations. Four control rooms were used for this evaluation: two at Edwards AFB and two in St. Louis. Control room 1 in St. Louis sent simulated live data and aircraft audio, live video, and live room-to-room communications to control room 2 at Edwards AFB. Control room 3 at Edwards AFB sent simulated live data and aircraft audio, live video, and live room-to-room communications to control room 4 in St. Louis. The communication connections between the control rooms were transposed initially, and the team troubleshot and corrected the issues during the checkout. There were no noticeable latency increases or issues with DREN performance; therefore, the test team does not anticipate bandwidth issues for future simultaneous DTO missions.

Latency

During flight test, the control room was required to monitor aircraft parameters to make safety-of-flight determinations, evaluate maneuver quality, and analyze data between test maneuvers. For example, to avoid ground impact during test maneuvers, the control room monitored aircraft airspeed, altitude, dive angle, bank angle, and acceleration to make “abort” calls to the pilot if the aircraft was going to exceed pre-determined safety margins.

The most pressing safety concern when establishing DTO was the latency between the aircraft and the two test sites. The team needed to ensure that the remote test site received aircraft data and could communicate a safety decision back to the primary test site with no noticeable delay, as if the remote control room was co-located with the primary control room.

The team programmed a latency measurement into the control room data displays. This latency measurement calculated the difference between the aircraft time when it sent a data package and the control room time when it received the data package.

This latency measurement was local to each control room, so each control room monitored the latency from the aircraft to their own control room. For aircraft operations in St. Louis, the Edwards AFB control rooms typically experienced latencies of 120-140 ms. Comparing that to the local latency in St. Louis indicated that the average latency increase due to sending data across the DREN via was 40-80 ms.

Latencies in both control rooms increased to ~300 ms when a telemetry repeater was used to relay data from the aircraft to the control room in St. Louis. However, the remote control room only suffered the standard 40-80 ms delay as compared to the primary control room. In the DTO missions to date, the latency in the remote control room was imperceptible to experienced control room personnel, and the timing of communication and data seemed comparable to the timing of a locally-executed control room mission.

A safety review board, comprised of experienced flight test professionals independent of the T-7A program, determined that latencies under 500 ms were acceptable for safety-of-flight calls for the first phase of T-7A testing. This latency threshold may change for future testing, based on the type of test and lessons learned from the first phase of DTO missions.

The latency displays on the control room data screens were programmed to alert the test conductor if the latency exceeded the 500 ms threshold. While the team has not seen latencies higher than 500 ms to date, the concept of operations mandates that if the latency exceeds the allowed threshold, the test conductor will make a “knock-it-off” or “abort” call to pause aircraft testing until the latency delay is resolved.

Concept of Operations (CONOPS)

The establishment of T-7A DTO involved both technological developments and organizational agreements to align processes, techniques, guidelines, and procedures between the government and contractor organizations. The government and contractor test teams co-authored and agreed upon a combined Concept of Operations (CONOPS) document that outlined the ground rules and procedures for DTO during flight test.

The CONOPS defined roles and responsibilities for test team members. Each control room had a test conductor who led the personnel in that control room. The test conductor at the primary test site maintained the responsibility of communicating with the test aircrew, while the test conductor at the remote test site acted as the primary communicator from the remote control room to the primary test conductor. During normal operations, the remote test conductor did not communicate directly with aircrew, enabling aircrew to communicate with a single point of contact for test information. Specialized discipline engineers could be located in either or both control rooms.

Examples of how the CONOPS brought two different organizations together to align guidelines were crew rest requirements and duty day limitations. Crew rest is mandatory off-time between duty days to ensure adequate rest before participating in aerial or control room activities. Duty day is a limitation on the amount of time spent performing official duties. The Air Force regulations and contractor standards for aircrew and control room personnel had different crew rest requirements and duty day limitations. Therefore, to ensure compliance across the combined T-7A team, the most conservative crew rest and duty day limitations from the Air Force and contractor requirements were written into the CONOPS and applied to the entire test team.

Another example of an organizational factor was resource scheduling. The CONOPS defined the scheduling processes and timelines for each test site. The test conductor at each site was responsible for scheduling resources for their respective site. The primary test conductor was responsible for preparing test cards for each mission and sending the mission materials to the remote test conductor, and the remote test conductor was responsible for distributing the materials to personnel at the remote site.

There were several types of software files required to load the IADS screens for each control room mission. Mission-specific files, prepared at the primary site, had to be sent to the remote site prior to each mission to ensure proper IADS functionality. The CONOPS outlined the required timelines for these files to be sent from the primary site to the remote site. This process also ensured version control to confirm that both sites operated with the same file revisions and viewed the same data.

Flight test briefings were led by the primary test conductor, as the overall lead personnel for flight test activities. Test team personnel at the primary site attended the briefings in-person, and personnel at the remote site called into the briefings.

The CONOPS defined the buildup approach to establish confidence in real-time safety-of-test data monitoring and communication from the remote site. The remote participants started with observation-only permissions, which allowed the test team to become comfortable with the DTO CONOPS and battle rhythm of working in/with a remote control room. The next step was progression to remote monitoring of mission-critical data to build confidence in the ability to communicate data quality or technical calls effectively across test sites. This allowed the team to identify any applicable considerations before implementing safety-of-test monitoring from the remote site. Once the combined government and contractor test team was confident in the ability to perform mission-critical monitoring from the remote site, controlled scenarios would be used to simulate making real-time safety-of-flight calls from the remote site. These scenarios were designed to exercise the necessary communication in the control rooms between both test sites, as well as communication to the aircrew that could be encountered during a live mission. Finally, the remote site would be permitted to make safety-of-flight calls real-time.

While the goal of DTO was to create a single virtual control room where engineers had the same responsibilities regardless of whether they were physically located in the primary or remote control room, the T-7A combined test team did impose restrictions on training control room personnel during DTO missions. Since good instruction relies heavily on observing the student's behavior, the decision was made to restrict formal instruction of new engineers to the same control room as the instructor. Additionally, engineers at both locations had to follow a formalized T-7A control room training plan.

Communication checks were performed prior to and during each DTO mission to ensure that the two control rooms retained communication with each other. Before each DTO mission started, the primary test conductor requested a direct “comm check” call from every engineer participant, regardless of whether the engineer was in the primary or remote control room, to ensure each engineer had operational communications. Then, prior to each test point, the primary test conductor asked for a “room ready” check-in from all participants; all discipline engineers gave a thumbs-up sign to their respective test conductor, and the remote test conductor relayed a “remote room ready” call to the primary test conductor. This process ensured that a communication check between the primary and remote control rooms was conducted prior to every test point.

A safety mitigation during flight test missions was that any control room engineer was able to make a safety-related “knock-it-off” call at any point in the flight. A “knock-it-off” call meant that the aircrew should cease aircraft maneuvering, de-conflict from any formation aircraft, and return to level flight in a safe flight envelope to evaluate further actions. This mitigation was also true for DTO missions; any participating engineer, regardless of control room, was empowered to make a safety-related “knock-it-off” call to the primary test conductor at any time.

The CONOPS described procedures to be followed if data or communication failures occurred during DTO. If telemetered data was lost in either or both control rooms, the primary test conductor would be informed immediately and relay that information to the aircrew. If communication between the two control rooms was lost, the remote test conductor or remote range control officer would use an independent telephone to call the primary control room and inform them of the communication dropout. If either test site lost monitoring of mission-critical or safety-of-test parameters, testing would be halted until the issue was resolved. Additionally, for DTO missions where the remote control room was making safety-of-flight calls, the latency to the remote control room (discussed above) was considered a safety-of-flight parameter.

In the event of an aircraft mishap, both control rooms would follow their organization’s pre-defined mishap procedures to secure data and begin the proper notification protocols. The addition of DTO participation would not change the mishap investigation responsibility.

As the test team encountered challenges and lessons learned during DTO execution, the CONOPS was updated to improve processes and increase efficiency for future DTO missions.

Challenges Encountered and Lessons Learned

Technical, organizational, and contractual challenges were encountered during the establishment of T-7A DTO. As the test team overcame many of these challenges, lessons learned were documented.

The most notable technical issue encountered to date was data dropouts to the remote control room. Data dropouts occurred twice in a single mission in August 2020. The first data dropout lasted thirty-one seconds, and the second dropout lasted three minutes and thirty-six seconds. During the dropouts, the remote control room lost aircraft telemetry and hot mic audio, but maintained communication with the primary control room and thus was able to inform the primary control room of the dropouts. The test team troubleshot the dropouts but was unable to diagnose the root cause. Data dropouts remained an item of interest for the test team, although no data dropouts occurred during the other 55 missions to date. Of note, no communication dropouts occurred on any of the 56 missions. Based on the strong performance of the data and communication via the DREN to date, the test team expects to maintain reliable communication and telemetry during future missions.

Another unexpected technical issue was radio interference from the remote site. During one DTO mission in November 2021, radio communication from a local frequency at the remote site interfered with DTO radio communications, causing confusion due to extraneous radio transitions. This radio bleed-over was immediately diagnosed as a hang-up between the data line bridging the communication channels, and the communication team was able to perform a reboot of the affected communication switch and resolve the issue.

Some challenges were both technical and organizational in nature. For example, the government and contractor test teams did not have a shared data network. As a result, transferring large files between government and contractor personnel was challenging. There were multiple file transfers required prior to every DTO mission to enable the control rooms at both locations to use the same data screens. The test team explored various file exchange services and determined that the Department of Defense (DoD) Secure Access File Exchange (SAFE) best fit this application. The team had to overcome security challenges to enable the contractor personnel to initiate file transfers with this service.

A technical issue with an organizational solution was a common file structure and naming convention was required to operate the control room displays. The IADS displays used several input files that were stored on a shared drive. Initially, the test sites had different names for their shared drives, which prevented IADS at the remote location from loading the input files. To remedy this, both locations renamed their shared drives identically, which enabled the IADS input files to load properly at both test sites.

Naming conventions were not the only difference between control room setups; hardware differences also proved challenging. For example, one test site had computer monitors with a 16:9 ratio, and the other site had monitors with a 4:3 ratio. The IADS screens were initially designed to fit 16:9 ratio monitors. During the first DTO checkout, the team discovered that the displays were compressed on the narrower 4:3 monitors, rendering the displays unreadable. After collaboration, redesign, and testing, the team concluded that the displays must be initially sized to fit the smaller monitors (4:3), then scaled up for the larger monitors (16:9) to maintain readability across both monitors.

An organizational challenge was that the government and contractor sites had different processes and timelines for scheduling resources required for DTO. For example, one of the sites had significantly more flexibility in rescheduling control rooms for DTO. Both test sites reserved control rooms for DTO on planned mission days, but when factors such as weather or maintenance drove the program to reschedule flights, DTO opportunities were missed when only one test site was able to reschedule control rooms.

To minimize the effect of missed DTO opportunities due to rescheduled flights, the test team increased the number of days they requested control rooms for DTO, then canceled their control rooms on days the T-7A was not flying. However, the team was unable to reserve control rooms every day because the control rooms were shared with other test programs. A limitation of DTO is that it increases the number of resources required overall; two control rooms (one at each location) are required for each DTO mission, and the additional resource demand was a limiting factor.

Another schedule-related challenge was the test sites had a two-hour time zone difference, resulting in mission briefs as early as 0330 for the remote site. In addition to the early missions presenting physiological challenges, there were difficulties scheduling control rooms at the remote site for early morning DTO missions. Mission times outside of available control room hours were a limitation that resulted in missed DTO opportunities.

Increased organizational communication was necessary for DTO missions. For example, the addition of remote personnel meant that a significant portion of the test team was not present for any in-person mission updates – such as maintenance or weather delays – that occurred after the mission brief concluded. Therefore, proactive communication was required from the primary test conductor to the remote test conductor to convey any updates that occurred after mission brief concluded.

DTO contractual challenges were identified and overcome. The government wrote a dedicated contract for DTO support. The initial DTO contract limited the program to a maximum of eight DTO missions per month, which resulted in missed opportunities for DTO. Through execution, it became apparent that the cost of establishing DTO for a single aircraft was the same whether one, two, or three flights were observed that day; thus, the financial limitation in the contract should be based on number of days – not number of flights – of DTO missions. The follow-on DTO contract allowed for up to 20 days of DTO per month, which incorporated the improvements of counting days versus flights as well as increased the allowable count per month.

Future Growth and Conclusions

The T-7A test team intends to use DTO as part of standard operations for future testing that will occur over the next several years. This includes the continuation of missions executed in St. Louis with a remote site at Edwards AFB, adding DTO missions executed at Edwards AFB with a remote site at St. Louis, and executing simultaneous DTO missions with aircraft flying at both locations.

A future goal of T-7A DTO is fully-remote test conduct, where the test control room is independent of the aircraft location. For example, an aircraft flying in St. Louis could utilize a single control room at Edwards AFB, without a control room staffed in St. Louis. The team intends to build up to this goal over the course of a couple years, after gaining more experience with DTO missions at each test location.

The T-7A team is in the process of establishing a connection between a T-7A hardware-in-the-loop simulator in St. Louis to a simulator control room at Edwards AFB. This connection would allow personnel at Edwards AFB to participate in simulator activities via DTO when aircrew fly the simulator in St. Louis. Applications of this include flight control law development, maneuver development, mission rehearsal, and miscellaneous analysis. Flight control law development occurs when engineers are designing the software that defines how the aircraft's control surfaces will act under various flight conditions. It often involves trial and error in the simulator, and it typically occurs at least a month prior to flight test on a given software version. Maneuver development occurs when the test team uses a simulator to test and mature different aircraft maneuvers to determine which maneuvers, test conditions, and recovery procedures will result in the desired data. Maneuver development typically occurs several weeks to months prior to flight test. Mission rehearsal is completed by the test team (aircrew and control room personnel) who will execute the actual mission. It serves as a practice mission, and the engineers gather IADS data during the rehearsal to use as predictions of key parameters in the actual mission. Mission rehearsal typically occurs one to eight days prior to flight test. The capability for simulator DTO would increase participation in these critical simulator activities and reduce test team travel.

As a result of the successes of the T-7A DTO program to date, numerous other test programs across the Air Force test enterprise are planning to use DTO for upcoming testing.

T-7A DTO demonstrated successes in both technological development of capability and in organizational unity to align processes, techniques, and procedures to accomplish a common mission. The long-term capability to minimize personnel travel and participate in test missions remotely will greatly improve quality of life for test team personnel and increase the ability of both organizations to participate in flight test.

DISTRIBUTION STATEMENT A. Approved for public release; distribution is unlimited.

412TW-PA-22148

DOI 10.5162/ettc2022/1.3

Modern High Speed FTI Recorders and Switches Requirements and Use Cases

Brandon Rosso
Curtiss-Wright, 15 Terry Dr, Newtown, PA, 18940, USA
brosso@curtisswright.com

Abstract: As Flight Test instrumentation (FTI) architectures increasingly migrate to airborne "network" systems – comprised of distributed sub-systems of data acquisition, processing, and recorders – the role of network switches that form the network switch fabric become critical. Likewise, the FTI recorders – whether a single large or multiple distributed data sinks – is also increasingly critical as it relates to the data formats suitable for ground processing, given the number and types of data sources. This paper discusses the factors influencing the switch and recorder units, for a Distributed FTI (DFTI) System.

Keywords: DFTI, IEEE-1588, IEEE-1394, 10GBASE-SR, PTP, QoS, TmNS, PCAP, DAR, IRIG, iNET, UDP

1. Introduction

The FTI architectures are rapidly evolving to airborne "networks" comprised of various network elements, i.e., Data Acquisition Units (DAUs), switches, recorders, gateways, and network manager sub-systems/units. The previous CAIS-based architectures, using aggregators for PCM outputs from multiple DAUs are now transitioning to DAUs that are part of the network and multi-cast acquired data to the network. The network DAUs include traditional measurands, e.g., accelerations, temperatures, pressures, and, also increasingly, avionics bus traffic, e.g., MIL-STD-1553, IEEE-1394, 10GBASE-SR, and ARINC-818. The network traffic also include data from cameras, whether high-definition or high-speed, that are delivered as Internet Protocol (IP) messages. The amount of data collected, especially for new airborne platforms, has increased significantly, with the bus traffic far outstripping the data from traditional measurands. The new type of network DAUs allow multi-cast of different data sets, i.e., all collected data aka "bulk" data and selected messages/data aka "Cherry-Pick" data.

The collected data and data rates are far more than the available RF bandwidth for real-time Telemetry (TM), thus necessitating the use of airborne recorders for storing the collected data and, as applicable, providing a subset of safety and time-critical data for TM. In the near-term, the need for Data-Retrieval-on-Demand (DRoD), driven by ground station commands using bi-directional RF links, will require recorders that not only record the collected data, but provide selected data sets (DRoD) for TM.

In an networked architecture, the TM data can be generated as PCM (clock/data) for a RF transmitter, by either a centralized recorder or a Gateway unit that filters all selected messages/data from the various network sub-systems and creates a single PCM for the entire network.

The FTI architectures, even for the network systems, can vary depending on the platform, mission requirements, and the system integrator preferences. Alternatives include using multiple recorders that provide redundancy and a means to distribute the network units across the entire platform, instead of dedicating/sacrificing a single large section of the platform for a centralized recorder.

The dichotomy in the FTI architectures can even extend to the entire FTI system, above and beyond the decision on the recorder type. Does the platform support the Size, Weight, and Power (SWAP) – including thermal management – for centralizing the entire FTI systems of DAUs, switches, recorders, and gateways; or does an alternative method of distributing the various FTI sub-systems throughout the platform, often closest to the measurands and their DAUs, provide better benefits and fully leverage the "network".

In either scenarios, the FTI network requires some key elements for it to be fully functional. These include time synchronization throughout the network with one network sub-system/unit providing the master reference; system wide programming and control e.g., through Simple Network Management Protocol (SNMP); multi-casting of bulk and selected message/data; data aggregation and port mirroring to multiple data sinks (recorders and gateways); and source data type agnostic network paths. As the FTI networks grow larger with potential for latencies, especially for safety and time-critical traffic, the network should provide capabilities to establish a

DOI 10.5162/ettc2022/1.3

Quality-of-Service (QoS) for critical data. In the long-term, the FTI networks may evolve to include Time-Sensitive-Network (TSN) capabilities for these types of traffic.

The network recorders should be capable of receiving data from multiple sources with different message types, e.g., from DAUs or from platform sensor-suites, and be capable of recording them in formats that are suitable for ground processing. Depending on the data source, some formats may be better suited for some message types, e.g., PCAP for sensor-suite IP traffic and IRIG Chapter 10 for other traffic types.

The FTI network considerations drive the requirements and use cases for the switches and recorders. This paper discusses these factors and their impact on the switches and recorders, through a few use cases.

2. Generalized FTI Network

A generalized FTI network is shown in Figure 1. The network includes DAUs that acquire analog sensor data, e.g., acceleration; switches (5-port, 12-port, and 16-port); recorder (nREC-7000); recorder control panel (RCP); gateway (nGWY-2000); and transmitter.

The 16-port switch (NSW-16GT-1), henceforth NSW-16 acts as the master reference in this network, with its timing referenced to GPS signal that it supports. The entire network uses IEE-1588-2008 (v2) for time synchronization, with other switches, e g., 5-port switch (NSW-5GT-1, henceforth NSW-5) and 12-port switch (NSW-12GT-1, henceforth NSW-12) providing either Boundary Clock (BC) or Transparent Clock (TC) modes of operation.

The DAUs acquire analog data and bus data and multi-cast them on the 100Base-T, GbE, or higher data rate ports. The analog data in each acquisition stack may be formatted as PCM and the PCM frames are packetized and multi-cast as TmNS (IRIG Chap. 21 – 26), IRIG Chapter 10/11, or as DARv3 (Curtiss-Wright proprietary format) that is widely used in the FTI industry. Some protocols, e.g., TmNS and DARv3 are better suited for networking, with Chapter 10/11 becoming more prevalent for some system integrators. The DAUs can also select specific messages and/or data, especially from acquired bus traffic, and multi-cast it for devices, e.g., network gateway (nGWY-2000, henceforth nGWY) to convert to PCM for real-time TM. The DAUs may also multi-cast their status, metrics and, in the future, may support QoS for time-critical data.

Other data sources, e.g., cameras are also part of the FTI network and will also multi-cast IP traffic. The cameras may capture high definition display data or high-speed event data for on board recording, and possible TM of camera pre-view data.

Other data sources may include the platform sensor-suites that are rapidly advancing in dates from less than 1 Gbps to 10Gbps, and in the future to 100Gbps. The capture and processing of these high data rate sources will require improvements to the current FTI capabilities.

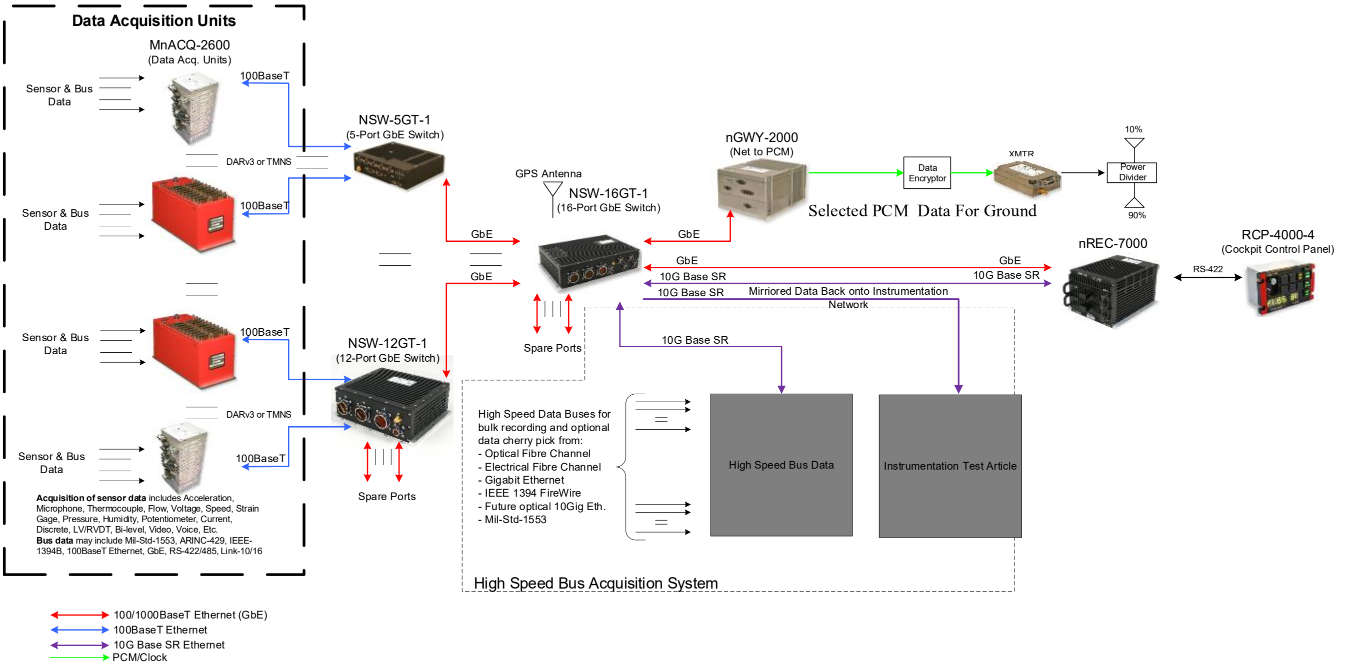

Figure 1: Generalized FTI Network

The onboard recorder (nREC-7000, henceforth nREC) represents one of the of the data sinks of the network. The nREC may be used to record the entire FTI network data including all bulk and selected message/data and the status and metrics of all the network sub-systems/units. Thus, the nREC should be capable of supporting multiple message types from the different data sources and record them in formats suitable for ground processing. The time stamping of the recorded data varies by the specified standard with some formats supporting the 64-bit resolution while others revert to 48-bit resolution. Some message traffic types, e.g., from sensor-suite may be better suited for recording as PCAP while other data, especially from DAUs that capture analog data, preferable to be recorded as IRIG Chapter 10. FTI recorders should provide the requisite flexibility in recording formats.

The recorders may additionally provide other capabilities depending on the FTI system architecture. If there is only one centralized recorder with no nGWY, the recorder may need to provide data/message selection and their conversion to PCM. Thus, the recorder, in this instance, functions as a gateway. The recorder may optionally multi-cast selected messages to a nGWY if the gateway is part of the FRI network. In an DFTI architecture, the selected message/data from each data source will be filtered by the nGWY for conversion to PCM. The PCM formats would also depend on the data sources within the FTI system. A FTI system that requires only analog data to be provide as TM, may use the bandwidth efficient IRIG Chapter 4 PCM format. If the FTI system includes traffic from network sources, e.g., video messages for TM, the PCM needs to be formatted as Chapter 7/4.

Other functions that the recorders need to perform include DRoD, thus necessitating design and implementation changes on the file formats and journaling for rapid retrieval of data. The implementation of DRoD, especially with a bi-directional transceiver, e.g., nXCVR-3140 that provides an uplink for ground station commands, will have implications on latency, QoS, and in future, TSN.

The network configuration, programming, and monitoring also pose requirements for the switches and recorders. The network may be configured, programmed, and managed by SNMP. Other methods include vendor specific software, e.g., TTCWare (Curtiss-Wright software) that supports the entire network for a “Total Systems Solution”. In the future, the FTI industry may adopt the IRIG Chapter 23 Meta Data Language (MDL) programming for the network. In a fully networked FTI system, the entire network will be programmed on the ground using Ground CheckOut Panel (GCOP) interface. The network may also be controlled during flight by Recorder Control Panel (RCP) or Cockpit Control Panel (CCP) units, e.g., RCP-5000 that supports GbE.

One of the critical functions in the FTI architecture definition and management is the estimation and management of the network switch fabric traffic loads, and the required aggregation of data from multiple data sources to one or more data sinks. The network switch fabric may be required to provide a layered aggregation of data, e.g., using a NSW-5 to aggregate all the data from DAUs underneath the left wing. Additional switches may aggregate the data from multiple NSW-5 culminating in the NSW-16 that supports four (4) 10Gbps optical inputs/outputs. Any of the switch ports could also support port mirroring, where data received on one port is copied and mirrored back to another port. These features enable network traffic to be directed to a bulk recorder, while the copy is sent to a unit that carries out data/message selection and/or gateway functions.

3. Recorder Centric Flight Test Systems

There is a growing need to provide a compact recorder unit for FTI applications that may only require the need to capture avionics data buses. There are situations where initial flight testing has been completed and the aircraft has moved into production. In these cases, when there is a need to requalify for a new specification or increased capabilities of the aircraft, a compact recorder unit would suffice, and the data can be pulled from the avionics buses located on the aircraft. The optimal solution is a compact recorder that could easily be inserted into the aircraft, and act as a permanent piece of test hardware. This provides the team with limited wiring to deal with, and a low weight addition to the aircraft. The compact recorder would perform similar operations as a full blown DFTI system, except in a much more reduced size and scale.

In terms of inputs, the DFTI system interfacing to specific digital buses, e.g., MIL-STD 1553, IEEE 1394, Fibre Channel, ARINC 429, Serial Buses, Ethernet Buses will typically contain the necessary information on aircraft that has completed the initial flight test qualification.

As in the DFTI system, there is typically a need for telemetry or TM in this application as well for some type of safety of flight, or potentially some type of onboard display. The idea in this system would be the ability to select specific data from the input interfaces, and output this data via a PCM output, that needs to be formatted as Chapter 4 or 7 for telemetry. As well as the need to provide a UDP multicast output, a data format that can be sent over the network via UDP multicast traffic as TmNS (IRIG Chap. 21 – 26), IRIG Chapter 10/11, or as DARv3 (Curtiss-Wright proprietary format) that is widely used in the FTI industry.

DOI 10.5162/ettc2022/1.3

In summary, the needs of every aircraft are different. However, by identifying what buses need to be captured, we can tailor a specific recorder box that be used in these specific applications.

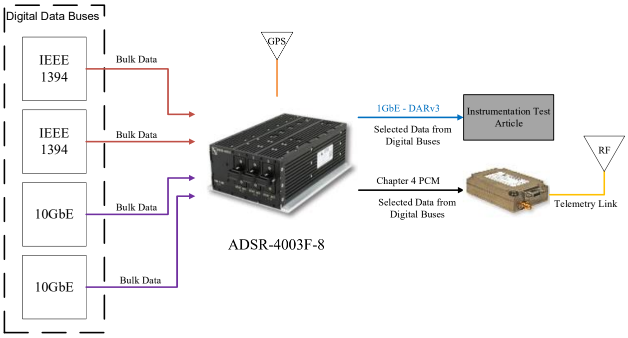

Figure 2: Recorder Centric Flight Test Acquistion System

Figure 2 represents an example of a compact recorder box (ADSR-4003F-8) that is being used to accomplish the above outlined task, of providing a one box solution for a compact recorder box. The unit is interfacing with four different avionic buses – 2-Channels of IEEE 1394, and 2-Channels of 10GbE that are bulk recorded in a Chapter 10/11 format for post processing. In addition, the data from these buses is filtered, and the filtered/selected data is sent to ground via PCM (Chapter 4) output. Moreover, the same stream is sent out over the network as UDP packets to interface with the aircraft devices, e.g., display.

Curtiss-Wright provides several Commercial-Off-The-Shelf (COTS) units, as different ADSR-4003F-x variants for different customer and platform needs. Table 1 below show the currently available ADSR variants

DOI 10.5162/ettc2022/1.3

	ADSR-4003F-1	ADSR-4003F-2	ADSR-4003F-3	ADSR-4003F-5	ADSR-4003F-6P	ADSR-4003F-7	ADSR-4003F-8	ADSR-4003F-10
ADSR Base	1*	1*	1*	1*	1	1	1	1
1 Channel GPS & PCM Output					1	1	1	1
2 Channel IEEE 1394 Card					2		2	
2 Channel 10G Base - SR							1	
4 Channel MIL-STD 1553 Card						2		3
1 Channel HD-SDI Input		4						
1 Channel DVI/ HDMI Input			4					
2 Channel 1GbE Input				1				

Table 1: Supported Interfaces

4. High Speed Camera System

Some DFTI applications have a need to capture images at extremely high rates, e.g., 1000-5000 frames per second. These systems function like the described DFTI network, comprised of the same type of elements: Data Acquisition Units (in this case the cameras themselves), switches, recorders, gateways, and network manager sub-systems/units. As in the DFTI system, the switches (NSW-16GT-1) are responsible for synchronizing to an external time source, such as GPS, and providing 1588 time synchronization to all the high speed cameras (nHSC-36-S1), recorder (nREC-7000), and nMGR-2000. This is to ensure that all cameras can be time coherent when analysing their images in post flight.

The most common application is to capture a separation event from the aircraft. The system is installed as a “distributed, networked architecture”; the customer may install the individual high-speed camera units in a variety of locations throughout the aircraft (in the fuselage, wings, etc). The high-speed camera equipment will be wired to power, network interfaces and control instruments by the customer.

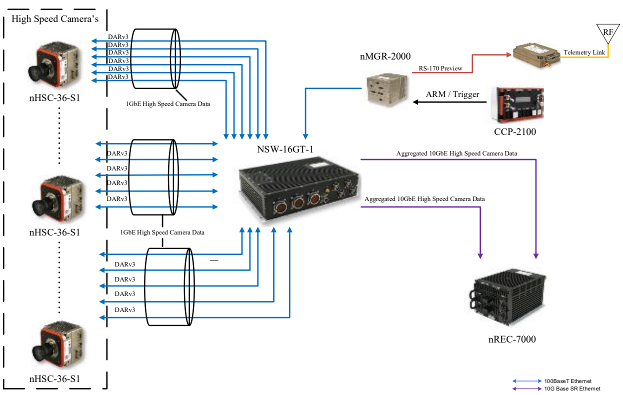

Figure 3: High Speed Camera System

Figure 3 shows a system that uses a manager (nMGR-2000) to configure and control the cameras. The nMGR-2000 sends the capture command when initiated by the control panel via SNMP commands to the High-Speed Camera (nHSC-36-S1’s).

Once the camera captures the images, they will be held in the camera’s internal buffer memory until a transfer request is initiated by the nMGR-2000. This is mainly to manage the traffic on the switches properly. The high-speed cameras will typically be transferring GigaBytes of data, with each camera potentially sending a full buffer of 8GB. One of the issues with the current generation of high-speed network camera systems with large number of cameras (greater than six) is the speed required to transfer the images from the high-speed camera to the recorder. Due to the amount of data being sent, there needs to be a balance between the rate at which the data is being sent, and what is an acceptable time to wait for an entire buffer to be cleared. Typically, the two other factors in this is the pipeline or bandwidth of the Ethernet link, and the media write speed of the recorder.

In our previous systems we would be limited by the 1GbE link of the Switch & Recorder. When accounting for the combination of limits between the media write speed, and the bandwidth limitations of the switch, the maximum amount of camera’s high speed data the user can send to the recorder is limited to 3 at once, per Ethernet port, when the link is limited by 1GbE. This port limitation is both a factor on the switch, and the recorder.

By providing a switch that can support 10GbE such as the NSW-16GT-1, and a recorder such as the nREC-7000 that has the capabilities to link at 10GbE, we eliminate this connection bottle neck. From a bandwidth perspective this would increase the theoretical increase the transfer capabilities high speed camera network to that of 30 camera's per Ethernet link.

The advantage of this allows the 10GbE system to be ready for another set of captures significantly faster than a 1GbE system. The bottleneck could then be put on the recorder's media, which typically was not being hit on a 1GbE network. This development would allow users to theoretically be able to utilize more camera's when imaging events due to the fact that the camera system could be ready significantly faster then what was previously possible in a 1GbE based system.

Due to the way most high speed camera systems are planned out, this capability would typically only require the addition of a 10GbE switch (NSW-16GT), and a 10GbE Recorder (nREC-7000) that has the capabilities of reassembling, and recording the images of the high speed cameras. The user could simply leverage their existing hardware of a 1GbE with the various 1GbE based switches, and simply rely on the NSW-16GT, and the network manager (nMGR-2000) to properly manage the data being sent to the nREC-7000.

7. Conclusions

As discussed, the planning of an FTI system requires a lot of planning to determine the needs of not only the current goals of the system, but potentially the need to provision for increased data rates, or an adaptation of requirements.

By designing our products based on applications with system architecture in mind, we have been able to quickly adapt our recorder and switch products in various ways covered in this paper. It has allowed us to provide existing DFIT systems to quickly integrate with high speed data buses by utilizing our nREC-7000 & NSW-16GT to manage the high speed data buses , provide permeant fit solutions to post flight test aircrafts by leveraging our ADSR-40003 platform with COTS I/O cards, and decrease the down time of the high speed camera system by utilizing the 10GbE pipeline that is provided by the nREC-7000 & NSW-16GbE link.

7. Glossary

DAS: Data acquisition system
EMC: Electromagnetic compatibility
EMI: Electromagnetic interference
FPGA: Field programmable gate array
FTI: Flight test instrumentation
GCOP: Ground Checkout Panel
GPIO: general purpose input output
HD: High definition
IP: Internet Protocol
NTP: network time protocol
PCM: Pulse code modulation
PTP: Precision time protocol
RF: Radio frequency
RTP: real-time protocol
RTSP: real-time streaming protocol

DOI 10.5162/ettc2022/1.4

FTI Wireless DataBuses Interface

Mª del Pilar Vicaria Torralbo
Airbus Defence and Space. Avd. De John Lennon s/n, Getafe Madrid, Spain

pilar.vicaria@airbus.com

Abstract

The objective of this paper is to present the evaluation of feasibility of a wireless system for acquiring, recording and monitoring Databuses for flight test instrumentation and the production of a prototype capable of performing these tasks.

Three main phases have been tackled:

-Feasibility study phase: study of feasibility of the wireless technology applied to the acquisition of the common Databuses required for flight test. The result of this study would be the identification of the Databuses which are suitable for wireless management.

-Hardware and firmware architecture definition phase: the definition of the hardware and software architecture of the wireless system that would implement the acquisition of the Databuses identified.

-Prototype production phase: the manufacture, program and configuration of a prototype system that complies with the previous architecture.

Key words: Wireless, Databus, Instrumentation, Flight Test, FTI.

Wireless Application in Flight Test Instrumentation.

In this paper when speaking about wireless applications in Flight Test Instrumentation (FTI) it is referred to installations devoted to the measuring and acquisition of data in an aircraft when is instrumented for a flight test campaign using pieces of equipment that transmit the information in a wireless mode opposite to a wired one. Data gathered from instrumented aircrafts come mainly either form sensors or from databases that interchange information between computers.

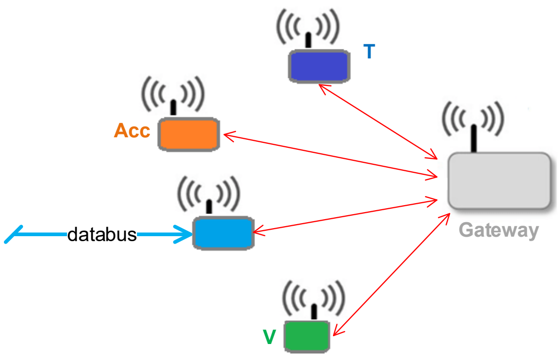

Fig 1 Wireless schematic system

During the last years the wireless technologies have been developing exponentially and their usefulness is being demonstrated in all fields. In the Flight Test environment it has been proven that they may be useful for the acquisition of certain analogic measurements referring to temperatures, voltages, and other discrete signals and there are in the market manufacturers of sensors like Lord Microstrain or BeanAir that transmit the information they sense in a wireless mode as depicted in the figure 1. But no studies or test have been conducted to determine the suitability and feasibility of acquire and transmit complex digital signals, like databus or streaming, being these abundant and widely used in the FTI of military and commercial aircraft, today is a field little explored, mainly due to the absence of specific hardware oriented to this matter.

The amount of data acquired in one flight test aircraft the quantity delivered in data buses is very high and increases every day more. As a figure, in the light and medium transport platforms the required instrumentation of data buses is of 20% of the total measurements but the parameters inside are of more than 85%. In the case of flights dedicated to evaluation for customers or in service anomalies the ratio is much higher being even of the 100%.

The wireless solutions have been demonstrated to have a positive impact in several aspects of the final FTI solutions either when using wireless sensors or for databuses wireless acquisition devices.

- Higher degree of wire reduction. Local acquisition of Databuses would reduce the wiring of a big quantity of parameters.
- Higher degree of autonomy. The FTI system would tend to a plug and play solution reducing the work load of a number of organizations.
- Higher reduction in the installation and uninstallation activities: reduction in the amount of documentation produced by the Design department and in the modifications in the aircraft.
- Reduction of time required to install and deinstall the FTI in the aircraft, with the associated impact in schedule.

Having into account the previous circumstance and that the aircraft systems are everyday more fitted with Databuses dedicated for flight test, having the capacity of acquiring this amount of data wirelessly would improve dramatically the advantages of a wireless FTI system.

Feasibility Study

The ARINC429 databus has been identified as the most suitable for been used in this prove of concept for being acquired by a wireless node.

For reaching this conclusion it has been identified and analyzed the most commonly required communication buses in FTI. In this way it has been summarized the different types and their main characteristics, evaluating the suitability to be acquired and transmitted wirelessly, taking into account the maturity and technological limitations existing in the current wireless transmission systems [Fig.2], as well as its current use in traditional flight test acquisition (wired).

DATA BUS TYPES

The traditional FTI wired installations of modern aircrafts includes tons of orange cables, many of them are dedicated to transporting communications buses to the FTI data acquisition rack.

The following are the bus or information transmission line types most commonly acquired in FTI by wired methods:

<u>ARINC 429</u>

Description

ARINC 429 implements serial line communication and was one of the first standards specifically targeted at avionics applications. Unlike in modern networking protocols, the sender always sends to the line, and the recipients always read from it. The number of maximum number of recipient is 20.

The bus can operate at low or high speed. Low speed uses a variable clock rate and a nominal throughput of 12-14 kbps, while the high speed mode requires a fixed clock rate and allows 100 kbps.

Transmission from the source LRU is comprised of 32 bit words containing a 24 bit data portion with the actual information, and an 8 bit label describing the data itself.

Impact in FTI

Surely ARINC 429 is the most frequently acquired bus in Flight Test, some A/C like A330 MRTT has around one hundred ARINC 429 lines acquired during flight test development, and therefore a wireless system to acquire these buses can contribute to reduce cost, works and weight into the FTI deployment.

<u>CAN</u>

Description

CAN Bus is a message based protocol, designed originally for multiplex electrical wiring within motor vehicles, developed by Bosch as an automotive data bus in 1983, but also can be used in many other contexts like A/C. The CAN-bus has emerged as a future technology, also known as ARINC 825. The CAN Bus can work at Low or High speed, The High-Speed ISO11898 Standard specifications are given for a maximum signaling rate of 1 Mbps with a bus length of 40 m and a maximum of 30 nodes. It also recommends a maximum un-terminated stub length of 0.3 m. The Standard defines a single line of twisted-pair cable with the network topology.

Impact in FTI.

The CAN Bus is used in modern aircrafts like A400M, but now the massive implantation of devices is low, two or three FTI bus lines not seems quite to justify a wireless system. Furthermore the high-speed modes get over the current wireless bandwidth performance, for this reason

CAN bus implantation and wireless bandwidth evolution must be kept and re-evaluated.

MIL-STD-1553B

Description

MIL-STD-1553, the *Aircraft Internal Time Division Command/Response Multiplex Databus*, is widely used in military aircraft. The standard was evolved from the initial data rate of 1 Mbps to the extended and hyper variants, which use newer hardware to offer 120 and 200 Mbps respectively. The MIL-STD-1553B has an extremely low error rate of 1 word fault per 10 million words, on a dual-redundant architecture. MIL-STD-1553B defines the interconnection of up to 31 remote terminal (RT) devices. The cabling defined is set of two pairs of twisted-shielded pair transmission line made up of a main bus and a number of attached stubs.

Impact in FTI

This bus is widely used in wired FTI acquisition systems, commonly a unique set of dual-pair connections is taped. The MIL-STD-1553B bus has a low fail-rate, redundancy and reliability defined in MIL-STD-1553 specification that seems difficult to meet with wireless systems, this together with the minimum bandwidth of 1Mbps does that this bus works too fast compared with the state of art of actual wireless systems.

RS232

Description

The EIA introduced the 232 standard in 1962 in an effort to standardize the interface between DTE and Data Communication Equipment (DCE). The communication typically begins with 1 start bit, 8 data bits, 1 stop bit. This is typical for start-stop communications, but the standard does not dictate a character format or bit order. The standard does not define bit rates for transmission, except that it says it is intended for bit rates lower than 20,000 bits per second. In the real word, and after more than 40 years of RS232 use and evolution is common use bit rates from 9,600 to 230,000 bits per second or more.

Impact in FTI

The maturity of this interfaces after half century in the market achieved that today we can see RS232 ports easily in most of the pieces of equipment inside or outside of aircrafts. FTI installations commonly include tapings of this ports, although it is not the most common, for against, the simplicity of protocol and relative low baud rates would be the feasibility for wireless interfacing.

RS422/485

Description

RS422 and R485 is similar standard differential port for serial communications. The main difference is that in 485 up to 32 transmitter receiver pairs may be present on the line at one time vs the 10 of 422.

Impact in FTI.

As RS232, the RS422/485 ports are easily present in most pieces of equipment inside or outside of aircrafts. FTI installations commonly include tapings of this ports, although is not the most common, for against, the simplicity of protocol and relative low baud rates would be the feasibility for wireless interfacing.

ARINC 664 (AFDX)

Description

Avionics Full DupleX Switched Ethernet (AFDX) is a standard that defines the electrical and protocol specifications (IEEE 802.3 and ARINC 664, Part 7) for the exchange of data between Avionics Subsystems. One thousand times faster than the old ARINC 429, it builds upon the original AFDX concepts introduced by Airbus. AFDX End systems, or LRUs communicate based on VLs (virtual links) with traffic shaping through the use of BAGs (bandwidth allocation gaps), which are the minimum intervals between transmitted Ethernet frames on a VL.

Impact in FTI

The AFDX Bus is used in modern aircrafts, today the massive implantation of devices in FTI systems is low, but surely in the future will be massive. In addition the base of Ethernet does that wireless technology could be easily implemented , however the bit rate increase fast over wired lines (1Gbit now), but wireless systems have limitations, consequently the application will be limited to low transfer rates or streaming lines like video given the latency.

See the following two tables summarizing the characteristics of the database analyzed before and the compilation of the state of the art of the more common wireless transmission protocols that could fit for this project.

BUS	BANDWITH	FTI IMPACT	REMARKS	FEASIBILITY
ARINC 429	Max 100Kbps	Very high	Simply/Robust	Very high
CAN	Max 1Mbps	Low	Robust	Medium
MIL-1553B	1Mbps >	High	Redundant	Low
RS232	> 230Kbps	Low	Simply	High
RS422/485	> 230Kbps	Low	Simply/Robust	High
AFDX	>1Gbps	Low	Complex	Medium

Table 1. Bus Evaluation Table

TECHNOLOGY	AUTONOMY	BANDWITH	RANGE	SYNCHRO NIZATION	DATABUS ACQUISITION	BEHAVIOUR IN A/C	COMMON USE
ZIGBEE	Weeks	250Kbps	>100mts	32 μs	Candidate	Advisable	Commonly used for sensors and IoT connections
BLUETOOTH	Days	250Kbps	10mts	N/A	Discarded	Not recommend	
WIFI	Hours	From 1 to 10Mbps	100mts	30ms	Discarded	Not recommend	Commonly used for PAN. TCP/IP protocol.
ULTRAWIDE BAND	Hours	6Mbps	10mts	30ms	Discarded	Not recommend	Used for indoor applications

Table 2 State-of-Art suitable for instrumentation purposes

SUMMARY

Actually the state of art or wireless technologies focused to sensor networks and measurements handle bandwidths of about 250Kbps, some recent protocols out of IEEE 802.15.4 achieve some improvements and would reach theoretical bandwidths up to 1Mbps. With this maturity the feasibility of transmit by wireless the data buses commonly present FTI systems is limited first to the bandwidth.

Having into account the state of the art of the present wireless technologies and after the analysis of the different databuses more often used in instrumented aircrafts the optimal databus for evaluation of wireless feasibility is ARINC 429, as commented this bus is widely used and could be a substantial improvement to FTI systems.

The next candidates would be RS232-RS422/485, this not is widely used but in some conditions could be an advantage to install wireless, the maturity of wireless technology make it possible.

A special remark to AFDX networks, this could be investigated due to the proximity to Ethernet LAN Wi-Fi systems, some disadvantage like latency and others should be investigated, but could be possible the feasibility for limited environments, like Video Streaming or others.

This information is of origin Airbus Defense and Space/Spain and does not contain any export controlled information
Airbus Amber releasable to ETTC

DOI 10.5162/ettc2022/1.4

Hardware and Firmware Architecture

The requirements for the system are described in the table below.

The architecture, figure 3, of the system has been selected in a node-gateway policy.

REQUIREMENT	TARGET	COMPLECTION
Nb of Bus	2 HS	1 HS
Global Bandwidth	512Kbit/s	250Kbps
Max latency	To be measured	To be measured
Max sampling per parameter	60%bus payload managing	100%
Battery restriction	Battery and external supply	Got
Autonomy	hours (no first objective)	Got (first prototype)
Transition retry protection	YES	Got
Storage at the sensor node level	NO	N/A
Storage at the receiving Gateway	YES	Started
Max nb of nodes	1 node as study concept	Got
Receiving node real time output protocol	IENA	Started (no difficult envisaged)
Storage format	RAW	Got
Time synchronization	PTP / GPS	PTP compatible
Time synchronization accuracy	32 µs	To be measured
Time stamping	YES	Got
Time stamping resolution & accuracy	1 ms	Got (by design)
Environment	N/A as study concept	Next Step
Dimension	Max 100X70 mm	90X40 (first prototype)
Antenna	Embedded as first target	Got

Table 3 Requirements and Complexion Status

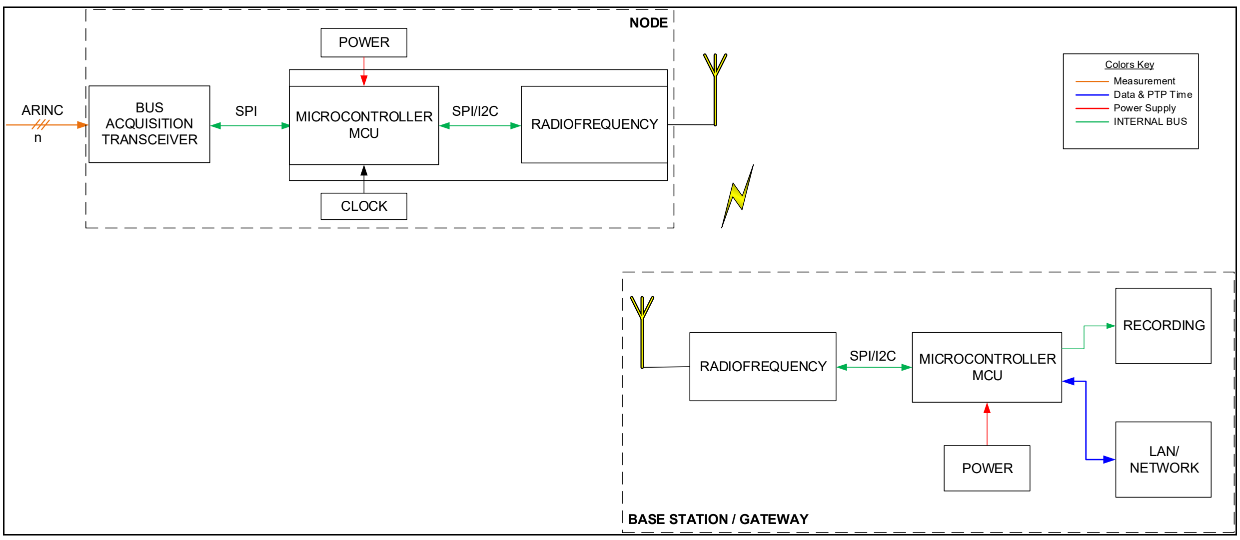

Fig 3.Wireless Node-Gateway Architecture

This information is of origin Airbus Defense and Space/Spain and does not contain any export controlled information
Airbus Amber releasable to ETTC

DOI 10.5162/ettc2022/1.4

In this probe of concept it has been defined one node and one gateway in the system but the quantity could be increased making profit of more transmission channels defined in the standard.

The node interfaces the ARINC429 databus and acquires, time stamps, processes and transmits the data to a base gateway where data is sent to recording and put available to be sent to the network in IENA format assuring total compatibility with other elements of the flight test instrumentation network. Additionally the gateway has two additional functionalities: the time is obtained from the network in PTPV1 protocol and managed to be sent to the node and signals of control, acknowledge and status between the base and the node are managed.

To comply with this architecture three main components are involved: the ARINC 429 transceiver, the microcontroller that manage the format translation, the data timestamping and the transmission protocol, the clock which drives the time stamp of the acquired data and the radiofrequency stage in charge of transmitting the data using the maximum possible, the optimum, bandwidth. There will be minor elements such us connectors or housing also important for future onboard requirements but not paramount now.

The interface protocols used for communication between the electronic components have been SPI and I2C, robust and widely used in this kind of electronic components and compliant with the requirements of the acquired signals and the instrumentation global requirements.

It has been selected the following elements:

- Arinc429 Transceiver. Manufacturer Holt Integrated Circuit with SPI interface.
- RF Tx-Rx Transceiver with microcontroller integrated. Manufacturer ATMEL 2.4Ghz AVR series with MCU integrated. This piece of equipment integrates the microcontroller and the radiofrequency part.
- Real Time Clock. Extremely accurate RTC with integrated crystal. Manufacturer MAXIM.

TRANSMITTING NODE

The transmitting node main functions are: data acquisition, data time stamping and data transmission.

The components are:

ARINC 429 Transceiver

The bus transceiver interfaces the ARINC429 bus. It acquires the bus and translate it into an SPI stream suitable for been manage by the microcontroller.

The transceiver supports different configurations. It is able of parsing, label filtering, the bus labels or can acquire the whole bus stream. The bus speed has to be configured.

The transceiver has the capacity of acquire one bus, either high or low speed bus, but in the market can be find other chips for acquiring different number of inputs.

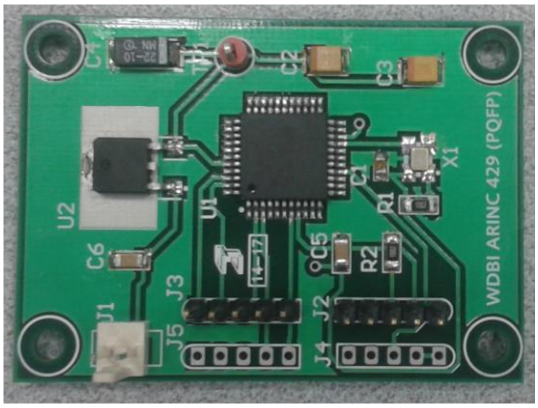

Fig 4.Node Mother Board Equipped

Microcontroller and RF

The SPI signal that caries the logical information of the bus is processed by the selected microcontroller.

The data processing, programmed in C language, enables the packetization of the data and its delivery to the RF stage.

Real Time Clock

The extremely accurate clock allows the system to synchronize or time-stamp events to a time reference that can be easily understood by the user.

This clock has been selected with a SPI interface due to the type of processor being used. The crystal oscillator is one of the most accurate circuits available for providing a fixed frequency, a 32,768Hz crystal is used for most RTCs. By dividing down the output of the oscillator, a 1Hz reference can be used to update the time and date. The accuracy of the RTC is dependent mainly upon the accuracy of the crystal. Tuning-fork crystals have a parabolic frequency response across temperature. This circuit manufactured by Maxim Integrated offer an error of 2ppm that is about 1 minute per year and is compensated in temperature with an integrated temperature sensor.

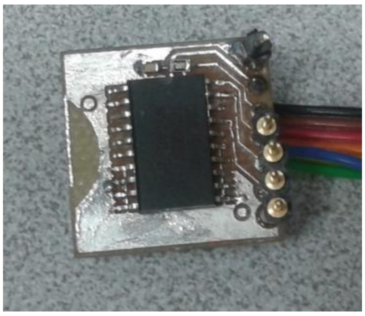

Fig 5.Clock

RECEIVING GATEWAY

The gateway main functions are: data reception, data recording, data distribution and time acquisition from the PTPV1 source.

The components are:

Microcontroller and RF

It receives the transmitted data and produce the data stream, in IENA format, that is going to be, in one hand, delivered to the network and in the other hand sent for recording.

SD Recording Module

A module for recording is available in the gateway in case no other recording device there is in the system. The recording is done in raw format.

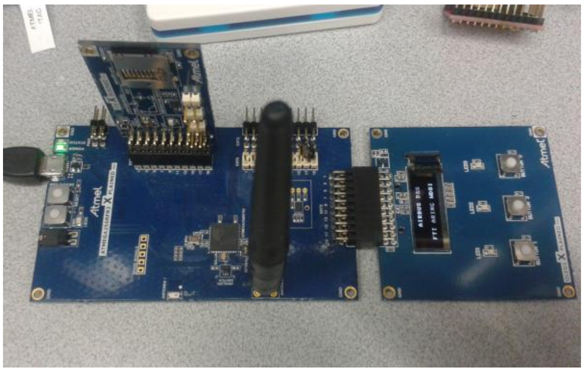

Fig 6.Gateway Mother Board Equipped

FIRMWARE

The data management: acquisition, transformation and processing, from acquisition from the ARINC429 source to the reception in the Gateway and recording in the SD card have been performed by programming both microcontrollers in C program language.

This is a complex task due to it requires a considerable long coding for controlling all the hardware elements involved system and the customization of some protocols and the composition of some data formats (IEEE, IENA, SPI, SD…).

Initially the ARINC429 data are obtained in its standard electrical levels. The levels are translated to TTL, which are electrical levels more suitable for the process of the following stage.

The microcontroller communicates with the ARINC429 transceiver and the clock using the SPI protocol:

- It obtains the data from the transceiver when are available in the bus.
- It obtains the time from the clock.

The following action is ordering and dating the data and their process in the proper format for transmission.

The final format, the structure of the message in the figure 7, contains not only the data and their acquisition time but also other relevant information for the transmission of the message and its identification in the gateway when received.

When the message is received in the gateway the contrary process is done: the frame is identified, its origin, it is processed and an acknowledge message is sent. After that it is translated in SPI protocol to be recorded in the SD card and in IENA format for delivering to the network.

It has also been implemented a transmission retry process for assuring the minimum lost o packets.

16	8	16	16	16	8	8	16	16	4	4	0/16	Variable	0/32	16
Frame Control	Sequence number	PAN ID	Destination Address	Source Address	Frame Control	Sequence number	Source Address	Destination Address	Source Endpoint	Destination Endpoint	Multicast Header	Variable	MIC	CRC
MAC Header					Network Header							Payload	MIC	CRC

Fig 7.Protocol Example

Conclusion

This project is a proof of concept that has demonstrated the feasibility of having a wireless system able to manage data coming from databuses.

It is clear that there are a wide variety of uses cases in which having small footprint instrumentations based in wireless solutions can reduce the cost of the flight campaigns drastically, saving in several areas involved in the campaign.

From the production of this demonstrator to the time of this paper the availability of pieces of equipment that can manage data wirelessly have increase and the technologies involved have evolved equally having nowadays wireless hardware, designed and oriented to this applications, able to manage payloads of several Mbps.

In this context, it is worth continuing exploring this solutions and investing in their development.

References.

ARINC SPEC 429. AECC Specification for ARINC 429.

ARINC SPEC 664. AECC Specification for ARINC 664 (AFDX).

ARINC SPEC 825. AECC Specification for ARINC 825 (CAN).

CAN SPEC 2.0. Bosch CAN Specification V2.0.

MIL-STD-1553B. DoD Interface Standard Specification Data Bus.

EIA/TIA-232-E. EIA RS232 Specification standard.

EIA/TIA-422-B. EIA RS422 Specification standard.

IEEE 802.15.4. IEEE Standard for Local and metropolitan area network.

IEEE 802.3. IEEE Standard for Etherner network.

ISO11898. Standard Road vehicles -- Controller area network (CAN).

DOI 10.5162/ettc2022/2.1

SKYbox: the new range of Flight Test Installation

P. Berthouze[1], D. Cumer[1]
[1] AIRBUS Operations SAS, 316 route de Bayonne 31060 Toulouse, France
pascal.berthouze@airbus.com, david.cumer@airbus.com

Abstract:

Flight testing is one of the key activities required to certify and deliver aircraft to our customers. To this end, we carry out flight tests on prototypes known as flight test aircraft but also in serial aircraft or production aircrafts ready to be delivered to Airlines.

The SKYbox project aims to offer a new range of Flight Test Installation (FTI) solutions. These less intrusive and more modular solutions ease the installation and provide FTIs at the cutting edge of technology.

Key words: Flight Test Installation, Architecture, SKYbox, Trolley.

Introduction

Flight testing is one of the key activities required to certify and deliver aircraft to our customers. To this end, we carry out flight tests on prototypes known as flight test aircraft. Throughout a programme life cycle, these aircrafts are used to validate the various changes.

In some cases, these aircrafts are not sufficient, as they may lose their representativeness compared to in-service aircrafts. A flight test aircraft is not, in fact, necessarily upgraded with all changes in the programme and can not represent all the aircrafts of the fleet in service. Therefore customer aircraft just coming off the Final Assembly Line (FAL) and at the latest standard are used.

At the same time, Airbus must also respond to their customers about major in-service problems (MISP). The analysis of such problems may require tests on aircraft already in service, in order to troubleshoot and to provide a rapid response to our customers.

The first FTI equipment were installed from the beginning of the Airbus A300 programme in the early 70s and were built specifically for each aircraft and program. The still in-service FTI solutions date back to the A380 programme (first flight in 2005) and the A350 programme for the most recent ones (first flight in 2015). Some FTI solutions are therefore starting to become obsolete.

Today, flight test aircrafts are used by engineers on a daily basis to exhibit enhancements and innovations during flights thus making our products more competitive. This modifies the testing profile and pace and therefore requires an increased agility.

Within this context, the SKYbox project aims to offer a new range of FTI solutions to meet all types of tests for all types of aircraft. The main driver is to ease the installation providing a more modular and less intrusive FTI based on the cutting edge of technology.

The first short-term target refers to the installation on board aircraft just coming off the FAL and equipped with their cabin.

These solutions are then extended to more heavily instrumented flight test aircraft.

Architecture concepts

The architecture follows two main drivers:

1/ Core functions concentration
2/ Distributed architecture

The selected strategy consists in moving some equipment closer to their customers in order to reduce the number of wires to be installed:

- Data acquisition closer to the sensors thanks to remote acquisition unit [1]

DOI 10.5162/ettc2022/2.1

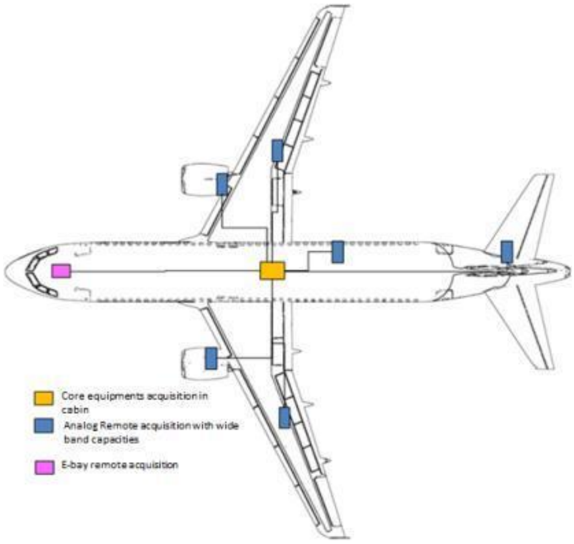

Fig.1.Generic remote architecture principle.

- Commands closer to the equipment to be piloted thanks to remote I/O system

- Video encoder closer to the video cameras

All these remote equipment are connected to the core FTI thanks to Ethernet connections.

The SKYbox range focuses primarily on 3 solutions:

1/ An avionic bay module grouping together the FTI's core functions for development tests on FAL aircraft

2/ A cabin trolley, which can be installed in a galley and complements the functions of the avionics bay module for development and certification tests on FAL or flight test aircraft

3/ A cabin bay, as a replacement for the trolley, on aircraft requiring a heavy test installation

These 3 solutions are complemented by a display and test steering station with a new FTES (Flight Test Engineer Station).

Fig.2.Architecture and Installation synoptic for medium installation.

The complete Skybox range will make it possible to renovate existing installations and be more efficient on new installations thanks to a reduced footprint, increased ease of installation and increased modularity:

<u>Modularity</u>: SKYbox solutions allow to cover the scope of all flight tests while keeping a functional architecture common to all these solutions.

They are able to adapt to changing requirements during a test campaign by adding additional modules (such as additional computing power) or additional functions.

<u>Footprint</u>: New technologies significantly reduce FTI congestion. To illustrate: a state-of-the-art computer - for processing test data in real time - can replace 10 older generation computers

DOI 10.5162/ettc2022/2.1

such as those present on the FTI of the A350 development. On a complete installation, the space saving (reduction of a factor 8) and mass is remarkable:

Fig.3.Previous solution with corresponding core functions - weight ~450kg.

Fig.4.SKYbox trolley - weight ~100kg.

<u>Easy installation</u>: The smaller dimensions allow the use of form factors that facilitate installation on board aircraft. For aircraft with an already equipped cabin, for example, a trolley can be used, which can be installed in the galley like a conventional food trolley.

New solution description

A new FTI system (format ARINC600 / avionic computer) has been developed in order to put more functionalities in the same volume as the current system, thanks to miniaturization of components: time base and DGPS capabilities have been added to current bus acquisition and recording capabilities. This system is installed in the avionic bay and can be used alone, possibly connected to a laptop for real time visualization.

For more demanding test needs, this avionic bay module can be linked to a FTI trolley. This trolley concentrates the main core FTI functions in a very reduced volume:

- Data processing
- Network (FTI data and intersystem communication)
- Recording
- Electrical sources selection (2 sources and output power up to 17kVA)
- Electrical generation and distribution

In order to display the information provided by the avionic bay module and the trolley, a new Flight Test Engineer Station (FTES) is developed with the same drivers: modularity, reduced footprint, easy installation.

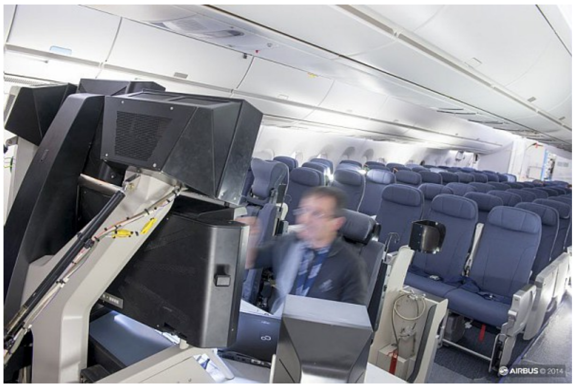

Fig.5.Installation of a FTES in a cabin A/C.

Conclusion

Part of the new SKYbox solutions has been flying on development aircraft since September 2020 with expected gains in ease of installation and modularity, hence a better customer satisfaction.

These solutions are defining our policy for flight test installation for the coming years.

In order to continuously improve the non intrusivity and the installation of our FTI equipments, we need now to prepare the next generation by using smaller size equipment, new technologies available on the market (less wire, wireless, optical fiber, MEMs sensors, mini and micro computer systems, ...) and cost efficient solutions.

References

[1] S. Martin, C. Perret, Adapted acquisition systems for future FTI architecture, *ETTC 2013*;

DOI 10.5162/ettc2022/2.2

High quality measurements for helicopter applications using sensor telemetry

Dr.-Ing. Ernst Manner[1], Dr.-Ing. Stephanie Manner[2], Dr. Julia Manner[3]
[1,2,3,] MANNER Sensortelemetrie GmbH, Eschenwasen 20, 78549 Spaichingen, GERMANY
manner@sensortelemetrie.de

Abstract:

More and more players on the market try to get in the game of sophisticated helicopter manufacturers. There are several interesting industries that helicopters are needed for. The famous ones like military and air transport for air lifting are now extended by new mobility concepts like the electrical urban air mobility.

But all have the same challenges with innovations on drives and transmission leading to many newly designed critical rotating components where temperature, strain, force or acceleration measurements for durability and operational strength need to be exercised.

In this paper, MANNER shortly sums up the challenges that come with the engineering and development of a high-quality, high accuracy telemetry measurement system. A system withstanding all environmental constraints and mechanical challenges but being flexible for the customer as well as for the different measurement tasks in every mean.

Sample timestamping and data structure need to be taken into account for accurate measurements in such big measurement tasks.

The request for IENA and Precision time protocol (PTP V2) has been realized as one way to go with the new generation of telemetry systems.

The aim of this paper is to provide the reader a good insight on the challenges of telemetry systems on helicopters and the solutions that have been found to realize a highly reliable, highly accurate yet very flexible measurement system that now is an answer to all measuring tasks on a helicopter.

Key words: - sensor telemetry, helicopter applications, time synchronized data acquisition of rotor signals, Precision time protocol (PTP V2) with IENA, Complex measurement tasks, Strength and Durability measurement.

Harsh environments and measurement tasks

There are several locations where a telemetry for measurement task is needed. Weather it is due to small installation space, or high and low temperatures, function a high altitude, high vibration level or steel surroundings. The measurement has to be performed for either health and usage monitoring, maintenance or for qualification reasons.

Installation space:

Not always is a space for installation resyulting during the development of the helicopter and its components. Often there has to be done a retrofit, meaning a measurement system placed in a location where there has never been the thought of implementing a system for measurement purposes. This often resulting in installation challenges that can hardly be overcome.

Environmental conditions that are prominent not only in aircrafts but are even more prominent and demanding in helicopters are summed up in the DO160 or CS29 specification.

The most known ones are vibration, temperature, altitude.

The vibration level and the resonant frequencies of the mechanical and physical components are diverse.

The long-term mechanical integrity as well as electrical function under vibration has to be guaranteed.

DOI 10.5162/ettc2022/2.2

One term is micro phonic disturbances but there are more. All this has to be taken into account when developing a system for aircraft applications.

The temperature rages can be extreme. Ranging from -50°C to 160°C or even higher, depending mainly on the measurement task and installation location.

Light weight and minimized dimensions are of extraordinary importance. Due to the challenge of retrofit or post engineering and post design fit, there is often few to no space available. Nevertheless, the measurement is crucial for qualification or further optimization of the part.

The telemetry system, especially the rotating components have to be minimal in size and weight and show a large range of flexibility like the choice of sensors and filter settings.

The flexibility of a telemetry measurement system makes it customizable in short time. This is often a game changer in fast development cycles. To be able to define the sensor and measurement signals necessary on the fly helps to realize this short development cycles.

All these mentioned challenges as

- EMI/EMC proofness
- Vibration robustness
- Temperature range
- Pressure altitude
- humidity
- Installation place and situation
- Rotation speed

Have to be overcome by a system and partner to perform the measurements satisfactory.

Different protocol types and the way to go for fully synchronized measurements

There are a lot of protocols available on the market. Thus, making this whole task even more demanding.

The aim for a fully synchronized measurement is clear. On a complex system as a rotorcraft or aircraft, it is very important to bring the different samples back to one master clock. Then being able to compare the parameters and visible conspicuous data.

IENA PTP v2 protocol

One of the most promising way to go is the IENA PTP v2 protocol accessible via ethernet.

The precision time protocol (PTP) allows to have one master clock e.g. GPS grand master and to synchronize every sample with this master clock.

By performing this every sample is defined in time with very high accuracy.

The time accuracy is about 10 ns and also depending on the sample rate.

Time stamping

The time stamping can be performed on the rotor side, meaning prior to the transmission into the stationary system. This is achieved by time stamping each sample prior to transmitting it.

A second possibility is to correct the time that is necessary for a sample measured on the rotor side to be transmitted to the stationary side. This time depends on filters and the transmission path but is constant for each system. This allowing a correction in time without loss of accuracy.

High flexibility in telemetry measurement systems

Prior mentioned the flexibility of a telemetry measurement system has many dimensions.

Once the project is planned, there is a set of measurement points that has been agreed on. Considering the lead time of a costume made telemetry systems not taking into account the certification for the measurement of critical aircraft systems (DO160 or CS29) may vary between 6 months and 2 years.

The problem with these systems often is that they are custom-fit and very inflexible. Often there is nothing that really can be changed after the delivery.

There is no such thing as adding a few more channels or changing filters or sample rates.

To overcome all these disadvantages and challenges there has been a development at MANNER.

A totally new generation of telemetry measurement systems designed to obey the high flexibility demands of the industry has been realized.

Not only have been there met major goals for highest flexibility but also all these possibilities:

- Change of number of sensors
- Change of channel count by adding more modules
- Change of sensor type per channel (1/4 bridge, ½ bridge, full bridge, TC, PT100/1000, acceleration sensors and so on)
- Change of data rate and transmission technology
- Shutting off damaged channels
- Daisy chain and star structure
- Settings all changeable via software
- Calibration via software
- Data recording via software

Because of the high level of flexibility by software customizing the electronics, the system can be adapted to all of the needs.

There is no need to send the telemetry system back and change e.g. the configuration. To order more electronics and change software settings will solve the issue.

Accurate data without loss

Besides our radio telemetry solutions powered by batteries the majority of systems are engineered with our inductive telemetry.

The inductive transmission path is very robust and secure against disturbance or signal loss.

Due to the nature of an inductive transmission path there is no data loss.

High data rates

MANNERS new technology can handle up to 128 channels within one system data rates up to 50 Mbit/S

Conclusion

The high demands on measurement systems with the challenges that come with the environment, helicopters and other aircrafts operating often resulted in sacrifices. So far, a very custom specific telemetry system was feasible to engineer by an experienced manufacturer, but then the system was highly specific for one application or instrumentation and because of a huge engineering part, the lead time was long.

With new technologies developed by MANNER those systems are now highly flexible (number of sensors, sensor types, filter frequencies, data rates, transmission type and more) by software configuration and the modular structure. This is even accessible by the customer to change settings.

Amplifier modules with each 1 or 4 measurement channels onboard are cascadable in a bus structure but also in a star structure for applications where it is highly preferable to keep the bus running with as much channels working as possible in case of an unforeseen event e.g. a collision of the rotor.

The evaluation units of our system can be routed as a daisy chain and provide even more flexibility.

The measurement of the telemetry sensor can easily be compared to other measurements because of the time stamping and the use of a network protocol as IENA PTPv2.

DOI 10.5162/ettc2022/2.3

Universal Modular Full Flight-Testing System

Jointly issued by G.Steiner[1], C.Douglas[2]
[1] imc Test & Measurement GmbH, Voltastr. 5, D-13355 Berlin, Germany,
[2] JDA Systems, Gutenbergstrasse 4, D-26632 Ihlow Riepe, Germany
gregor.steiner@imc-tm.ch , cdouglas@jda-tele.com

Abstract:

Driven by the need for a next generation flight test data acquisition and signal conditioning system, this presentation describes a new solution to fulfill that need. The on-board system design covers all aspects of signal measurement technology from high-precision analog signal processing (even in the high-voltage range for e-drive / battery measurements) to aircraft BUS acquisition and the embedding of existing proprietary user protocols.

The modular system is fully compliant with the latest IRIG 106 standards and include real time uplink ground control of the airborne system utilizing IRIG106 Chapter 7 capabilities. These include the complete signal conditioning system configuration, the IRIG106 Chapter 10/11 recorder control, the structure of the IRIG106 Chapter 7 telemetry downlink, the pilot and any local engineering display setups, the transmitter frequencies, modulation types and power levels. The total system timing is GPS based and utilizes the NTP and PTP network timing standards within the air vehicle under test.

This presentation should be of interest to anyone interested in air vehicle testing.

Key words: data acquisition system, embedding proprietary user protocols, aircraft BUS acquisition, IRIG 106, full duplex telemetry link.

Introduction

The definition of new standards, particularly IRIG 106 Chapter 7, 10 and 11, have opened the door to a new way of thinking about onboard flight test signal conditioning systems. These must not necessarily continue to be considered as systems that are setup in a predefined manner to match the requirements of a specific flight test scenario, but perhaps rather should be looked at as a flexible resource that can be, to a certain extent, changed in real time to match a series of flight tests which have different requirements.

Having realized this fact our thinking about what is an on-board flight test system, and how it is to be used, should also change.

This presentation introduces a new type of flight test system that takes advantage of this realization to offer new ways of working for flight tests engineers, ways that may reduce their workload and open new doors.

The Basics

To start with it is clear that in order to be efficient and successful in modern flight testing, you need solid precision measurement technology for the analog world, but with that said we must also deal with BUS based sensors and devices as more of these types become available and are put into use.

Many of these BUS based sensors and devices have proprietary bus protocols based on Ethernet, Serial, etc. and it is becoming clear that the fast, adaptive acquisition of such data sources is now just as important as that of analog sources.

Measuring Islands

These measure directly at the source and are remote data acquisition systems that help both to save cable effort (weight) and improve signal quality.

New Instrumentation Challenges

Measurements on electric-powered aircrafts make it necessary to pay particular attention to the insulation resistance of the measuring amplifiers and sensors. Examples are, temperature measurement in the high-voltage environment and general differential voltage measurements on batteries that require high common-mode levels. Temperature measurements in this area can be covered either optically using FBG technology (fiber Bragg grating) or conventionally with RTDs or thermocouples and corresponding high-voltage measurement modules.

Figure 1 Example of optical FBG sensor system

Instrumentation Layout

To achieve a high level of flexibility the application of internationally recognized standards was key to the implementation of the system, these include:

- IRIG 106 various chapters (4,7,8,9,10,11)
- Ethernet 1000/100/100
- GPS position and timing synchronization
- NTP and PTP network timing
- ONVIF video capture and camera control

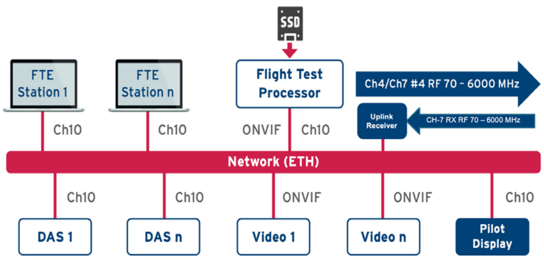

Figure 2 Ethernet based on-board system layout

As an overview, the onboard flight test system consists of the following main elements:

- Chapter 10/11 Ethernet DAS modules
- Chapter 10/11 Ethernet camera feeds
- Pilot display, Ethernet
- Engineering workstation displays, Ethernet
- Intelligent packet combiner/recorder
- Intelligent ethernet based Chapter 7 RF transmitter TIER0, TIER1 and TIER2 (L, S & C band)
- Intelligent ethernet based Chapter 7 RF receiver TIER0, TIER1 and TIER2 (L, S and C band)
- Modular airborne antennas with integrated amplification (L, S and C band)
- Ethernet backbone

Flight Test Processor

The heart of this flight test system is the Intelligent packet combiner/recorder which provides the functions of:

- IRIG106 Chapter 10/11 data packet combiner
- IRIG106 Chapter 10/11 recorder
- IRIG106 Chapter 10/11 packet selector/filter for telemetry link
- GPS synchronized NTP and PTP network Time Server
- Selected packet decoder and data server for pilot display and any airborne engineering workstations
- IRIG106 Chapter 7 telemetry encoder
- RF transmitter TIER0, TIER1 and TIER2 (L, S and C band) (suitable for use with modular airborne antennas with integrated amplification)
- Intelligent IRIG106 Chapter 7 RF receiver controller
- IRIG106 Chapter 7 uplink decoder

The system is distributed in structure in that all Chapter 10/11 data transfers are encapsulated, and therefore time stamped, within the data acquisition units themselves. To provide sufficiently accurate timing for this process the NTP and PTP ethernet time protocols were selected, with a system developed that provides timing to an accuracy of 0.000001 seconds in the data acquisition units.

A mechanism is included to provide accurate information regarding the relationship between the system time and the internal 10MHz counter originating from the combiner/recorder, which is required to conform to IRIG106 Chapter10/11 standard.

The setup of the entire airborne flight test system is managed from the DAS-setup software via the generation of IRIG106 Chapter 9 (TMATS) files, which are fed into the combiner/recorder over one of its available interfaces on that unit

DOI 10.5162/ettc2022/2.3

(Ethernet, RS232, USB, Chapter 7). The TMATS files are used to setup the entire system and also as the basis for a the TMATS header, which is the first packet in any Chapter 10/11 recording.

One of the new functions of the intelligent packet combiner/recorder is its ability, under customer control, to decode selected Chapter 10/11 data packets on the fly. Extract and calibrate the parameter data before distributing that recovered information to the Pilot Display and any connected airborne engineering display workstations.

As the combiner/recorder is also an IRIG106 Chapter 7 telemetry encoder, the incoming data is available to be sent over that Chapter 7 telemetry downlink, which may be any combination of the decoded parameter data and/or selected Chapter 10/11 encapsulated data packets.

The system design takes advantage of the Chapter 7 ability to provide a control uplink to the vehicle under test.

As the entire airborne system is configured via uploaded Chapter 9 (TMATS) files then sections, or a whole new, TMATS files may be sent over the uplink to the combiner/recorder even while the flight test is in progress.

These uplinks can control:

• The downlink Chapter 7 telemetry contents, data rates and structure.

• The downlink RF characteristics including data rate, transmission frequency, modulation type etc.

• The downlink transmission power.

• The content of the Pilot and any engineering displays.

• The control for the recorder start/stop/new file etc.

• The Chapter 10 data packet selection for decoding, recording, RF transmission etc.

In other words, the configuration of the airborne system may be changed at any time via a Chapter 7 uplink from the ground station, thus saving time and money on a flight test program by allowing multiple disparate tests to be carried out during a single flight.

One of the most important features of the total system design is the ability, through the use of internationally recognized standards throughout, to integrate customer supplied legacy equipment, with minimal effort, into the systems infrastructure.

Another important feature is the minimal internal cabling required within the air vehicle under test. Basically, just ethernet and 28V power is sufficient to bring the system together.

On the ground a standard telemetry antenna configuration (with optional uplink capability) is used along with unmodified telemetry data receivers.

The data thus recovered is decoded by the systems software and is then available for distribution to local or remote engineering stations.

The Chapter 7 uplink capability is provided by the same ground software and can take the TMATS files generated by the DAS-setup software and send them in a secure manner via the Chapter 7 uplink to the aircraft under test.

Conclusion

A new class of onboard flight test systems that uses internationally recognized standards to go beyond fixed configurations in airborne test systems offering new more efficient flight test capabilities.

This has applications to the issue of more efficient telemetry bandwidth usage, as well as for unforeseen data needs during a test flight.

The intelligent integration of previously separate functions along with control via the uplink, makes this a state-of-the-art solution, while still providing the ability to integrate customer existing equipment into the overall system.

The best news is that this is all immediately available.

DOI 10.5162/ettc2022/2.4

From Automotive to Flight Test Instrumentation: Wiring Reduction Using New Ethernet Standard.

Joaquín Antonio Pablos Palomino[1],
[1] Airbus Defence and Space, San Pablo Sur FTC, Seville, Spain,
joaquin.pablos@airbus.com

Abstract:
The electric car has required the development of a new vehicle architecture , use of new sensor technologies (cameras, UWB, radar,) and networking extension (cloud gateways) to support new requirements of connectivity, safety, security and reliability, enabling not only current but future services (infotainment and communications). Supporting this architecture has been possible thanks to a new Ethernet standard that will reduce significantly the wiring needed: Ethernet over a single pair cable.

This article introduces the main features of the new Ethernet standards related with single pair Ethernet and how Flight Test can make use of them. Currently most of FTI components have Ethernet interfaces (acquisition systems, sensors, cameras …) so the adoption of the new standard in current architecture can be done smoothly at different paces. The proposal of new FTI architectures for some use cases are presented to show major improvements from this standard. Finally, future expected advantages for FTI components are analyzed as the adoption of Ethernet for new sensors, the use of AI devices at the edge and the co-existence with wireless and IoT technologies

Key words: Single Pair Ethernet (SPE) , Flight Test Installation (FTI)

1. Introduction: Ethernet Role in FTI

Ethernet has become the backbone solution for communications in Flight Test Installations in the last 20 years. The movement has allowed to benefit of all the new advances in this technology such as time synchronization, traffic priority and segregation or easy upgrade to new speeds.

One of the main benefits of Ethernet is to simplify the installation of remote acquisition units near measurement zones (wing, engines), reducing the wiring to the zone to power supply and Ethernet communications channels.

Since the first use of Ethernet in flight test for acquisition systems, more FTI equipment are adopting Ethernet standard such as cameras or pressure scanners. This is increasing the use of Ethernet wiring and the complexity of installation of Ethernet harnesses.

In addition flight test campaigns are being developed more often in customers' aircrafts. This is requiring to design flight test installations more compact and pushing to reduce harnesses to avoid impact in customers' aircrafts.

Keeping all the functionality of Ethernet and reducing the wiring needed for it would simplify installations. This article introduces a new Ethernet technology named Single Pair Ethernet (SPE) developed for automotive sector that uses single pair cable for full-duplex Ethernet communications. This means to reduce from two pairs to one for 100 Mbps and four pairs to one for 1Gbps. This technology has been created and standardized thanks to automotive sector as it will described to show the origins in first place.

Second a description of the different standards developed is introduced. Third the current status of technology supporting the technology is shown. Fourth the results of some tests carried out internally will be presented. These tests have been done using standard FTI equipment, single pair Ethernet converters and standard flight test wiring. Finally use of SPE in current and future flight test installations are analyzed.

A previous study of Time Sensitive Networks and Ethernet over Single Pair Cable was done for avionics use when the standards were in development [1]. This article also completes this analysis with all recently published standards related with Single Pair Ethernet and the application to flight test.

DOI 10.5162/ettc2022/2.4

2. Automotive Network Evolution

The automotive sector is living a revolution pushed by electric car and new systems as Advanced Driver Assistance System (ADAS) and Infotainment (information and entertainment). For supporting these technologies a problem raised to transmit the volume of data required. Just upgrading the firmware of all the systems was becoming a problem. This was the initial use of standard Ethernet in cars though pins of OBD port (On-board diagnostics). The first use of Ethernet had as objective to reduce the time required to upgrade the car systems from 16 hours using Controller Area Network (CAN bus) interface [2]. This application detected a problem of use of standard Ethernet UTP (Unshielded Twisted Pair) cables in automotive sector, emissions were higher that allowed by automotive normative radiated emissions limits [3]. So standard Ethernet over UTP was right because the car was in a garage for the specific flash upgrade function but could not be used when car was in the runtime.

Considering this problem an innovation program leaded by BMW [2] was launched and had good results to develop an Ethernet physical transceiver based on an unshielded single pair cable that met the emissions required by automotive sector.

This new network technology is key to support the evolution of architecture in cars currently based on several automotive protocols LIN, CAN, MOST or Flexray with lower data rates (see Table 1).

Table 1 – Main automotive buses

Protocol	Speed	Distance	Physical Media
LIN	19.2 Kbit/s	40m	Single wire
CAN	125kbps/5 Mbps	500m/40m	Twisted pair
MOST	25/50/150Mbps	-	Fiber/UTP/Coax
Flexray	10 Mbps	24 m	1 or 2 UTP

The volume of SPE nodes in a car is expected to grow exponentially. This need has led to semiconductors companies to develop physical transceivers compatible with SPE.

Finally the technology developed has become a standard published by IEEE. This is very important in automotive sector, to allow the integration of equipment from different vendors avoiding proprietary solutions for intra communication in the vehicle. In this way a car manufacturer can choose independently the best sensor and the best processing unit for processing the sensor data. The standardization by IEEE has become important also for the use in other sectors as industry.

3. IEEE Standards

Initially Single Pair Ethernet was developed by Broadcom that provided the required modifications for owned technology to support automotive sector. This technology is known as BroadR-Reach.

The interest in standardization led to a group of automotive and semiconductors' companies to create a group called OPEN Alliance SIG in 2011 (more than 300 members now).[4] This group has developed the Ethernet specifications related to automotive [5].

As other sectors as industry considered this technology useful, at the same time IEEE started to develop the IEEE 802.3 related standards. The standards that have been developed so far are:

- 100Mbit/s specification: IEEE Std 802.3bw™-2015 [6]
- 1000Mbit/s specification: IEEE Std 802.3bp™-2016 [7]
- 10 Mbps/s specification: IEEE 802.3cg-2019 [8]
- 2.5 Gb/s, 5 Gb/s, and 10 Gb/s: IEEE 802.3ch-2020 [9]
- Power over Data Lines (PoDL) : IEEE Std 802.3bu™-2016 [10]

These standards describe the functions of the physical layer (named PHY).

The specification IEEE 802.3bw [6] (100Mbps) defined for each copper port a single balanced twisted-pair link segment connection of up to 15 m in length. For supporting full-duplex communications over a single balanced twisted-pair it uses echo cancellation. The 100BASE-T1 PHY leverages 1000BASE-T and 100BASE-TX PHY technologies in operation at 100 Mb/s adopting Pulse Amplitude Modulation 3 (PAM3) to provide trade-off between bandwidth and EMI performance.

The PHY converts the stream of 4-bit words at 25 MBd to a stream of 3-bit words at 33.333 MBd. The bits are then scrambled and converted through PCS encoding to a stream of code-groups (pairs of ternary symbols).These ternary symbol pairs are then multiplexed to a serialized stream of ternary symbols at 66.666 MBd

The link segment defined in the standard supports up to 15 m single balanced twisted-pair cabling with up to 4 in-line connectors and two mating connectors

The standard [6] defines the characteristics of the cable up to 66 MHz (impedance, insertion/return loss…). As we will see later physical transceiver developed are capable of longer distances than defined in the standard.

The standard IEEE 802.3bp [7] (1 Gbps) operates using full-duplex communications over a single twisted-pair copper cable with an effective rate of 1 Gb/s in each direction simultaneously.

It supports operation on two types of link segments:

a) An automotive link segment supporting up to four in-line connectors using a single twisted-pair copper cable for up to at least 15 m (referred to as link segment type A)

b) An optional link segment supporting up to four in-line connectors using a single twisted-pair copper cable for up to at least 40 m to support applications requiring extended physical reach, such as industrial and automation controls and transportation (aircraft, railway, bus and heavy trucks). This link segment is referred to as link segment type B.

The 1000BASE-T1 PHY utilizes 3 level Pulse Amplitude Modulation (PAM3) transmitted at a 750 MBd rate. A 15-bit scrambler is used to improve the EMC performance. To maintain a bit error ratio (BER) of less than or equal to 10e–10, the 1000BASE-T1 PHY uses Reed-Solomon Forward Error Correction.

The standard IEEE 802.3cg [8] (10 Mbps) defines two different physical layers:

- 10BASE-T1L: specification for a 10 Mb/s Ethernet local area network over a single balanced pair of conductors up to at least 1000 m reach. The 10BASE-T1L PHY is a full-duplex PHY specification, capable of operating at 10 Mb/s. The PHY supports operation on a link segment supporting up to ten in-line connectors using a single balanced pair of conductors for up to at least 1000 meters. The 10BASE-T1L PHY utilizes 3-level Pulse Amplitude Modulation (PAM3) transmitted at 7.5 MBd on the link segment.
- 10BASE-T1S: specification for a 10 Mb/s Ethernet local area network over a single balanced pair of conductors up to at least 15 m reach. It is specified to be capable of operating at 10 Mb/s in several modes. All 10BASE-T1S PHYs can operate as a half-duplex PHY with a single link partner over a point-to-point link segment (four in-line connectors and up to at least 15 meters in reach), and, additionally, there are two mutually exclusive optional operating modes: a full-duplex point-to-point mode over the link segment, and a half-duplex shared-medium mode, referred to as multidrop mode, capable of operating with up to 8 stations (bus length of 25 m). The 10BASE-T1S PHY utilizes two level Differential Manchester Encoding (DME). A self-synchronizing scrambler is used to improve the EMC performance.

The IEEE 802.3ch-2020 [9] define the 2.5GBASE-T1 PHY, 5GBASE-T1 PHY, and 10GBASE-T1 PHY that operate using full-duplex communications over a single balanced pair of conductors with an effective rate of 2.5 Gb/s, 5 Gb/s, or 10 Gb/s in each direction simultaneously while meeting the requirements (EMC, temperature, etc.) of automotive environments. The PHY supports operation on an automotive link segment supporting up to four in-line connectors using a single balanced pair of conductors for up to at least 15 m. The 2.5GBASE-T1, 5GBASE-T1, and 10GBASE-T1 PHYs utilize 4-level pulse amplitude modulation (PAM4) transmitted at 1406.25 MBd, 2812.5 MBd, and 5625 MBd rates, respectively.

The IEEE 802.3bu [10] describes the specification for providing a device with a unified interface for both data and power it requires (see Figure 1). The standard defines the electrical characteristics of two power entities: a PoDL Powered Device (PD) and PoDL Power Sourcing Equipment (PSE) for use with supported single balanced twisted-pair Ethernet Physical layers (see Table 2).

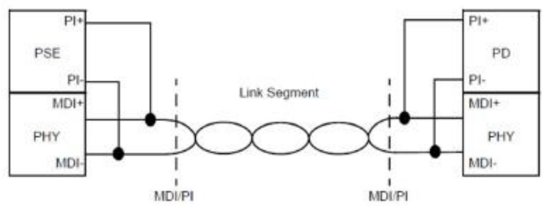

Figure 1 - PoDL block diagram [10]

The total resistance through two conductors looped at one end of the link (direct current loop resistance) shall be less than 6 Ω for 12 V unregulated classes. The direct current loop resistance shall be less than 6.5 Ω for 12 V regulated, 24 V regulated and unregulated, and 48 V regulated classes.

This information is of origin Airbus Defense and Space/Spain and does not contain any export controlled information.

Table 2 -PSE classification [10]

	12 V unregulated PSE		12 V regulated PSE		24 V unregulated PSE		24 V regulated PSE		48 V regulated PSE	
Class	0	1	2	3	4	5	6	7	8	9
Pmax (W)	0.5	1	3	5	2	3	5	10	30	50

The use of power over data line can raise EMC problems to be analyzed. The use of power over data line will also increase the size of the gauge required.

Finally an important standard related with single pair Ethernet and aeronautics was published in 2020. This document specifies the ARINC 854 Cabin Equipment Network Bus (CENBUS) [11] utilizing a new, serial communications protocol based on IEEE 802.3 Clause 96 (100BASE-T1) operating at 100 Mbps.

4. Technology Maturity

As introduced before, although technology was developed by one manufacturer (Broadcom) the creation of OPEN group later led to several semiconductor companies related with automotive sector to develop physical layers IC for the different standards that cover Single Pair Ethernet. Currently the most available PHY IC is the 100BASE-T1. The following table show the ICs provided by the main manufacturers.

Table 3 - Physical layer transceivers for Single Pair Ethernet

	Manufacturers				
Standard	Broadcom	TI	Marvell	Microchip	NXP
100BASE-T1	BCM89820	DP83TC81x	88Q120xM 88Q111x 88Q1010	LAN8770	TJA1101BHN TJA1102AHN
1000BASE-T1	BCM89882 BCM89880	DP83TG720			
10BASE-T1L		DP83TD510			
10BASE-T1S				LAN8670/1/2	
10G/5G/2.5GBASE-T1	BCM89890		88Q4364		
100BASE-T1/ 1000BASE-T1	BCM89881 BCM89883		88Q222xM 88Q211x		
Switch 100BASE-T1, 1000BASE-T1 PHYs	BCM89571 (8 ports) BCM8956X				
Switch 100BASE-T1	BCM89559 BCM8954X BCM8955X BCM8953X BCM89549		88Q5072 88Q5050 88Q5030		SJA1110 (PREPRODUCTION)

Most of the physical layer transceiver ensures that that length for 100BASE-T1 is at least 15 m but others like TI with DP83TC814R-Q1 and DP83TC811R-Q1 announces maximum cable lengths of 49 m and 60 m. It has to be considered that this length is for an unshielded single pair cable, if we use a better cable the distance can be longer. A distance of 40 m for 100Base-T1 is considered to be reachable with a cable with enough quality.

The physical layer integration in the electronics design is simple, it has a typical MII (Media Independent Interface), RGMII (Reduced Gigabit MII) or SGMII (Serial Gigabit MII) interface depending on the link speed. Any existing physical Ethernet transceiver could be replaced by minor changes in software driver to configure it.

The external components required between phy and the external connector of the 100BASE-T1 phy are (see Figure 2): ESD protection, common mode termination, DC block capacitors, common mode choke and low pass filter (it can be integrated in the PHY). Transformers are not used in the automotive application so isolation is different of standard Ethernet. The transformer is replaced by a Common Mode Choke (CMC) to meet EMC in automotive sector.

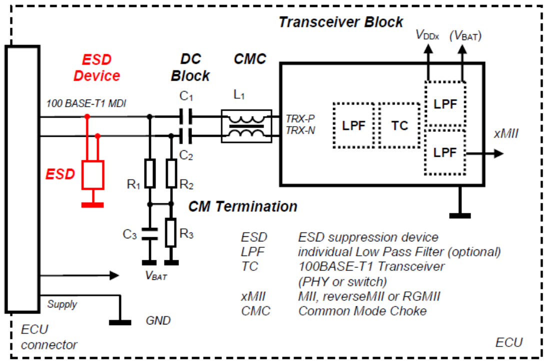

Figure 2 - External components of Phy for 802.3w[5]

For keeping isolation of standard Ethernet some application notes treat how to modify the automotive solution [12].

In addition to the electronics components needed for updating or designing new equipment, commercial/industrial equipment are also available.

Test equipment manufacturers [13] have developed products to analyze OPEN Alliance requirements of 10BASE-T1S, 100BASE-T1, 1000BASE-T1 and 2.5G/5G/10GBASE-T1 (see Figure 3).

Figure 3 - Oscilloscope with SPE test capabilities

In the market there are also available [14] converters for testing and validating applications/equipment with automotive Ethernet connections (like MATEnet or

Molex/mini50) for 100BASE-T1 and RJ45 connection for 100BASE-TX (see Figure 4).

Figure 4 - Ethernet converters

Ethernet switches supporting SPE that are a key element in deployment of new standard are also available [15].

The main manufacturers of connectors/cables are developing products for automotive, but also for other sectors interested in single pair Ethernet as industry or aeronautics [16].

Therefore we can conclude that all the elements of this technology are ready to be used.

5. Testing with FTI Wiring and Equipment

Previous studies have analyzed the use of Single Pair Ethernet for aerospace application performing EMC tests with CAT 5 cable [17,18] and cabin existing wiring of an A321 [19].

As an approach to single pair Ethernet technology some tests connecting FTI equipment have been done using two typical FTI wiring.

As converter module to connect 100Base-Tx equipment using 100Base-T1 standard an evaluation board from TI has been used. The DP83TC811EVM [20] supports 100-Mbps speed and is IEEE 802.3bw compliant. This evaluation board is a media converter to enable bit-error rate testing, interoperability testing and PMA compliance.

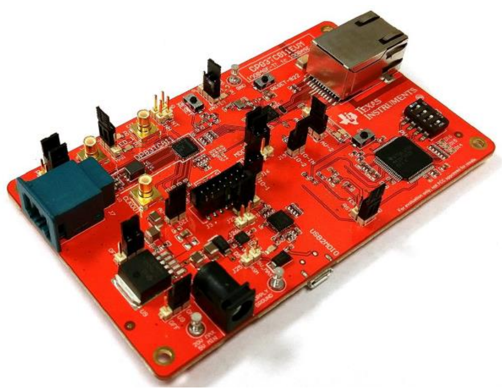

Figure 5 - Evaluation board used as converter

FTI equipment used were a rugged Ethernet PTP master switch, a recorder and two different remote acquisition units.

The wiring used during the tests have been a standard FTI Ethernet cable and a standard two-cores FTI cable [21]:

- KD24: 100 ohms shielded quad core cable, used for high speed data transmission (Ethernet networks) 100 Mbit/s and in-flight entertainment application.
- ASNE 0411 TV: 2 core shielded cable used mainly for connecting sensors to remote acquisition channels. The use of this cable is not expected to pass EMC tests and it is done only for testing robustness of physical layers with non-qualified Ethernet standard wiring.

The following test have been performed:

- Test 1: Connection of a FTI recorder to a remote acquisition unit with 16 meters of KD24 (using one of the two pairs for bidirectional communications). The bit rate of the link was 5 Mbps working without errors (see Figure 6 & 7).

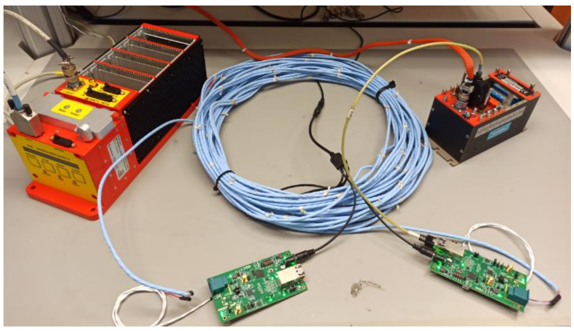

Figure 6 – Test 1 set-up

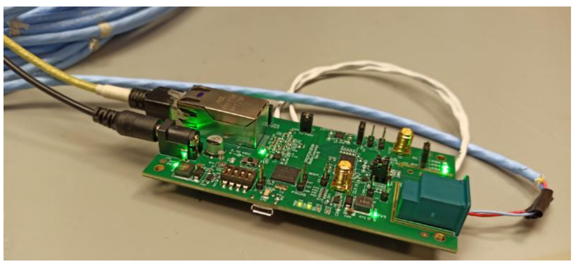

Figure 7 – Detail of test 1 set-up

- Test 2: connection of a FTI switch to a remote acquisition unit with 16 meters of KD24 (using one of the two pairs for bidirectional communications, see Figure 8). The bit rate of the link was 6.5 Mbps working without errors.

This information is of origin Airbus Defense and Space/Spain and does not contain any export controlled information.

Figure 8 - Test 2 set-up

- Test 3: connection of a FTI switch to a remote acquisition unit with 20 meters of TV (see Figure 9). The bit rate of the link was 6.5 Mbps working without errors.

Figure 9 - Test 3 set-up

- Test 4: connection of a FTI switch to a remote acquisition unit with 50 meters of ZTV. The bit rate of the link was 6.5 Mbps working without errors.
- Test 5: connection of two PCs with 16 meters of KD24. For this test a software tool "iperf" was used to check performance of the link. Using a traffic of 90 Mbps no packet was lost during the test. If the traffic is configured to 95 Mbps some errors are detected (maybe produced by converters).

As performed tests show, existing technology is very promising, even with a not considered "Ethernet wiring" as the TV, in the end it seems to provide a good communication link.

6. FTI Architecture with SPE

FTI architecture rely on Ethernet infrastructure for the main functions (see Figure 10): data acquisition, recording and monitoring. It has become the backbone that connect most of the FTI systems [22].

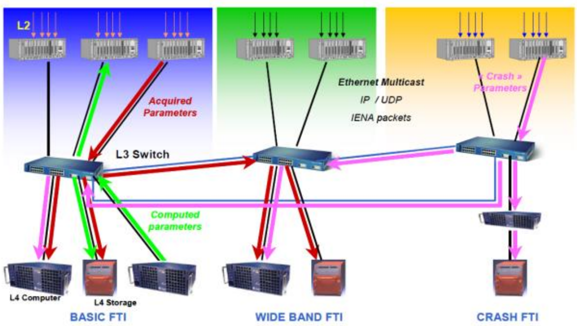

Figure 10: A380 IENA FTI LAN (Acquisition mode)

Remote acquisition units has reduced the wiring of sensors but has increased Ethernet wiring. Other FTI equipment as cameras are moving to Ethernet technology, so Ethernet wiring is growing and being one of the main problems. Ethernet growth implies additional connectors, increase of pressure seals occupation and new need of drilling holes in normal installation (see Figure 11).

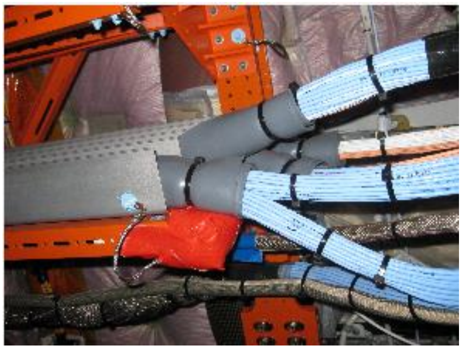

Figure 11 - Ethernet wiring in Flight Test

The benefits of using Single Pair Ethernet is clear: we can reduce the size/weight and cost of wiring of the current installation by a half. In addition the building of the installation is simplified because less connectors have to be assembled.

The following figure shows a typical A400M light FTI architecture:

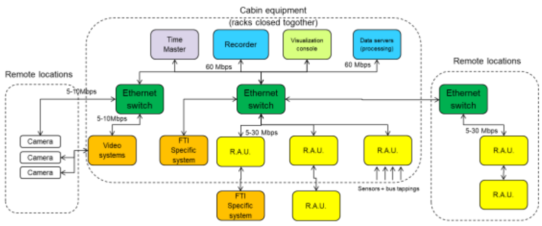

Figure 12 - A400M Light FTI

In one of the A400M prototypes with a light FTI the use of SPE would reduce the Ethernet pairs from 86 to 27, so only one third of the number of existing pairs would be needed and less connectors used. In the case of heavy FTI where many racks are interconnected with Ethernet wiring the savings taking into account cable length and weight would be even more noticeable. One of the main cable manufacturers claims [16] that specific SPE cable would save 14 % of weight compared with standard cable (2 pairs) required for 100Base-Tx and 62 % compared with standard cable (4 pairs) required for 1000Base-Tx

The main problem to adopt SPE is that none of the existing equipment have network interfaces that support it. FTI Ethernet switches should

DOI 10.5162/ettc2022/2.4

support SPE as a first step for future growth. New ARINC 854 standard will help to have this kind of device available and qualified for aircraft with standard connectors and wiring [25].

Current installations can benefit of SPE technology using converters and existing Ethernet wiring to avoid modifying installation in not accessible zones. These converters would simplify the update when a higher speed for a connection is needed or the number of Ethernet channels has to be increased. As a typical case we can consider to increase the number of remote acquisition units in an engine or a POD without needing to increase the Ethernet wiring from Cabin to the remote acquisition zone (see Figure 13). We would need two converters in each end and the same KD24 wiring would support the increase of channels.

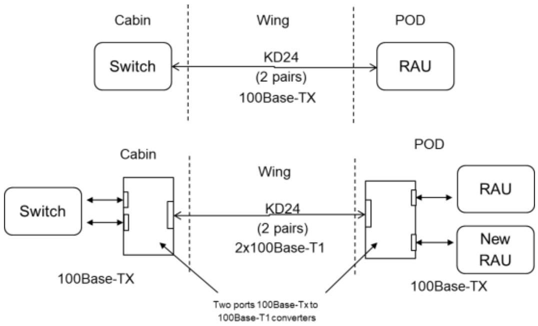

Figure 13 - Use of converters in current FTI

One of the advantages of supporting SPE in FTI is that will allow to make use of new devices developed for automotive that could have application in flight test such as cameras or other kind of sensors/devices.

As Ethernet cameras and micro acquisition systems (6-8 inputs) are recent FTI elements that have a promising future (see Figure 14), supporting SPE can make more attractive the use of these elements. Not only data but power could be provided through a single pair for this kind of elements as they don't have a high power consumption.

Figure 14 - Examples of micro acquisition system and Ethernet camera

Integrating this technology in existing and new devices will simplify flight test installations. The technology for 100 Mbps and 1 Gbps is available and is currently being used in automotive sector. The technology for 10 Mbps and PoDL will allow to integrate new equipment with only one pair cable and longer distances. Use of this technology by automotive and industrial sectors will ensure that it will be supported and updated.

One of the first documented uses of SPE technology in flight test has been a Flight Test Pod on board a Panavia Tornado [1] with good performance even when technology was not mature (2014).

7. Future Applications of SPE in FTI

The main elements required to support the evolution to SPE in FTI architecture are the following (see Figure 15):

- Ethernet switches supporting 100 Mbps/1Gbps communications and PoDL.
- Ethernet Cameras supporting 100 Mbps / 1 Gbps communications and PoDL.
- Micro data acquisition units supporting: 100 Mbps / 1 Gbps communications and PoDL.
- Remote acquisition units with support of 100 Mbps / 1 Gbps communications.
- Specific Ethernet FTI equipment (pressure scanners, specific sensors …) using most convenient SPE speed and PoDL.
- Access points for wireless technologies with SPE support for communications and PoDL.

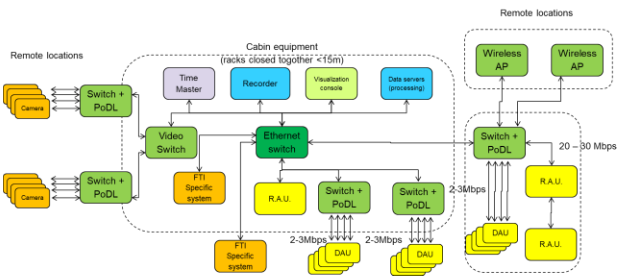

Figure 15 - Future SPE FTI architecture

SPE use for FTI in drones can be key to maximize the autonomy range optimizing size and weight while keeping support of high bandwidth (1 Gbps).

Although SPE can be seen as a reason to avoid use of wireless technology, it can help to power

This information is of origin Airbus Defense and Space/Spain and does not contain any export controlled information.

and communicate with the access points simplifying the routing to the best place for radio coverage.

Currently many aircraft and FTI equipment make use of protocols such as CAN, LVDS, … that can have now an easy migration to Ethernet using reduced wiring and enhancing the speed if needed. This process has been done in automotive and industry sectors to replace the use of old field buses. In the industry a group of leading suppliers and standards development organizations are working in the development of Ethernet advanced physical layer (Ethernet-APL [23]) based on 10 Base-T1L to meet the requirements for the field of process plants.

Every new FTI device / sensor should consider SPE for data transmission to reduce the wiring impact in aircraft and to avoid dependencies or other communications protocols.

Finally future use of IoT devices with new microprocessors & tools that will provide intelligence at the edge will need a way to transmit information. Although wireless technology is being considered in many use cases [24], the use of SPE can be an alternative for these applications, especially when communications reliability and data rate are important. The power over data line feature is another advantage of SPE standards to become an advanced platform for Internet of Things. The use of SPE will simplify use of Ethernet for digitalization at the edge.

8. Conclusions

In this paper the main IEEE standards related with Single Pair Ethernet has been introduced. The technology is ready to be used and several tests have been done with FTI equipment. Automotive sector has been the main developer of this technology and new sectors as aviation and industry are adopting it, defining related standards.

The main technological advance is to support from 10 Mbps to 10 Gbps Ethernet based on a single pair cable in harsh environments, reducing weight and installation of Ethernet networks. Flight Test Installations make use currently of 100 Mbps and 1 Gbps Ethernet interfaces, so it could benefit from this technology to reduce wiring and harnesses as in the use cases described.

The FTI systems that will take the most advantage of the new standard have been analyzed to define a future FTI architecture. Use of SPE for communications with remote locations are the main application in transport platforms. For small platforms as drones the use of SPE can help to reduce the FTI footprint.

The main advantages that justify the use of SPE for FTI are reduced cost, easier and faster installation, and higher bandwidth if needed. This simplification of Ethernet will facilitate the use of new emerging devices with capabilities of machine learning in flight test.

9. References

[1] Wilfried Steiner, TTTech Computertechnik AG, Vienna, Austria, Peter Heise and Stefan Schneele, Airbus Group, Munich, Germany - “Recent ieee 802 developments and their relevance for the avionics industry” - *2014 IEEE/AIAA 33rd Digital Avionics Systems Conference (DASC)*

[2] Kirsten Matheus, Thomas Königseder: “Automotive Ethernet” 2nd Edition, Cambridge University Press

[3] Donovan Porter: “100BASE-T1 Ethernet: the evolution of automotive networking” – Texas Instruments whitepaper April 2018

[4] OPEN Alliance (One-Pair Ether-Net) - https://www.opensig.org/

[5] OPEN Alliance Automotive Ethernet Specifications : http://www.opensig.org/Automotive-Ethernet-Specifications/#

[6] IEEE 802.3bw-2015 - IEEE Standard for Ethernet Amendment 1: Physical Layer Specifications and Management Parameters for 100 Mb/s Operation over a Single Balanced Twisted Pair Cable (100BASE-T1)

[7] IEEE 802.3bp-2016 - IEEE Standard for Ethernet Amendment 4: Physical Layer Specifications and Management Parameters for 1 Gb/s Operation over a Single Twisted-Pair Copper Cable

[8] IEEE 802.3cg-2019 - IEEE Standard for Ethernet - Amendment 5: Physical Layer Specifications and Management Parameters for 10 Mb/s Operation and Associated Power Delivery over a Single Balanced Pair of Conductors

[9] IEEE 802.3ch-2020 - IEEE Standard for Ethernet--Amendment 8:Physical Layer Specifications and Management Parameters for 2.5 Gb/s, 5 Gb/s, and 10 Gb/s Automotive Electrical Ethernet

[10] IEEE 802.3bu-2016 - IEEE Standard for Ethernet--Amendment 8: Physical Layer and Management Parameters for Power over Data Lines (PoDL) of Single Balanced Twisted-Pair Ethernet

[11] ARINC Specification 854 - https://www.aviation-ia.com/products/854-cabin-equipment-network-bus

[12] SPE Industrial Partner Network – “Single pair ethernet for industrial applications (application note)” - https://single-pair-

ethernet.com/sites/default/files/2021-03/202103speapplikationnotespe-integrationv10en_anp085.pdf

[13] Rohde-schwarz – "Excellence in automotive Ethernet solutions" : https://scdn.rohde-schwarz.com/ur/pws/dl_downloads/dl_common_library/dl_brochures_and_datasheets/pdf_1/Automotive_Ethernet_fly_en_5216-0267-32_v0100_120dpi.pdf

[14] Keysight – "Automotive Networking Tools" - https://www.keysight.com/es/en/assets/3120-1066/data-sheets/Automotive-Networking-Tools.pdf

[15] Technica Engineering – 100BASE-T1 Products - https://technica-engineering.de/en/product-category/100base-t1/

[16] Martin Cullen, Robert Moore, Clint Schlosser, Mark Benton:" Connecting the future of flight" – TE whitepaper

[17] A. Thain, F. Le Sergent, C. Marot, B. Pasquier: "Suitability of 2-wire ethernet solutions for aerospace applications" - *2016 ESA Workshop on Aerospace EMC (Aerospace EMC)*

[18] R. Perraud , C. Marot, G. Martins, V. Kretzschmar,, B. Theillaumas , J. Sperandio : "EMC Investigations on Ethernet Link for Avionic Application" - *2019 ESA Workshop on Aerospace EMC (Aerospace EMC)*

[19] Alexandros Elefsiniotis, Sebastian Hahn: "Aircraft harness measurement campaign and investigations on introducing one pair Ethernet" - *Telecommunications Network Strategy and Planning Symposium (Networks), 2016 17th International pp.207 - 212*

[20] DP83TC811 100BASE-T1 to 100BASE-TX automotive Ethernet PHY media converter evaluation module https://www.ti.com/tool/DP83TC811EVM

[21] Nexans catalogue - A complete range of wire & cable solutions for aerospace applications Issue 9 - June 2013

[22] Natalie Revaux – Frédéric Abadie: "A380 Flight Test Architecture : Switched IENA from Pulse Code Modulation to Ethernet LAN", ETTC 2003

[23] Ethernet APL - Two-Wire Ethernet For Process Automation - https://www.ethernet-apl.org/about-moksha

[24] P. Durand Estebe, V. Boitier, M. Bafleur, J-M. Dilhac : "Power Supply for a Wireless Sensor Network: Airliner Flight Test Case Study" - *The 2014 International Power Electronics Conference*

10. Glossary

SPE: Single Pair Ethernet

IEEE: Institute of Electrical and Electronics Engineers

FTI: Flight Test Installation / Instrumentation

UWB: Ultra Wide Band

IoT: Internet of Things

AI: Artificial Intelligence

ADAS: Advanced Driver Assistance System

CAN: Controller Area Network

UTP: Unshielded Twisted Pair

LIN: Local Interconnect Network

MOST: Media Oriented Systems Transport

SIG: Special Interest Group

PoDL: Power over Data Lines

PHY: Ethernet physical layer

PAM: Pulse Amplitude Modulation

BER: Bit Error Rate

EMI: Electromagnetic interference

EMC: Electromagnetic compatibility

PD: PoDL Powered Device

PSE: PoDL Power Sourcing Equipment

CENBUS: Cabin Equipment Network Bus

ARINC: Aeronautical Radio, Incorporated

ESD: electrostatic discharges

CMC: Common Mode Choke

MII: Media Independent Interface

RGMII: Reduced Gigabit MII

SGMII: Serial Gigabit MII

DME: Differential Manchester Encoding

LVDS: Low Voltage Differential Signaling

DOI 10.5162/ettc2022/3.1

Assessment of GNSS based equipment in the context of AEBS based on the UNECE R152

Ernst P. Mrohs[1], *Marcel Visser*[2]
NavCert GmbH, Schwanthalerstr. 14, 80336 Munich, Germany
[1]*phillip.mrohs@navcert.de*
[2]*marcel.visser@navcert.de*

Abstract

For safety-critical systems in the automotive industry the assessment of all sensors and systems is mandatory using calibrated measurement equipment. In the last decade GNSS based sensors are used in a variety of applications starting in the context of information, merging to commercial and now entering safety critical applications. With the pan-European emergency call 112 eCall for the first time a regulation specified mandatory requirements for performance and assessment of GNSS based systems were defined. This trend progresses with new requirements in other areas like EETS and smart tachograph (see implementing regulation EU 2021/1228 [1]) in which the usage of GNSS based systems has become mandatory Similar concepts are specified in the field of driving assistance and automated driving, like the UNECE R152[2].

Conformity to such defined requirements is assessed by notified entities in this context. The calibration of measuring instruments is an essential prerequisite for the reliability of testing (see metrological traceability ISO 17025[3]). Since the observations of GNSS based reference measuring instruments are not directly traceable to SI units and accordingly cannot be calibrated through accredited calibration schemes, an ISO 17025[3] conform assessment, validation and qualification of the reference measuring systems must be performed instead of calibration.

For this purpose, NavCert has developed a test procedure for the assessment of GNSS reference receivers based on existing standards. The respective test scheme replicates for the calibrations the assessment of performance values for GNSS based equipment. The process is presented for exemplary assessing values in the area of time, position, speed and distance with certain devices. As an outlook, currently discussed further use cases and systems are briefly presented.

Key words: ISO 17025, Assessment, GNSS, AEBS, UNECE R152

INTRODUCTION

The UNECE R152[2], where the fourth and latest amendment was released in December 2021, describes the approval for advanced emergency braking systems for M1 and N1 vehicles.

In the chapters “5. Specifications” and “6. “Test procedure” of the UNECE R152 and its amendments [2] requirements regarding the assessment in the area of speed, centreline offset and distance are defined. Hereby it needs to be mentioned that the distance is not directly addressed, but in form of the time to collision as function of distance and relative speed of the of the subject vehicle and the target.

These requirements are for example that the subject vehicle shall approach the target in a straight line for at least two seconds prior to the test with a subject vehicle to target centreline offset of not more than 0.2 m and that the tests shall be conducted with a vehicle travelling at different speeds with a tolerance of +0/-2 km/h [2].

These requirements are verified with reference equipment from the notified bodies or mandated accredited laboratories. Which reference equipment is used by these entities and if additional requirements apply is defined for each entity in standard operating procedures which follow quality standards like the ISO 17025 [3]. Hence the calibration of measuring instruments and references is an essential prerequisite for any laboratory to perform tests with reliable results.

In the UNECE R152 context the usage of GNSS based reference equipment is widespread, but also creates and issue, because one of the “default” requirements following ISO 17025[3] is the need of accredited calibration of the reference equipment.

According to the valid version of DIN 1319-1 [5], calibration is described as "determination of the relationship between a measured value (...) and the associated (...) correct value". Here, the correct value is defined according to the definition of the PTB [6] by means of measurement standards, which is a representation of an SI unit based on fundamental physical constants.

Thus for GNSS based measuring instruments a calibration by definition is not feasible, since the relevant measured quantities are not directly traceable to SI units.

The following presented work is a revision and update of the previous NavCert internal project presented in [7].

STATEMENT OF THE PROBLEM

Typically a calibration certificate needs to be issued for all kinds of measuring instrument used in laboratories, because according DKD-L 13-1 [8], an issued calibration certificate is the proof of traceability to national standards, as required by DIN EN ISO/IEC 17025 [3].

Based on the developments in the last years and upcoming ones, GNSS receivers and GNSS based equipment are used as reference measuring instruments during type approval by notified bodies and qualification and voluntary certification tests by accredited laboratories. Current fields of application for GNSS receivers or GNSS based equipment as test objects in the automotive industry are for example the tests in the context of the type approval of advanced emergency braking system, see [2], for the measurement of speed, centreline offset and distance necessary (see chapter 5. and 6. of [2]). For these topics different test scenarios are defined like for example the warning and activation test with a stationary vehicle target like defined in [2] chapter 6.4 ff., where the defined speeds of 20, 42 and 60 km/h with a tolerance of 2 km/h, the time to collision of at least 4 seconds and a maximum centreline offset of 0.2 m need to be independently measured. Similar applies to the other applicable test cases like for moving pedestrian targets (see [2] 6.6.1).

For these measurements a reference measurement equipment is needed. The most common used measurement systems are either GNSS receiver or GNSS based equipment (e.g. INS).

Due to the typical system design of such units and usage of non-deterministic algorithms the PVT-output of such systems is nearly impossible to traceback to SI-units and currently not calibratable.

Due to the thus non-existing calibration possibility such system needs to be assessed according to laboratory requirements like stated for example in the ISO 17025 [3].

Additionally it needs to be mentioned that this applies not only the core reference system, but also to other services which are used together with the reference equipment (e.g. augmentation in the form of RTK-correction).

If such system (e.g. GNSS-RTK-Systems) has not been calibrated and validated, the proof of the quality of the measured values (e.g., reliability, accuracy, availability, integrity) is missing and the test result is doubtful.

To solve this problem as an accredited laboratory for GNSS NavCert conducted an internal project.

INITIAL ANALYSIS

As a first step, an initial measurement and error analysis of typical GNSS receivers and GNSS based equipment was performed. The initial work for this was done in [7] and for the here presented revision an update in the area of inertial measurements was conducted. Hereby typical measurement quantities as well as output protocols are considered.

According to [8] chapter 3.3, the following measured quantities are the typical observed quantities of GNSS receivers:

- Pseudo range or code phase
- Carrier phase
- Doppler frequency shift

These typical observables can be outputted in the form of RINEX data in the observation part with additional information, such as information regarding observation time from specific receivers, and supplemented with the RINEX navigation part. In the past, receivers which could output RINEX were usually professional ones. However, this is changing in recent years due to the release of raw GNSS data in Android environments [9] for example. Usually RINEX data is used for GNSS post-processing, which is currently used for certain applications (e.g. determination of coordinates of static reference points). Currently the assessment of RINEX-data is not within the scope of the defined internal project and thus they are not further discussed in the current project phase.

Another standard output format in various forms and versions is NMEA, which is supported by quite every receiver. It is a real-time output protocol which provides information for example about visible satellites as well as the current position fix of the GNSS receiver. This document focuses on NMEA-0183 v 4.11 with RMC, GGA, VTG, GSA and GSV -message as defined in [10] as follows, which are for example used for tests according to DR 2017/79 Annex VI [4]:

- RMC: Recommended Minimum Specific GNSS Data
    - Includes time, date, position, speed, status, heading information.
- GGA: Global Positioning System Fix Data
    - Contains time, date, position, quality, altitude information, which is supplemented by the number of satellites used and information regarding correction data used.
- VTG: Course Over Ground & Ground Speed
    - Contains course, speed and status information
- GSA: GNSS DOP and Active Satellites
    - Contains status and satellite information regarding navigation satellites actively used for positioning, which is supplemented by PDOP, HDOP and VDOP
- GSV: GNSS Satellites in View
    - Contains information about possible and seen satellites

In addition to the two presented formats, there are further formats which are not discussed in this document.

Besides the GNSS measurement in this document also on IMU measurements are discussed on a high-level. These are according to [11] linear accelerations and angular rates. These measurements can be outputted by IMUs by using usually by the manufacturer defined output formats.

If the IMU is used in combination with a GNSS receiver or other sensors in a more complex localisation sensor system, we are speaking usually of an INS, where these measurements are combined internally via sensor data fusion algorithms with the GNSS measurements in one of the three typical data fusion levels (loosely, tightly, ultra-tightly).

Besides these measurements also the output of used augmentation/ correction services was analysed. The project is focused currently on NTRIP based RTK services which provide their correction data according to the RCTM definition [12]. These corrections originate from one or a network of GNSS reference stations and cover a large are of data, e.g., RTCM 3.3 message 1004 contains the extended L1 & L1 GPS observations.

Additionally to the measurement analysis and uncertainty analysis for the GNSS, IMU and RTK was conducted and the impact on the measurement results was evaluated. This analysis and its outcome are used to define certain critical scenarios or feared events which shall be acknowledged in the later test scheme.

The analysis followed the described process in [6] and [13] and usually contains six steps. But for the usage as for definition of the critical scenarios only the first four steps are from major importance. These steps are:

1. Description of the measurements
   The underlying measurements for the tests and of the equipment were described here based on the outcome of the initial analysis.
2. Modelling of the measurements
   The described measurements are modelled according to the process described in [14], whereby all impacting topics/input variables like for example personnel, environment, method, equipment are analysed and listed upon their impact
3. Evaluation of input variables
   The identified input variables are evaluated based on their probability, quantify and severity. Hereby the impact on the accuracy was the main focus, but also other performances like the integrity were evaluated.
4. Calculation of the best estimate and combined standard measurement uncertainty
   For the variables assessed as essential for the further process the best estimate quantity is calculated and carried over to the calculation of the combined uncertainty.

Hereby its needs to be highlighted that most of the critical scenarios which apply to the GNSS receiver also apply to the assessed correction services due to the usage static GNSS reference receivers for the generation of the correction data.

The detailed analysis is not highlighted in this paper due to its extend.

As outcome of the analysis it was determined that for this revision of the testing scheme the focus shall be put first on the integration of GNSS specific critical scenarios like:

- Shadowing
- Non-availability
- Multipath

- Jamming/ Interference
- Meaconing
- Spoofing

STANDARDS

The next step was an analysis of available standards for the assessment. The following standards were selected for the:

- Definition of the performance requirements
- Definition of test setups and test description

Tab. 1: Overview of standards

Number	Version
ETSI TS 103 246-3 [15]	V1.3.1 (2020-10)
ETSI TS 103 246-5 [16]	V1.3.1 (2020-10)
DIN EN 16803-1 [17]	2021-07
DIN EN 16803-2 [18]	2021-07
DIN EN 16803-3 [19]	2021-07
ISO 17123-1 [20]	15.08.2014
ISO 17123-8 [21]	15.06.2015
DIN ISO 5725-1 [22]	1997-11/1998-09
ISO 5725-2 [23]	2019-12
ISO 5725-4 [24]	2020-03
DIN ISO 5725-6 [25]	2002-08

METRICS

Based on the standards listed above, the metrics of the assessment scheme was defined. For this the following represents the metrics scope for this phase of the internal project for the basic performance part. It was defined that the GNSS equipment performance is asset for the horizontal position and the horizontal speed and the timing quality.

Hereby for the horizontal position and for the horizontal speed the focus was laid on the accuracy and availability. For the timing the focus was laid on the general performance, availability, and continuity.

Additionally, if correction services are used from the GNSS equipment, it was defined to also evaluated the correction service’s availability and continuity.

Background of this decision is that the accuracy is one of the fundamental and most crucial performances which has an effect on several system functionalities. The same applies to the topics of availability and continuity.

As second part of the test scheme the critical scenarios are defined like described in the chapter “Initial Analysis”. Here besides the above defined metrics also the integrity is considered in this phase of the internal project.

The following table represents the definition of the metrics, which follows definitions from the references [15] chapter 5.4.1 ff and [17] chapter 5.5 ff.:

- Position Quality
  - Horizontal Accuracy: The horizontal position accuracy is defined by the horizontal error of the valid position data in comparison to the reference.
  - Availability: The positions availability is described as the percentage of operating time intervals of length T_b during which the system provides at least one valid output.
- Distance quality between two systems
  - Horizontal Accuracy: The horizontal distance accuracy is defined by the horizontal error of the differences of the valid position outputs in comparison to the reference.
  - Availability: The horizontal distance availability is described as the percentage of operating time intervals of length T_b during which both systems provide at least one valid output.
- Speed Quality
  - Horizontal Accuracy: The speed accuracy is defined by the error of the valid speed outputs in comparison to the reference.
  - Availability: The speed availability is described as the percentage of operating time intervals of length T_b during which the system provides at least one valid output.
- Time Quality
  - General performance: The general timing performance is defined by the time to first fix under cold start conditions warm start as wells as the reacquisition time.
  - Availability: The timing availability is described as the percentage of operating time intervals of length T_b during which the system provides at least one valid output.
  - Continuity: The timing continuity is described as the percentage of operating time intervals of length T during which the system provides valid outputs at the required rate and without interruptions.

- Relative delay: The timing delay of the is described as the relative time offset of the recorded trajectory between of the SUT and the reference determined by a cross-correlation analysis.
- Correction Service Quality
  - Availability: The correction service availability is described as the percentage of operating time intervals of length T_b during which the system provides at least one valid output.
  - Continuity: The correction service continuity is described as the percentage of operating time intervals of length T during which the system provides valid outputs at the required rate and without interruptions.

As expression of these metrics in the test scheme the following representations are used:

- Accuracy: Mean error, standard deviation and the 75th and 95th percentile (see [15] chapter 5.2.2)
- Availability: Percentage (see [18] 5.5)
- Continuity: Percentage (see [18] 5.5)
- General timing performance: Mean value

TEST DESCRIPTION

As a next step, based on the requirements for laboratories of ISO 17025 [3], a description of the tests to be performed and a detailed analysis regarding the test topics, e.g. a measurement uncertainty analysis, was carried out based on the processes described in ISO Guide 98-3 [26], in DKD-L 13-1 [6] and DKD-L 13-2 [13].

For the measurement uncertainty analysis the process which is highlighted in the chapter "Initial Analysis" was used.

This process consists of six steps, which are highlighted in the following with the focus on the test scheme and used reference for the tests:

1. Description of the measurements: The underlying measurements for the tests and of the equipment were described here based on statements from [2] and the outcome of the initial analysis. The required measurements can be highlighted as followed:
   - Assessment of GNSS based reference equipment under consideration of used correction services in the domain of position and distance between two systems.
   - Assessment of GNSS based reference equipment under consideration of used correction services in the domain of velocity.

   As measurement method for the assessment different methods need to be considered due to the difference of the used systems, which is highlighted in the following:
   - GNSS receivers: A simulation-based approach based on [3] under consideration of inputs from [2] applies here where the output of the SUT is compared to the simulation reference.
   - GNSS-IMU-systems: A field testing approach based on [18] under consideration of [2] applies here where the output of the SUT is compared to a validated PVT-reference.
   - Correction services: The field-testing approach, which is described in [21], applies. It contains to steps, the static approach and the dynamic approach, which resemble a modified approach from [21] under consideration of [2].
2. Modelling of the measurements
   The described measurements are modelled according to the process described in [14], whereby all impacting topics/input variables like for example personnel, environment, method, equipment are analysed and listed upon their impact. This analysis applies to the described high level measurement methods described before and the chosen reference.
   Based on the requirements from [2] (for example velocity accuracy better than 2 km/h and position accuracy better than 0.1 m) and the analysis outcome the initial requirements for the reference for the assessment tests was defined. Hereby it was defined that the reference shall be in optimal case ten times better than the requirement.
3. Evaluation of input variables: The identified input variables are evaluated based on their probability, quantify and severity. Hereby the impact on the accuracy was the main focus, but also other performances like the integrity were evaluated.
4. Calculation of the best estimate and combined standard measurement uncertainty: For the variables assessed as essential for the further process the best estimate quantity is calculated and carried over to the calculation of the combined uncertainty.
5. Determining the expanded uncertainty: Based on the conducted sample analysis (see below) and under consideration of the prior analysis the expanded uncertainty is determined.
6. Specifying the complete measurement results: Based on all the previous information the expected uncertainty of the

reference and the measurement method is statistically analysed and determined.

Additionally to support the measurement process as further topic a sample analysis according to [27] was performed, which is described in the following on a high level.

In order to obtain a sufficient significance of the test results, a certain confidence must be achieved, which influences the sample size and further values. Within the project, the confidence levels of 99% and 99.9% regarding the binomial distribution at an infinite population were considered. They were considered via the factor of 2.57583 and 3.29053, respectively, according to [27] A.5.

This results under consideration and inclusion of other parameters into a minimum sample size of about 16,600 resp. about 27,000 samples for each respective test.

During the presented analysis also all relevant topics regarding the test method like signal strength for the simulated signals, applicable GNSS environments for simulation and field tests, test setup are discussed and under consideration of the available standardisation defined. For example the open and urban environment (see Fig.1 and 2) was defined for certain tests.

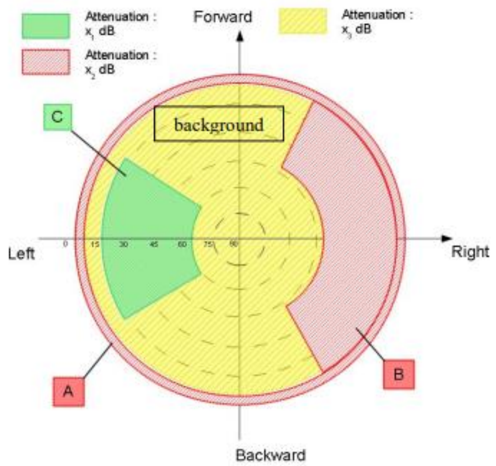

Zone	Elevation range (deg)	Azimuth range (deg)	Attenuation (dB)
A	0 to 5	0 to 360	$x_2 = 100$
B	5 to 60	30 to 150	$x_2 = 100$
C	10 to 60	230 to 310	$x_1 = 0$
Back-ground	Angles out of Zones A, B, C		$X_3 = 15$

Fig. 1: Asymmetric GNSS-Environment according to [4] A..3.2

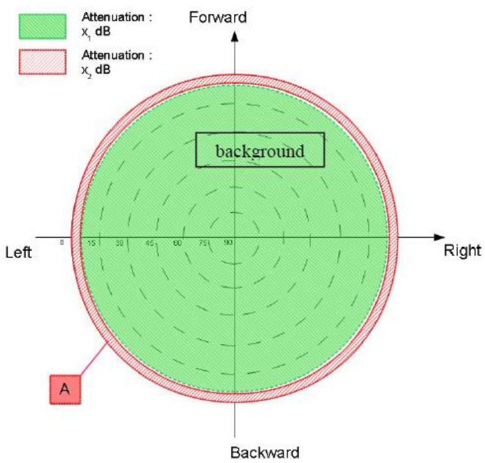

Zone	Elevation range (deg)	Azimuth range (deg)	Attenuation (dB)
A	0 to 5	0 to 360	$x_2 = 100$
Back-ground	Angles out of Zone A		$x_1 = 0$

Fig. 2: Open GNSS-Environment according to [4] A.3.2

In total three basic environment are defined according to [15] for the assessment. Hereby for the field tests a procedure is defined to determine the applicable environment on test side.

The kinematics for the tests are defined following requirements from [2] and [15]. Hereby generically static and dynamic movements are defined, whereby the kinematics are defined in the standard test case according [15] A.4. These are amended by the movement on straight lines following the description and requirements from [2], e.g. travelling speeds like 20,42 and 60 km/h.

Based on the initial analysis regarding critical scenarios the second part of the test scheme is defined, assessing the system's performance and behaviour under influence of such. The effect of shadowing and non-availability are already covered by the basic performance assessment. Like indicated in the initial analysis the test scheme covers the impact of

- Multipath
- Jamming
- Interference
- Meaconing
- Spoofing

Hereby the definitions from [15], [16] and [19] are followed. Due to the impact of such threats to the public the critical scenarios tests cannot usually be performed in open environment and thus a special environment is required. This can be either a shielded environment or a special restricted place.

As next part of the test scheme the assessment of the correction service is conducted. This follows the accredited NavCert testing schemes PPP80013 [28] and PPP80019 [29] which were adapted to represent the use case testing of reference measurement equipment for AEBS type approval according to [2]. The approach assesses the addressed quality of the service and the performance of the services together with the used receivers. The performance assessment of the services is combined with the basic assessment of the GNSS based systems in fields tests. The correction service quality on the topic of availability and continuity is asset via an QM-review of the service provider, long time data logs of the provider and spot checks during the tests.

Besides the single system performance assessment also the synchronic performance of two systems for the measurement of distance or relative positions are assets in this test scheme. For this in the current phase of the project the test systems are mounted for a field test to a moving platform with which at least three different independently asset distances can be set. Similar to the position assessment the test is conducted with different speeds and in different environments to determine the quality of the distance output of the combined system.

For the test setup different setups apply. In the standard operating procedure for this test scheme the following test setups are defined:

- GNSS simulation test setup
    - Shielded environment
    - Wired connection
- GNSS based equipment field test setup
- GNSS correction services test setup
- GNSS critical scenario setup
    - Shielded environment
    - Restricted testing area
- Distance test setup

In the following as representatives the setup for basic performance assessment for GNSS receiver testing (see Fig. 3 and 4) and the distance test setup (see Fig. 5) are presented.

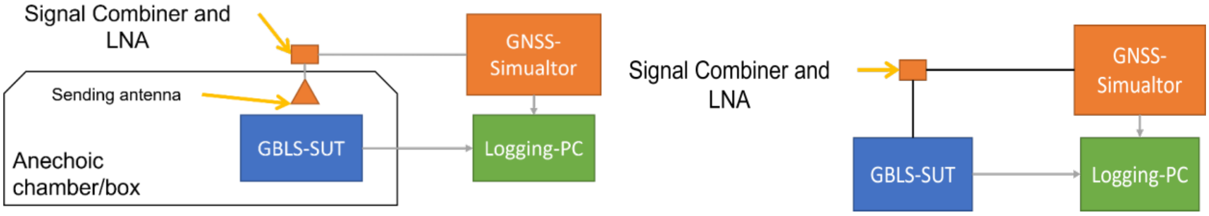

Fig. 3: Test setup according to [16] Annex A A.1 System set up for tests in anechoic room and [16] Annex A A.2 System set up for tests with wired connections

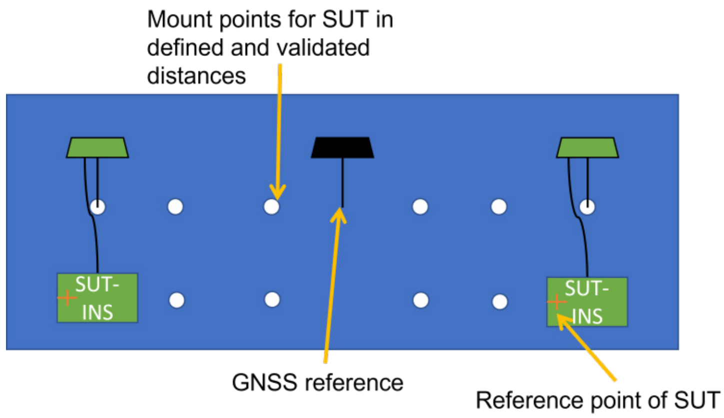

Fig. 4: Test setup for distance assessment

The test setups for the GNSS receiver simulation test follow the description [5]. The test setup for the distance assessment is a self-developed approach. It contains beside the mount points for the GNSS based SUT (e.g. an INS) with evaluated distances to each other also a validated GNSS reference for checking the applicable environment and further topics which are required to create reproducible results.

At the end of the test scheme additional statistical tests are included to check and deliver proof that during the testing no errors for example were conducted. Examples for these statistical tests are for example null hypothesis testing, comparison of the critical range with the range of results and Cochran's test (see for example [23]).

EVALUATION

To conclude in the following the according [3] required initial validation, verification and review including initial results are presented. The results are based partially on the previous work conducted in [7]. In the following three topics are presented and discussed:

- Determination of the position and speed error in simulation mode based on basic performance assessment
- Determination of the time error in simulation mode based on basic performance assessment
- Determination of distance error in field testing based on basic performance assessment

The first step after the definition of laboratory is the validation according [3]. This step is required and is here highlighted only. For the standardized methods a validation is only proposed, but due to the nature of the here presented a validation needs to be conducted to assure that the quality of the method. According to [3] different possibilities for the validation are available, which are not further detailed here. The initial validation of the presented methods was conducted successful, concluding that the chosen methods ensure the required quality.

After the successful validation the initial verification of the test scheme and its methods was conducted upon their suitability to the intended use. For this the required measurement equipment, the available measurement range and the respective accuracies are compared to the required measurement ranges for each method to assess that the full range of measurements is covered and can be assessed. Additionally, a prototypical test campaign is conducted using suitable equipment as the SUT. The initial results of the verification are presented in the following. Due to the ongoing project the formal topic of review is currently not conducted but will be conducted after finalization of the next phase.

For the verification here the results of the including prototypical test campaign are presented. Like described before the assessment of position, speed, time and distance will be shortly presented.

In the following the error vector, mean error and standard deviation are presented as way are the base for the definition of the values mentioned in the chapter "Metrics".

In the course of the subsequent laboratory verification of the test procedure, the NMEA data of a timing receiver and a geodetic receiver were compared with the validated reference data of the GNSS simulator within the project for the addressed simulation test methods. The following results were obtained:

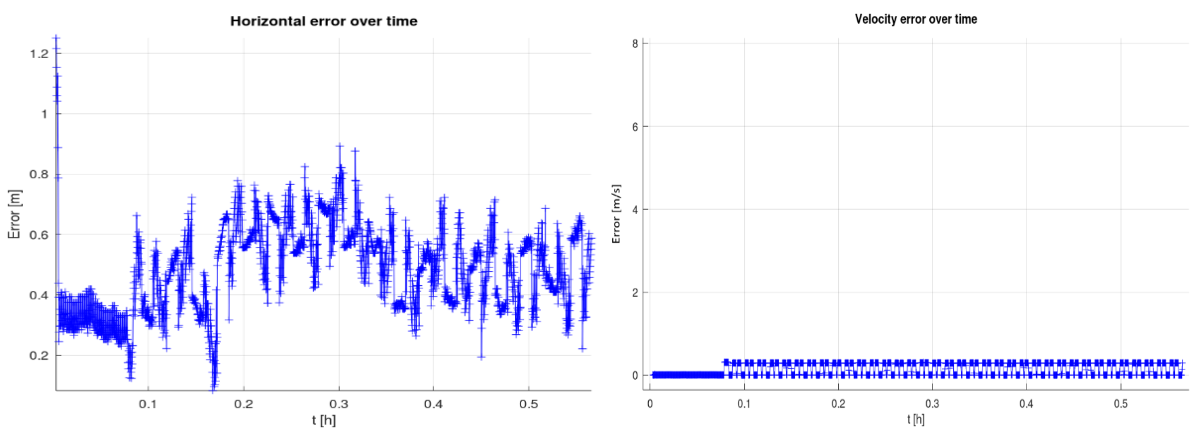

Fig. 5: Horizontal error over time for the chosen timing receiver and speed error over time for the chosen geodetic receiver

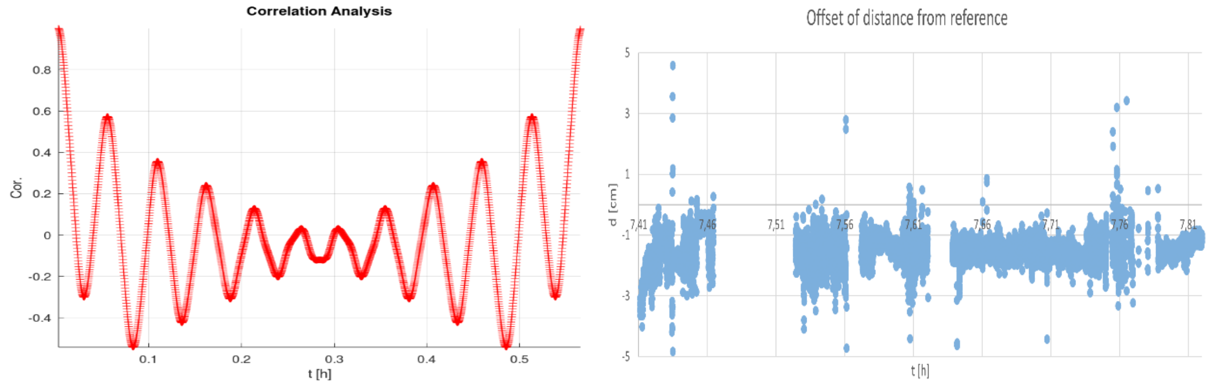

Fig. 6: Cross-correlation results of the geodetic receiver and excerpt of distance analysis data for the high-quality solution

Here, the geodetic receiver achieved a comparable time quality considering the resolution of 10 ms of the reference. The timing receiver achieved the same result regarding time quality, which was expected.

Regarding the position and the speed, values below 1m for the horizontal position error and below 0.25 m/s for the horizontal speed error were achieved in the SBAS mode for both receivers.

For the assessment of the distance a high-quality solution and a high-quality solution were checked. Hereby for the high-quality solution an uncertainty of the distance of 1,49 cm+/- 0,53 cm and the low-quality solution uncertainty of the distance of 1,02 m +/-3,88 m was determined.

CONCLUSION AND OUTLOOK

As initially presented, calibration for GNSS based measuring equipment is due to the definition of calibration problematic. Accordingly, instead of calibration, an evaluation, validation and qualification of used systems need be conducted.

Based on current outcome it can be stated that the presented method shows a valid initial approach which can already be used for certain type of equipment. The performed and ongoing validation and verification of the test procedure according laboratory requirements hereby ensures that the developed procedure meets the initial expectations and can be used as a basic procedure for assessment, validation and qualification.

However, it provides only an initial assessment. Therefore, further refinement and elaboration is needed, like addressed before. This is currently under work and will be done in further ongoing of the project within NavCert. Here, for example, the planning is to include also RINEX data in the assessment and thus to check other GNSS observations such as pseudo-distance.

Additionally to widen the scope of the assessment further use cases and augmentation sensors and services need to be included in the scheme.

References

[1] EU, COMMISSION IMPLEMENTING REGULATION (EU) 2021/1228 as regards the requirements for the construction, testing, installation, operation and repair of smart tachographs and their components

[2] UN, UN Regulation No. 152 with amendments 1 till 4: Uniform provisions concerning the approval of motor vehicles with regard to the Advanced Emergency Braking System (AEBS) for M1 and N1 vehicles

[3] DIN, DIN EN ISO/IEC 17025 :2018-03- General requirements for the competence of testing and calibration laboratories

[4] EU, COMMISSION DELEGATED REGULATION (EU) 2017/79 establishing detailed technical requirements and test procedures for the EC type-approval of motor vehicles with respect to their 112-based eCall in-vehicles systems, of 112-based eCall in-vehicle separate technical units and components- ANNEX VI

[5] DIN, DIN 1319-1: 1995-01- Fundamentals of metrology-Part 1: basic terminology

[6] PTB-DKD, DKD-L 13-1 Praxisgerechte Ermittlung der Messunsicherheit, Revision 1, 2012-02, doi: https://doi.org/10.7795/550.20191105

[7] E.P. Mrohs, S. S. K. Machiraju, Assessment of a GNSS reference in the context of calibration, *ION ITM 2022*

[8] Manfred Bauer, Vermessung und Ortung mit Satelliten, 7. Edition, Wichmann, Berlin, 2018

[9] Google LLC, Raw GNSS Measurements (last updated 2021-08-05), https://developer.android.com/guide/topics/sensors/gnss, accessed 2021-08-10

[10] National Marine Electronics Association Inc., NMEA 0183, Version 4.11, 2018-11

[11] Ch. Jekeli, Inertial Navigation Systems with Geodetic Applications, Berlin, de Gruyter, 2001

[12] RTCM, RTCM Standard 10403.3 Differential GNSS (Global navigation satellite systems) services – Version 3 with amendments 1 and 2, 2021

[13] PTB-DKD, DKD-L 13-2 Validation of measurement uncertainty budgets, Edition 10/2020, doi: https://doi.org/10.7795/550.20211118

[14] JCGM/BIPM, JCGM GUM-6:2020 Guide to the expression of uncertainty in measurement — Part 6: Developing and using measurement models, 2020

[15] ETSI, ETSI TS 103 246-3- Satellite Earth Stations and Systems (SES); GNSS based location systems; Part 3: Performance requirements, V1.3.1 (2020-10)

[16] ETSI, ETSI TS 103 246-5, - Satellite Earth Stations and Systems (SES); GNSS based location systems; Part 5: Performance Test Specification, V1.3.1 (2020-10)

[17] DIN/EN, DIN EN 16803-1- Use of GNSS based positioning for road Intelligent Transport Systems – Part 1: Definitions and system engineering procedures for the establishment and assessment of performances, 2021-07

[18] DIN/EN, DIN EN 16803-2- Use of GNSS based positioning for road Intelligent Transport Systems – Part 2: Assessment of basic performances of GNSS based positioning terminals, 2021-07

[19] DIN/EN, DIN EN 16803-3- Use of GNSS based positioning for road Intelligent Transport Systems – Part 3: Assessment of security performances of GNSS based positioning terminals, 2021-07

[20] ISO, ISO 17123-1- Optics and optical instruments - Field procedures for testing geodetic and surveying instruments - Part 1: Theory, 15.08.2014

[21] ISO, ISO 17123-8- Optics and optical instruments — Field procedures for testing geodetic and surveying instruments — Part 8: GNSS field measurement systems in real-time kinematic (RTK), 15.06.2015

[22] ISO, ISO 5725-1- Accuracy (trueness and precision) of measurement methods and results - Part 1: General principles and definitions, 1997-11/1998-09

[23] ISO, ISO 5725-2-Accuracy of measurement methods and results - Part 2: Basic method for the determination of repeatability and reproducibility of a standard measurement method, 2019-12

[24] ISO, ISO 5725-4-Accuracy of measurement methods and results - Part 4: Basic methods for the determination of the trueness of a standard measurement method, 2020-03

[25] DIN/ISO, DIN ISO 5725-6-Accuracy of measurement methods and results - Part 6: Use in practice of accuracy values, 2002-08

[26] ISO/IEC, ISO Guide 98-3 Uncertainty of measurement- Part 3 Guide to the expression of uncertainty in measurement, 2008

[27] Wolfgang Polasek, Schließende Statistik, Springer, Berlin, 1997

[28] NavCert, Ernst Phillip Mrohs, PPP80013C:2020 Ground Based Augmentation Systems, 2020

[29] NavCert, Ernst Phillip Mrohs, PPP80019D:2020 RTK Services for Dynamic Applications, 2020

DOI 10.5162/ettc2022/3.2

Certification of automotive GNSS receivers using aerial image data

Paulo Mendes[1], Franz Kurz[2], Veronika Gstaiger[2], Hartmut Runge[2], Ernst Phillip Mrohs[1], Collins Akhimien[1]
[1] NavCert GmbH, Schwanthalerstr. 14, 80336 Munich, Germany,
[2] German Aerospace Center (DLR), EOC, Weßling, Oberpfaffenhofen, Germany
paulo.mendes@navcert.de

Abstract:
A new method for calibration, validation aiming at certification of GNSS receivers used in the automotive industry addressing the levels 3 and 4 of automation under real world conditions is presented. The method uses simultaneously acquired high-resolution aerial image data, from a helicopter, which is precisely georeferenced with Ground Control Points. The method provides a reference trajectory for vehicles in GNSS critical areas, e.g., GNSS-denied type environments. The images obtained contain the vehicle's roof with the signalized GNSS receiver antenna. Together with a precise height model of the road surface, the absolute position of the GNSS receiver in world coordinates can be derived from the position in the image. The main results of a test campaign, performed in July 2021, using the method are presented. It was investigated how the quality of the GNSS sensors is influenced by the environment (Rural, Highway and Urban) and what added value the method provides. The method proved to be resilient and robust to situations where the GNSS position accuracy degrades, even when RTK is used, as local effects do not impact the new method. The method provides high-precision reference trajectories facilitating calibration, validation, and conformity testing. In this contribution the focus will be set on the validation and testing process leading to certification.

Key words: Certification, GNSS, Aerial imagery, Validation.

Introduction

Determining the absolute position of a vehicle with a high degree of accuracy is a relatively new and considerable challenge in the automotive industry. This is due to the high complexity of the hardware and software systems involved, their complex interaction and dependence on, e.g., environmental conditions, physical properties of the terrain and landscape, the use of different data types, GNSS correction data services, e.g., Real-Time Kinematic (RTK) data, and other factors. To date, the main need for positioning in the automotive sector has mainly been in applications where the requirements for positioning accuracy are not so high. The vehicle position determination has only been used as a commodity of convenience for basic functions such as navigation or for the provision of points of interest (PoI's). However, these requirements change for vehicles with automated driving functions.

Vehicles with automated driving functions specifically designed for SAE-L3 (L3) or SAE-L4 (L4) definitions [1] are bound by the highest reliability and data quality of positioning systems due to their safety requirements. Since automated driving functions require accurate absolute position information derived from GNSS data with optional support from auxiliary sensors such as INS and odometers, it is necessary to ensure that GNSS receivers meet and maintain the position requirements. This means that GNSS sensors must be tested regarding the position accuracy during development and integration before they are deployed on the road. This assessment process requires a method that provides a ground-based reference trajectory (GTRT). This trajectory is compared with the trajectory of the vehicle measured by a GNSS sensor. To date, GNSS-INS, or high-quality devices for dynamically determining a ground reference trajectory have been widely used on the road, but there are few alternative methods for independently validating these devices under realistic conditions. It is assumed that by using a high-quality GNSS system, an accurate and error-free GTRT can be determined. This approach has the disadvantage that the same system-intrinsic GNSS errors cannot be identified and most likely both the reference system (RS) and the system under test (SUT) are affected simultaneously. The extent of the system-intrinsic errors affecting both the GNSS RS and the GNSS SUT generally remains unknown without calibration, validation, or a test process.

Currently there is an urgent need for a reliable and independent method for verifying accuracy guidance when using GNSS data in the context of autonomous driving. Especially as OEMs and Tier 1 companies are looking for exactly such methods for the validation process of required key performance indicators (KPI), such as the absolute position accuracy of the vehicle. Independent reference trajectories of known quality can finally be used to characterise GNSS-based solutions and support their development and validation.

Two viable approaches to determine a GTRT (position, velocity, orientation and time) are relative positioning using robotic total stations, and absolute positioning using aerial imagery in combination with ground control points (GCP) derived from the TerraSAR-X satellite based on radargrammetric measurements or from static GNSS equipment.

The Objective

The main objective was to develop a conformity scheme based on test principles that can be used to support the calibration, validation and in particular a certification process of GNSS sensors used in the field of automated driving. A conformity assessment process comprises a set of procedures to demonstrate that a product, service, or system meets the requirements of a standard, regulation, law, etc. Conformity assessment brings several benefits, including additional consumer and stakeholder confidence, competitive advantage, or assurance to regulators that all specified requirements and conditions have been met.

In the context of automated driving, there is no defined GNSS-based standard or regulation that addresses the absolute accuracy of positioning KPIs. The standardisation organisations CEN/CENELEC and ETSI have worked extensively on the development of standards for the use of GNSS sensors in automotive applications. This work focused on the more traditional automotive users, i.e., it did not consider the high positioning accuracy requirements needed for automated driving. This situation will certainly change in the near future. The CEN/CENELEC standard series EN 16803 [2] - Use of GNSS-based positioning for intelligent transport systems (ITS) in road transport - and the ETSI standard series TS 103 246 [3] - GNSS-based positioning systems (GBLS) - are examples of this important work in road transport. These standard series were used as a starting point and inspiration for the defined accuracy KPI metrics, the associated performance classes and the use cases developed in this work. For position accuracy, the horizontal and vertical position errors (HPE, VPE) were defined as the main KPIs, with the 68.3rd, 95.4th and 99.7th percentiles as associated metrics. The proposed HPE and VPE KPIs and associated metrics are used to establish pass/fail criteria in this particular case in the context of conformity assessment, i.e., in the context of a certification scheme based on testing activities.

The Method

The newly proposed calibration and validation method allows absolute positioning using simultaneously acquired aerial imagery from a flying platform [4] (see Fig. 1) in combination with ground control points (GCPs) derived from the TerraSAR-X satellite based on radargrammetric measurements [5] (see Fig. 2) or acquired from stationary GNSS equipment. The latter require medium- to long-term measurement series of defined GCPs along the test track(s).

Fig. 1. Artistic depiction of the concept. A flying platform equipped with a DLR 4k camera system mounted on the fuselage of a helicopter follows a test vehicle obtaining imagery along the test track.

This method is based on the idea of comparing the measurements of a GNSS receiver on board a test vehicle with those of a validated and GNSS-independent RS, which provides higher accuracy and coverage even in GNSS-denied areas by using aerial imagery.

The method enables for the first time the calibration and validation of automotive GNSS receivers under real-world conditions through the use of aerial imagery and GCPs and, unlike previous calibration and validation test methods, is independent of GNSS-related sources of error.

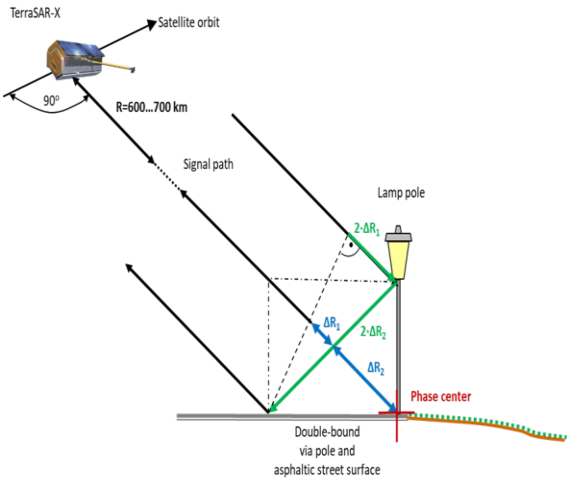

Fig. 2. Radargrammetric measurement principle using the TerraSAR-X satellite for the extraction of a GCP position data from a streetlamp pole. The method can use other GCP types, e.g., derived from mid or long-term stationary GNSS measurement series.

This method enables the absolute positioning of moving objects with the help of aerial images by forward intersection of image objects. For forward intersection, an image beam is defined from the precisely defined position and orientation of the aerial camera and the position of the vehicle in the image. To determine the position of the vehicle along this image beam, the beam must be intersected with a digital terrain model (DTM). By applying the collinearity equations for all image beams in the high frame rate image sequences, the reference position, velocity, orientation, and time of the mobile GNSS receiver antenna on the vehicle roof can be determined.

The derivation of 3D positions of objects from a 2D image requires additional information from the DTM. Therefore, the method requires GNSS-independent height information at the position of the GNSS antenna on the vehicle roof, which can be used to derive the horizontal position of the GNSS antenna (X and Y). The absolute height of the vehicle GNSS antenna is a central parameter that is simply the sum of the absolute road surface height from the DTM at that position and the height of the GNSS receiver relative to the ground. The aerial imagery is georeferenced by a bundle adjustment using GCPs, on-board GNSS/inertial measurements and automatically high-density tuned link points. The method is independent of the type of GCPs provided. The GCPs are measured as standard with a stationary GNSS device with an accuracy of one centimetre. The base points of lampposts or road signs are usually used as reference points, which can often be clearly identified radar satellite data as well as in the aerial images. After georeferencing the images, the reference trajectory of the vehicle is derived. This is then used to evaluate the trajectory of the SUT derived from the GNSS sensors by calculating the various KPI metrics using the vehicle position obtained from the imagery and GCPs as the reference trajectory.

For any test procedure, be it calibration, validation, or conformity assessment, it is important to evaluate the reference system theoretically and practically. From a theoretical point of view, the expected accuracy of the method is better than 10 cm compared to the accuracies of GNSS receivers of more than 100 cm. The overall accuracy of the method was analysed in the field under good GNSS conditions and using SAPOS GNSS data corrections for post-processing. The average differences between the positions of the aerial vehicles and the post-processed GNSS data were better than 10 cm and thus in line with the theoretical assessment [6].

Test framework

The architecture of the test frame consists of the elements associated with the new method, i.e., the DLR 4k optical camera system (see Fig 1) and the associated processing algorithms, as well as the test object, i.e., the GNSS receivers of the vehicles. Two nadir-viewing cameras of the DLR 4k system with different focal lengths of 35 mm and 50 mm are used to record the aerial image sequences. In order to enable automated measurement of the position of the GNSS receiver in the aerial images, it is necessary to uniquely recognise the vehicle and to be able to measure the exact position of the receiver on the car roof. For this purpose, a magnetic sticker with eye-catching colours and high contrast was placed on the roof of the target vehicle (see Fig 3).

DOI 10.5162/ettc2022/3.2

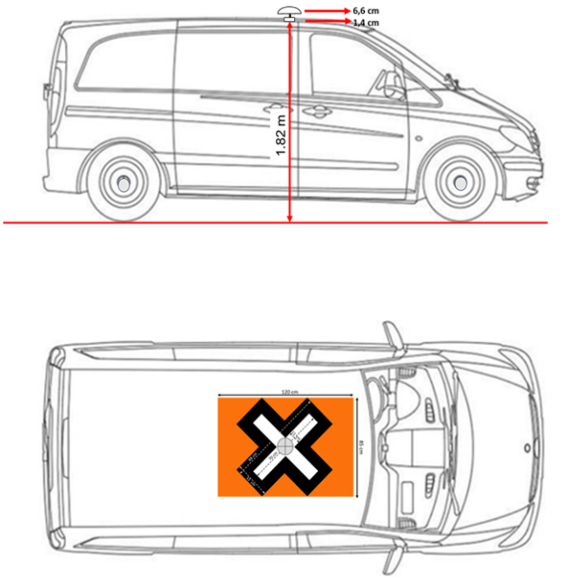

Fig. 3 Magnetic sticker with cross installed on the vehicle roof to enable the automatic tracking during image data processing. The GNSS antenna was installed in the center of the cross mark. The antenna height is an important parameter.

Figure 4 provides an example of the image resolution in terms of the Ground Sample Distance (GSD) using the 35 mm and 50 mm optical cameras at a height of 500 meters. The defined image data rate is of 1 Hz. Each aerial image frame is synchronized with GNSS and inertial navigation system capturing the GNSS position and the image attitudes (i.e., the exterior orientation of the camera system) at the time of exposure.

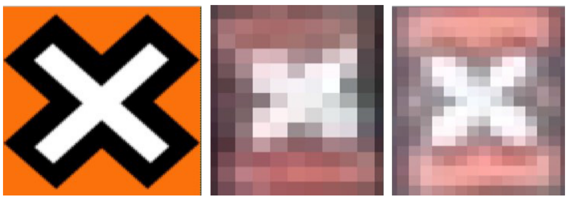

Fig. 4 Resolution comparison between the original magnetic sticker marker and the imaged magnetic sticker with 10 cm GSD and 7 cm GSD, respectively.

Determining the exact position of the GNSS antenna in the image sequence is an important part of image processing and is done automatically. It is based on an NCC matching algorithm, see Fig. 5. The aerial images are then georeferenced by a bundle adjustment method using GCPs, onboard GNSS and inertial measurements associated to the images, and automatically highly dense matched tie points. The method is independent of the type of GCPs provided for the method. The most important aspect to consider in relation to the GCPs is accuracy, which should ideally be in the centimetre range.

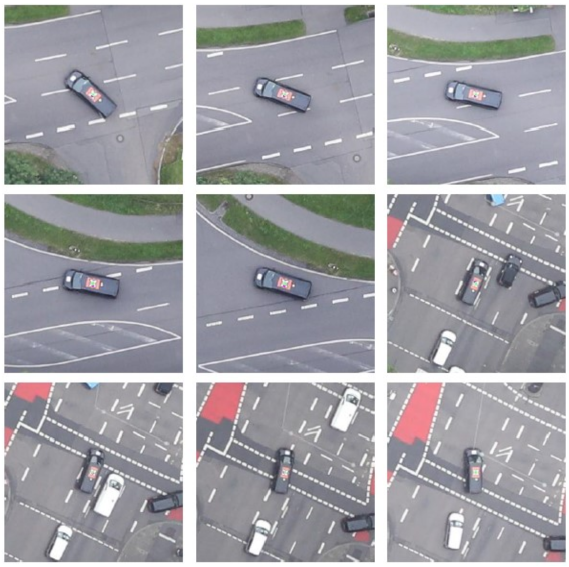

Fig. 5 A series of aerial image sequences with the cross center in the middle of the image patch obtained during the test campaign.

The test architecture allows several SUTs, in our case several GNSS receivers, to be tested simultaneously. This is also important for certification purposes. Two different types of GNSS receivers were used as part of a test campaign. A high-quality GNSS receiver (multi-constellation and multi-frequency) that can use RTK corrections and a GNSS receiver for the automotive industry (multi-constellation and single frequency) were used (see Fig. 6).

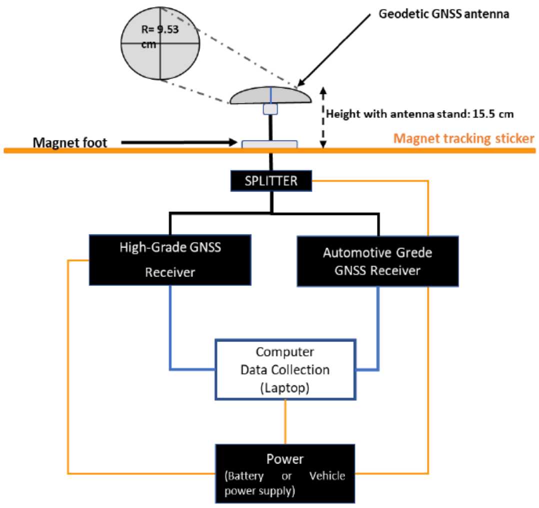

Fig. 6 Architecture used during a test campaign. During which two different GNSS grade receivers were tested.

In July 2021, the procedure was put into practice in a test campaign. The test campaign was conducted on two consecutive days. On the first day, the GNSS RTK corrections from the high-quality GNSS receiver could be used.

On the second day, the same test architecture was used, but this time without GNSS RTK corrections for the high-quality GNSS receiver. This allows the performance and behaviour of the GNSS receivers to be compared.

Two nadir-looking cameras of the DLR 4k camera system on a helicopter were used to record the aerial image sequences. The predefined test routes included various real environmental scenarios in the Munich area and in the city. In this way, it was investigated how the quality of the GNSS sensors is influenced by the environment and what added value the new method can offer. The test tracks include three different test cases: in the countryside, on the motorway and in the city of Munich and its surroundings (see Fig. 7). These cases can be traced back to the scenario types described in the CEN/CENELEC EN 16803 series [2]. This aspect is important when developing or defining a certification scheme, as the certification scheme can be based on standards or elements of existing standards. An example of scenario type is "*standard old big cities with relatively narrow streets, but sometimes large avenues or ring roads, with buildings from medium height to tall, masking angles up to 60° generating frequent multipath and non-line-of -sight phenomena*" which applies to the city of Munich.

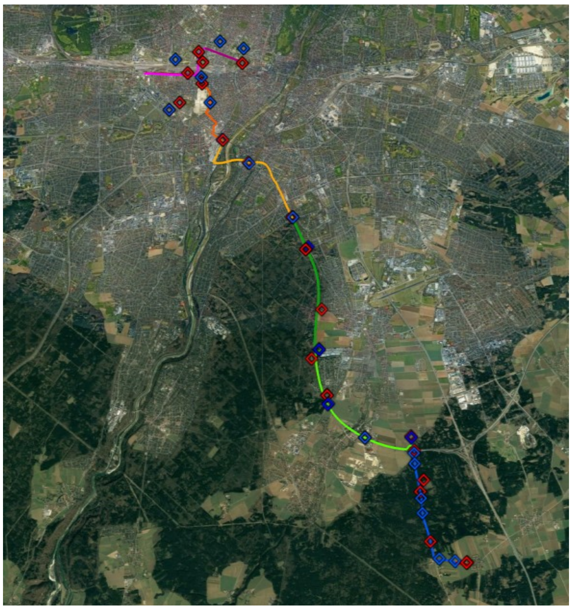

Fig. 7 Test cases: rural (in ***dark blue****), highway (in* ***green****) and urban (in* ***light and dark orange****, and* ***purple****). The diamond symbols depict check points (in* ***blue****) and ground control points (in* ***red****), respectively.*

As can be seen in Fig. 8, deviations of different degrees are seen for both high-end and automotive receivers. This is particularly surprising for the high-quality receiver, as this receiver used RTK corrections on the first day of the campaign.

Fig. 8 Examples showing deviations regarding the derived vehicle positions by the high (in ***red****) and automotive (in* ***blue****) grade receivers as compared with the new method (in* ***yellow****). During this test GNSS RTK corrections were used.*

On the second day of the test campaign, the same settings were used, except that the high-grade GNSS receiver did not use RTK corrections.

Figure 9 shows situations where the position solution of the high-quality GNSS receiver deteriorates significantly when using multiple constellations and multiple frequencies. In these situations, the position solution is even much worse than that of a typical automotive GNSS receiver.

The new method proved to be resilient and robust to situations where GNSS position accuracy degrades, even when RTK is used, as local effects do not affect the method.

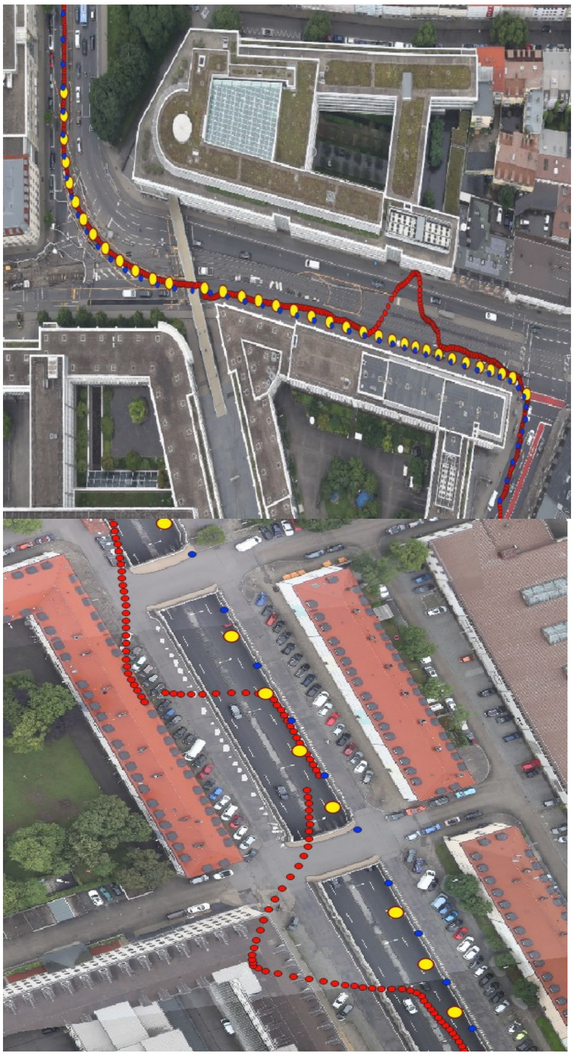

*Fig. 9 Examples showing deviations regarding the derived vehicle positions by the high (in **red**) and automotive (in **blue**) grade receivers as compared with the new method (in **yellow**). During this test **no** GNSS RTK corrections were used.*

These situations show that using a high quality GNSS receiver as an RS to build a GTRT can be problematic, as it operates on the same principles and is therefore subject to the same errors and problems as the GNSS receiver under test. It is therefore important to use test methods that are as independent as possible from the operating principles of the SUT. The new proposed method goes exactly in this direction by avoiding the use of GNSS measurements at the level of the vehicle, where problems often occur, as is the case with multipath effects.

Certification results

As described in the previous sections, the proposed method has been shown to be resilient and robust to situations where the derived position accuracy of a purely GNSS-based reference system degrades. This has also been observed when using RTK-GNSS corrections, as local effects affecting GNSS signals have no impact on the airborne method used. Since the proposed method provides more accurate data than the SUT and performs very well in all use cases, it can also be used for conformity assessment. One form of conformity assessment is certification. The certification aspect is very important for OEMs and Tier 1 companies as it increases confidence in a product by ensuring that the specified requirements are met and thus certified GNSS equipment has a distinct market advantage over equipment without certification. We have developed a test scheme for certification purposes. The certification scheme and certification content include three categories of accuracy levels associated with horizontal and vertical position errors. These accuracy levels or classes are linked to the use case, i.e., highway, urban or rural. This certification system allows the selection of one or more accuracy classes. We have followed the principles proposed in standards [2] and [3] in defining the classes and criteria, except that we have defined our values based on the value of 20 cm at 68.3rd percentile proposed in [7]. This scheme was defined for the case where an OEM, Tier 1 or manufacturer is interested in certifying its GNSS sensor(s) for only one class. In the context of testing and certification activities, in addition to defining the classes, it is important to define the metrics to be applied, the pass/fail criteria and the sample size. The proposed pass/fail criteria are based on the mean values of HPE/VPE and in particular on the 95.4 percentiles of HPE/VPE as defined in Table 1.

Tab. 1: Proposed accuracy classes definitions and associated pass/fail criteria for the proposed certification scheme.

Accuracy Metrics	Position Error		
	Class I - Urban	Class II – Rural	Class III - Highway
	Maximum Horizontal Position Error [m]		
HPE | 68.3^{th} percentile	≤ 0.20	≤ 0.25	≤ 0.33
HPE | $\mathbf{95.4^{th}}$ percentile	$\leq \mathbf{0.40}$	$\leq \mathbf{0.50}$	$\leq \mathbf{0.66}$
HPE | 99.7^{th} percentile	≤ 0.60	≤ 0.75	≤ 1.00
	Maximum Vertical Position Error [m]		
VPE | 68.3^{th} percentile	≤ 1.00	≤ 1.20	≤ 1.50
VPE | $\mathbf{95.4^{th}}$ percentile	$\leq \mathbf{2.00}$	$\leq \mathbf{2.40}$	$\leq \mathbf{3.00}$
VPE | 99.7^{th} percentile	≤ 3.00	≤ 3.60	≤ 4.50

The minimum sample size required for each class is based on the statistical consideration that the measurement error must be ten times better than the confidence level of 95.4 defined for the selected accuracy class. With these considerations in mind, 625, 400 and 230 measurement samples were defined for classes I, II and III, respectively. This is also a requirement for the proposed method, as this minimum number of samples must always be achieved during the test campaign for both the proposed method and the SUT. After the test campaign, the data were processed. The aerial photo data were used to define the GTRT. The high-grade and automotive grade type GNSS receiver's trajectory position data were then compared to the GTRT. The analysis and position error results show that only one GNSS receiver would be eligible to receive certification, and only for one class type. The main certification results are summarised in Table 2.

Tab. 2: Main results of the of accuracy analysis according to classes definitions for the proposed certification scheme. The results show that only one GNSS receive, the high-grade GNSS receiver, could be certified for the highway class type and, solely, when using RTK corrections.

Track Case/ Device	$p_{HPE}^{68.3th}$ [m]	$p_{HPE}^{95.4th}$ [m]	$p_{HPE}^{99.7th}$ [m]	$p_{VPE}^{68.3th}$ [m]	$p_{VPE}^{95.4th}$ [m]	$p_{VPE}^{99.7th}$ [m]
Rural						
High-Grade (RTK)[1]	0.33	1.24	1.81	0.25	2.76	4.60
High-Grade [2]	0.30	1.20	3.71	0.68	1.06	1.45
Automotive-Grade [1]	1.56	2.75	3.07	2.22	5.65	6.90
Automotive-Grade [2]	2.12	2.90	5.73	2.08	4.71	7.79
Highway						
High-Grade (RTK) [1]	0.21	**0.34**	0.62	0.07	**0.11**	0.37
High-Grade [2]	0.41	0.60	1.05	0.24	0.47	0.83
Automotive-Grade [1]	0.60	0.90	1.09	1.27	2.97	3.32
Automotive-Grade [2]	1.25	1.79	3.96	2.63	3.94	4.45
Urban						
High-Grade (RTK) [1]	0.29	0.86	4.74	0.06	1.26	16.8
High-Grade [2]	1.51	4.33	26.46	1.90	5.90	20.1

Automotive-Grade [1]	1.18	2.23	3.48	2.30	4.01	6.39
Automotive-Grade [2]	1.21	2.48	5.82	3.90	5.75	6.41

[1] First day of the testing campaign. [2] Second day of the testing campaign.

Generally, certification is based on standards or regulations. However, the certification of GNSS devices for autonomous road vehicles supporting automated driving functions is currently neither standardised nor regulated. As there are currently no bidding GNSS-based standards or regulations for automated driving, certification would be based on a voluntary scheme .For the proposed voluntary certification system with the defined pass/fail criteria, only high-quality receivers and only when using RTK corrections could be certified as Class III - highway. As shown in the main results in Table 2, neither the high-quality receiver itself using RTK corrections, nor the GNSS receiver for vehicles could meet the proposed criteria. However, with the advancement of technology and the use of more GNSS constellations and frequencies by the receivers, it is expected that better performance will be achieved, so it is likely that the proposed pass/fail criteria will be met and thus certification based on a voluntary scheme can be obtained.

Conclusions

A conformity process based on testing principles is introduced. The conformity process is based on a certification scheme aiming at certifying and validating GNSS receivers, in the automotive domain, addressing the L3 and L4 levels of automation under real world conditions. The certification system uses a new method that provides a GTRT based on high-resolution aerial imagery from a test vehicle equipped with a GNSS receiver. The imagery is precisely geo-referenced with high accuracy GCPs, allowing accurate positions of the vehicle of ~10 cm to be derived. This new method has proven to be resilient and robust to situations where the GNSS position accuracy of the receivers used has degraded due to local effects, even using RTK-GNSS corrections. The presented method provides a reference trajectory for motor vehicles in GNSS critical areas, e.g., in environments where GNSS is denied, subject to multipath effects, etc., which are not only a problem when evaluating the intrinsic GNSS performance of the equipment during testing, but also when the reference system is GNSS-based. This method can be used by OEM and Tier 1 companies during development and test activities to facilitate calibration, validation and performance evaluation of their positioning and navigation systems. As an independent method that provides highly accurate position data, it can also be used as a certification tool that GNSS receiver manufacturers can apply for to certify their products. From now on, the new method can be used for calibration and validation, supporting the developed conformance scheme required for certification activities, which will be used commercially by NavCert. As a certifier, NavCert can offer a voluntary certification service for GNSS receivers by issuing a certificate and providing the TÜV SÜD certification mark as proof of the achieved performance. The results show that this method can be used successfully for the process of certifying automotive type grade GNSS receivers aiming to reach L3 and L4 levels of automation

References

[1] SAE, International Technical Standard (2014). *Terminology for Motor Vehicle Automated Driving Systems*, https://www.sae.org/news/press-room/2014/10/sae-international-technical-standard-provides-terminology-for-motor-vehicle-automated-driving-systems

[2] EN 16083 Series (2020). Use of GNSS-based positioning for road Intelligent Transport Systems (ITS), CEN/CENELEC

[3] ETSI TS 103 246 Series (2020). GNSS based location systems, ETSI

[4] F. Kurz., D. Rosenbaum, D. Meynberg, O. Mattyus, P. Reinartz, (2014). *Performance of a real-time-sensor and processing system on a helicopter*. ISPRS - International Archives of the Photogrammetry, Remote Sensing and Spatial Information Sciences, 189-193.

[5] U. Balss, C. Gisinger, X. Cong, R. Brcic, S. Hackel, and M. Eineder (2014). *Precise Measurements on the Absolute Localization Accuracy of TerraSAR-X on the Base of Far-Distributed Test Sites*. In Proceedings of the 10th European Conference on Synthetic Aperture Radar (EUSAR), pp. 993-996. VDE Verlag. EUSAR 2014, 3.-5. June 2014, Berlin.

[6] Kurz, F., Mendes, P., Gstaiger V., Bahmanyar, R., d'Angelo, P., Azimi, S.,

Auer, S., Merkle, N., Henry, C., Rosenbaum, D., Hellekes, J., Runge, H., Toran, F., Reinartz, P., 2022, Generation of reference vehicle trajectories in real-world situations using aerial imagery from a helicopter, ISPRS Annals, Nice, France - Accepted.

[7] EUSAP Report (2019). *Report on road user needs and requirements*. GSA-MKD-RD-UREQ-250283, Revision 2.0, July 2019

DOI 10.5162/ettc2022/3.3

A novel Robust and Precise Timing Facility for Galileo

P. Kindl, L. Agazzi, T. Schilling, M. Schmitt, and J. Furthner
DLR Galileo Competence Center
Oberpfaffenhofen, D-82234 Wessling, Germany

pia.kindl@dlr.de

Abstract:
A fundamental component in each Global Navigation Satellite System is the timing facility, which is responsible for the synchronization of all elements within the ground segment as well as for the satellites in space. Different concepts exist to provide a time scale that fulfils all requirements, e.g. master clock principle, weighted clocks or composite clock algorithm. In the European Global Navigation Satellite System Galileo, the so-called Precise Timing Facility (PTF), located in Oberpfaffenhofen, Germany, and Fucino, Italy, has the task to provide the Galileo System Time (GST). The actual published design of the PTF depends on a master clock principle and is therefore sensitive to failures of individual units within the GST generation [1].

At DLR Galileo Competence Center we propose an alternative design for such a timing facility, which is called Robust Precise Timing Facility (RPTF). The focus of the concept is on mitigating technical vulnerabilities and increasing the tolerance to the failure of any of the components of the existing PTF.

In this paper we present the concept, current status and future plans for such a RPTF to generate robust system timescales for the next generation of the European satellite navigation systems. The aim is to build, test and characterize the RPTF under the aspect of a 24/7 operational service. The key element is the combination of all the individual atomic clocks in the facility via the composite clock approach to generate a weighted average, the so-called Implicit Ensemble Mean (IEM), and to provide redundancy and test opportunities in case of hardware and software failures.

Key words: Galileo, Robust Precise Timing Facility, active hydrogen maser, short- and long-term stability, composite clock

Introduction

The task of the Precise Timing Facility (PTF) is to generate, maintain and distribute the Galileo System Time (GST) with the aim of providing a very stable time reference for navigation purposes and of disseminating timing information synchronized to UTC/TAI to the Galileo users. Therefore, it is very important that the PTF provides both short- and long-term stability.

The setup of the PTF is shown in Fig. 1. The so-called master clock principle, employing a high-precision clock with very good short-term stability, an active hydrogen maser (AHM), is used as basis for the GST generation. The derived timing signals are subsequently distributed to all Galileo segments. A second AHM is used as backup source and its output signals are steered to the signals of the master AHM in order to avoid a frequency offset and an integrated time offset. The medium- and long-term stability is guaranteed by cesium clocks and by using the measurement data provided by the Time Service Provider (TSP) for UTC/TAI. If the master clock or one PTF component shows an error or fails while generating the system time, no correct time scale will be provided and the end customer will not able to use the Galileo system for position determination. Therefore, in order to avoid “single points of failure”, two PTFs are operated in the Galileo system. They are located in Oberpfaffenhofen (Germany) and in Fucino (Italy) and are synchronized to a certain degree of accuracy via satellite connections: Two-Way Satellite Time and Frequency Transfer (TWSTFT) and GPS All-in-View (AV). However, in the case of regular maintenance of one of the PTFs, there is no further redundancy in the system. This led to the failures of the Galileo system in autumn 2018 and summer 2019, with the last incident lasting more than five days. As upgrades and replacements of system components are to be expected in the ongoing and future operations of Galileo, it is foreseeable that during their occurrence, due to the consequent lack of further delocalized and redundant PTFs in the Galileo system, any disturbance or fault may result in reduced availability, degradation, or failure of the PTF, the GST, and potentially of the entire Galileo system.

Examples of such disturbances and faults include but are not limited to:

- frequency and phase jumps of the clocks and of other PTF elements
- errors in the measurement instruments
- wrong GST time distribution to other elements of Galileo Ground Segment
- loss of TWSTFT or AV, e.g. due to jamming and/or spoofing of the received satellite signals
- non-availability of backup PTF in case of maintenance
- software failures, especially when abnormal situations occur that are often not considered or tested
- missing monitoring capabilities/parameters to assess the operational status of the PTF

In order to mitigate these technical vulnerabilities and to increase the tolerance to the failure of any PTF component, we propose the concept of the RPTF. Its design is based on the introduction and integration of the features described in the following section. Its architectural implementation is presented in Fig. 2, along with the connection to external partners.

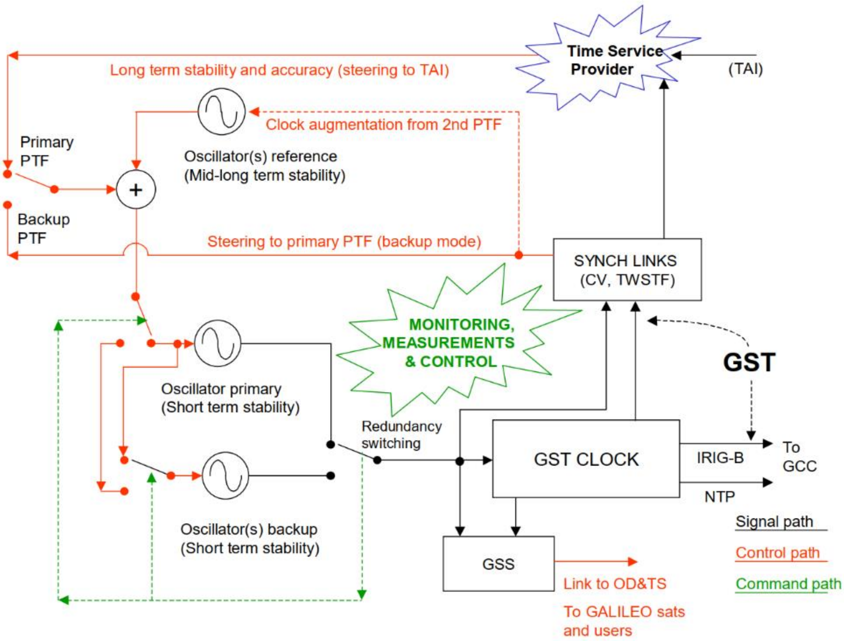

Fig. 1. Functional operation of the Galileo PTF, actual published scheme from [1]. The master clock principle, with primary and backup oscillators, and the two PTFs are depicted.

DOI 10.5162/ettc2022/3.3

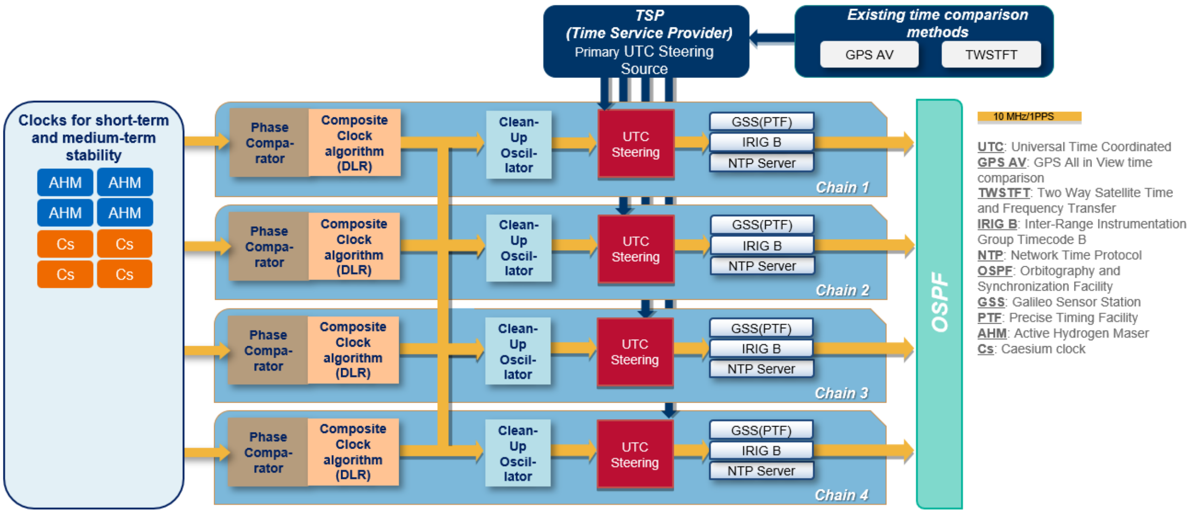

Fig. 2. The proposed RPTF architecture, including all four chains

Realization of the Robust and Precise Timing Facility

One of the main objectives of the RPTF is to increase the reliability of the system. Instead of the master clock principle, with its intrinsic weaknesses, a Composite Clock Algorithm (CCA) based on Kalman filters as proposed in [2] will be implemented. This generates an Implicit Ensemble Mean (IEM) of all available clocks located at the RPTF, i.e., a weighted average of the contributions of each clock, and it generally outperforms each clock in the ensemble in terms of stability. Currently, four (4) AHMs (T4Science iMaser 3000 and MicroChip MHM 2020) and four (4) cesium high-performance frequency standards (MicroChip 5071A HP) are used to realize the RPTF (see Fig. 2), but the algorithm can be expanded so that any number of clocks can also be added, e.g., from the ground and the space segments. Besides the improved stability another advantage of the IEM is the robustness of the output against phase and frequency jumps, failures or replacement of clocks. In extreme cases, up to seven of the eight existing clocks in the RPTF can fail without any major restrictions on the generation of the system time. Of course, depending on the failed clocks, the accuracy of the generated time scale may be reduced, but it is still available for the Galileo system and no general system failure can occur. These arguments make the use of the IEM for the generation of system time a straightforward choice.

To elaborate further on this point, the clocks are measured with respect to each other in a multi-channel phase comparator. The measured signals are then fed into a Kalman filter which estimates the future states of each clock and implicitly provides the system time of the ensemble in terms of the IEM, a so-called paper clock. As mentioned, the IEM generally exhibits a better stability for all sample intervals than every single clock in the ensemble. However, this quantity is not directly available in hardware, since it requires knowing the exact state of each clock at each time step, which is not directly measurable. Nonetheless, it can be realized by steering a clock signal towards the IEM with a dedicated control loop containing a second Kalman filter and a regulator which computes the control action to be applied. This way, the output of the steered clock provides a physical realization of the IEM. This CCA implementation is based on more than ten years of both theoretical and applied experience gathered at the Institute of Communications and Navigation at the German Aerospace Center (DLR) [3].

Another important aspect of the RPTF design is that not only the clocks, but also the measuring instruments (e.g., phase comparators) will be acquired from at least two different manufactures for the same functionality and similar quality (dual source), so that a direct comparison of the measuring instruments under the same conditions can be performed. This applies not only to the hardware but also to the software. For example, the same CCA could be implemented in two different programming languages.

Furthermore, the RPTF elements will be arranged in four chains, each running an independent comparison of all the clocks and generating an independent IEM. The physical representation of the IEM for each chain is then fed as input to a clean-up oscillator that acts as a failover clock switch: it tracks all selected input channels and switches automatically between them in case of failure of the selected main input channel while maintaining phase coherence. Assuming all IEMs are identical when suddenly a chain is faulty or an IEM input at the clean-up oscillator goes missing, no change at the output of the clean-up oscillators will be seen, as the device automatically switches between the four IEM chains. Afterwards, the output of each clean-up oscillator is steered to UTC. The primary source for steering is the product of the Galileo Time Service Provider (TSP) whose results are based on TWSTFT and GPS AV measurements for the GST. In our case, we have no access to the results of a TSP and no TWSTFT station at Oberpfaffenhofen. Therefore, we steer the IEM/clean-up oscillator output to UTC only by GNSS All-in-View. This steered output is provided to a GNSS receiver, which measures the clock offset of each individual GNSS satellite to the system time, and to a Network Time Protocol (NTP) server for distributing the resulting system time to all system elements where date and time is needed. In addition, the timing signal is also distributed with IRIG-B. Besides, there are further developments that should be taken into consideration while implementing the RPTF: Precise Time Protocol (PTP) and White Rabbit. Both modern protocols can improve the robustness of Galileo.

The choice to use four chains is based on the following arguments:

- two chains already offer higher redundancy compared to one only. However, as soon as one element in one of the two chains shows faults, fails and needs to be replaced, or undergoes standard maintenance, or the software of the CCA is updated, the redundancy of this approach is removed.
- the addition of a third chain increases the redundancy and enables the self-indication of the best system time representation in the RPTF via the three-cornered hat method. Therefore, in order to detect anomalies in the chains one can check if the generation of the IEM in the different chains is identical. This way an error in the chains, e.g., a phase jump after the clean-up oscillator can be detected immediately. These three chains represent the operational chains.
- the setup of a fourth chain has the advantage that it can serve as test bed for new algorithms or hardware components. It acts as a backup-chain for troubleshooting activities and in case one of the other three chains is in maintenance.

Fig. 3 shows the detailed structure of a single chain, whereas Fig. 5 shows pictures of two of the four AHMs, the cesium clocks, and one of the four RPTF chains, being arranged in a single rack. Besides the elements already mentioned above Fig. 3 displays various frequency and pulse per second (PPS) distribution units that amplify and distribute the signals within the RPTF, and measurement equipment that compares the states of the four chains. Not only the 10 MHz frequency signals but also the 1 PPS timing signals will be compared to each other, the latter via time interval counters (TIC). Multiple comparisons occur: after generating the four IEMs, the clean-up oscillator, the UTC steering, the time distribution (NTP), and the GNSS receivers. These “check elements” combined in orange shade in Fig. 3 represent the necessary measuring instruments needed for the investigation of availability and accuracy of the system time of the RPTF after different steps of generation. They are part of an agent-based health manager with the task of checking the output of the RPTF versus expected values and ensure that error states are not transferred to further elements, for example the Galileo system. The health manager has capabilities in continuous monitoring, anomaly detection, diagnostics and prognostics so that element failures can be promptly detected and compensated for during operational use. The health manager also allows a detailed view of all processes in the past and supports the analysis in case of troubleshooting. Additionally, combining the results of the health manager and the information of the behavior of the used equipment (e.g., aging processes) one can predict the behavior of the RPTF system time generation.

This, together with the dual source concept, will ensure that supplier-specific weaknesses or errors will not be able to affect the availability of the system. Even a replacement of equipment, e.g., within a necessary calibration cycle, is made possible with this approach and the multiple redundant setup, without the risk of a complete failure of the system time generated by the RPTF.

DOI 10.5162/ettc2022/3.3

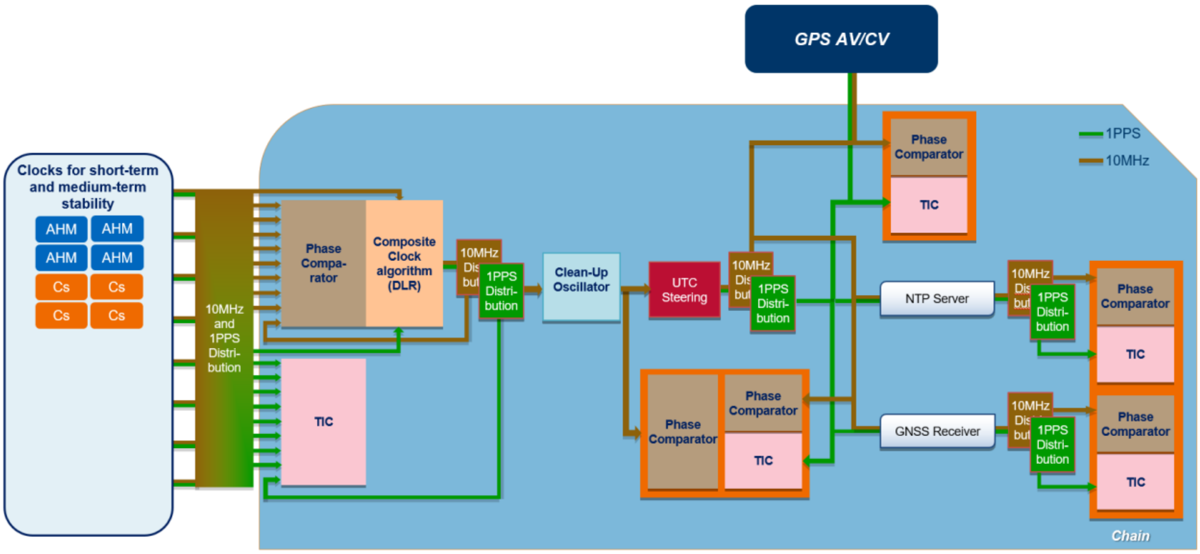

Fig. 3. Detailed structure of a single chain.

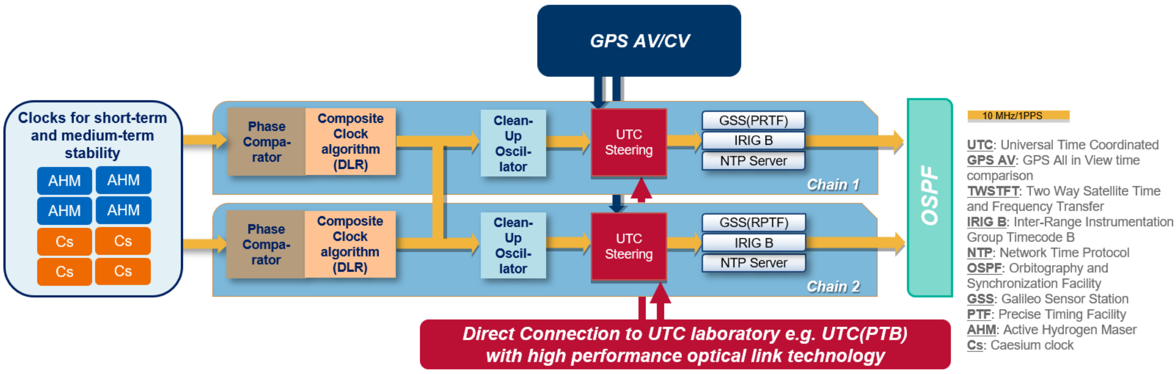

Fig. 4. Fiber link implementation demonstrated on 2 chains.

Fig.5. From left to right: two of the four AHMs; the cesium clocks; one of the RPTF chains, arranged in a rack.

DOI 10.5162/ettc2022/3.3

In recent years it was shown that the current spatial diversity in Galileo given by the two locations of the PTFs in Oberpfaffenhofen and Fucino alone cannot guarantee the desired reliability of Galileo. Therefore, alternative connections to external time laboratories are presently being researched to achieve higher availability, redundancy and increased robustness of the GST. To this end, the proposed RPTF foresees a fiber link connection of the RPTF to the Physikalisch-Technische Bundesanstalt (PTB) which is responsible for the legal time in Germany (Fig. 4). This way, the system time generated in the RPTF can be compared directly with the German time and the UTC world time. The fiber link connection promises an accuracy below 100 ps in the long-term behavior which represents an improvement by at least a factor of 10 compared to actual standards used in the Galileo system; not to mention the much higher data rate exchange (e.g., every second) if compared to other standard methods such as GPS AV or TWSTFT.

Outlook

In conclusion, with our suggested approach of the RPTF, we assume that the currently published Galileo PTF will be significantly improved in terms of robustness.

The hardware and software implementation of the RPTF is currently under realization. A detailed evaluation of the RPTF elements with regard to reliability, availability, maintainability, and safety (RAMS analysis) is forthcoming. This analysis will classify the RPTF elements according to failure conditions and will clearly ensure that a failure of one or more elements only reaches a certain risk status of the RPTF and thus of the Galileo Systems.

Future developments include, but are not limited to:

- testing of advanced methods for distributing the RPTF-generated system time to all elements of the Galileo ground segment, e.g., PTP and White Rabbit
- testing against non-nominal satellite signals by using GNSS signal simulators
- and finally, the integration of atomic clocks in the time laboratories of other well-established European metrological institutions (in addition to PTB), to generate an even more robust, accurate, and geographically diverse GST by means of fibre optical connections and the composite clock approach

The start of operations of the proposed Robust and Precise Timing Facility is planned for the beginning of 2023.

References

[1] X. Stehlin, Q. Wang, F. Jeanneret, P. Rochat, and E. Detoma, “Galileo system time physical generation,” Proceedings of the 38th Annual Precise Time and Time Interval Meeting (PTTI), pp 395–406, December 2006.

[2] K. R. Brown Jr., “The theory of the GPS composite clock,” Proceedings of the 4th International Technical Meeting of the Satellite Division of The Institute of Navigation (ION GPS), pp. 223–242, September 1991.

[3] C. Trainotti, T. D. Schmidt, and J. Furthner, “Comparison of clock models in view of clock composition, clock steering and measurement fitting,” Proceedings of the ION Precise Time and Time Interval Meeting (PTTI), pp. 265–283, July 2019

DOI 10.5162/ettc2022/3.4

Performance Monitoring for Galileo and other GNSS at the Galileo Competence Center

Katharina Lutz[1], Lukasz Greda[1], Marios Smyrnaios[1], Wolfgang Dilg[1], Thomas Schilling[1], Ilinca Ioanid[1], Steffen Thölert[2], Gerardo Allende Alba[2], Martin Kriegel[3], Luca Spataro[4], Philipp Rosauer[4], Annika Meinecke[4], Rebecca Brydon[4], and Johann Furthner[1]
[1] DLR Galileo Competence Center, Oberpfaffenhofen, D-82234 Wessling, Germany,
[2] DLR Institute of Communications and Navigation, Oberpfaffenhofen, Germany,
[3] DLR Institute for Solar-Terrestrial Physics, Neustrelitz, Germany,
[4] DLR Institute for Software Technology, Cologne and Oberpfaffenhofen, Germany,

katharina.lutz-lloyd@dlr.de

Abstract:
Satellite navigation has become a vital part of our daily lives by ensuring navigation on land, in air and at sea, and by providing precise timing information for the energy, communications and finance sector. It is therefore essential to monitor the performance of the four main global navigation satellite systems (GNSS) Galileo, GPS, GLONASS and BeiDou. The Galileo Competence Center (GK), part of the German Aerospace Center (DLR), is dedicated to the further development of the European GNSS consisting of Galileo and EGNOS. Within the SigPerMon project, the GK monitors the reliability and quality of navigation signals with comparable metrics for all four GNSS, and detects deviations from the nominal state of navigation systems. Necessary data are sourced from a global network of GNSS receiver stations. These data are used to compute performance indicators to monitor and analyse the availability and health status of navigation signals, and the precision of positioning and timing solutions. In the future, machine learning models will be used to detect anomalies in the satellite signals. A summary of the results will be presented on a dedicated webpage, which provides both detailed analyses for authorized researchers and personnel, and interactive data visualizations for the general public.

Key words: Global Navigation Satellite Systems, Performance Monitoring, Machine Learning, Webpage, Receiver Network

Introduction

We present the new Global Navigation Satellite System (GNSS) performance monitoring system, which is currently being implemented at the Galileo Competence Center (GK).

The Galileo Competence Center was founded in 2019 as part of the German Aerospace Center (DLR). GK aims at furthering the development of the European GNSS Galileo and EGNOS, and at advising national and European government bodies as well as companies in the field of navigation technologies.

In this context, we are developing a comprehensive GNSS performance monitoring suite. We have started to analyse and monitor the reliability and quality of navigation signals. Furthermore, we want to detect any deviation from the nominal state of GNSS systems. In the future, we will disseminate warnings and information about detected errors to users and applications.

For each GNSS minimum performance levels have been defined by the respective governing bodies. GNSS operators regularly publish performance reports indicating how well the respective GNSS meets the minimum performance levels [1 – 4]. However, the performance indicators are at least partially different (e.g. the definition of healthy satellite signals is not identical for the four systems). In addition, the data used for the aforementioned computation are also not identical and are collected at different station locations using different equipment. Thus, a direct performance comparison of the different global navigation satellite systems is challenging and, in many cases, restricted to only a few performance indicators. Therefore, we aim to use, as far as possible, the same data processing framework to compute performance indicators for all four

GNSSs and perform the computation using the same global network of ground tracking stations.

To that end, we will establish and operate a dedicated GNSS receiver network with real-time data transfer capability and global coverage. The data from this network will be used for monitoring and an extensive and fair comparison of the performance of the four global navigation satellite systems. In addition, the receiver network will support the generation of real-time corrective data for precise point positioning services. Collected data will be stored in a dedicated database.

In this paper, we will give an overview of our current performance monitoring system and present future plans.

Data collection and storage

The data necessary for performance analysis and monitoring are stored in a dedicated database. Until our own global network of monitoring stations is fully deployed, we use RINEX observation files from the International GNSS Service (IGS) stations [5]. We selected stations, such that they are distributed around the globe and that receivers are set up as homogenously as possible.

Data from these stations are stored in our database, as are daily multi-GNSS merged navigation files and other auxiliary data sets. Most of these files are accessed via Nasa's Crustal Dynamics Information System (CDDIS) archive [6]. Data sets from other external and DLR internal archives are also stored in our database. These data sets can, for example, include reference station metadata, space vehicle information, ionospheric maps, and satellite orbits from other sources. Upon collection, the data are parsed, transformed into internally defined formats and stored in PostgreSQL tables, which are organised to best serve our needs. The input RINEX files are archived as well.

The database is structured such that it allows both a long-term analysis of the performance of all four GNSS, and a simple visualisation of the most important performance indicators on our webpage. The long-term analysis might either be a classical statistical analysis of key performance indicators (KPIs) or the usage of machine learning models to detect outliers in the data. In both cases, a major challenge is the identification and removal of faulty data. Such errors might be caused by receivers during data capturing, during data conversions, coming from data traffic, from data processing tools or other sources and can result in false anomaly detections [7]. A data cleaning process or quality check for the identification of errors not coming from the navigation systems themselves but rather from other sources can be significantly sped-up via the use of the database structures.

Performance indicators and deviation analysis

In cooperation with other DLR institutes, we are implementing and validating GNSS KPI and metric evaluation algorithms. Our goal is to compute and measure these parameters for all four GNSSs, so that we can establish a monitoring framework for each GNSS. The characterisation of their performances will be carried out in real-time or in post-processing, depending on the computed parameter.

We are particularly interested in evaluating:

- the availability of a GNSS for positioning and timing applications
- the accuracy of the information (e.g. clock and orbit parameters) sent by individual satellites
- the accuracy of positioning and timing solutions

To this end we are developing a monitoring system with real-time and reporting capabilities: We use recorded data from our database for a specified time range (e.g. a month) and calculate the statistics of availability and accuracy over this time range. Furthermore, we capture real-time data streams and evaluate the current status of the GNSSs. In both cases, data would be collected by the same network of reference stations distributed around the globe. Performance reports of the different navigation systems are published every few months by the respective operators. The parameters presented in these reports are not necessarily comparable. For our performance monitoring system, we will focus on performance parameters that are calculated in a similar way for all GNSSs and are thus comparable.

In addition, we also want to know in real-time how well the GNSSs are providing their services: does a user get a reliable and good positioning or timing solution right now? To answer this question, we need to analyse GNSS signals for a sufficiently large set of GNSS monitoring stations in real-time. This analysis will include parsing a stream of incoming real-time data, reading the health

DOI 10.5162/ettc2022/3.4

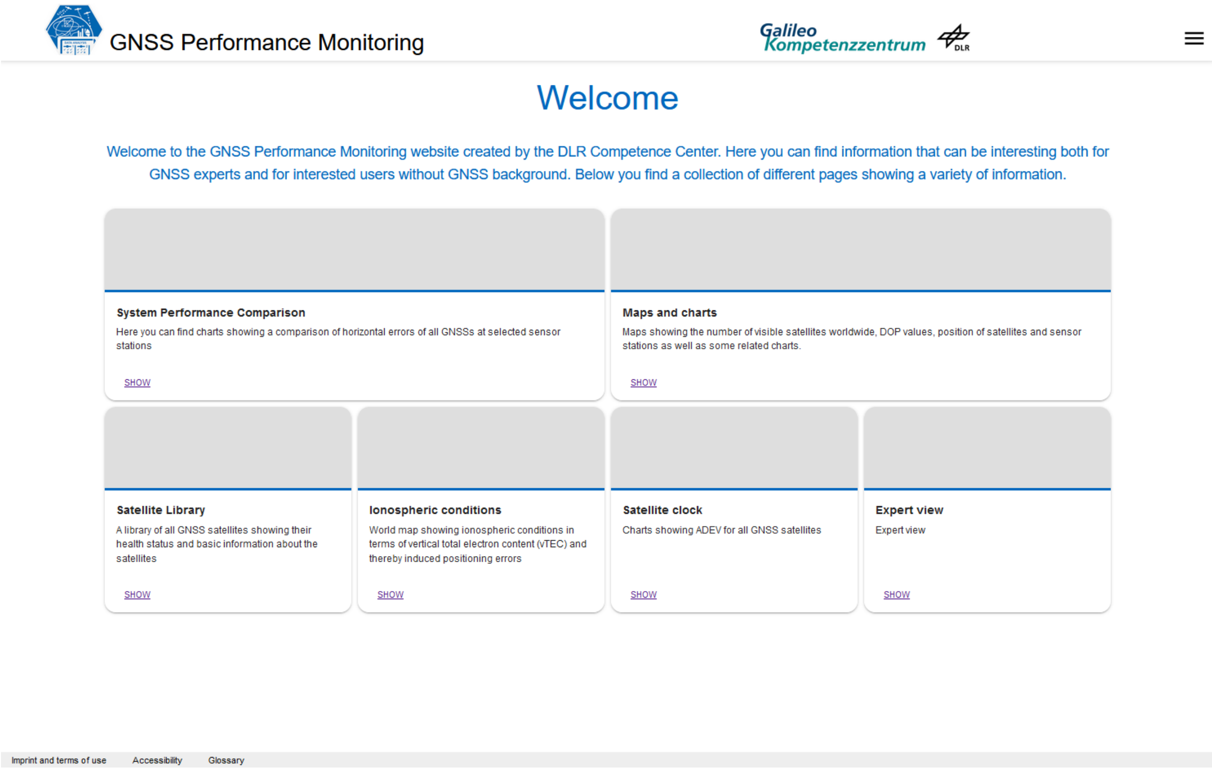

Fig.1.Landing page with overview of available features.

status of satellites, estimating the accuracy of their orbital parameters, calculating the position of the monitoring station, and comparing that result with the reference position for that station. Since the data rate we are using is one measurement per second, our algorithms need to be fast and efficient to tackle these large amounts of data in real-time.

While some irregularities in determining timing and positioning solutions can be deduced from comparing real-time results to long term statistics, we expect to get a more comprehensive deviation analysis with the help of suitable machine learning models. The dataset to train our models on will consist not only of observed data from sensor stations, but will also need to include simulated data. The simulated data are to be provided by a GNSS simulator and signal generator. This combination of different data sources for the machine learning training dataset is vital, because for example jamming and spoofing events are rare, but still need sufficient representation in a balanced training set. Besides a supervised machine learning approach based on neural networks in a long short-term memory architecture [8], the usage of unsupervised learning methods (e.g. auto-encoders, clustering models or a combination of both) will be essential to find unexpected or little-known faulty behaviour in observed data.

In summary, we are developing a multitude of methods to monitor the performance and quality of global navigation satellite systems in real-time and for long-term statistics. This information will in part be provided on our webpage.

A dedicated performance monitoring webpage

To visualise some of the computed GNSS performance parameters, we created a dedicated user-friendly website, which reads data from our database and illustrates a selection of performance parameters of all four GNSSs.

Fig. 1 shows the landing page of the website and provides a first overview of available features:

- System Performance Comparison: a visualisation of the comparison of the horizontal positioning accuracy of the four GNSSs
- Maps and Charts: a world map, on which positions of satellites and sensor stations are shown. As overlay, dilution of precision or visible satellite count maps at a given point in time may be selected. Time series of these data may also be visualised.

- Satellite Library: a library of all GNSS satellites informing about their current health status, orbit parameters as well as some additional basic information
- Ionospheric conditions: a world map with an overlay visualising the ionospheric conditions in units of vertical total electron content and the position error subsequently induced by the ionospheric conditions
- Satellite Clocks: Charts presenting the Allan deviation of GNSS satellites. This is a measure for the stability of the clocks onboard the satellites.
- Expert view: all of the above with extended possibilities to change settings.

The functionality and design of the website are continuously evolving [9]. In the following sections, we will describe the current features in more detail and provide an outlook for future developments.

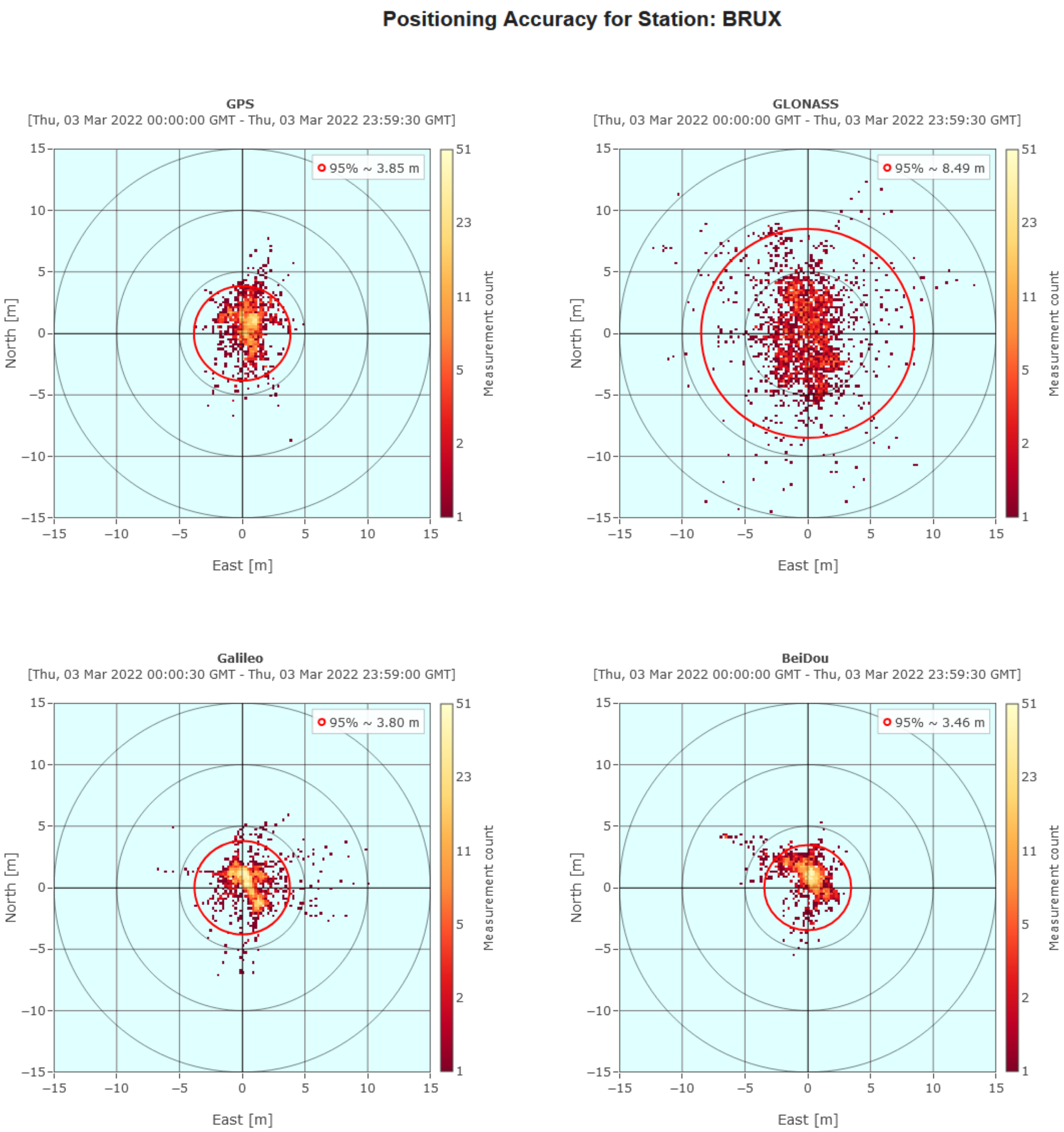

Fig. 2. Positioning accuracy in Northerly and Easterly direction for GPS, GLONASS, Galileo and BeiDou (left to right, top to bottom) at IGS station BRUX on 2022-03-03. The red circle indicates the 95th percentile of the error distribution.

DOI 10.5162/ettc2022/3.4

System Performance Comparison

To visualise the horizontal error in determining the user position, we calculate the user positions from observations in RINEX files of IGS stations. These files provide measurements for every 30 sec. The North and East-wards distance between the calculated single point position and the known, precise station position are then displayed on our website (see Fig. 2).

In the future this feature will be extended to use real-time data at a higher rate (measurements every 1 instead of 30 sec).

Fig. 3. Different Visualisations of calculated DOP values. (a) PDOP for Galileo with satellites included as soon as they rise more than 5deg above the horizon. (b) PDOP for Galileo in urban canyons, i.e. satellites are only included above elevations of 20deg. (c) Time series of all DOP values in Nuremberg over a week in April 2022.

Maps and Charts

This feature allows to visualise world maps and time series of dilution of precision (DOP) values and visible, healthy satellite counts. Moreover, positions of sensor stations and satellites are shown. Stations and satellites can be connected depending on whether or not satellites are currently visible from the sensor station given the selected elevation mask.

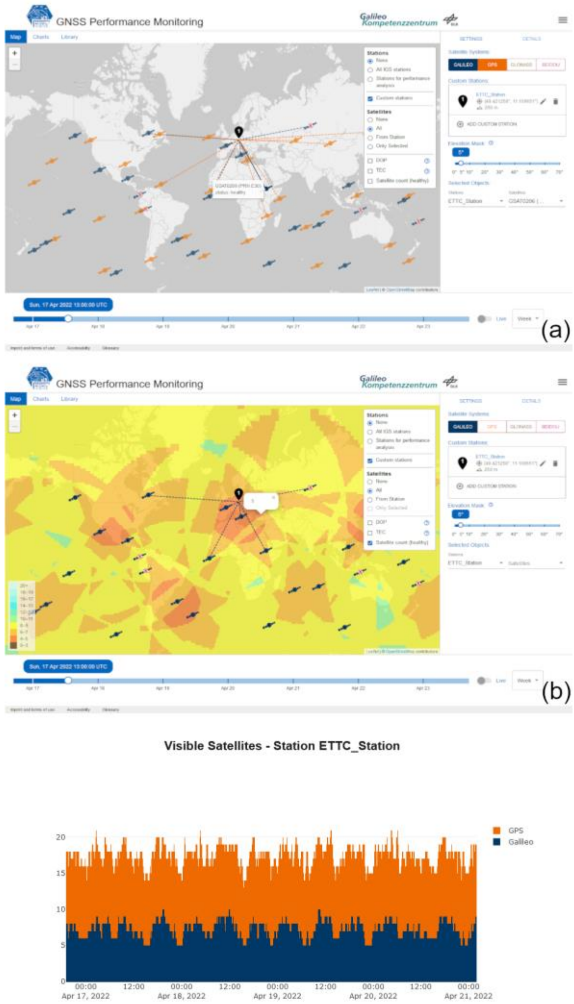

Fig. 4. Visualising satellite positions and availabilities. (a) Location of all GPS (orange) and Galileo (blue) satellite around lunch time on 2022-04-17. Satellites that are visible from Nuremberg are connected with the user-defined station marker. (b) A map of the number of visible satellites. (c) A time series of the number of satellites visible from Nuremberg during a week in April 2022.

The calculation of different DOP values (PDOP, GDOP, VDOP, HDOP, TDOP) requires the position and velocity of the GNSS satellites. These are based on orbital parameters in NORAD Two-Line Element (TLE) Set Format provided by CelesTrak [10]. For the calculation of DOP values all visible and healthy satellites are used. The user has the option to set the cut-off elevation angle and to exclude any satellite. For examples of different visualisations of the calculated DOP values see Fig. 3.

Similarly, the number of visible GNSS satellites at any point on the 2D world map is calculated using TLE data for all healthy satellites. Examples for visible satellite number and satellite position visualisation are given in Fig. 4.

Satellite Library

The satellite library aims to be a one stop shop for all information regarding single satellites. This information includes the health status of satellites, their current orbit parameters and more details such as their launch date, NORAD identifier or nicknames. An example is shown in Fig. 5.

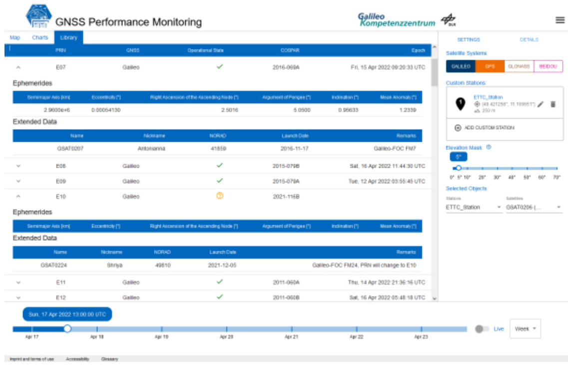

Fig. 5. The satellite library with details displayed for E07 and E10. Note how the status of newly launched GSAT0224 is still set to testing while other Galileo satellite are healthy and operational.

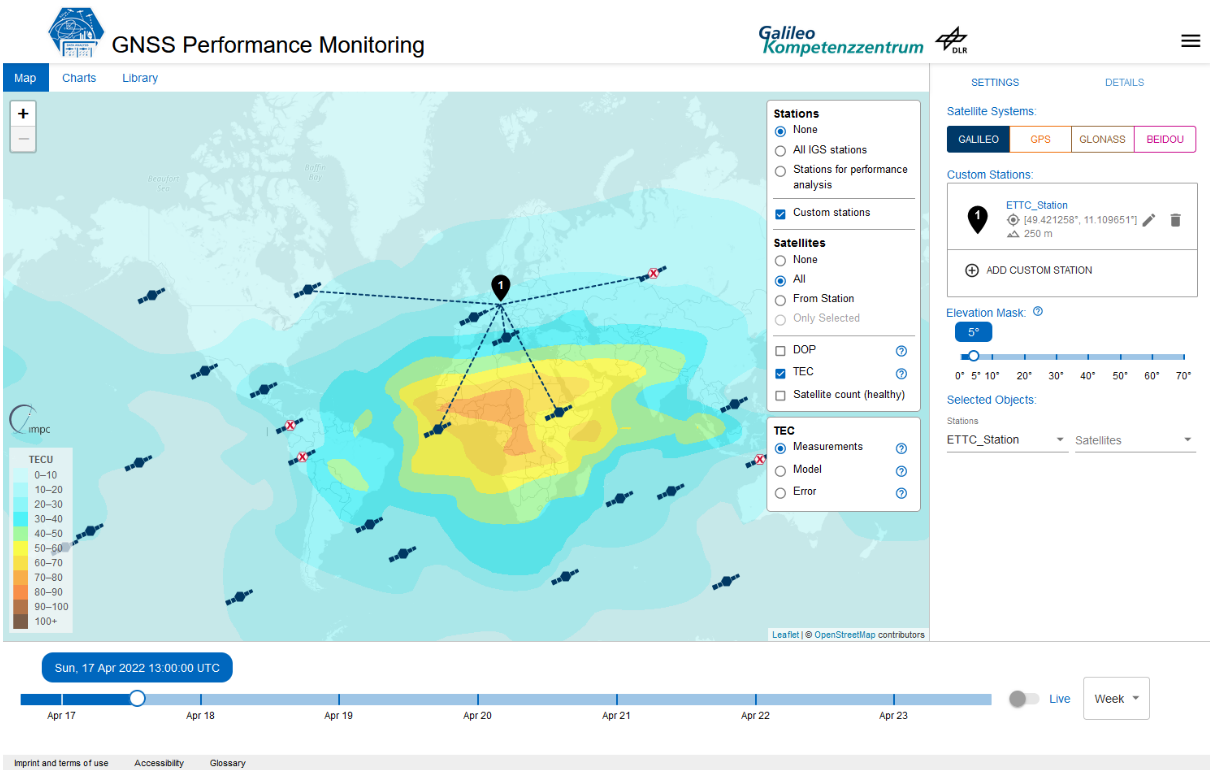

Fig. 6. Ionospheric conditions around lunch time on 2022-04-17.

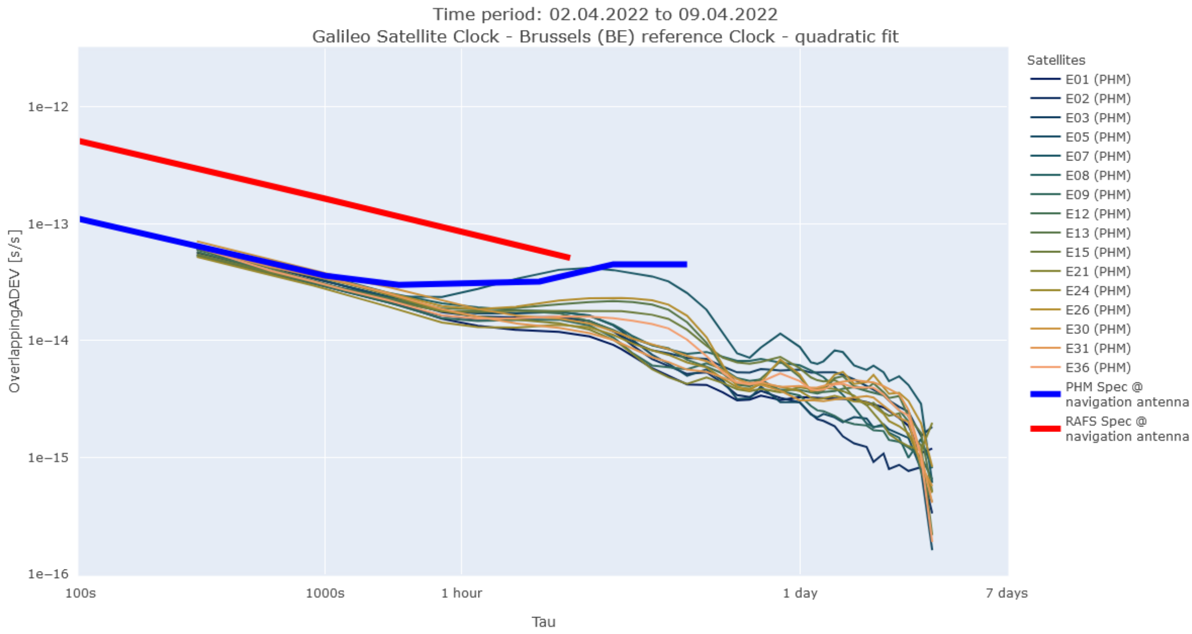

Fig. 7. The overlapping Allan Deviation for all healthy Galileo satellites for the time range from 2022-04-02 to 2022-04-09.

Ionospheric conditions

Space Weather related effects such as solar flares, coronal mass ejections (CMEs) and radio bursts can severely affect GNSS performance by causing rapid changes of the Earth's geomagnetic and atmospheric conditions (e.g. increased ionization, strong plasma density irregularities and associated gradients) at various temporal and spatial scales. To monitor ionospheric conditions, the website offers a two-dimensional visualisation of vertical total electron content (vTEC) on a world map. The user can switch between measured, modelled and error data (see Fig. 6). The vTEC data are provided in near real-time by DLR's Ionosphere Monitoring and Prediction Center (IMPC) [11], with an update rate of 5 minutes.

Satellite Clocks

The frequency stability of a clock can be characterised by measuring its overlapping Allan deviation. We obtain these measurements for GNSS satellite clocks using precise clock corrections from GFZ Potsdam [12]. The calculations are run with a Python script making use of the package AllanTools [13].

Expert View

While the above views will be limited to only a few user settings, we will also offer an expert view. The expert view is aimed at users, who work in the field of satellite navigation and need very detailed analyses. We want the expert users to be able to select options that are most suitable for their use case. In other words, the expert view is envisioned as a contrast to the other views, which come with many pre-set options and should make the usage of the website easy for the interested public and political decision makers. Furthermore, detailed analyses will be made available, which are not necessarily useful or helpful for users from outside the field of satellite navigation.

Outlook

The new performance monitoring system will not be limited to pure provision of KPIs. It will also include newly developed algorithms for error detection and analysis using advanced methods for detection metrics. One example is the use of machine learning for the automated detection of known and still unknown GNSS errors or anomalies. This also includes key parameters for characterising the impact of Space Weather on GNSSs which are currently being developed at the DLR Institute for Solar-Terrestrial Physics and can be included in the future.

In the coming years, we will combine the navigation signal monitoring at user level, as described in this paper, with more detailed raw signal analysis using the DLR 30 m parabolic reflector high gain antenna. As very large amounts of data will be gathered by recording I/Q data for all GNSS satellites, we will use appropriate machine learning algorithms for error detection, distinguishing between nominal and abnormal signal states and determination of ageing effects. Based on the combined evaluation of all data, possible errors can then be analysed extremely reliably and with high precision.

We expect the webpage to be available end of May 2022 under www.GNSS-Monitoring.dlr.de .

References

[1] Galileo Performance Reports, [Online]. Available: https://www.gsc-europa.eu/electronic-library/galileo-serviceperformance-reports [Accessed: 2022-02-07].

[2] GPS performance, [Online]. Available: https://www.gps.gov/systems/gps/performance/ [Accessed: 2022-02-07].

[3] BeiDou Monitoring and Eval., [Online]. Available: http://en.beidou.gov.cn/SYSTEMS/Monitoringandevaluation/ [Accessed: 2022-02-07].

[4] GLONASS System documents, [Online]. Available: https://www.glonass-iac.ru/en/documents/ [Accessed: 2022-02-07].

[5] G. Johnston, A. Riddell, G. Hausler, The International GNSS Service. *Teunissen, Peter J.G., & Montenbruck, O. (Eds.), Springer Handbook of Global Navigation Satellite Systems (1st ed.)*, 967-982 (2017). Cham, Switzerland: Springer International Publishing; doi: 10.1007/978-3-319-42928-1

[6] C. Noll, The Crustal Dynamics Data Information System: A resource to support scientific analysis using space geodesy, *Advances in Space Research*, 45, 1421-1440 (2010); doi: 10.1016/j.asr.2010.01.018

[7] L. Heng, G. X. Gao, T. Walter, and P. Enge, GPS Signal-in-Space Anomalies in the Last Decade: Data Mining of 400,000,000 GPS Navigation Messages, *Proceedings of the 23rd International Technical Meeting of the Satellite Division of The Institute of Navigation (ION GNSS 2010)*, *Portland, OR*, 3115-3122 (2010); doi: NA

[8] S. Hochreiter and J. Schmidhuber, 'Long Short-Term Memory, *Neural Computation*, 9, 1735–1780 (1997); doi: 10.1162/neco.1997.9.8.1735

[9] L. Greda et al., Performance Analysis for Galileo and other GNSS at DLR Galileo Competence Center, *Proceedings of NAVITEC 2022*, 41 (2022); doi: NA

[10] CelesTrak, [Online]. Available: http://celestrak.com/NORAD/elements/ [Accessed: 2022-02-07]

[11] DLR's Ionosphere Monitoring and Prediction Center (IMPC). [Online]. Available: https://impc.dlr.de [Accessed: 2022-04-21]

[12] B. Männel, A. Brandt, T. Nischan, A. Brack, P. Sakic, M. Bradke, GFZ rapid product series for the IGS, *GFZ Data Services*, (2020); doi: 10.5880/GFZ.1.1.2020.003

[13] A. E. E. Wallin, D. Price, C. G. Carson, F. Meynadier, Y. Xie, E. Benkler, AllanTools, [Online] Available: https://allantools.readthedocs.io [Accessed 2022-04-20]

DOI 10.5162/ettc2022/3.5

New developments for GNSS precise positioning and timing

Michael Schulz[1], Jürgen Rüffer[1]
[1] ALLSAT GmbH, Sokelantstr. 5, 30165 Hannover, Germany
michael.schulz@allsat.de

Abstract:
The latest developments in the GNSS precise positioning and timing receivers from JAVAD GNSS include the option to replace the classical TCXO (Temperature Compensated Crystal Oscillator) by an OCXO (Oven Controlled Crystal Oscillator). This internal OCXO delivers an unmachted short term frequency stability 2x10-12 (@1sec) and 5x10-12 (@10sec). The position and timing signals measured using this OCXO will have great advantages, especially for flight test measurements with high dynamics or ionosphere scintillation measurements both requiring high update rates for raw measurement and positioning (up to 200Hz supported).

For the long term frequency stability, the latest JAVAD GNSS receivers have the ability to precisely synchronize the internal receiver clock with external 1 PPS signal without any additional equipment. In this mode the receiver uses the external frequency as the reference, but the time offset between 1 PPS and 10 MHz signal is measured inside the receiver and can be recorded. All the observations are performed in the epoch defined by an incoming 1 PPS signal. Receiver synchronizes its internal time scale to input 1 PPS signal with accuracy less or equal 0.4 ns, without any external time interval counter. This is the optimal solution for network timing or to synchronize FTI.

Key words: GNSS, time synchronization, OCXO, FTI, JAVAD GNSS

Introduction

To achieve the highest accuracy and precision in PNT applications, the most essential hardware part of the GNSS receiver is the internal oscillator. The stability of the internal reference frequency delivered by an OXCO oscillator is the key factor to measure short term effects like ionosphere scintillations and TEC, which require sampling rates up to 200Hz. Also for high dynamic applications like flight tests or autonomous navigation in the automotive industry, the short term frequency stability is essential for delivering precise trajectories.

For the long term frequency stability, i.e. essential for time synchronization of FTI, the highly stable PPS or NTP output signals require the ability to precisely synchronize the internal receiver clock with atomic satellite time without any additional equipment.

Highest stability of reference frequency [1]

The latest developments in the GNSS precise positioning and timing receivers from JAVAD GNSS include the option to replace the classical TCXO (Temperature Compensated Crystal Oscillator) by an OCXO (Oven Controlled Crystal Oscillator). This internal OCXO delivers an unmachted short term frequency stability 2x10-12 (@1sec) and 5x10-12 (@10sec).

The OCXO oscillator can be installed as an option in the receiver DeltaS-3S to provide the highest stability of the reference frequency. No special configuration efforts from the end user are needed. The comparison between two receivers one with the OCXO and one with a conventional TCXO is shown below.

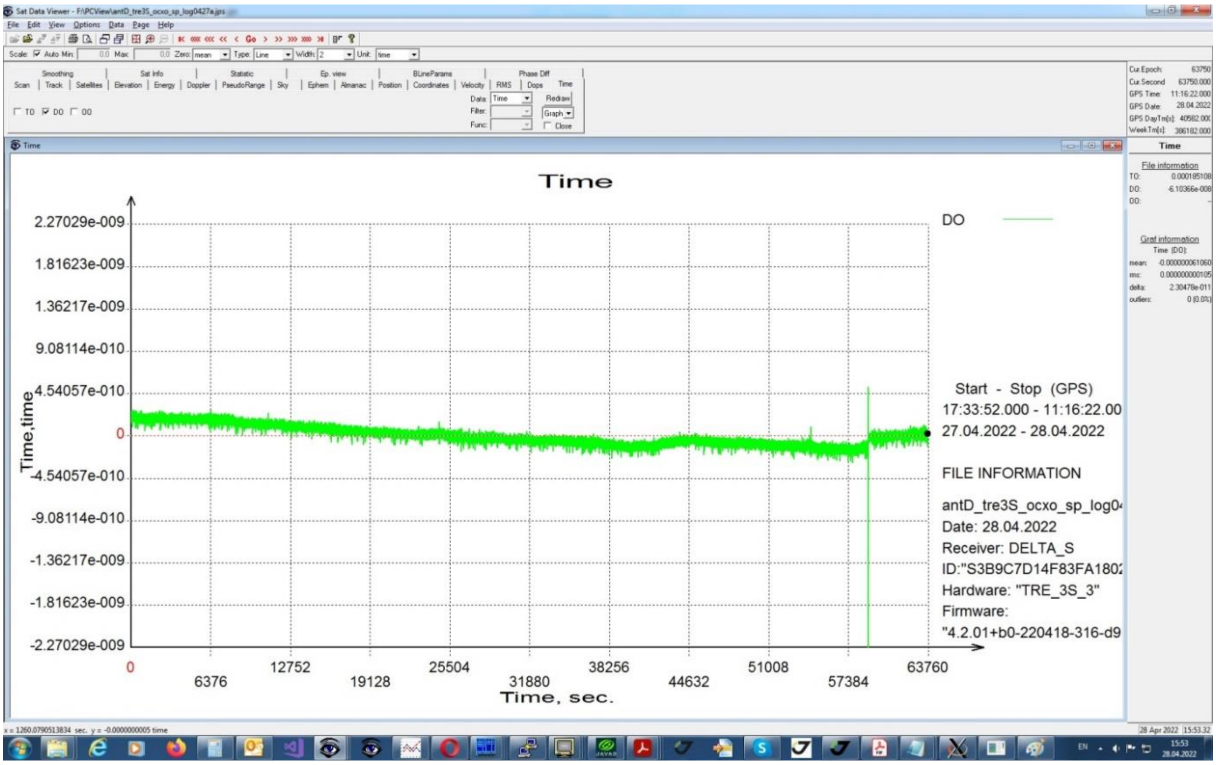

Fig.1. GNSS Receiver with new OCXO (offset of reference frequency from nominal value)

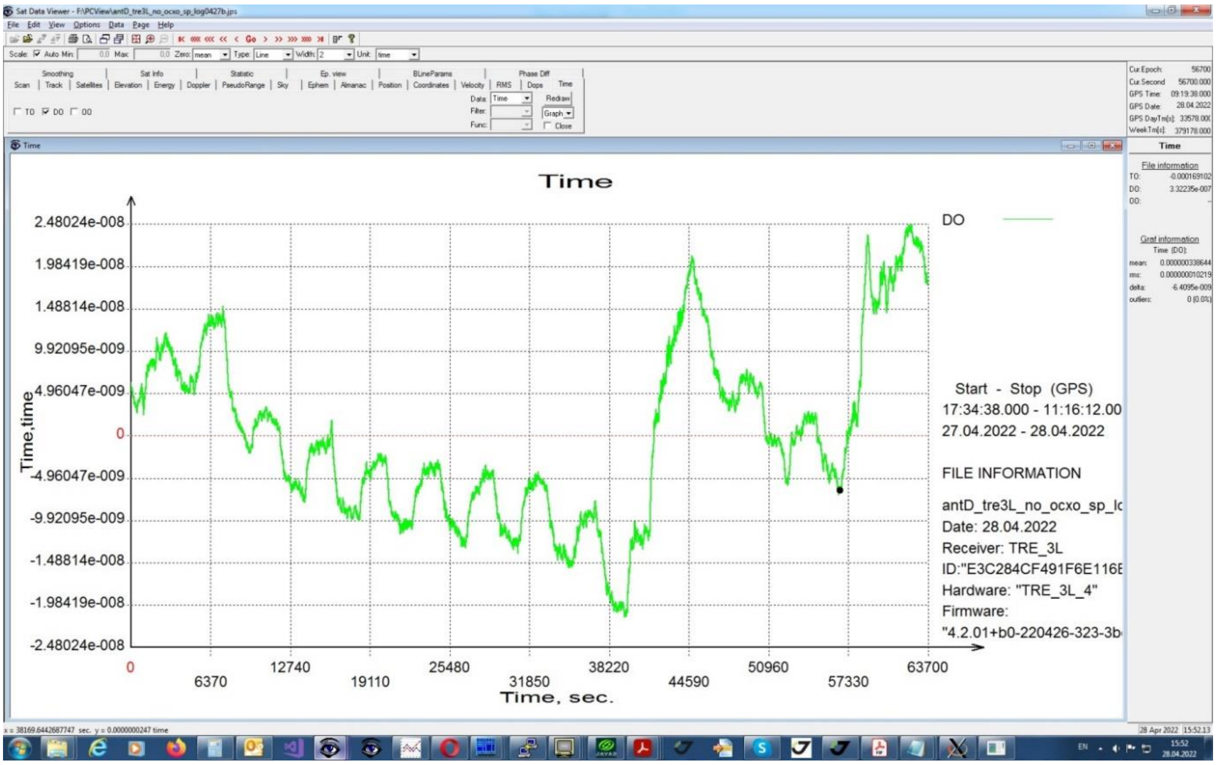

Fig.2. GNSS Receiver with standard TCXO (offset of reference frequency from nominal value) at the same place at the same time connected to the same antenna

The two charts cleary show temperature fluctuations affecting the precision of the reference frequency of the standard TCXO (Fig. 2), whereas the new OXCO (Fig. 1) controls temperature by its internal oven shows significantly more stable frequency. It can be noted that even small temperature changes, e.g. from the operation of the air conditioner, as well as from the morning airing of the room, are clearly visible.

High stability of reference frequency can be used in different applications such as timing applications or applications that need low noise measurements for example the GNSS antenna phase-center calibration or Ionosphere Scintillation monitoring and Total Electronic Content (TEC) computation.

TEC is computed using iono-free combinations of range measurements refined by corresponding phase measurements. Since the measurements inside the receiver have hardware biases the calibration of measurements needs to takes place before the computation of TEC. Calibration is performed at the time of minimum ionospheric activity using an analytical model of the ionosphere.

There is special command to activate calibration:

%%set,/par/raw/tec/calib/mode,on

TEC values in TECu units are outputted for all tracked satellites by special JPS message [te]:

Struct SatVTEC {nSats+1} {F4 VTEC[nSats];U1 cs;};

Raw data from all existing GNSS in JPS format can be logged with up to 200Hz either into internal receiver memory or to a file on the PC. The free JPS-File Analyzer software can be used to visualize the VTEC measurements. JPS-File Analyzer decodes raw JPS-data, presents them in charts and tables, and calculates their statistics. Processed data are presented on the panels organized as a tree.

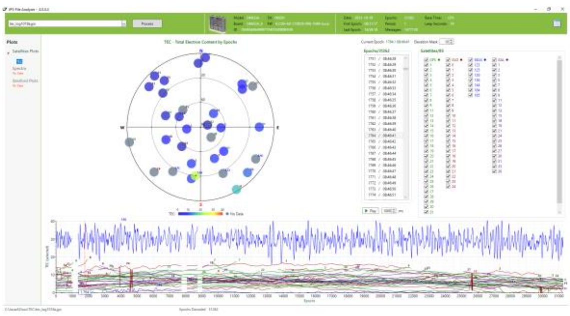

Fig.3. TEC graphs. All satellites are selected.

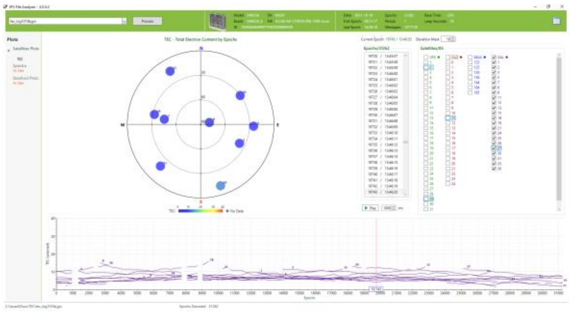

Fig.5. TEC graphs. Galileo only satellites are selected.

TEC panel contains a 2D graph in axes epochs-TEC. Y-values represent Total Electron Content calculated for a satellite. The sky plot shows the position of the satellites for the current epoch. Each satellite is displayed by the circle colored according to the TEC value from blue to red. The smallest values are blue, biggest -red, gray – value is unavailable.

JAVAD Receiver for Time Transfer (Timing receiver) [2]

For the long term frequency stability, the latest JAVAD GNSS receivers have the ability to precisely synchronize the internal receiver clock with external 1 PPS signal without any additional equipment. In this mode the receiver uses the external frequency as the reference, but the time offset between 1 PPS and 10 MHz signal is measured inside the receiver and can be recorded.

Delta(S)-3S receiver is a universal high precision GNSS receiver with an additional "time transfer" feature. It utilizes the unique calibration hardware, which allows to measure (and then compensate in data processing) the delay between the input PPS signal and the internal receiver's time reference. The accuracy of such calibration is about 20 picoseconds. The presence of such a schematic simplifies the overall hardware setup (see Figure 5). There is no need for the so-called "time interval counter", which is usually a rather big and expensive device.

The receiver supports the on-board generation of CGGTTS-V2E files, widely used in the time transfer community. Not only GPS-based data are available. Time transfer may be obtained using any GNSS system, including Galileo and BeiDou.

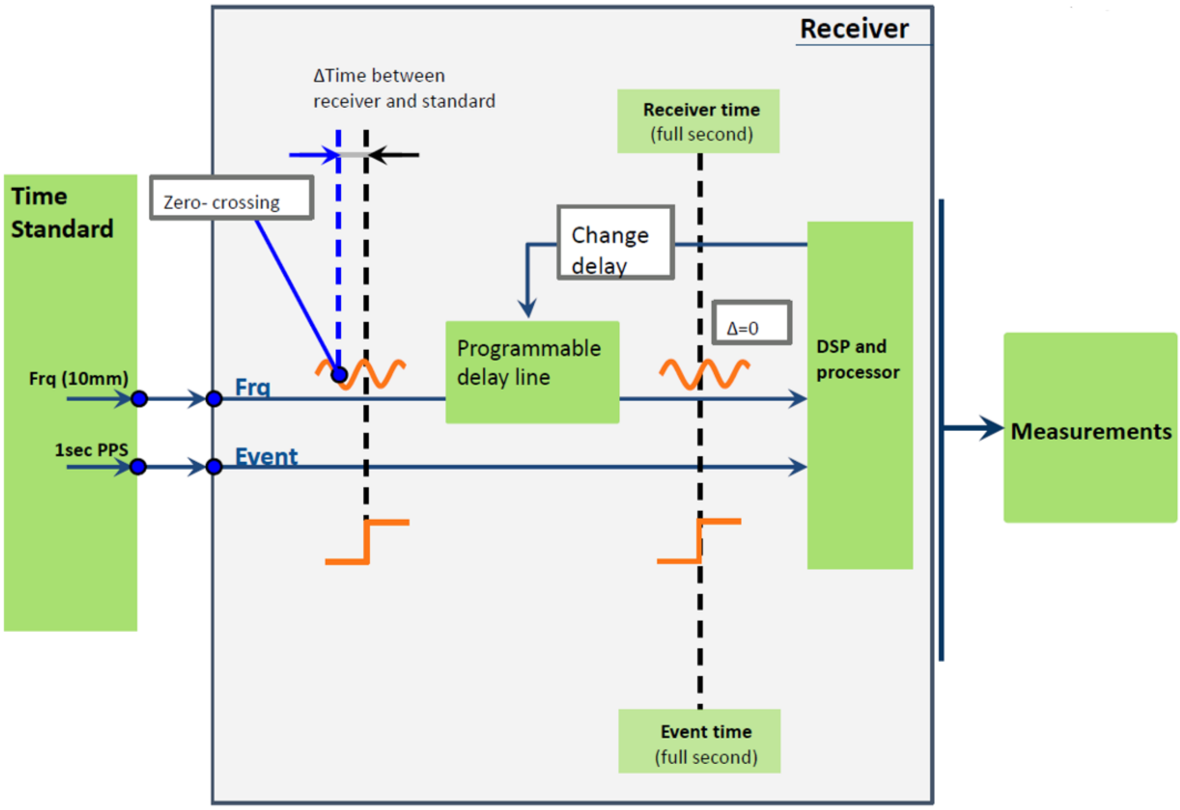

Fig.5. JAVAD Receiver for Time Transfer (Timing receiver)

Conclusion

For GNSS precise positioning and timing applications the position and timing signals measured using an internal this OCXO will have great advantages, especially for flight test measurements with high dynamics or ionosphere scintillation measurements both requiring high update rates for raw measurement and precise position calculation with GNSS receivers.

For the long term frequency stability, the latest JAVAD GNSS receivers have the ability to precisely synchronize the internal receiver clock with external 1 PPS signal without any additional equipment. This is the optimal solution for network timing or to synchronize FTI.

References

[1] V. Zhukov, S. Yudanov, O. Tubalin, Highest stability of reference frequency with OCXO oscillators

[2] V. Zhukov, S. Yudanov, O. Tubalin, JAVAD Receiver for Time Transfer

The challenge of e-mobility and eVTOLs on measurement technology with vibration and acceleration sensors.

Stefan Meyer
PCB Synotech GmbH
Porschestraße 20-30
41836 Hückelhoven

Abstract

The influences of trouble signals on measurement technology have recently changed significantly due to new technologies. Due to the technology shift to more electric drives and hydrogen technology, sensors should also provide reproducible and reliable data even in this environment. In order to continue to ensure the quality of the measurement results, sensors and cable concepts must be reconsidered, modified and tested. The aim of this presentation is to point out these problems in connection with vibration and acceleration sensors with piezoelectric ICP®- and MEMS-DC technology and to show examples of improvements and solutions. Product improvements will be presented and measurement results from a test series in the field of e-mobility will be shown. Practical suggestions for optimal wiring, cable selection and ground concepts will be discussed. The perspective on the use of placebo sensors to verify measurement results is addressed. The findings and suggestions for improvement are a good help for test and measurement engineers in the development field of E-Mobility as well as eVTOLs for Urban Air Mobility (UAM) in selecting sensors and their use.

Key Words

ICP®-Technology, DC MEMS-Accelerometer, Electric and Magnetic Fields, Pseudo Transducer, Ground and Case Isolation.

The new challenges for NVH sensors in eMobility and eVTOLs applications.

Hybrid and electric vehicles present NVH testing (Noise, Vibration, Harshness) challenges due to vehicle complexity and potential for problems with electrical shielding. NVH issues related to the addition of new electrical devices, gear whine, and vehicle resonances increase the number of NVH areas to be tested.

Our broad line of accelerometers is engineered to meet these challenges, by incorporating ground and case isolation. Electrically isolated accelerometers help avoid measurement errors and poor test data that can result when ground loops and stray electrical signals are present during testing.

The aim of this paper is to point out these problems in connection with acceleration sensors with piezoelectric **ICP® -** and MEMS-DC technology, as they are used in such applications.

External influences on vibration sensors

There are some environmental influences that can affect the output signal of an accelerometer and therefore the accuracy and fidelity of a measurement.

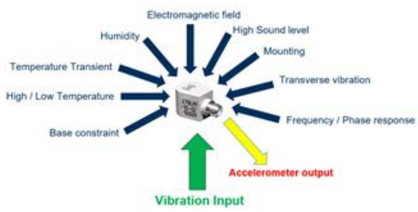

Typical electrical noise sources

Capacitively coupled

the varying electrostatic field between input and ground is electrically coupled by some stray capacitance, ex: power lines, electric motors, adjacent circuitry (multi-channel printed circuit boards without channel isolation/shielding).

DOI 10.5162/ettc2022/4.1

Magnetically coupled

the varying magnetic field around (poorly shielded) cable, ex: changing current in cables found near AC power distribution paths (machinery, transformers, etc.).

Current coupled

current other than the vibration signal is introduced into the measurement system via a common path, where impedance generates extraneous signals, ex: shaker drive circuits providing conduction currents through multiple ground points.

Triboelectric effect

relative motion/separation between the cable dielectric and the outer shield, ex: cable "whip"

Ground loops/potentials

line frequency and harmonics, ex shaker power systems

The sensor technology for NVH applications

ICP® -Accelerometers (IEPE)

ICP® is a PCB® registered trademark that stands for "Integrated Circuit Piezoelectric" and identifies sensors that incorporate built-in microelectronics. The electronics convert a high-impedance charge signal generated by a piezoelectric sensing element into a usable low-impedance voltage signal that can be readily transmitted, over ordinary two-wire or coaxial cables to any data acquisition system or readout device.

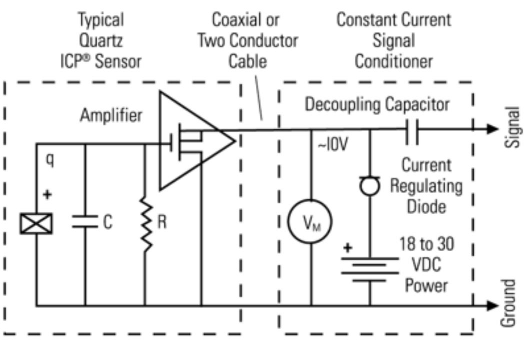

ICP® System Schematic

Capacitive Accelerometers

MEMS stands for micro electro mechanical system and applies to any sensor manufactured using microelectronic fabrication techniques. These techniques create mechanical sensing structures of microscopic size, typically on silicon. When coupled with microelectronic circuits, MEMS sensors can be used to measure physical parameters such as acceleration. Unlike ICP® sensors, MEMS sensors measure frequencies down to 0 Hz (static or DC acceleration). PCB® manufactures two types of MEMS accelerometers: variable capacitive and piezoresistive. Variable capacitive (VC) MEMS accelerometers are lower range, high sensitivity devices used for structural monitoring and constant acceleration measurements. Piezoresistive (PR) MEMS accelerometers are higher range, low sensitivity devices used in shock and blast applications.

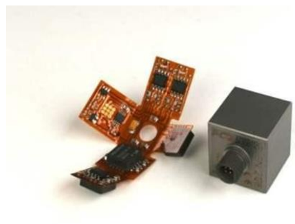

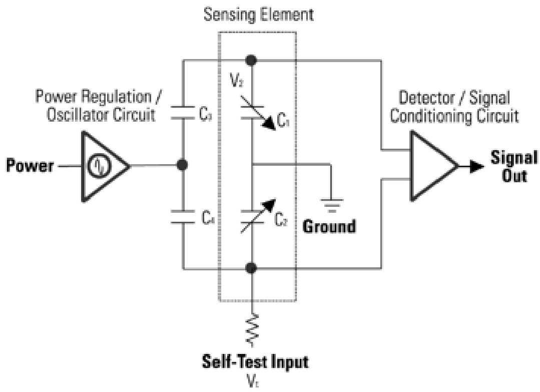

DC MEMS System Schematic

Study 1:

Influence of Electric Vehicle High Voltage Electromagnetic Fields on NVH Sensors

(Test Paper WPL 84)

The development of NVH sensors for automotive applications, in the past, has been without regard for HV EM Fields that are now present with EVs and HEVs. Consequently, there are concerns about what
influence or effects HV EM Fields impose on microphone and accelerometer signals when implemented for operational testing of EVs or

HEVs. To address and understand the influences of EV HV EM Fields on microphone and accelerometer signals a study was performed to asses these effects on an EV. Ten different models of PCB NVH sensors, including several cable types for some of the sensors, were evaluated local to various HV EM Field sources on an EV. The microphone and accelerometer signals were recorded along with signals from adjacent transducers that measure the EM Field strength. Assessment of the influence of the HV EM Fields is based on the coherence function between the NVH sensor signal and the corresponding EM Field transducer signal – where higher coherence values indicate a higher influence of HV EM Fields on the NVH sensor signals.present during testing.

Ten types of PCB Piezotronics NVH Sensors were evaluated at nine different HV EM Field sources on an EV. Six of the NVH sensors, all of which were an ICP type, were evaluated with two different cables.

PCB Piezotronics SENSOR DESCRIPTION					PCB Piezotronics CABLE DESCRIPTION			
					CABLE A		CABLE B	
TYPE	MODE	FEATURES	AXES	M/N	M/N	VARIANTS	M/N	VARIANTS
Microphone	ICP	pre polarized	uniaxial	378B02	003D20	Low Noise Coax	024AC015AC	Twisted Pair
Accelerometer	charge	charge converter	triaxial	356A70	003G10	Low Noise Coax	n/a	n/a
Accelerometer	ICP	standard	triaxial	356A02	010AY015NF	Grounded Shield	010S10	Non-grounded Shield
Accelerometer	ICP	filtered	triaxial	HT356A63	010AY015NF	Grounded Shield	010S10	Non-grounded Shield
Accelerometer	ICP	TEDS	triaxial	TLD356A16	010AY015NF	Grounded Shield	078G10	Non-grounded Shield
Accelerometer	ICP	case isolated	triaxial	354A04	010AY015NF	Grounded Shield	036G20	Non-grounded Shield
Accelerometer	ICP	ground isolated	triaxial	J356A43	010AY015NF	Grounded Shield	036G20	Non-grounded Shield
Accelerometer	DC	single ended	triaxial	3713B11200G	037M29	Multi Conductor	n/a	n/a
Accelerometer	DC	differential	uniaxial	3741F12100G	integral	Multi Conductor	n/a	n/a
Accelerometer	CVLD	case isolated	uniaxial	355M87A	integral	Coax	n/a	n/a

Table 1 – Sensor and Cables subject to EV HV EM Field evaluation

Measuring Points on the eMobile

Each PCB sensor/cable is evaluated at 9 different HV EM Field locations on the EV (the EV was a BMW i3)

EV HV EM FIELD LOCATIONS FOR SENSOR EVALUATION	
LABEL	DESCRIPTION
EME TOP	Power electronics module with HV inverter, HV converter, DC-DC converter, top surface
ELEC HEAT CABLE	Cable for high voltage heat system
KLE SIDE	Charging electronics module, side surface
KLE TOP	Charging electronics module, top surface
EME KLE CABLE	Cable connecting power electronics module to charging electronics module
LOCAL HV BAT CABLE	Local to high voltage battery cable, offset to one side of the parallel cables
HV BAT CABLE	Immediately adjacent to high voltage battery cable, above but centered between the parallel cables
EKK BOTTOM	Air conditioner compressor motor, bottom surface
EM BOTTOM	Vehicle electric motor, bottom surface

Table 2 – EV HV EM Field locations implemented for NVH sensors/cables

Test Conditions

Operating measurements were obtained for EV conditions that yield a high or maximized EM Field to assess a maximum influence on the NVH sensors / cables.

VEHICLE OPERATING CONDITIONS FOR HV EM FIELD INFLUENCE ASSESSMENT		
OPERATING CONDITION DESCRIPTION / PARAMETERS	OBJECTIVE	ACTIVE SYSTEMS
vehicle power off	Baseline EM Field Levels (reference zero)	none
accelerate up-hill	Max Load - DC and AC systems	HV BAT, EME, EM, EKK
air. cond. max		
windows down		
constant speed	Max Load - AC heat system	EME, ELEC HEAT CABLE
max heat		
windows down		

Table 3 – Vehicle operating conditions

Data Analysis – Coherence Function

Assessment of the influence of HV EM Fields on the NVH sensors/cables is accomplished using the coherence function between the NVH sensor signal (system output) and the locally measured EM Field transducer signal (system input) – where the NVH sensor / cable and the corresponding EM Field transducer define a single system.

The coherence function has values that range from 0 (zero) to 1 where a value of 0 indicates no causality between the system output signal and the system input signal, and where a value of 1 indicates causality between the system output signal and the system input signal. As related to the NVH sensor/cable coherence data, frequencies with low coherence indicate less susceptibility of the sensor/cable to the

local EV EM Field and frequencies with high coherence indicate more susceptibility of the sensor/cable to the local EV EM Field.

In an ideal situation the coherence function between the sensor signal and the EM Field will be 0 (zero) – no causality. This means the sensor signal only contains information about the desired measured phenomena (acceleration / acoustic pressure) and is not influenced by the EM Field (electrical noise).

Comparison of coherence functions of NVH-Sensors

The coherence spectrum is useful for assessing the performance characteristics of the NVH sensors/ cables at the various EM Field locations or for comparing performance between sensors/cables at the same EM Field location.

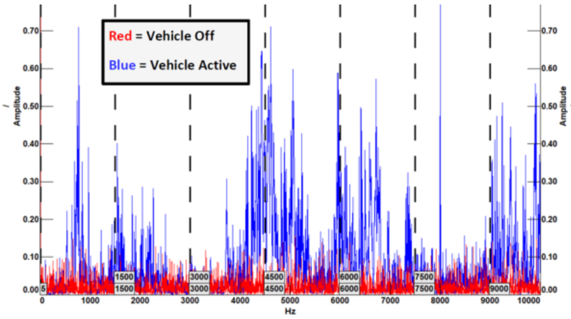

Figure 4 – Coherence functions comparing NVH sensor performance characteristics between an active EV HV EM Field (blue) and the same EV HV EM Field switched off (red) and Frequency bands for average coherence.

Results – Normalized Average Coherence

The relative ranking of NVH sensor/cable performance at different EM Field locations is not easily assessed with average coherence data given the sensors are not identical (differences include; circuitry, sensitivity, shielding, housing, power source, etc.) and the EM Field sources are not identical (differences include; circuitry, power levels, power functions, switching and duty cycles, etc.). Therefore, the average coherence data for the 5 Hz to 9 kHz frequency bands are normalized to determine a relative ranking performance for the sensors/ cables.

The normalized average coherence is determined from ratios between each sensor's average coherence at each EM Field location (for the 5 Hz to 9 kHz band) and the EM Field location with the maximum average coherence for that sensor (one of the nine EM Field locations). Thus, the normalized average coherence values will theoretically range between 0 (zero) and 1. A further consequence of the normalized average coherence process is each sensor / cable will have one EM Field location with a maximum value of 1 (corresponding to the EM Field location that is most influential on a particular sensor/cable).

Consolidating the normalized average coherence values into tables provides an overview for assessing sensor / cable performance at different EM Field locations and for sensor to sensor comparisons. The normalized average coherence data are organized into two tables; Table 5 for the sensors with Cable A and Table 6 for the sensors with Cable B.

A color scale is superimposed on the normalized average coherence values to distinguish between low, moderate, and high values. The color scale fades from green to yellow to orange to red which corresponds to low, low-moderate, moderate-high, and high coherence values, respectively. The color scale applies across the table rows (per sensor performance at each EM Field location), as well as down the table columns (sensor to sensor comparison at each EM Field location), and between the Cable A data and the Cable B data.

PCB SENSOR DESCRIPTION				EM FIELD LOCATION									
TYPE and M/N	MODE and AXES	FEATURES	REF. AXIS	EME TOP	ELEC HEAT CABLE	KLE SIDE	KLE TOP	EME KLE CABLE	LOCAL HV BAT CABLE	HV BAT CABLE	EKK BOTTOM	EM BOTTOM	AVERAGE PER SENSOR
MIC 378B02	ICP UNIAX	pre-polarized	X Y Z	0.806	0.325	0.854	0.581	0.611	0.683	0.940	0.368	0.853	0.669
ACCEL 356A70	CHARGE TRIAX	charge converter	X Y Z	0.398	0.167	0.314	0.719	0.393	0.676	0.483	0.336	1.000	0.498
ACCEL 356A02	ICP TRIAX	standard	X Y Z	0.276	0.232	0.592	0.530	0.366	0.517	0.379	0.348	0.996	0.471
ACCEL HT356A63	ICP TRIAX	filtered	X Y Z	0.539	0.253	0.708	0.473	0.457	0.645	0.572	0.408	0.911	0.552
ACCEL TLD356A16	ICP TRIAX	TEDS	X Y Z	0.339	0.284	0.799	0.496	0.375	0.675	0.630	0.409	0.787	0.533
ACCEL 354A04	ICP TRIAX	case isolated	X Y Z	0.250	0.215	0.295	0.425	0.293	0.535	0.577	0.315	1.000	0.434
ACCEL J356A43	ICP TRIAX	ground isolated	X Y Z	0.373	0.270	0.416	0.425	0.485	0.573	0.320	0.376	1.000	0.471
ACCEL 3713B11200G	DC TRIAX	single ended	X Y Z	0.266	0.248	0.279	0.254	0.273	0.362	0.308	0.320	1.000	0.368
ACCEL 3741F12100G	DC UNIAX	differential	X Y Z	0.202	0.120	0.202	0.188	0.167	0.275	0.218	0.145	1.000	0.280
ACCEL 355M87A	CVLD UNIAX	case isolated	X Y Z	0.318	0.472	0.518	0.403	0.436	0.445	0.284	0.296	1.000	0.464
AVERAGE PER EM FIELD LOCATION				0.377	0.258	0.498	0.450	0.385	0.539	0.471	0.332	0.955	

COLOR SCALE for NORMALIZED AVERAGE COHERENCE DATA

NO DATA	low	low - mid	mid	mid - high	high

Table 5 – Averages of normalized average coherence data (5 Hz to 9 kHz) for sensors with Cable A.

PCB SENSOR DESCRIPTION				EM FIELD LOCATION									
TYPE and M/N	MODE and AXES	FEATURES	REF. AXIS	EME TOP	ELEC HEAT CABLE	KLE SIDE	KLE TOP	EME KLE CABLE	LOCAL HV BAT CABLE	HV BAT CABLE	EKK BOTTOM	EM BOTTOM	AVERAGE PER SENSOR
MIC 378B02	ICP UNIAX	pre-polarized	X Y Z	0.854	0.344	0.886	0.575	0.494	0.760	0.959	0.399	0.755	0.670
ACCEL 356A70	CHARGE TRIAX	charge converter	X Y Z	n/a	n/a	n/a	n/a	n/a	n/a	n/a	n/a	n/a	n/a
ACCEL 356A02	ICP TRIAX	standard	X Y Z	0.316	0.328	0.610	0.393	0.395	0.567	0.505	0.372	0.933	0.491
ACCEL HT356A63	ICP TRIAX	filtered	X Y Z	0.448	0.295	0.689	0.596	0.455	0.525	0.402	0.479	1.000	0.543
ACCEL TLD356A16	ICP TRIAX	TEDS	X Y Z	0.397	0.319	0.600	0.596	0.487	0.749	0.533	0.465	0.969	0.568
ACCEL 354A04	ICP TRIAX	case isolated	X Y Z	0.393	0.365	0.540	0.654	0.503	0.765	0.434	0.488	0.918	0.562
ACCEL J356A43	ICP TRIAX	ground isolated	X Y Z	0.379	0.355	0.503	0.548	0.495	0.769	0.483	0.488	0.985	0.556
ACCEL 3713B11200G	DC TRIAX	single ended	X Y Z	n/a	n/a	n/a	n/a	n/a	n/a	n/a	n/a	n/a	n/a
ACCEL 3741F12100G	DC UNIAX	differential	X Y Z	n/a	n/a	n/a	n/a	n/a	n/a	n/a	n/a	n/a	n/a
ACCEL 355M87A	CVLD UNIAX	case isolated	X Y Z	n/a	n/a	n/a	n/a	n/a	n/a	n/a	n/a	n/a	n/a
AVERAGE PER EM FIELD LOCATION				0.464	0.334	0.638	0.560	0.471	0.689	0.553	0.448	0.927	

COLOR SCALE for NORMALIZED AVERAGE COHERENCE DATA

NO DATA	low	low - mid	mid	mid - high	high

Table 6 - Averages of normalized average coherence data (5 Hz to 9 kHz) for sensors with Cable B.

Summary of the WPL 84 test (Study 1)

Influence of electromagnetic radiation from electric and magnetic fields on the measurement chains of acceleration sensors using different connection cables (A & B) in electric vehicles.

ICP® sensors

- Largest influence at the measuring point on the electric motor.
- Benefits of NF-cable (Grounded Shield) version.
- The model Triax 354A04 with the best result. (case isolated sensor model!)

DC MEMS sensors

- The sensors with the least influence on the electric and magnetic fields.
- Differential output with the best result.

DOI 10.5162/ettc2022/4.1

Study 2:

EMI issue on vibrational ICP-Sensors (Lab Test)

Test bench:

- Test of electro magnetic interference onto ICP® - vibrational sensors.
- Evaluation of different sensor designs, cable configurations and DAQ front end grounding set ups.
- Test bench consist of an electric motor, driving a shaft for RMA test (running mode analysis).
- Motor speed about 20 Hz.
- Magnetic interference EMI measured with magnetic field probe (h-probe).

Sensors

- J356A45 ground isolation ICP
- 356A15 Standard ICP
- M354A05 case isolation ICP
- 639A91 case isolation IMI ICP

Cable

Shield and Ground **NOT** connected:
034G10 BNC plug **JW option**
010S10 BNC plug **JW option**

Shield and Ground connected:
034AY003NF BNC plug **NF option** (non-standard)
034RB-LEMO-9M

Result with JW cable (ground/shield splice not connected)

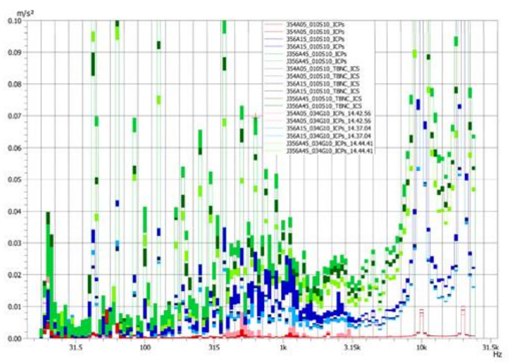

- All not case isolated sensors show a significant noise signal and/or EMI interference at certain singular frequencies (harmonic(s) of rotating frequency
- The case isolated models shows quite low noise level, no predominance of any EMI issue!

Result with NF cable (ground/shield splice connected)

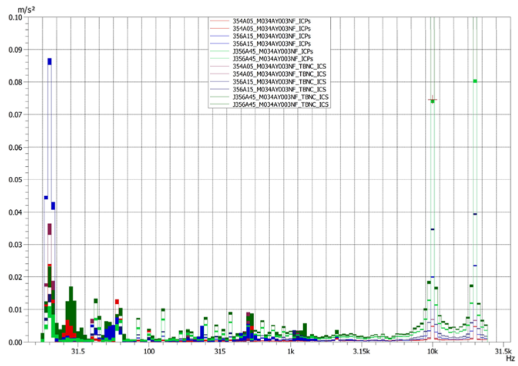

- Case isolated model and not case isolated sensors show quite similar low noise level, no predominance of any EMI issue.

Example Nr. 1:

Modal Test at machine tool

Spikes on Triaxial ICP® -Accelerometer

Bad noise effects:

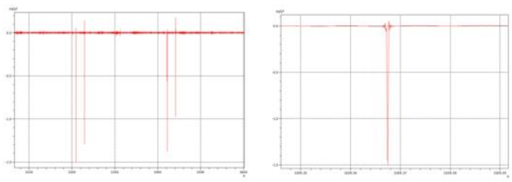

Standard Cable "JW"
Shield & Ground NOT connected

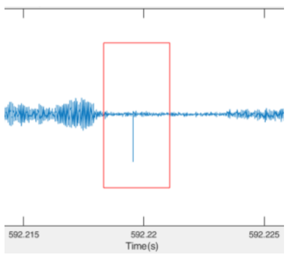

No-Standard Cable "NF"
Shield & Ground connected

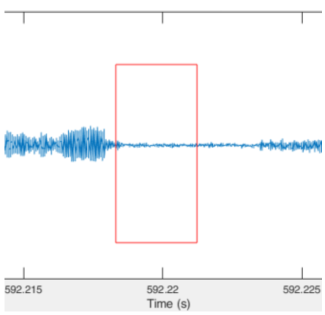

DOI 10.5162/ettc2022/4.1

Example Nr. 2

Aerospace Customer

Spikes on Triaxial ICP® **-Accelerometer**

Electric Motor / Electromagnetic interference (EMI)

Problem:

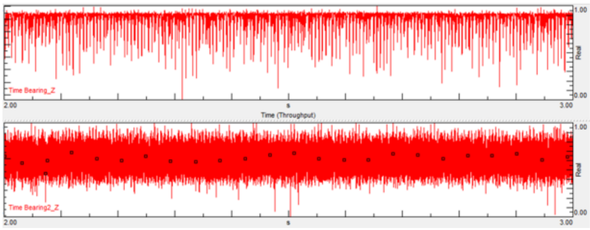

Standard Cable „JW“
Shield & Ground NOT connected
034G20

Solution:

No-Standard Cable „NF“
Shield & Ground connected
034G20

No-Standard Cable „LEMO“
Shield & Ground connected
FRE-078-AY-LEMO-3M (9-pin)

Ground isolated

Sensor Improvements

Case isolated triaxial ICP® **accelerometer**

Model 354B04 / 354B05 / TEDS

- Case Isolation
- No need for special isolation bases, coatings and insulated mounting screws

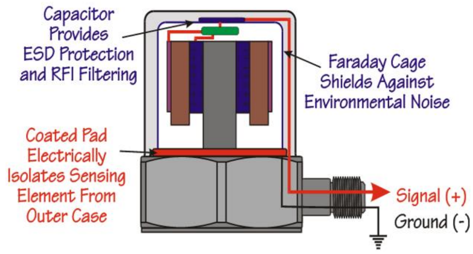

Schematic case isolation

DAQ Improvements

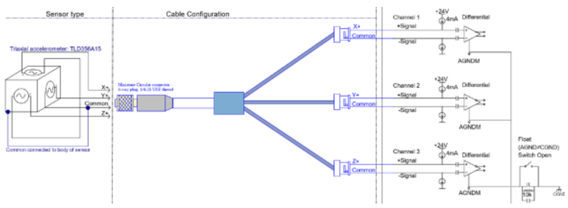

DAQ with differential input best solution.

Placebo Transducer a Tool for Data Validation

For any testing in which the environmental operating conditions of a transducer vary with time and/or location, several requirements must be fulfilled before measurement uncertainty analysis is justified. Included among the requirements are good measurement system design practices, such as adequate low- and high-frequency response and data-sampling rates, appropriate anti-aliasing filter selection, proper grounding and shielding and much more.

In addition to these requirements, data validation must be performed to establish that each transducer responds only to the environmental stimulus for which it is intended. For piezoelectric and piezoresistive transducers, “placebo” (IEST-RP-DTE011.1) transducers enable data validation to be accomplished. The referenced IEST standard defines a placebo transducer as ‘identical to a “live” unit in every parameter except for mechanical sensitivities.’ The placebo transducer should respond only to extraneous “environmental factors.” Ideally, its output would be zero. Any signal output from it would indicate that signals from the “live” transducers could be corrupted.

Placebo Sensors

Summary

- eMobility and eVTOLS have increased the requirements for NVH acceleration sensors due to magnetic influences.
- PCB has conducted studies with users on an e-mobile and a test bench to verify NVH triax sensors and various cable designs.
- For the sensors, isolated mounting or versions with isolated signal output are recommended.
- With triax NVH sensors, attention must be paid to the grounding in the cable and to the grounding concept of the measurement chain.
- The input circuit of the ICP® -signal conditioning can influence the quality of the measurement (single-ended/differential).
- In special cases, placebo sensors are a possibility for validation.
- DC MEMS capacitive accelerometers with true differential output are the most stable.

References

[1] Electric & Hybrid Vehicle Testing & Development (PCB Piezotronics).

[2] TN-16 Placebo Transducers: A Tool for Data Validation (PCB Piezotronics).

[3] Influence of Electric Vehicle High Voltage Electromagnetic Fields on NVH Sensors (PCB Piezotronics).

[4] TP323 Understanding the Endevco variable capacitance accelerometer electrical characteristics (Endevco),

DOI 10.5162/ettc2022/4.2

Tailoring Flight Test Instrumentation with Additive Manufacturing

Andreas A. Machnik[1], Thomas Decker[1], Robert J. Ashworth[2]
[1] Vectoflow GmbH, Gilching - Germany,
[2] Evolution Measurement Ltd, Andover – United Kingdom.
andreas.machnik@vectoflow.de

Abstract:
The project “Surface Module Approach for Rapid Testing in Flight Test Instrumentation” (SMART-FTI) is part of the “Clean Sky 2 - Joint Undertaking” (CS2). Innovative aerodynamic measurement technology is being developed and the preliminary results are shown in this paper. With the design freedom of additive manufacturing or “3D-printing”, measurement equipment can be tailored to seamlessly integrate into the loft of any aircraft. Through topology optimization, weight saving measures are applied while keeping strength to allow for flight test applications. The direct integration of the data acquisition (DAQ) into measurement modules supports quick and easy assembly as well as high frequency pneumatic measurements. A fully integrated aerodynamic measurement system approach with PTPv2 – IEEE 1588 is a novelty in FTI.

Key words: additive manufacturing, topology optimization, high frequency measurement, integrated aerodynamic measurement, PTPv2 – IEEE 1588

Introduction

Goal of the project SMART FTI is to develop aerodynamic flight test instrumentation (FTI) for the innovative Airbus Helicopters “RACER”. The RACER is a high-speed helicopter demonstrator developed by Airbus supported within the CS2 frame. With its aerodynamic configuration in service of high speed, aerodynamic flight testing needs are a logical consequence. The aircraft/helicopter hybrid is distinguished by a main rotor and two lateral rotors with additional aerodynamic surfaces. The concept is shown in Fig. 1.

Fig. 1. Rendering model of the RACER concept by Airbus Helicopters [1]

FTI for detailed collection of aerodynamic test data of the complex flow around the new aircraft concept is envisioned. Details on the complex flow can be obtained in Wentrup et al. [2]. For the data collection, several module types and a novel, compact scanner with direct integration into FTI modules are in development. For high frequency measurements, pneumatic links are to be kept to a minimum to avoid lag and damping, a common phenomenon known by pitot systems of aircrafts.

Benefits for Aerodynamic Testing

Although CFD is spreading and generating great guidance for design, the need for validation also rises. In addition, complex configurations, and aerodynamic interaction with structure and rotating elements exhibit a challenge. Consequently, aerodynamic testing in the aircraft industry is performed from concept phase to certification and even beyond. From university research of innovative aerodynamic elements to scaled model testing in the wind-tunnels to flight testing campaigns on prototypes.

In the past advanced aerodynamic flight testing was very complex and limited. Therefore, indirect measurements have been used. For example excessive vibration of a vertical fin has often been tested using strain gauges and accelerometers, although the source of that behavior may come from the propulsion system or aerodynamic interference.

In conclusion, aerodynamic flight test equipment allows for verification of CFD and wind tunnel experiments. It also enhances root cause analysis possibilities for aerodynamic effects that could for example effect engine performance/stability, vibration, handling qualities and aerodynamic performance/stability. Typical aeras of investigation are:

- Engine inlet flow;
- Flow over wings, stabilizers and control surfaces;
- Accelerated flow of the propulsion systems.

Ambition of SMART-FTI

The innovation here is primarily to take known pieces of aerodynamic measurement solutions, puzzle them together and levitate its technology readiness level (TRL) by proving its capabilities in flight testing on the RACER high-speed demonstrator.

Vectoflow, together with Evolution Measurement and Any-shape are forming a strategic partnership bringing in its natural competences and know-how in designing, additive manufacturing, testing, and data acquisition. The resurrection of non-conventional airplanes, helicopters and drones is triggering a demand in aerodynamic testing. The general demands for fuel efficiency and aerodynamic drag reduction can be answered with aerodynamic testing. Also challenges for passenger comfort and noise can be detected with FTI. The consortium is mastering new demands in data communication, new design freedom with additive manufacturing, and recent advances in materials and processes. Finally, the goal is to achieve a one-fits-all concept, that allows easy adoption for future FTI programs.

SMART-FTI Process

Secondary FTI is developed in the SMART-FTI project, under the premise: no permission of modification of the aircraft structure. The following work packages have been formulated forming the process of the SMART-FTI project:

- Region of Interest (ROI) definition and Requirements:
  Definition of measurement points and data to obtain; Requirements engineering.
- Conception of Scanner:
  Development of scanner and concept for direct integration into the FTI modules.
- Conception of FTI modules:
  Development of measurement concepts for surface modules and conception of Vectoflow's conventional rakes and probes for measurement tasks; validation of additive manufacturability.
- Design/Integration:
  Detailed design on specified ROIs including the minimal invasive integration into the RACER helicopter and fast/easy installation to the airframe.
- Substantiation of loads:
  Simulations to obtain Permit to Fly (PtF)
- Manufacturing:
  Additive Manufacturing of the polymer and metallic modules.
- Flight Testing:
  Data acquisition and post processing.

Currently, the design and integration stage are being concluded and a PtF is targeted.

Additive Manufacturing

Additive manufacturing is an umbrella term for manufacturing technologies, which build parts by adding increments to a build platform totaling up to the final part. [3] Recent advances in these technologies and its qualification for flight applications lead to a broader use in aerospace as demonstrated in Blakey-Milner et al. [4]. While there are several technologies available, the present article will focus on the laser powder bed fusion (LPBF) process for metals and organic polymers, used to produce the FTI.

The LPBF process of building parts is a continuous repetition of the following steps: powder deposition, laser exposure, lowering the build platform. [3] A detailed graph of the LPBF setup is given in Fig. 2.

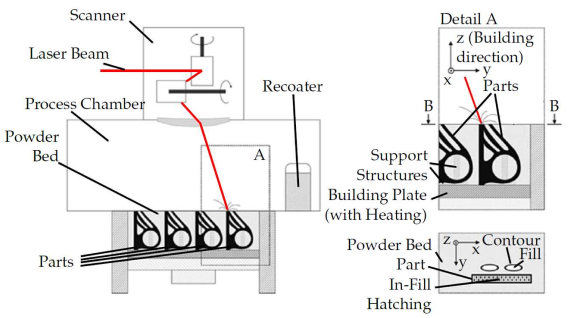

Fig. 2. Graph of LPBF Process (laser powder bed fusion), modified from [5]

The layer-wise process allows for a high design freedom, which can be used to introduce lightweight structures e.g., lattices or honeycombs, or internal channels. [6] These features make the process predestined for the manufacturing of flow probes and FTI with internal channels. With AM, lightweight parts with integral internal channels for pressure measurements can be manufactured in one piece using a single process.

As the process does not require any tooling, short lead times of several hours to days can be

DOI 10.5162/ettc2022/4.2

realized, making the process suitable for rapid prototyping. [3]

Surface Modules

The main topic of the SMART FTI project is the development of surface modules to measure pressure gradients. While, in this project, the ROIs follow curves in 2D-planes around profiles, the pressure mapping can be placed nearly arbitrarily across a module.

The module concept is a local thickening of 10mm of the aerodynamic surface at the ROI. This value is derived from the maximum scanner thickness of 10mm and to ensure smoothness for the added profile thickness. The scanner is integrated into the modules. The scanner specification is detailed in a later section. An overview for the surface module prototype is given in Fig. 3.

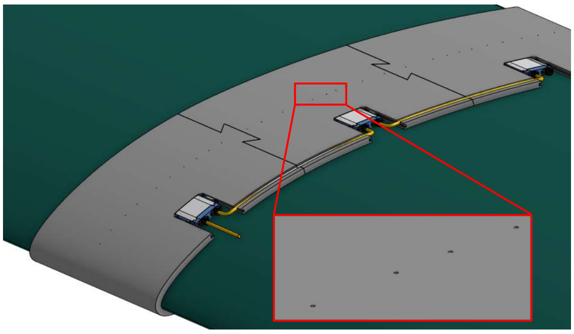

Fig. 3. Placeholder surface module – general layout of plastic module with integrated scanners on a generic airfoil – isometric view

A side view on the profile is given in Fig. 4. The overall thickness of $t_{max} = 10mm$ is kept around the profile.

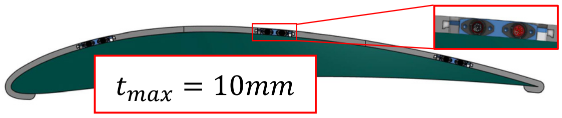

Fig. 4. Side view of the module concept on a generic airfoil

A 2D-simulation yielded an acceptable alteration of aerodynamic profile characteristics with the constant thickness increase. The influence on performance sank with having only a partial chord length instrumented with the module. Hence, in the first prototype shown in Fig. 6 only the first two thirds of chord length are equipped with the module.

Within the thickness, the developed EvoScann scanners sit on an intermediate piece, which is glued into the surface module. The concept is shown in Fig. 5. Airtightness is ensured with sealings, which are not shown in the presented CAD-model.

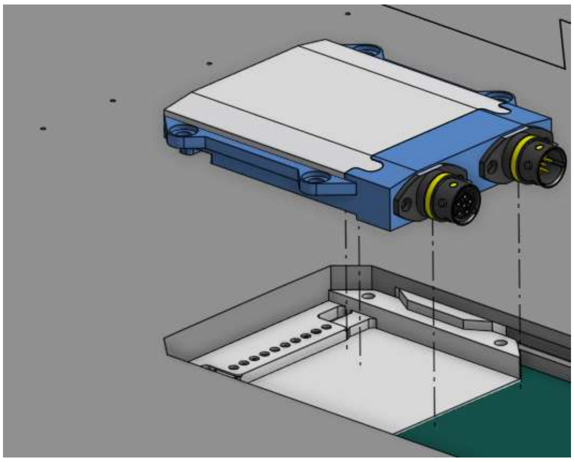

Fig. 5. Integration concept of scanner into the plastic module

In the final prototype, the connection to the aircraft is modelled in detail. Threaded inserts, so called Clickbonds, are glued to the aerodynamic surfaces. The surface modules can then be fixated with screws. Gaps and cable slots are sealed with aluminum tape. The concept is shown in Fig. 6.

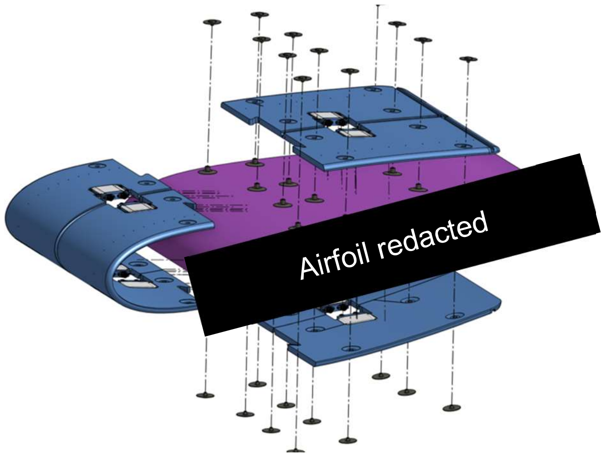

Fig. 6. Integration concept onto airfoils with clickbonds, airfoil redacted due to NDA

For the surface modules, an organic material (polyamide) has been chosen. The choice has been made according to the following requirements:

- Low density, due to weight constraints on the tail empennage;
- Manufacturability by LPBF;
- Thermal stability at elevated ambient temperature;
- Material flexibility for adaption to manufacturing tolerances of the aerodynamic surfaces.

Although the density of the used material is relatively low, the constant profile thickness yielded in a significant weight. Due to the large lever to the center of gravity of the aircraft, the weight needed to be reduced. Here, the high flexibility of the LPBF process comes in handy. Topology optimization by integration of a honeycomb or Voronoi structure comes with no penalty on the manufacturing side. A printed prototype is shown in Fig. 7. It is even beneficial for the manufacturing time as less material needs to be molten. The effort is on the design side. With the application of the weight saving measure, up to 55% of weight could be saved compared to the full material. In the future, topology can be further optimized by tailoring the honeycomb/Voronoi structure to the loads.

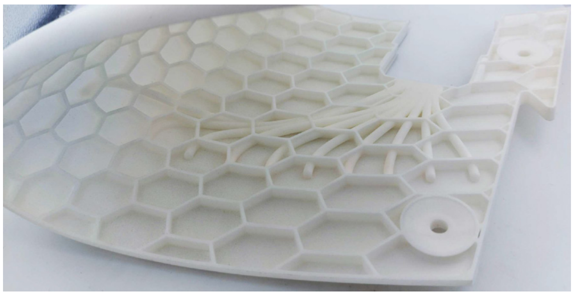

Fig. 7. Printed Prototype with honeycomb structure

An overview of the instrumented tail section of the RACER helicopter is given in Fig. 8.

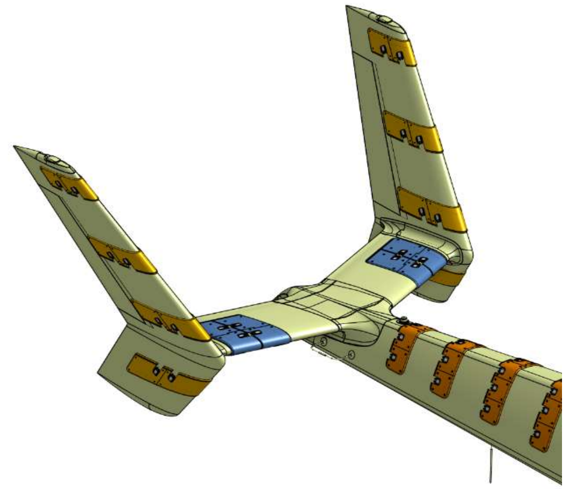

Fig. 8. Overview of the FTI installation on the tail-section of the RACER (aspect ratio modified)

The polymer PA-12 with a melting point of merely 187°C is used in colder areas. For higher temperatures, metallic modules are in use. Further, while the obtained data from the surface modules is valuable, sometimes more spatial resolution is required. The rakes and flow probes described in the next section can deliver the higher spatial resolution of measurements.

Rakes and Flow Probes

In higher temperature regions close to the main rotor and engines, plastic modules cannot fulfill the requirements. For installation on the RACER, metallic modules are envisioned. These consist of metallic flow probes, or rakes, which allow for higher temperature acceptance. The basic principle is a nearly unrestricted placement of measurement points, e.g., 5-hole probes or Kiel probes (Fig. 10). The probes are held by an aerodynamic profile, which contains internal pressure pneumatic channels as pressure tubes. Using the advantages of LPBF, these rakes can be manufactured in a single piece.

While metallic rakes are a standard product at Vectoflow with a high TRL, the innovation in this project lies in the mount of the scanners directly to the rakes. The latter eliminates the need for extensive plastic tubing to centralized, analog DAQs leading to fast frequency responses. An overview of the concept is given in Fig. 9.

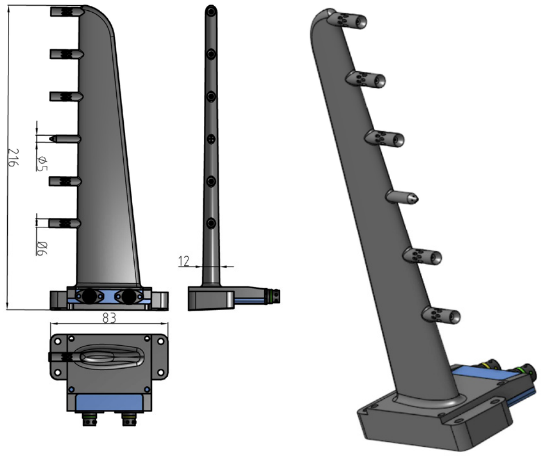

Fig. 9. Metallic rake concept with integrated scanner

Another novelty is the choice of material for this project. Due to low-weight requirements, rakes are printed in Scalmalloy®. It is a lightweight aluminum alloy with exceptional strength and ductility [7], exclusively developed for AM [8]. While AM of Scalmalloy® has been proven successful in aerospace [9], it has not yet been applied to LPBF of flow probes. Due to the larger extent of melt-pools for aluminum-alloys, resolution is lower. This was overcome by adaption of Vectoflow's standard geometry to the new requirements. The printed probes are shown in Fig. 10.

Fig. 10. Kiel-probe manufactured by LPBF from Scalmalloy®

First calibrations of the Kiel-probes show a recovery of 99% of the total pressure over an angle range of ±53° for yaw and pitch. Pitch-angle results are shown in Fig. 11.

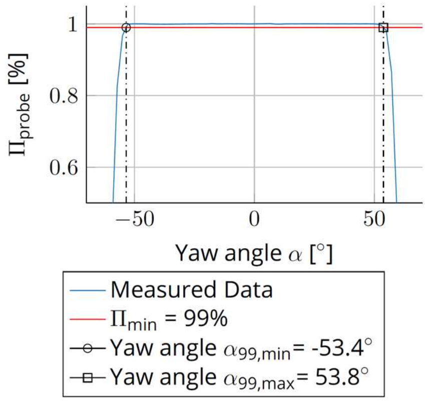

Fig. 11. Total pressure recovery over yaw-angle for calibration of developed Scalmalloy Kiel-probes at Ma=0.3

The rake geometry can be adapted to suit any measurement grid. For example, rakes can be curved to be fitted to freeform surfaces, as shown in Fig. 13. This allows for a 2D-mapping of external flow conditions in the plane of interest. For the integration of the scanner, the base can get bulky. To prevent aerodynamic perturbations, an aerodynamic cover, which is additively manufactured as well, might be added.

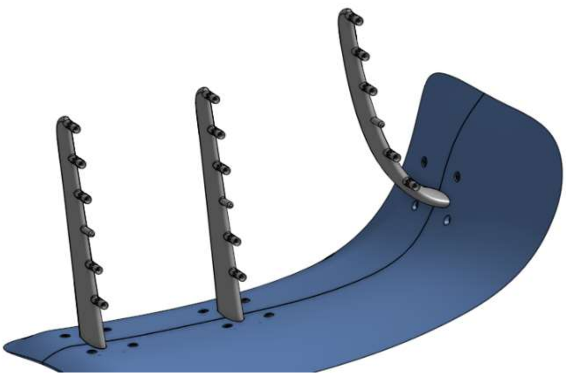

Fig. 13. Rake assembly adapted to freeform surface with aerodynamic cover

Scanner Features and Measurement Topology

Specifically for this project, a scanner is developed by Evolution Measurement using its experience from the EvoScann standard product as a base. A top-level requirement is the ease of installation without the need for extensive wiring, which is met with the measurement topology in Fig. 12: the potential to daisy-chain the scanners. This means only one cable between each scanner is required for data and power transmission. In the following, key-features of the novel scanner are listed.

Mechanical features:

- Low profile form factor <10mm to suit embedding into aerodynamic surfaces with minimum intrusion.
- IP67 Rating to allow uses in outdoor and varying environmental conditions.

Sensor features:

- 10 True-differential pressure measurement – ranges from +/-20mBar to +/-1Bar.
- Typical accuracy of measurement <0.1% FS
- Measurement resolution to 0.0006mbar
- Electronic resolution 24bit
- 1 Additional Absolute pressure channel to detect for local static pressure measurement deviations.
- High frequency synchronous measurement up to 4kHz across all channels.
- Wide Operating Temperature -40˚C to +110˚C.

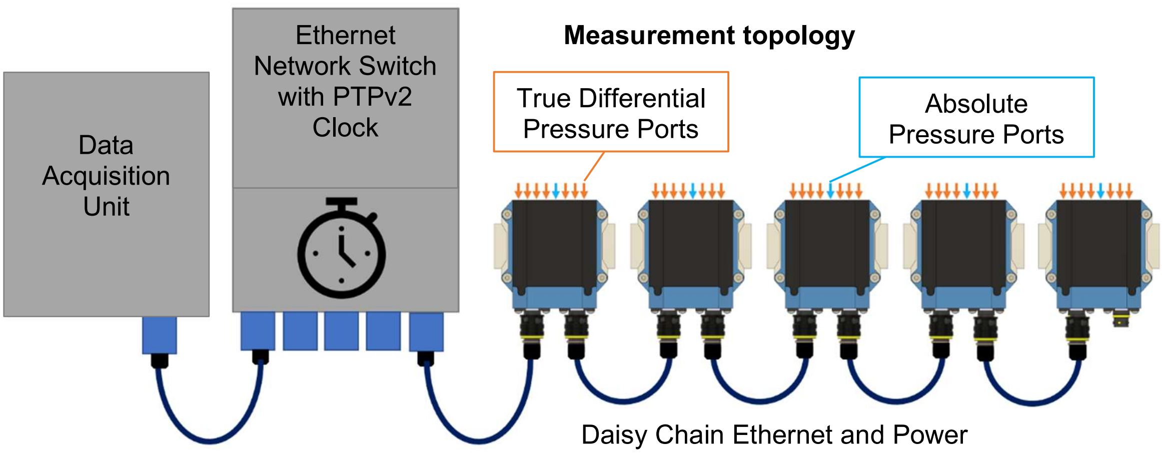

Fig. 12. Topology of data acquisition

- Direct coupling of scanner to test article maximizes frequency response to provide best measurement fidelity

Electrical features:

- Low Power consumption <1W per scanner.
- Power over Ethernet (PoE) compatible for ease of use and reduction in cabling to the scanners, whilst also proving full electrical isolation of the measurement.
- Embedded Ethernet Switch enabling multiple scanners to be daisy-chained reducing the complexity of the electrical Installation.
- IEEE 1588 PTPv2 compliant – accurate time stamping of data packets, allowing all scanners on the network scanners to be synchronized.
- Possible future software integration of flow probe and surface characteristics to provide direct velocity and angular information output

Impact for Future Programs

Within the SMART-FTI projects materials and processes for additive manufacturing of modules that are safe for flight are being developed. Probes and scanner technology are merged into modules which form a useful product with state-of-the-art connectivity. Future programs will benefit from the ability to go above and beyond in aerodynamic testing by generating larger sets of aerodynamic data in one test campaign. SMART-FTI modules are driving efficiency and usefulness of these campaigns.

These modules may have the number of measurement points that are typical for wool threads but with quantitative figures. They can also be used to get quantitative data for external flow, to generate the full aerodynamic data set. At high frequency rates this data allows to investigate more thoroughly the root cause and unsteady effects of the aerodynamic and propulsion elements of the aircraft configuration.

This innovative technology will help addressing key issues and unknowns with novel distributed propulsion systems, and aerodynamic optimization designs, just like the RACER, but in electrical vertical take-off and landing aircraft (eVTOL) businesses.

The modules with contributions from many different companies, in contrast to a self-assembled system, will reduce the complexity for the end-user: The consortium provides an all-in-one solution with a simple plug and play interface allowing to connect to modern FTI developments, e.g., in eVTOL developments shown in da Motta [10]. In addition, the rapid prototyping of FTI can take place early and in parallel to the prototype development. This saves costly development/improvement time and leverages the OEM into a better market situation.

References

[1] M. May, T. Haase, Y. Leost, Bird strike analyses on RACER fast rotorcraft, *AIAA SciTech Forum* (2019); doi: 10.2514/6.2019-1270

[2] M. Wentrup, J. Yin, P. Kunze, T. Streit, J.-H. Wendisch, T. Schwarz, J.-P. Pinacho, K.Kicker, R.Fukari, An overview of DLR compound rotorcraft aerodynamics and aeroacoustics activities within the CleanSky2 NACOR Project, *AHS International 74th Annual Forum* (2019); url: https://elib.dlr.de/123744/

[3] A. Gebhardt, *Additive Fertigungsverfahren* (2016); doi: 10.3139/9783446445390

[4] B. Blakey-Milner, P. Gradl, G. Snedden, M. Brooks, J. Pitot, E. Lopez, M. Leary, F. Berto, A. du Plessis, Metal additive manufacturing in aerospace: A review, *Materials & Design* 209 (2021); doi: 10.1016/j.matdes.2021.110008

[5] D. Herzog, V. Seyda, E. Wycisk, C. Emmelmann, Additive manufacturing of metals, *Acta Materialia* 117 (2016); doi: 10.1016/j.actamat.2016.07.019

[6] M.K. Thompson, G. Moroni, T. Vaneker, G. Fadel, R.I. Cmpbell, I.Gibson, A. Bernard, J. Schulz, P. Graf, B. Ahuja, F. Martina, Design for Additive Manufacturing: Trends, opportunities, considerations, and constraints, *CIRP Annals – Manufacturing Technology* 65 (2016) 737-760; doi: 10.1016/j.cirp.2016.05.004

[7] M. Muhammad, P.D. Nezhadfar, S. Thompson, A. Saharan, N. Phan, N. Shamsaei, A comparative investigation on the microstructure and mechanical properties of additively manufactured aluminum alloys, *International Journal of Fatigue* 146, (2021); doi: 10.1016/j.ijfatigue.2021.106165

[8] M. Awd, J. Tenkamp, M. Hirtler, S. Siddique, M. Bambach, F. Walther, Comparison of Microstructure and Mechanical Properties of Scalmalloy® Produced by Selective Laser Melting and Laser Metal Deposition, *Materials* 11(1):17, (2018); doi: 10.3390/ma11010017

[9] S. Begoc, F. Montredon, G. Pommatau, G. Leger, M. Gas, S. Eyrignoux, Additive manufacturing of Scalmalloy® satellite parts, *8th European conference for aeronautics and space sciences (EUCASS)* (2019); doi: 10.13009/EUCASS2019-677

[10] L.A.J. da Motta, How conventional Flight-Test Instrumentation concepts can contribute to the eVTOL aerospace development, *European Testing and Telemetry Conference* (2020) 84-88; doi: 10.5162/ettc2020/2.6

DOI 10.5162/ettc2022/4.3

Fiber Optic Sensing: the challenges of miniaturization, ruggedization and integration to enhance flight test instrumentation capabilities

Ghislain Guerrero[1], *Rémy Pelluault*[1], *Jan Koch*[2], *Wolfgang Schippers*[2], _Philip Guehlke_[2], *Christian Waltermann*[2], *Nassim Salhi*[3], *Didier Pohl*[3], *Minh Chau Phan Huy*[3]

1: Safran Data Systems, 5 Avenue des Andes, 91940 Les Ulis, France
2: FiSens GmbH, Salzdahlumer Str. 196, 38126 Braunschweig, Germany
3: Safran Tech, Rue des Jeunes Bois Châteaufort, 78772 Magny-Les-Hameaux, France

Abstract

One of the main challenges encountered by flight test instrumentation is to offer the adequate means to deliver accurately the continuously increasing number of data requested by design offices while minimizing the intrusiveness on the test vehicles. This contradictory trend applies to all stages of the instrumentation chain: sensing part, cabling, data acquisition units and communication.

Nowadays, new fiberoptic sensors are gaining ground in various industries due to their unique characteristics. However, their optical interrogation has been very challenging, particularly for the demanding environment in aerospace applications.

To overcome requirements interlinked between performance and miniaturization, a new innovative fiber-integrated approach is presented, with a focus on the reduction and optimization of all necessary materials and components.

This paper aims at highlighting the benefits of Fiber Optic Sensing technology compared to legacy sensing methods as well as sharing an initiative to integrate this technology in an existing compact and modular data acquisition unit compliant with harsh environments

Key words: Instrumentation, Flight Test, Fiber Optic Sensing, Fiber Bragg Grating, Spectrometer, Interrogation system

High-end aerospace instrumentation

In the aerospace domain, instrumentation, telemetry and data processing are key components to support the flight test campaign of a test vehicle whatever the type: civil or military aircrafts, rotorcrafts, UAV, eVTOL, HAPS, space launchers, missiles,…

Safran Data Systems (SDS) aims at developing solutions, such as devices, but also complete turnkey systems, combining high performances (accuracy, synchronization,…), low intrusiveness, ease of use, versatility and high level of reliability and ruggedization against shocks, vibrations, EMI/EMC, temperature, fluids, dust, pressure, vacuum and even radiations for space applications.

The more than 60-year experience of SDS in instrumentation has shown that each test vehicle brings its own unique set of functional and environmental requirements. SDS has developed and maintains a comprehensive toolbox in order to always be able to propose a tailored solution based on COTS bricks. These functional bricks are data acquisition units (DAUs), recorders (airborne & ground), data routers (e.g. Ethernet switches), data links (e.g. short and long distance transmitters, antennas, receivers and transceivers), data processing units, data display units and data replay units,…

Modular data acquisition unit

Whether they are hardware or software based, the functional bricks are most of the time attached to a modular architecture open to the final user. It is especially the case with the XMA data acquisition unit designed by SDS, which has been selected by major aircraft and rotorcraft manufacturers for more than a decade. The modules that compose this device can be of different types:

- Analog acquisition modules: intended to acquire electrical quantities (voltages, currents, charges, resistances, etc.) from sensors measuring different physical phenomena (temperature, acceleration, pressure, mechanical stress, displacement, position, etc…).
- Digital acquisition modules: intended to acquire digital information from sensors integrating signal digitization or from control/command systems and test vehicle avionics. The data can be conveyed under different standards (RS232/422/485, Ethernet, ARINC429, MIL-STD1553,…)
- Video (analog or digital)
- Data Storage
- Data transmission (wired or wireless)
- Customization :
  - o In terms of software, by hosting and running user defined algorithms
  - o In terms of hardware, by hosting and powering user defined electronics

Fig. 1: Example of XMA modular Data Acquisition Unit with 6 modules and a power supply

Analyzing technological trends and taking into account the news expectations expressed by the flight test community are definitely key factors when managing an instrumentation product line. As such, it appeared natural for SDS to explore the possibility to add Fiber Optic Sensing (FOS) capability to the XMA product. A fruitful teaming with Safran Tech and FiSens paved the way towards this goal and is described here after.

Safran Tech activities – Sensors Research unit

Safran Tech is the corporate Research and Technology center of Safran. It is responsible for developing and building innovative technology bricks for the aeronautics of the future. As part of its activities, S3AR (Safran Sensing Systems Application and Research) focuses on sensing technologies. FOS is part of S3AR activities.

Activities deal with all the building blocks of a fiber optic system. From the sensing element to the interrogation system. As well as methods and means for fiber optic integration.

To characterize these different blocks, tests are carried out in both laboratory conditions (To assess nominal performances) and on test rigs conditions (To get in line with real life applications).

Origins of Fiber Optic Sensing

Fiber optics are well known in the field of telecommunications as they made it possible to reach higher and higher data transmission rates over longer and longer distances.

In parallel, fiber optics found rapidly growing use in the field of sensing for various applications:

- Energy: Oil and Gas, dams, wind energy, nuclear plants…
- Civil engineering: Bridges, structures and tunnels monitoring…
- Transportation: Railway, Aerospatiale…
- Many others such as smart factories, biomedical…

Fiber optic sensing systems play an important role in SHM (Structural Health Monitoring), process control, predictive maintenance and smart structures.

The integration of fiber optic sensing systems in an increasing number of fields is made possible thanks to intrinsic characteristics of fiber optics. These specifications allow fiber optics to reach environments where conventional sensors cannot operate and densify the sensing capacity.

The main advantages of fiber optic sensors are listed below (Non-exhaustive list):

- Reduced weight and size.
- Immunity to Radio Frequency Interference and no emitted Radio Frequency.
- Compatibility with ATEX environments and harsh environments (high temperature and/or irradiated environments).

- High density of sensing points along the fiber optic and good metrological performances (Precision, sampling rate, measuring range…).
- Plurality of technologies/suppliers as most of the components come from the telecom field.

Fiber Optic sensing Technologies:

Many fiber optic sensing technologies are currently available in the market for industrial applications. Each one having its own pros and cons and its relevance for a given application. Fiber optic sensing technologies share a common architecture. The "brain" of the system is the interrogator, it consists of the active components that generate and collect light and the necessary electronics for data processing and transmission. The interrogator is coupled to the sensing fiber optic which will reach the DUT (Device Under Test).

The schematic architecture of a fiber optic sensing system is shown below:

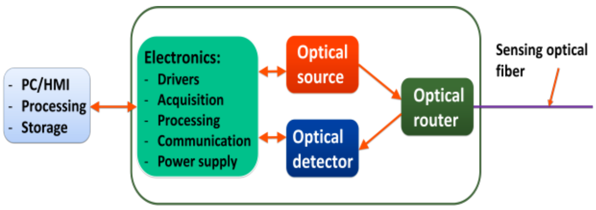

Fig. 2: Block diagram of fiber optic sensor interrogators

FOS technologies can be classified into three main families:

- **Distributed sensing systems**:

These systems allow to measure a high number (up to tens of thousands) of sensing points along the optical fiber. They are based on different backscattered phenomena (Rayleigh, Raman and Brillouin). Both OTDR (Optical Time Domain Reflectometry) and OFDR (Optical Frequency Domain Reflectometry) principles can be used to perform distributed fiber optic sensing. The drawback of these systems is the sampling rate which is quite low (in the order of the second) regarding the massive quantity of processed data.

The distributed sensing systems perform various types of physical measurements such as vibrations measurement using DAS (Distributed Acoustic Sensing) or temperature using DTS (Distributed Temperature Sensing).

- **Quasi-distributed sensing systems:**

These systems allow to measure a moderate number (up to approx. 100) of sensing points along the fiber optic. They are mostly based on FBGs (Fiber Bragg Gratings) which mainly utilize Wavelength Division Multiplexing (WDM).

These systems can reach sampling rates up to tens of kilohertz.

The Quasi-distributed sensing systems perform various types of physical measurements such as temperature, strain and displacement.

- **Point (Punctual) sensing systems:**

These systems allow to measure a single sensing point generally located at the tip of the fiber. They are based on several techniques (Interferometric cavities such as Fabry-Perot, power modulation…). They are often used for dynamic and static pressure measurement. The sampling rate can exceed 100kHz.

Fiber Optic sensing in the field of aeronautics

The field of aeronautics noticed many evolutions throughout the years. Among the evolutions, the number of sensing points inside the aircraft kept increasing in order to ensure reliability, improve safety and optimize performances. The field of aeronautics also noticed an increasing use of composite materials in order to reduce weight and thus consumption. New generations of engines tend to reach higher core temperature in order to increase thrust and optimize efficiency.

These new features benefited from the advantages of fiber optic sensors. A few examples of applications are listed below:

- Multiplexed temperature sensing for fire and overheat detection [1].
- Multiplexed strain sensing for various structural elements (Wings, landing gears, fuselage…) [2].
- Composite material process and lifetime monitoring to assess mechanical properties [3].
- FOD (Foreign Object Detection) in various aeronautical structures [4].

Challenges

Fiber optic sensors technology is already widely used in different fields of application. For the aeronautic field, its use implies to take into account specific challenges related to harsh environments:

- Interrogator: Capacity to be embarked (weight, volume), environmental stress (temperature, vibration, sealing…).
- Reliability: Due to the long lifetime of the devices, strong environmental constraints (thermal cycling…) and metrology (drift, hysteresis…).
- Metrology: Maintain the performance targeted by the application (acquisition frequency, number of sensors and measurement channels, accuracy, noise and stability ...).
- Integration: Ensure the integration of sensors, routing fibers along different paths and in harsh environments (Curvature radius, how to fix fibers, mechanical protection, maintenance…).
- Costs: Systems must be at an affordable price to be considered for deployment on a larger scale.

Focus on Fiber Bragg Grating technology

Fiber Bragg gratings (FBG) are known for more than 40 years [5] and consist in general of periodic changes of the refractive index within an optical waveguide leading to the reflection of a certain wavelength resonant to this refractive index pattern (fig. 3).

Fig. 3: Basic principle of fiber Bragg gratings: a periodic refractive index modification leads to a reflection of a specific resonant wavelength.

Spectroscopic techniques are obviously some of the most common tools to analyze reflected wavelengths of light. However, for about one hundred years the construction of dispersive high-resolution spectrometers has been following the same pattern: light enters the spectrometer through a narrow slit, a mirror or lens is used to collimate the light on a diffractive grating and finally a second imaging optic is used to create the wavelength resolved light distribution on a detector (e.g. [6]).

A precise interrogation of FBG wavelengths by means of a spectrum analysis requires a high optical resolution in the order of 0.1-1.0nm. To date this parameter can only be achieved by extending the overall optical path within a common spectrometer expanding the light cone essentially illuminating more lines or grooves of a diffraction grating. Unfortunately, this leads to bulky, heavy, and expensive devices with low light and energy efficiency.

In [7] and [8] FiSens first presented a fiber-integrated spectrometer which overcomes these limitations.

FiSens is a young company founded by a team of the Fraunhofer Heinrich-Hertz Institute in 2018. For more than 10 years the team has been focusing on the development of a Point-by-Point (PbP) femtosecond laser process for the inscription of FBG and other grating structures within optical fibers.
Utilizing this proprietary process FiSens also creates a precise periodic formation of ellipsoid nanostructures within the core of an optical fiber. By this patented apparatus [8] FiSens can encode all components for optical imaging usually needed for a common spectrometer (slit, lens or mirror, diffraction grating, lens) directly into the core of an optical fiber (Fig. 5). The resulting spectrometer requires only a second component: a detector (e.g., CMOS) to be placed in a lateral focal plane next to the fiber to capture all outcoupled and diffracted light with high intensities.

Fiber-Integrated Spectrometer:

To obtain an actual optical image at a predefined lateral focal distance to an optical fiber it is necessary to chirp the spacings between each point of the fiber-integrated diffraction grating. For instance, for a spectrometer in the visible region the required spacings between the grating points for the most efficient first order diffraction grating is in the range of 0.5µm with a change of the period of only slightly more than 10nm. Therefore, an extremely precise and reproducible setup for the PbP fs-laser inscription is required.
In the example shown below a diffraction grating has been simulated to support the simplest geometry for an actual visible spectrometer: a parallel positioning of detector and fiber and a wavelength sensitivity over the entire visible spectrum between 400 nm and 800 nm.

Figure 4 depicts simulated directions of constructive interference for different wavelengths: the Bragg angles for the first, the last and one pair of neighboring points in the middle of the grating are visualized. Additionally, the resulting focal position for each wavelength is marked. In this case the combined image appears quite symmetrically curved to the waveguide and the overall error for a parallel placed detector is minimized.

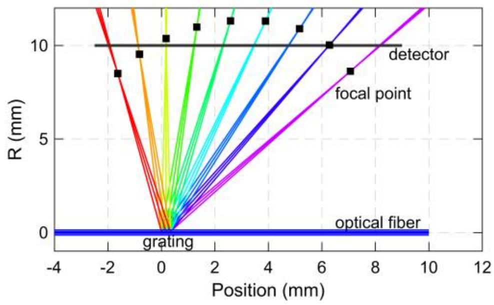

Fig. 4: Simulated directions of constructive interference of two neighboring points at the beginning, the middle and the end of an aspheric chirped grating

Applying the results of these brief simulations a fiber integrated spectrometer for the visible range has been created and no pre- or postprocessing has been performed on a polyimide coated standard single mode fiber.

Fig. 5 shows the fiber-integrated diffraction grating positioned above a simple sheet of paper, first illuminated by a red diode laser of 650 nm (a) and afterwards by a white light LED (b).

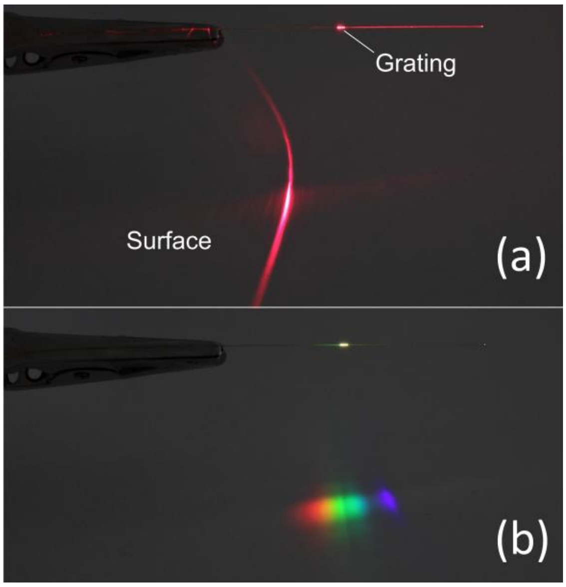

Fig. 5: a) red diode laser, b) white light LED imaged on a flat surface from a chirped first order PbP processed fiber-integrated diffraction grating by femtosecond laser pulses.

The laser light shows one singular bright red line, which focuses on the targeted distance from the core of the fiber at approx. 13 mm. For this wavelength a second order scattering occurs at a too small angle to leave the fiber due to total internal reflection. This second order is coupled to the cladding and coating of the fiber and results in an additional reddish glow beyond the grating. The white light leads to a clearly resolved rainbow including the LED-typical gap before the blue-UV region.

This fiber-integrated spectrometer represents the main building block for the analysis of reflected FBG wavelengths and can detect them with high optical resolution and light intensity.

Ultra-compact FBG-Interrogator

To accomplish the construction of an ultra-compact and high-performance FBG-Interrogator it is mandatory to inject high optical power into the waveguide, routing it to the FBG sensors and back to the spectrometer.

One highly space-consuming optical component within FBG-Interrogators is the routing of the optical fiber itself by means of optical circulators, couplers, switches, or fiber loops. By introducing the spectrometer into the optical fiber, the whole routing of it can be drastically reduced.

As seen in Fig 6. FiSens uses a bi-directional approach around a single monolithic optical fiber. The optical power of the light source is directly guided through the fiber-integrated spectrometer a first time while being routed to the FBG sensors. Since the fs-laser induced grating diffracts light at different angles dependent on the direction of light impinging on it, the light guided from the light source is outcoupled into an adverse direction and eliminated in a stray light trap. Only the light back reflected from the FBG sensors are directly imaged on the CMOS detector.

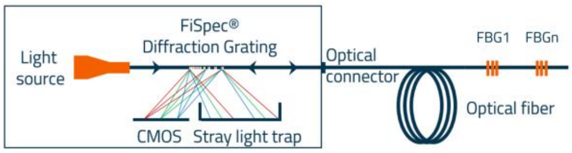

Fig. 6: Schematic illustration of a patented [4] FBG Interrogator around a single monolithic optical fiber.

Furthermore, the choice of operating wavelength for light source, detector and optical fiber plays a critical role. It is advantageous using 850nm over 1550nm due to the detector being silicon-based and only half the size. The higher attenuation at this wavelength can be neglected for applications of fiber lengths ranging up to 500m. The advantages of 850nm over 1550nm are:

- FBG sensor length of only 1-3mm for pin-point spatial resolution

- Critical fiber bending radius of only 5-6mm for tight routing
- Highly reduced costs and proven availability of CMOS detector
- CMOS detector with pixel-to-pixel pitch down to 5,5µm enabling high resolution

One of the key challenges with optical spectrometers and FBG-Interrogators are their ambient temperature dependent wavelength-drift. This effect occurs due the thermal expansion of detector and optical components. By shrinking the spectrometer build-up to only two very narrowly spaced components (i.e. fiber-integrated diffraction grating and detector) this effect can be reduced by several factors. Utilizing advanced materials like Invar36 around these two components can further minimize this effect. However, this alone will not be sufficient for a robust and stable sensor signal.

To overcome the full problem and stabilize the base line of the FBG sensor signal over the full operating temperature one can either actively thermally control the spectrometer (e.g., Peltier element) or passively compensate any base line drifts of the spectrometer using reference sensors inside the spectrometer. Hence, the most obvious solution is to use one FBG sensor of the available spectrum inside the single monolithic fiber of the FBG-Interrogator itself. This internal reference FBG sensor measures any changes in the device temperature and compensates against it.

Adding Fiber Sensing capability to the XMA

Among all the challenges anticipated, the mechanical integration has been the first roadblock encountered. As a modular product, it was mandatory to comply with the mechanical interface standard in order to keep hosting various type of modules in a single stack. This constrain would allow add-on capability to the thousands of XMA stacks currently in use and extend the combination of hardware configuration to meet future needs. Leveraging the mature mechanical design of the XMA, qualified and flight proven on numerous kind of test vehicles would be of great help to succeed in hosting and protecting the ultra-compact FBG Interrogator technology designed by FiSens. However, the volume offered by an XMA module housing is rather limited (50x80x11mm) as originally designed to high-end fine pitch electronics parts and not optical components.

The other challenges are the electrical interfacing (powering and data communication) and the synchronization / time stamping in order to provide consistent time aligned measurements that can be correlated with the other types of measurements.

Applying an agile methodology, SDS, Safran Tech and FiSens have decided to follow an iterative roadmap to integrate and ruggedize the FBG interrogator in the XMA product. Such approach has been eased thanks to the XMA-PRO and EXT modules which are off-the-shelf modules dedicated to host custom third party electronics in a standard XMA module housing.

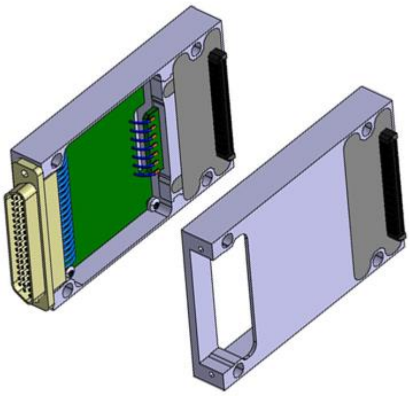

Fig. 7: XMA-PRO & EXT showing the surface allocated to host 3rd party components (in green)

This way of working allows focusing on the main challenges first, maximizing the probability to achieve a first flight capable version of the XMA-FBG interrogator module and minimizing the development effort. The counter part of this approach is that an additional module is required for the digital communication as the PRO&EXT modules only provide power supply voltages from the backplane. However, this additional module, which can be of different kinds (XMA-RSX, XMA-RSD, XMA-OBP,…), can be used to acquire the measurements coming from several XMA-FBG interrogators hosted in the stack or other serial and discrete signals needed for the application.

Thanks to the novel approach brought by FiSens and design simplification an ultra-compact FBG-Interrogator has successfully been integrated into the XMA form factor. (see Fig. 8). This first prototype of XMA-FBG combines a set of beneficiary properties:

- Dimensions of only 50x80x20mm
- Reduced weight of only 160g
- Low power consumption ~1W
- Simultaneous detection of all sensors (up to 30 FBG) without dead times
- High Precision of 1µe (@100hz, σ)

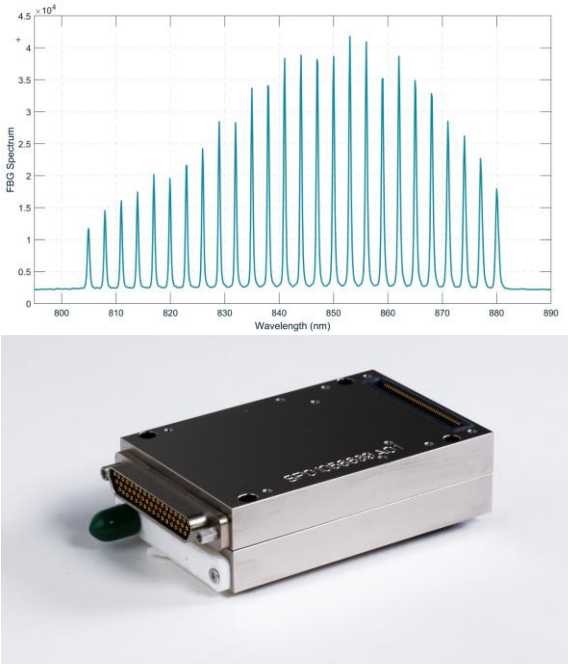

Fig. 8: 1st aerospace grade FBG-Interrogator prototype with availabe FBG spectrum at 808-880nm

The next steps will be to characterize the design in temperature, vibration/shocks and to run a first set of EMI/EMC testing. If needed, the design will be adapted following the same agile methodology.

Then, if all these test runs well, the target is to fly this first version of the XMA-FBG module on various test vehicles (fixed-wing and rotary-wing aircrafts) in order to meet quickly real flight conditions and to assess the benefits of this highly integrated FBG interrogator in a mature DAU.

Benefits of miniaturization and integration

Compared to stand-alone FBG interrogators, the miniaturization and modular approach offers the following benefits:

- **Mechanical installation in the test vehicle**: whatever the content of the XMA stack, only four mounting screws are required. External stand-alone interrogator would require additional mounting brackets or plate. This leads to time and cost savings. The high level of integration extends installation capabilities and offers more instrumentation channels for a given available volume.
- **Scalability**: one or several FBG modules can be hosted in a single stack whatever the form factor: XMA-CORE8, XMA-CORE16 or XMA-ROTOR

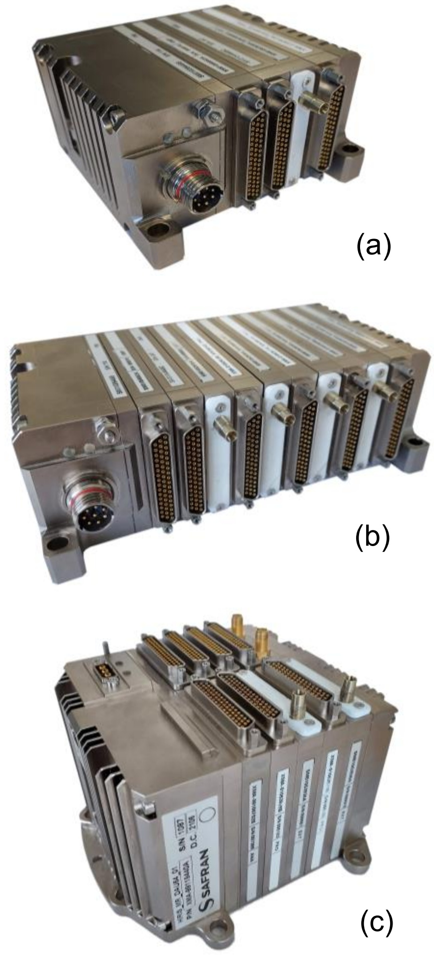

Fig. 9: a) XMA-CORE8 with 1 FBG interrogator + 2 other modules (top); b) XMA-CORE16 with 4 FBG interrogators + 2 other modules (middle); c) XMA-ROTOR with 2 FGB interrogators + 5 other modules (bottom)

- **Versatility**: capability to mix fiber sensing measurements with heterogeneous data types in the same data acquisition unit: legacy analog sensors (resistive strain gages, accelerometers, RTDs, thermocouples, pressure sensors,…), digital (avionic buses), discretes, video acquisitions,…
- **Homogeneous connectors**: obviously, the interface with the optical fiber implement a specific connector but data communication of the XMA-FBG module uses standard XMA microComp D-type connector.

- Electrical powering of the XMA-FBG modules comes from the XMA power supply module (XMA PSI / PSS) through the backplane and therefore take benefits of a fully isolated, DO-160 / MIL-STD704 qualified design.
- **Full integration** in SDS instrumentation system: configuration, synchronization, stand-alone or distributed architecture, wired or wireless network capability, standard compliant data stream (IRIG-106, IENA, …), on board recording, processing or telemetry,…
- **Ruggedization**: the ultra-compact FBG Interrogator will take benefits of the flight proven mechanical architecture of the XMA in order to be compliant with the demanding environments of flight-testing.

Conclusion and future perspectives

The collaboration between FiSens, Safran Tech and Safran Data Systems has led to a first successful integration of a downscaled FBG interrogator. The results obtained are promising but more developments are necessary in order to:

- Adapt the technical specifications for the targeted applications.
- Adapt the integration (mechanical and electrical) to be compatible with the standards and specifications.
- Reduce the cost.

However, the low intrusiveness, the high level of immunity, the compatibility with high temperature,… open promising perspectives in flight testing, but also in operations for health and usage monitoring (HUM) applications. As such, helicopter rotor blade monitoring appears definitely as a use case that could take benefits of such technology maturation and development effort.

References:

[1] PowerPoint Presentation (ftfsweden.se)

[2] Home - ALGeSMo - Advanced Landing Gear Sensing and Monitoring | Advanced Landing Gear Sensing and Monitoring

[3] 10.1007%2Fs13320-012-0065-4.pdf (springer.com)

[4] 77036042.pdf (core.ac.uk)

[5] B. S. Kawasaki, K. O. Hill, D. C. Johnson, and Y. Fujii, Opt. Lett. 3, 66-68 (1978)

[6] M. V. R. K. Murty, Opt. Eng. 13(1) 130123 (1974)

[7] C. Waltermann, P. Guehlke, J. Koch, W. Schippers, PhotonicsViews, Shaping Spectra within Optical Fibers (2019)

[8] C. Waltermann, US 10962415 B2, EP 3586177 B1

DOI 10.5162/ettc2022/4.4

Heavy-Duty Telemetry Systems based on SAW Sensors

René Fachberger[1], Marlien Stieger[1]
[1] sensideon GmbH, Ligusterstraße 4, Wels, Austria
rene.fachberger@sensideon.com

Abstract:
The suitability of telemetry systems based on surface acoustic wave sensor technology for applications like temperature measurement within the electric motor on a system level is demonstrated.

Key words: SAW, rotor temperature, wireless sensing

Problem

The challenge of the application of wireless telemetry systems lies in the elevated temperature and the very limited space available within engine and transmission components. Current telemetry systems are bulky and consist of active components, especially amplifiers, usually with a limited resistance towards temperatures beyond 125°C and fast changing electromagnetic fields.

As a result, new approaches come into consideration, to speed up and improve the development process of hybrid and full-electric drivetrains. One such approach is based on surface acoustic wave (SAW) technology.

Technology

Sensors based on SAW technology, are already known to be suitable for wireless sensing under industrial conditions [1]. The sensors are robust, work passively and due to a batteryless function, the sensors can be applied under fairly high temperatures.

The system configuration described in this paper is based on the principle, where the specific change in resonance frequency of the SAW device, brought about by a temperature change, is being measured and converted into a temperature value [2].

System Solution

Such systems are ideally suited for the digitalization of hot and fast rotating objects that are difficult to access as for example the rotor within an electric motor. As no pre-amplifier or similar electronic circuitry is needed on the rotating part, the transmitter and receiver modules are significantly smaller and more robust than in conventional telemetry systems.

The applied telemetry system (Fig. 1) uses a modular design consisting of a SAW sensor, a sensor antenna, a reader antenna and the reader electronics. The reader unit consists of a continuous wave radar operating at 2.4 GHz. Both, the reader unit as well as the resonating SAW sensor are connected to a fiberglass enforced printed circuit board antenna in form of a ring. All components are tailored flexibly to meet the geometrical requirements of almost any engine design, no matter the rotor diameter, magnet type, rotational speed, oil cooling or electromagnetic interference.

Due to the minimalistic design, the entire system gets mounted inside the engine housing without influencing oil jets or the performance of the electric engine.

Test Bench vs. In-Car Measurement

The environment of a test bench allows more flexibility when it comes to measurement systems. Cable routings may be more chaotic and it is possible to test single components of a powertrain separately. Telemetry systems can be relatively spacious since it is possible to mount them on shaft extensions for several reasons.

When it comes to the testing of encapsulated modules or testing of integrated components especially during vehicle driving operation, to validate the entire system, shaft extensions and complicated wire routings become an issue. The challenge is to integrate a telemetry system into a prototype without significant changes of the engine size. Fig. 2 shows an excerpt of measurements of a hybrid car with an integrated SAW telemetry system, recorded during driving performance tests in Sweden in winter 2019 [3]. Hybrid powertrains have even less available space when the engine is integrated into the gearbox.

Findings

SAW temperature measurement systems are an enlargement of existing telemetry solutions. It addresses the demand to perform sophisticated measurement tasks in the field of automotive electric engine development.

The system can be used in the most confined of spaces and can be fully integrated in any electric motor housing without significant adoptions. The components can flexibly be adapted to any dimension of the engine under test. The operation temperature covers a wide range of -40°C to +275°C and only a one-point calibration is needed for accurate and precise measurements. The robust system setup delivers constantly reliable measured values, even at the highest speeds or under the influence of lubricants. Another unique feature is the stability in electromagnetic fields which makes it ideal for use in electric engines.

The system provides reliable and dynamical data and allows temperature measurements in places, that have not been accessible with conventional telemetry systems so far.

References

[1] R. Fachberger, C. Werner, “Wireless temperature monitoring in an electrolytic galvanizing plant,” Proc. IEEE IUS, Prague, (2013)

[2] G. Bruckner, J. Bardong, “Wireless Readout of Multiple SAW Temperature Sensors,” Sensors, 19, 3077, (2019)

[3] H. Kurz, R. Fachberger, “SAW Temperature Sensing for Automotive Test Bench Systems,” Proc. ETTC, 2020

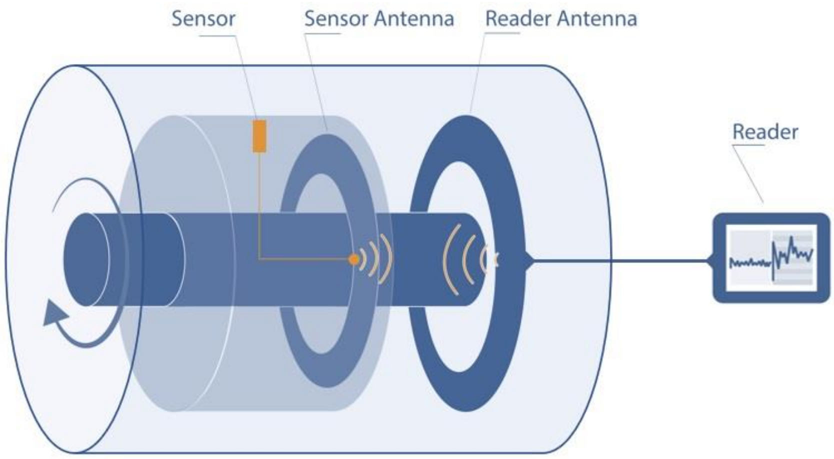

Fig. 1. System configuration SAW telemetry

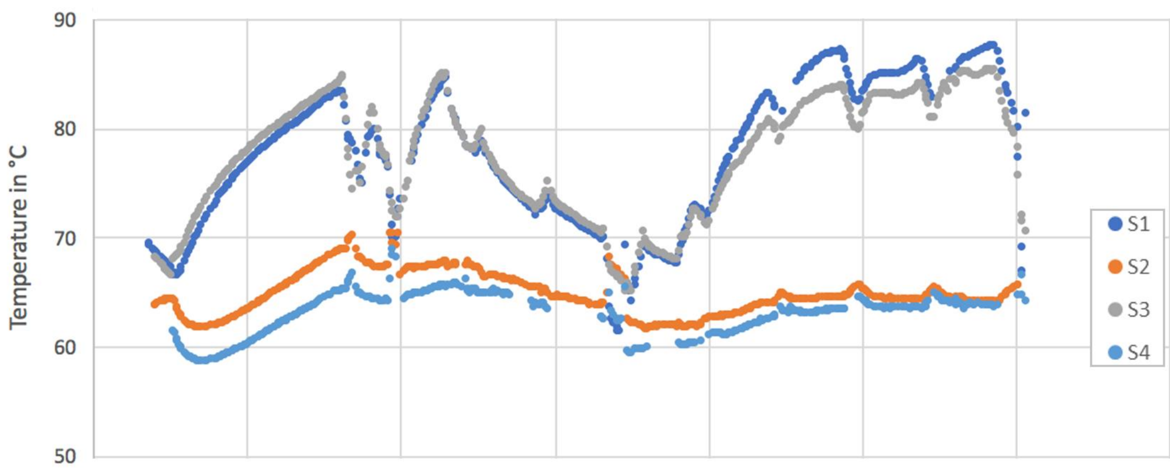

Fig. 2. Temperature plot over time (arb. unit) of a 4 channel SAW telemetry measurement with Sensors S1 to S4 during vehicle prototype tests in Sweden

DOI 10.5162/ettc2022/5.1

Aircraft Tracking with Single Camera and RF - System Synchronization

Volkan Tutay[1,2], İrfan Karagöz[2]
[1] Turkish Aerospace, Fethiye Mah. Havacilik Blv. No:17 Kahramankazan/Ankara , Turkey,
[2] Gazi University Engineering Faculty Electrical and Electronics Engineering Department 06570 Maltepe/ANKARA
volkan.tutay@tai.com.tr
irfankaragöz@gazi.edu.tr

Abstract:

Flight tests are carried out to complete the flight test campaigns. During flight test, safety and time factors are at the forefront. The safety of aircraft during flight, reducing flight test schedule are provided by telemetry systems. In some cases, such as GPS loss, jamming, the radio frequency tracking methods used in these systems may be insufficient. In order to eliminate this situation, auxiliary systems have been developed for telemetry systems. In this study, a camera system will be used as an auxiliary system since camera systems provide visual tracking and are inexpensive. The aim of this study is to perform visual tracking with a single camera with deep learning methods and to synchronize with these systems to assist RF tracking systems.

Key words: Telemetry, Flight Test, Aircraft tracking, Computer vision, Deep learning.

1. Introduction

It is used for object detection and tracking in telemetry systems, cameras, mobile phones, autonomous vehicle technologies, security, automation systems, aviation and space fields.

The telemetry system as in show in Fig. 1. provides real-time monitoring and recording of sensor data and bus messages acquisition from aircraft and at the ground station so visual monitoring of experimental aircraft is critical in flight tests. Within the scope of this study, the detection and tracking of an aircraft at any speed and altitude will be discussed. The telemetry antenna will be synchronized with the location information of the detected aircraft and the antenna and camera system will work together.

Many problems are encountered while detecting an aircraft from camera. These are; instantaneous movements of the aircraft, background cloudiness, light and visibility variations, target diversity, noise in the image and real-time processing requirements [1]. Many studies have been carried out to eliminate these problems.

Object detection is basically divided into traditional methods and machine learning methods. In traditional methods, background subtraction, optical flow and frame difference methods are generally used [1], [2]. Although these methods have been prior in use, machine learning and deep learning algorithms provide higher accuracy and speed. Deep Learning Methods firstly extract a feature with convolutional features then classifier networks are used to recognize the features of the objects. Generally, these networks try to detect the object by scanning the whole frame or any region on the frame [3].

Many object detection methods have been studied in the literature, RCNN [4], Fast RCNN [5], Faster RCNN [6], YOLOv3 [7] methods have more accuracy or speed. In this study, these models performances will be compared in relation to accuracy and speed than traditional methods such as Scale-invariant feature transform (SIFT), Histogram of oriented gradients (HOG) features. In this application, it is not sufficient to just detect and classify the aircraft. It is also necessary to track the moving aircraft. Also the direction of movement of the aircraft must be estimated. Tracking algorithms are of two types, traditional and CNN based.

DOI 10.5162/ettc2022/5.1

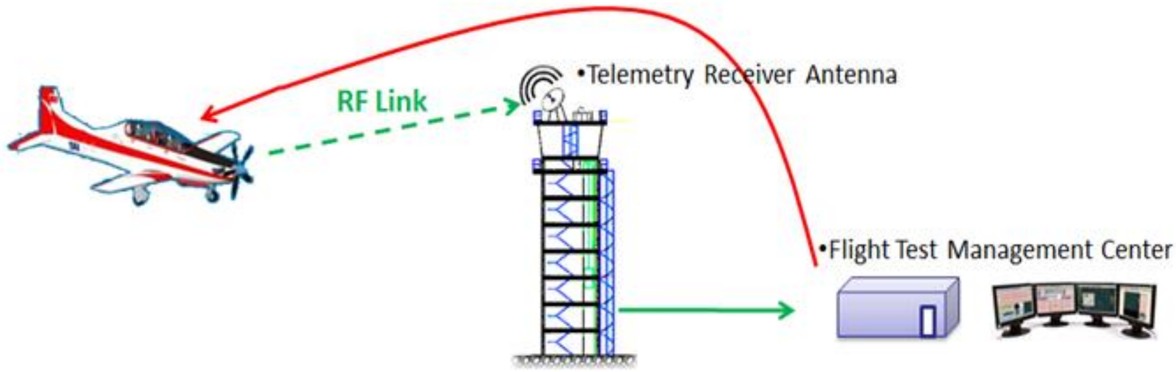

Fig. 1. Telemetry System

SORT, one of the most widely used tracking methods, will be used in this study.

The moving camera will be directed in accordance with the coordinates of the tracking aircraft. It will then move in synchronize with the telemetry antenna and camera.

2. Literature Review

There is no enough study in the literature within the scope of this study. For this reason, studies in which object detection and tracking are done with a moving camera are examined as separate subjects.

Dikbayır [8] used the Munich dataset, which includes cars, trucks, pickup trucks and buses in his study. The dataset includes vehicles photographed from different altitudes. Faster R-CNN and YOLOv3 algorithms were studied for each altitude. Although the YOLOv3 algorithm was successful in close vehicles, the Faster R-CNN algorithm was more successful in far vehicle photos. Although the YOLOv3 algorithm is faster for real time operations, it remains successful in detecting small objects. In this study, a new approach has been put forward by combining Faster R-CNN fed YOLOv3 algorithm and detection of vehicles was achieved with a higher success rate.

A performance comparison study was made by Wang et al. [9] using the Stanford University drone dataset with Faster R-CNN and SSD architectures on the RetinaNet algorithm. As a result of the study, they concluded that single-stage architectures successfully converged to two-stage architectures.

Another comparative study was done by Benjdira et al.[10]. In this study, they compared the one-stage YOLOv3 and two-stage Faster R-CNN model to realize vehicle surveillance and traffic monitoring. Dataset is created from images obtained from unmanned aerial vehicles. The performance evaluation and processing time of the models were examined. According to the results of the study, both algorithms achieved at least 99% and mention the object prediction accuracy in the dataset used. However, it was concluded that the YOLOv3 algorithm is more robust and has higher recall value than the Faster R-CNN model.

In the study conducted by Barış and Baştanlar[11], the classification of vehicles in traffic with PTZ camera was studied. The proposed method moves the camera according to the location of the detected object and then makes the classification of the vehicle. K-Nearest Neighbor method for object classification was tested in 4 different vehicle classes and the success of the method was 97.40%.

Maher et al.[12] proposed a target tracking system called deep-patch orientation network (DON) for tracking aircraft. This method predicts the direction of the target based on the training information. The DON method used the YOLOv3 and FrRCNN methods and the real-time tracking (SORT) algorithm. Experiments show that overall detection accuracy increases processing speed. Thus, the proposed method was more efficient for real-time operations.

3. Dataset and Methods

This section includes definition and preprocessing of dataset, object detection, object tracking and camera movements.

3.1 Dataset

In the literature, there are many data sets on object detection and tracking, but in this study, the data set was obtained from flight tests in Turkish Aerospace. This dataset was obtained by shooting 2 different fixed wing and 2 different rotary wing aircraft with different attributes from the ground camera. 1837 images were obtained from a total of 6 hours and 23 minutes of

DOI 10.5162/ettc2022/5.1

Fig. 2. Image labeling with LabelImg.

videos. These images were reproduced by mirroring, bleaching and rotation methods, which are data augmentation methods [13] and with the help of the augmentation methods 1837 images extended to 3280 images. The dataset split into training and testing as 70% of training, 30% of testing. To use in deep learning methods images need to be labelled so that create xml data for each images. Xml data include coordinate of image in frame and object class. Images were labeled with the LabelImg program as shown in Fig. 2.

3.2 Object Detection

Aircraft detection and classification were made in these images with R-CNN, Fast R-CNN, Faster R-CNN and YOLOv3, which are CNN based deep learning methods.

R-CNN method is the most basic model using the region recommendation approach as shown in Fig. 3. Fast R-CNN and Faster R-CNN are the developed and accelerated versions of this method. These models suggest regions with different sizes and in this model the window sizes are equalized by passing the relevant windows through conventional neural networks. At the end of the neural networks process, support vector machines (SVM) classifier is used to classify the object in that region. As a result of classification, it gives 4 coordinates indicating the location of the object in the image. On the other hand, Faster R-CNN classification is performed by linear regression. With the regression method used, the boundaries of the object are revealed [14].

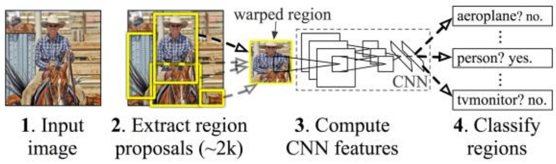

Fig. 3. R-CNN architecture

Unlike other deep learning methods, YOLOv3 does not operate with a regional-based approach, but in a convolutional network without fragmenting the image. It divides the image into grids of SxS, as shown in Fig.4., in accordance with its size and detects the object according to the similarity status [15]. In this way, the YOLOv3 algorithm is much faster than other deep learning methods. For this reason, it is widely used in the literature for object detection.

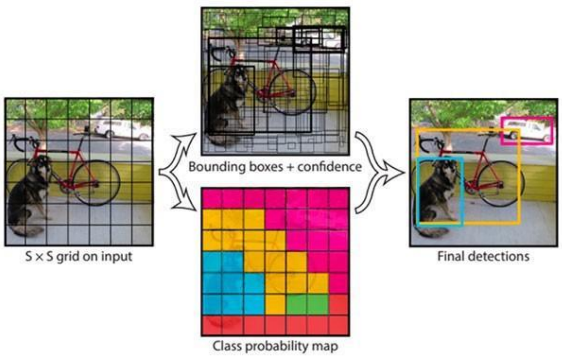

Fig. 4. YOLO SxS grid architecture

3.3 Object Tracking

SORT algorithm frequently used in real-time object tracking applicpations in the literature. SORT predicts the next location of the detected aircraft using the Kalman Filter. Intersection Over Union (IoU), one of the object association methods, is used in the SORT algorithm. This method makes object association according to the intersection of the previously detected

DOI 10.5162/ettc2022/5.1

object and the next location of which is estimated [16], as shown in Fig. 5.

SORT continues to track the object as long as the IoU score stays above a predefined threshold. If the object is lost for any reason, the tracking is interrupted and when the object is detected again, the tracking continues.

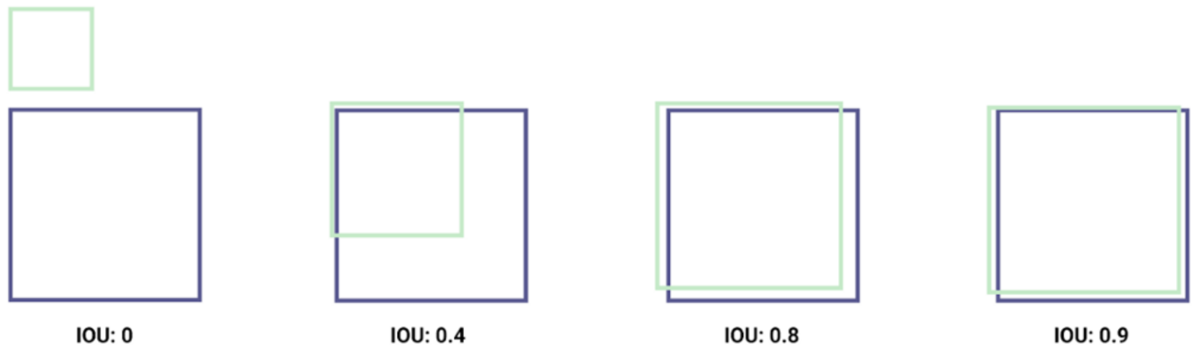

Fig.5. Sample IoU Scores

3.4 Camera Movements and Synchronization

The position values of the aircraft estimated by SORT are transmitted to the moving camera so that the camera can pan and tilt [17]. Camera movement is done according to the formula in (1).

$X = x + dx(1+\alpha),\ Y = y + dy(1+\alpha)$ (1)

The position values obtained after X and Y estimation, dx and dy instantaneous velocity values and the necessary variable for updating the α position are defined. Motion information is transmitted to the camera system via serial communication protocol (RS-232). With the generated PWM messages, the motors in the camera pedestal are moved accordingly.

The rate of change obtained from the movement of the camera motors is sent to the antenna control unit (ACU) of the telemetry antenna by RS-232. As a result of this, with the generated PWM messages, the antenna motors are moved synchronously with the camera motors.

4. Experimental Results

Four different methods used in object detection were compared. This comparison is provided by precision, recall, F1-Score, quality and IoU metrics.

Mean average precision (mAP) values obtained from precision, recall and IoU metrics. The results obtained with 3280 images are shown in Table 1.

Tab. 1: Metrics comparison

Method	mAP%
RCNN	86
Fast RCNN	90.4
Faster RCNN	94.2
YOLOv3	87.8

According to the test results, it was observed that the scores of the YOLO method were more successful. In addition to images, it has also been tested on videos from which the dataset was created. The fps values of the video of rotary wing aircraft performing taxi and take-off activities are given in Table. 2. In addition to these, the fps comparison of a section is as in Fig. 6.

Tab. 2: Average fps comparison

Method	Average fps
RCNN	30.7
Fast RCNN	4.8
Faster RCNN	43.1
YOLO	72.4

DOI 10.5162/ettc2022/5.1

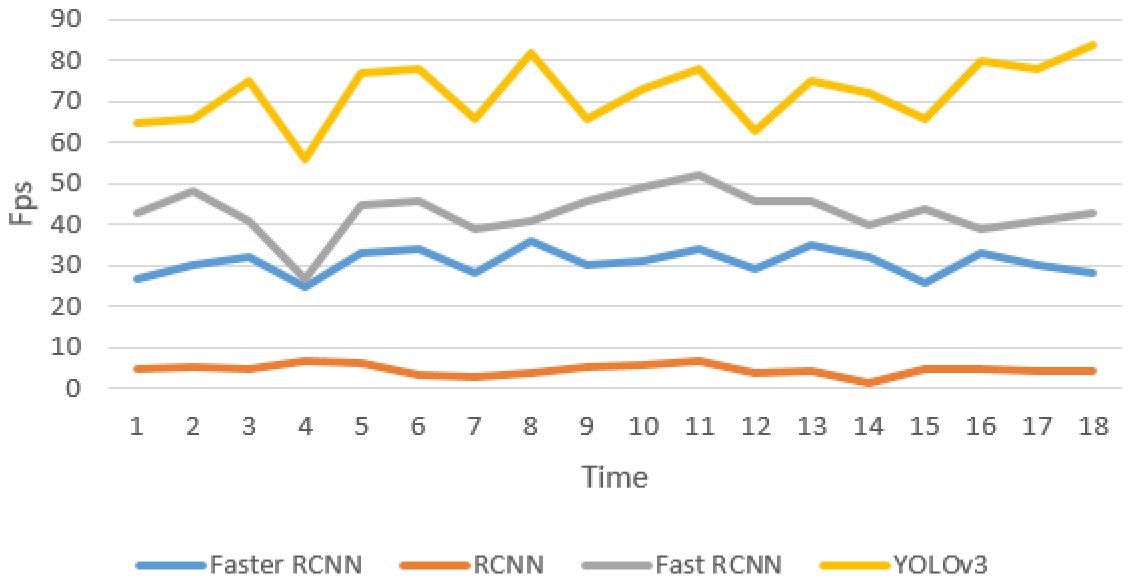

Fig.6. Fps comprision in video track

The sample results of the rotary wing aircraft detected by YOLOv3 are shown in Fig. 7 and Fig. 8.

Fig.7. Experimental result-1

Fig.8. Experimental result-2

DOI 10.5162/ettc2022/5.1

5. Conclusion and Future Works

In this study, metrics and frames per second (fps) values of RCNN, Fast RCNN, Faster RCNN and YOLOv3 models were compared for the for the detection of aircraft with motion cameras. Although the best mAP was obtained with the Faster RCNN model, the model with the highest fps value was YOLOv3. Since this application is processed in real-time, the YOLOv3 model is used.

SORT model was used for object tracking. Depending on the movement direction and speed of the tracked aircraft, the moving camera made pan-tilt movement and the camera and telemetry antenna synchronization was achieved.

In the future works, we will propose a new method that will be faster and have more accuracy.

6. References

[1] Liang, R., Yan, L., Gao, P., Qian, X., Zhang, Z., & Sun, H. (2010, October). Aviation video moving-target detection with inter-frame difference. In 2010 3rd International Congress on Image and Signal Processing (Vol. 3, pp. 1494-1497). IEEE.

[2] Pakfiliz, A. G. (2017). Automatic detection of aerial vehicle in cloudy environment by using wavelet enhancement technique. Radioengineering, 26(4), 1169-1176.

[3] Zhu, M., & Wang, H. (2017, October). Fast detection of moving object based on improved frame-difference method. In 2017 6th International Conference on Computer Science and Network Technology (ICCSNT) (pp. 299-303). IEEE.

[4] R. Girshick, J. Donahue, T. Darrell, and J. Malik, “Rich feature hierarchies for accurate object detection and semantic segmentation,” IEEE Comput. Soc. Conf. Comput. Vis. Pattern Recognit., pp. 580–587, 2014, doi: 10.1109/CVPR.2014.81.

[5] R. Girshick, “Fast R-CNN,” Proc. IEEE Int. Conf. Comput. Vis., vol. 2015 International Conference on Computer Vision, ICCV 2015, pp. 1440–1448, 2015, doi: 10.1109/ICCV.2015.169.

[6] S. Ren, K. He, R. Girshick, and J. Sun, “Faster R-CNN: Towards Real-Time Object Detection with Region Proposal Networks,” IEEE Trans. Pattern Anal. Mach. Intell., vol. 39, no. 6, pp. 1137–1149, 2017, doi: 10.1109/TPAMI.2016.2577031.

[7] J. Redmon, S. Divvala, R. Girshick, and A. Farhadi, “You only look once: Unified, real- time object detection,” IEEE Comput. Soc. Conf. Comput. Vis. Pattern Recognit., vol. 2016-Decem, pp. 779–788, 2016, doi: 10.1109/CVPR.2016.91.

[8] BÜLBÜL, H. (2020). DERİN ÖĞRENME YÖNTEMLERİ KULLANARAK GERÇEK ZAMANLI ARAÇ TESPİTİ.

[9] X. Wang, P. Cheng, X. Liu ve B. Uzochukwu, «Fast and Accurate, Convolutional Neural Network Based Approach for Object Detection from UAV,» arXiv.org, 2018.

[10] B. Benjdira, T. Khursheed, A. Koubaa, A. Ammar ve K. Ouni, «Car Detection using Unmanned Aerial Vehicles: Comparison between Faster R-CNN and YOLOv3,» arXiv, 2018.

[11] Barış, İ., & Baştanlar, Y. (2016, May). Classification of vehicles with omnidirectional and PTZ cameras. In 2016 24th Signal Processing and Communication Application Conference (SIU) (pp. 441-444). IEEE.

[12] Maher, A., Taha, H., & Zhang, B. (2018). Realtime multi-aircraft tracking in aerial scene with deep orientation network. Journal of Real-Time Image Processing, 15(3), 495-507.

[13] Shorten, C., & Khoshgoftaar, T. M. (2019). A survey on Image Data Augmentation for Deep Learning. Journal of Big Data, 6(1), 60. doi: 10.1186/s40537-019-0197-0

[14] Resul, D. A. Ş., Polat, B., & Tuna, G. (2019). Derin öğrenme ile resim ve videolarda nesnelerin tanınması ve takibi. Fırat Üniversitesi Mühendislik Bilimleri Dergisi, 31(2), 571-581.

[15] J. Redmon, S. Divvala, R. Girshick, and A. Farhadi, “You only lookonce: Unified, real- time object detection,” IEEE Comput. Soc. Conf.Comput. Vis. Pattern Recognit., vol. 2016-Decem, pp. 779–788, 2016,doi: 10.1109/CVPR.2016.91.

[16] Bathija, A., & Sharma, G. (2019). Visual object detection and tracking using Yolo and sort. International Journal of Engineering Research Technology, 8(11).

[17] G. Scotti, L. Marcenaro, C. Coelho, F. Selvaggi, and C. Regaz-zoni, “Dual camera intelligent sensor for high definition 360 degreessurveillance,” IEEE Proceedings-Vision, Image and Signal Processing,vol. 152, no. 2, pp. 250–257, 2005.

DOI 10.5162/ettc2022/5.2

A400M Image Processing Methodology to Calculate Relative Speed in Air to Air Refuelling

Israel López Herreros
Airbus Defence and Space, John Lennon s/n Getafe-Madrid, Spain
israel.lopez@airbus.com

Abstract:
The A400M deploys the hose and drogue to refuel fixed wind aircrafts and helicopters. This capacity called “air to air refuelling” provides multiple operations at long distances from home base. The helicopter must do contact at a reasonable speed within certain limits that allows a good coupling between the receiver probe and the tanker drogue. The relative speed between the tanker and the receiver is called closure rate.

This paper will explain the methodology used for this closure rate calculation and the flight test means. In general terms this process is based on virtual testing to validate the overall process, an onboard camera installed in the tanker and image processing algorithms developed in-house for the final calculations.

The outputs of this method are the 6-degrees of freedom of the receiver relative to the tanker reference axis, the speeds derived from that trajectory and a video with augmented reality to validate the calculated trajectory. This methodology was used to generate evidences to the certification process in those flight test points when the closure rate is extreme.

Key words: closure rate, air to air refuelling, image processing, augmented reality, photogrammetry.

1. Introduction

The A400M deploys the hose and drogue to refuel fixed wind aircrafts and helicopters. This capacity called “air to air refuelling” provides multiple operations at long distances from home base. The helicopter must do contact at a reasonable speed within certain limits that allows a good coupling between the receiver probe and the tanker drogue. This difference of the two velocities between the tanker and the receiver is called closure rate.

This paper will explain the methodology used for this closure rate calculation between the A400M and the helicopters. In general terms this process is based on virtual testing to validate the overall process, an onboard camera installed in the tanker and image processing algorithms developed in-house for the final calculations.

2. Test means

2.1. Tanker

Flight tests were performed on an A400M with the following AAR characteristics:

- Underwing pods
- Hoses
- Drogue
- Video cameras in fuselage

2.2. Receiver

France air force provided the Eurocopter Caracal, now called Airbus Helicopters H225M, for these flight tests. The A400M contract requires refuelling two helicopters simultaneously (See Fig. 1).

Fig. 1. A400M refuelling two H225M. View from chase aircraft.

2.3. Camera

The A400M development prototypes used for these flight tests have several cameras but for the closure rate calculation was used just one camera placed under the fuselage.

Characteristics of the camera:

DOI 10.5162/ettc2022/5.2

- Color
- Full high definition
- 25 frames per second
- Time synchronization with aircraft data

This camera covers the approaching of the helicopters to the drogues (See Fig. 2).

Fig. 2. Caracal view from camera under fuselage.

2.4. Simulation

Simulate the refuelling operation is crucial for the success of the flight tests. A geometric compatibility study is done with the different refuelling positions in order to characterise the risk of the operation (See Fig. 3).

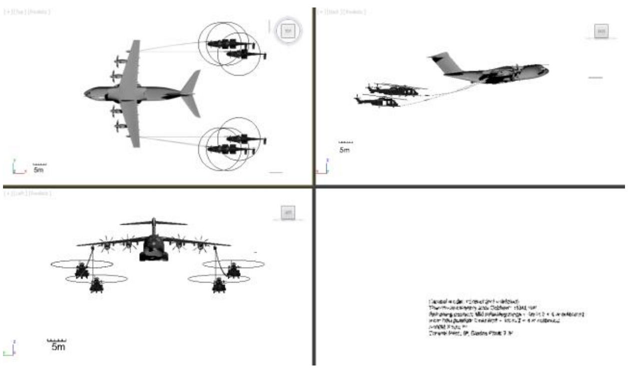

Fig 3. Geometric compatibility study.

Simulation also allows to render videos (See Fig. 4) from onboard cameras installed in the tanker in order to validate the methodology before the real flight tests.

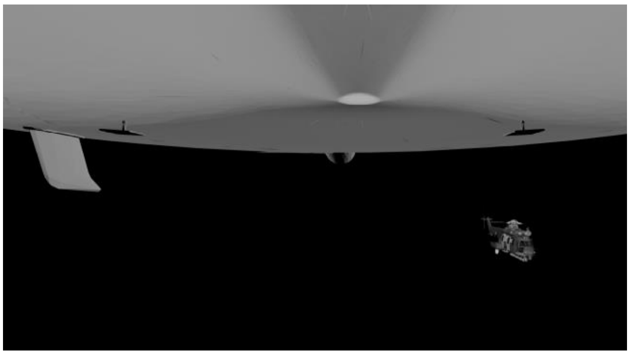

Fig. 4. Rendered image from onboard camera in the tanker.

3. Calibration and positioning of the camera

Using the 3DStudio Max software for scene simulation, the camera is initially positioned in order to cover the approaching of the helicopters to the drogues (See Fig. 4).

To calculate the receiver trajectory in tanker axis reference system it is necessary to position and calibrate the tanker camera. The camera position will be referred to the tanker reference system.

3.1. Tanker reference system

To define this tanker reference system it is necessary to know the coordinates of at least three A400M reference marks, provided by FTI design office (See Fig. 5 & 6).

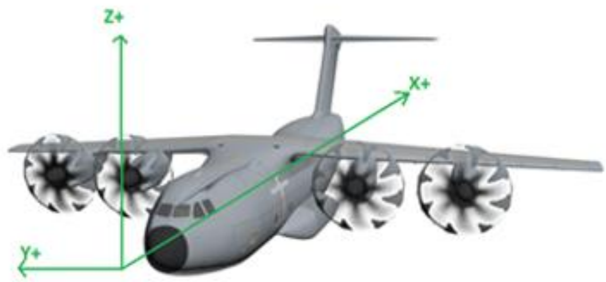

Fig. 5. A400M Tanker reference system.

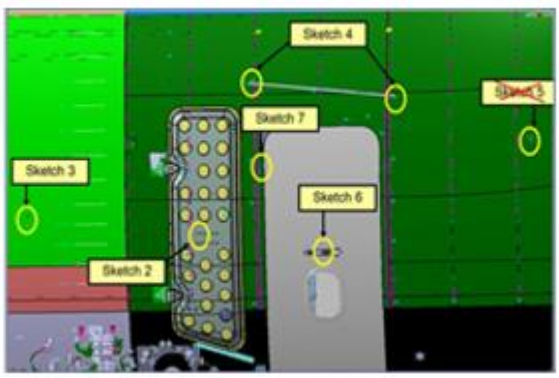

Fig. 6. A400M reference marks.

The algorithm of the closure rate calculation needs to start with the position and angles of the camera relative to the tanker reference system.

3.2. Camera calibration

The aim of the calibration process is to obtain the intrinsic optical parameters of the camera, more specifically of its lens, like focal length, principal point and distortion.

This has been done by means of Jean-Yves Bouguet's calibration toolbox [3]; taking pictures of a checked board of known dimensions (16x9 squares of 80mm) in different positions, varying distances and angles (See Fig. 7).

Fig. 7. Camera calibration.

3.3. Marks respect to the tanker reference system

Special stickers are used as marks by placing them within the cameras' visible field. With the aid of a tachymeter (See Fig. 8), the positions of the camera marks (See Fig. 9) and the reference marks (See Fig. 6) are measured in tachymeter coordinates. The position of the reference marks in tanker reference system are introduced manually in the software of the tachymeter, with this information the software of the tachymeter will transform the camera marks to the tanker reference system.

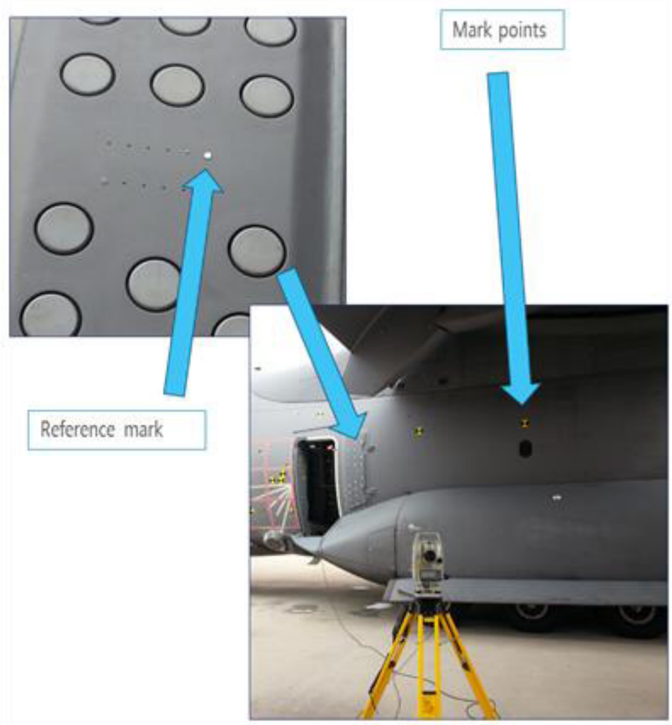

Fig. 8. Tachymeter used to measure marks in the aircraft.

Fig. 9. Calculation position and attitude of the camera using NEOS software.

3.4. Camera position and angles respect to the tanker reference system

The camera position and angles in tanker reference system is calculated through image processing and photogrammetry algorithms developed in-house in a software called NEOS.

NEOS software contains a function, based on the OpenCV solvePnP method [4]. The inputs of this calculation are the results from the camera calibration, camera marks in tanker reference system and 2D pixel coordinates of these marks (See Fig. 9).

4. Methodology to generate the closure rate

The helicopter must make contact at a reasonable speed within certain limits that allows a good coupling between the receiver probe and the tanker drogue. A minimum speed is required to produce a good coupling. A high speed can produce instabilities in the hose.

Measure the closure rate is part of the certification and qualification process. This section will explain the methodology used for this calculation between the A400M and the helicopters.

The closure rate will be derived from the receiver trajectory in tanker reference system. The trajectory calculated corresponds to one second before and after the contact. The section 4.1 will be applied in each frame in order to get the complete trajectory, the rest of the steps will work with the full trajectory to produce the final closure rate.

4.1. Calculate receiver position/angles in tanker reference system

4.1.1. Select marks in the receiver

NEOS needs at least four marks to calculate the 6DOF of the object. More marks are recommended for having greater accuracy and more robust solutions (See Fig. 10). Others recommendations to take into account are:

- Avoid coplanar marks as much as possible
- Maximize the space between marks
- Select marks that facilitate the tracking
- Avoid marks that can be hidden by others parts in the scene
- The 3D positions of the selected marks in the receiver reference system has to be well known
- Chose the geometric center of the receiver as the origin in the receiver reference system
- Select marks that produce minimum projection error (See Section 4.1.9)

Fig. 10. Marks in red selected by the user in the receiver.

4.1.2. Build transformation matrix from camera axis to receiver axis

This process calls the OpenCV method solvePnP [4] generally used in pose estimation, in this case it is used to estimate the orientation of the receiver based on the 2D image.

Inputs:

- Selected marks from the receiver in receiver reference system
- 2D pixel coordinates of these marks
- Camera calibration

Outputs:

- Transformation matrix from camera axis to receiver axis

4.1.3. Build transformation matrix from receiver axis to camera axis

Compute the inverse of the matrix of the last step.

Inputs:

- Transformation matrix from camera axis to receiver axis

Outputs:

- Transformation matrix from receiver axis to camera axis

4.1.4. Build transformation matrix from camera axis to tanker axis

Compute the rotation matrix compliant with the Tait-Bryan convention [5] followed by the camera translation. The following Python code shows this operation:

```
roll = cam.phi
pitch = cam.theta
yaw = cam.psi

R_x = np.array([[1, 0, 0],
                [0, math.cos(roll),
math.sin(roll)],
                [0, -
math.sin(roll), math.cos(roll)]])

R_y = np.array([[math.cos(pitch),
0, -math.sin(pitch)],
                [0, 1, 0],
                [math.sin(pitch),
0, math.cos(pitch)]])

R_z = np.array([[math.cos(yaw),
math.sin(yaw), 0],
                [-math.sin(yaw),
math.cos(yaw), 0],
                [0, 0, 1]])

R = np.dot(R_x, np.dot(R_y, R_z))

# Create rotation/translation
matrix
# Create identity matrix 4x4
R_4x4 = np.identity(4)
# Add rotation matrix
R_4x4[0:3, 0:3] = R
R_4x4[:, 3] = [0, 0, 0, 1]
# Add translation
R_4x4[3, 0:3] = [cam.x, cam.y,
cam.z]

return R_4x4
```

Inputs:

- Camera position / angles in tanker reference system

Outputs:

- Transformation matrix from camera axis to tanker axis

4.1.5. Build transformation matrix from receiver axis to tanker axis

Compute the dot product between the input matrices.

Inputs:

- Transformation matrix from receiver axis to camera axis
- Transformation matrix from camera axis to tanker axis

Outputs:

- Transformation matrix from receiver axis to tanker axis

4.1.6. Get receiver angles in tanker reference system

The receiver angles in tanker reference system are calculated as the Euler angles from input matrix [6].

Inputs:

- Transformation matrix from receiver axis to tanker axis

Outputs:

- Receiver angles in tanker reference system

4.1.7. Get receiver position in tanker reference system

The receiver position in tanker reference system is calculated as the dot product between the receiver position in receiver axis ([0, 0, 0, 1]) and the input matrix.

Inputs:

- Receiver position in receiver axis
- Transformation matrix from receiver axis to tanker axis

Outputs:

- Receiver position in tanker reference system

4.1.8. Add receiver position/angles to the trajectory

The position/angle of the receiver in tanker reference system is added to the trajectory.

4.1.9. Project receiver marks

Once the position/angles of the receiver are calculated the receiver marks selected by the user in section 4.1 are projected in the camera image as blue circles (See Fig. 11). The projection error corresponds to the distance between the red and blue circles. This errors will be used to choose the best set of marks.

Fig. 11. Marks in blue automatically projected in the camera image.

4.2. Trajectory visualization

A visual review of the components of the trajectory is mandatory to detect failures in the reconstruction. The graphics are also useful to check the expected behaviour of the receiver (See Fig. 12-17). This step will iterate during the complete process in order to validate the final trajectory.

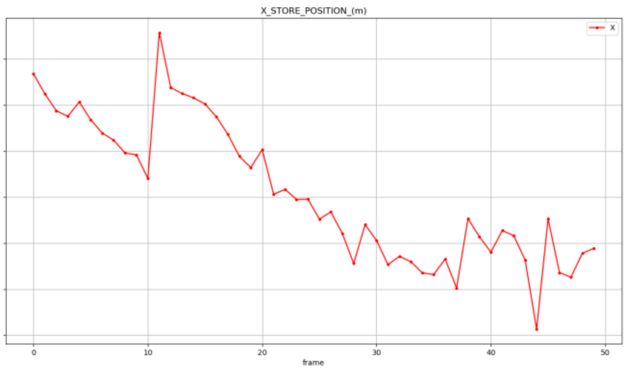

Fig. 12. X receiver relative position.

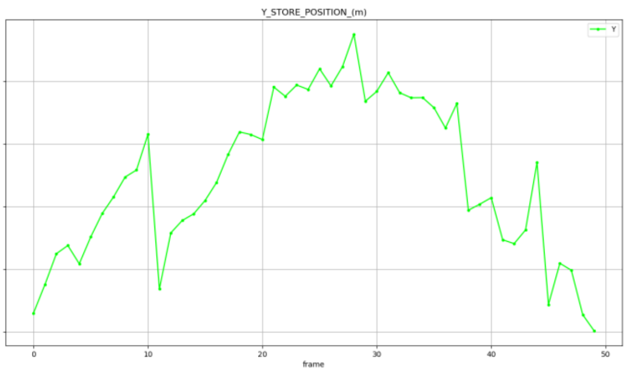

Fig. 13. Y receiver relative position.

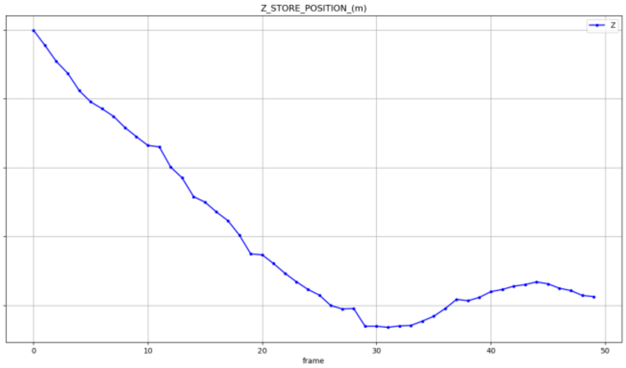

Fig. 14. Z receiver relative position.

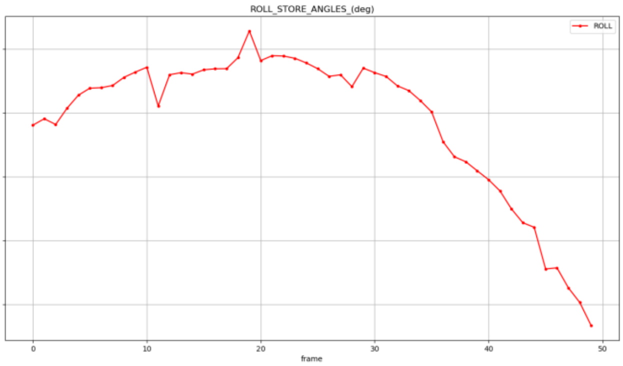

Fig. 15. Roll receiver relative angle.

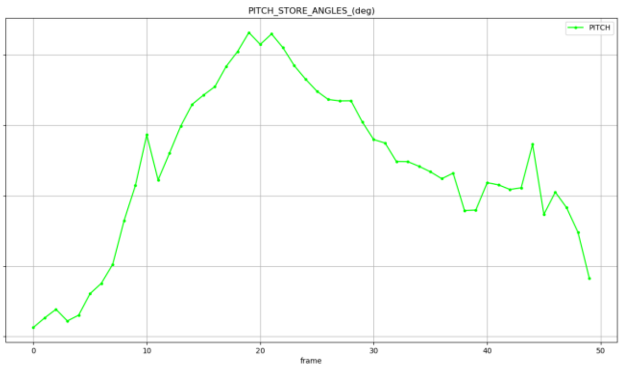

Fig. 16. Pitch receiver relative angle.

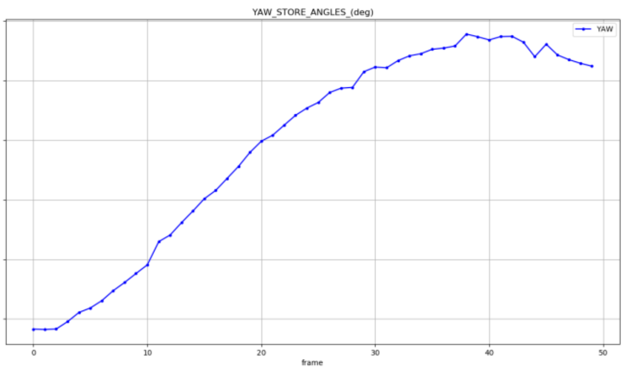

Fig 17. Yaw receiver relative angle.

4.3. Trajectory editing

In some cases the process detailed in section 4.1 generates wrong positions/angles of the receiver normally due to not enough accuracy in the marks receiver selection. In these cases there are two options:

a. Rework the marks in the receiver to gain in accuracy

b. Delete the position or angles of this frame and interpolate the hole with the information from the neighbors [7]

Option b is generally recommended when the hole is small.

4.4. Trajectory filtering

The trajectory calculated will be used to generate a relative speed to the tanker. The derivative process to calculate this speed will be more accurate if the trajectory is smoothed, therefore a filtering step [7] is highly recommended (See Fig. 18).

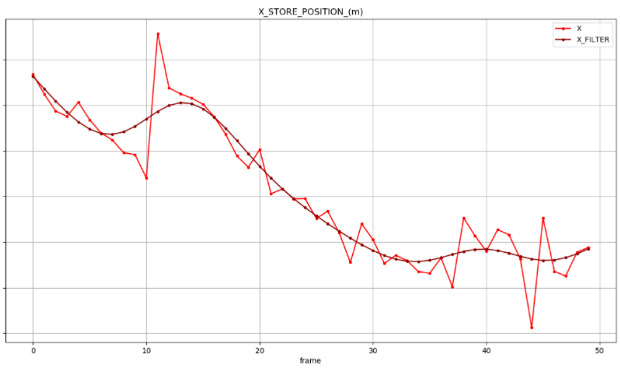

Fig. 18. X/X filtered receiver relative position.

4.5. Trajectory validation

A 3D bounding box with the dimensions of the helicopter is drawn in the camera image to validate the position and the angles of the receiver (See Fig. 19).

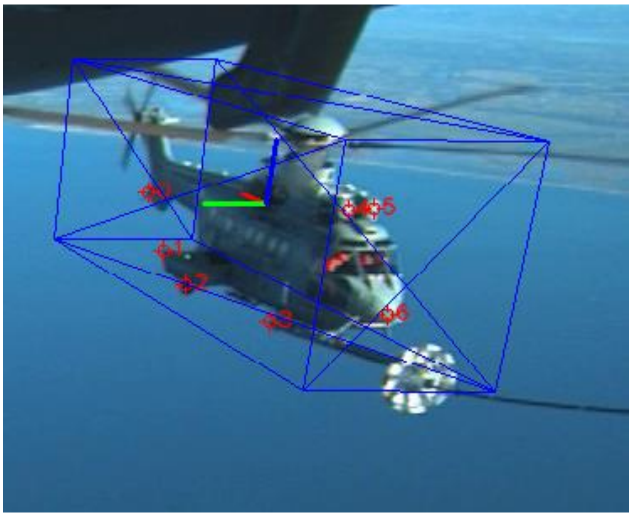

Fig. 19. 3D bounding box for validation.

These last steps could iterate several times until the trajectory is validated and sufficiently smoothed to produce a relative speed with the required accuracy.

4.6. Closure rate calculation

Once the relative trajectory of the receiver is obtained the closure rate can be calculated as a moving average speed of two elements in feet per second. In this step the three components of the speed and the speed absolute module are generated. A filter is applied to produce a smoothed speed (See Fig. 20).

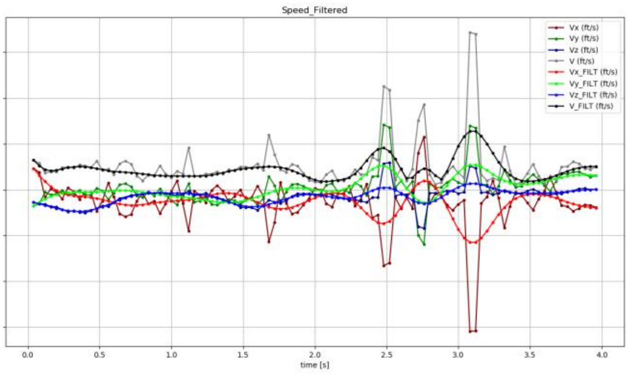

Fig. 20. Closure rate components and module. Raw and smoothed.

5. Methodology validation

The process explained in section 4 was applied to an artificial video generated by 3D Studio Max. The closure rate calculated with NEOS was validated against the theoretical speed used in the simulated video.

An empirical statistical accuracy study was done to check the error standard deviation in the generated trajectory respect to the theoretical one. The error factors considered in the study were:

- Error std in camera position / angles / calibration
- Error std in receiver marks selection

The error std in the closure rate was less than required, therefore the methodology was validated. One more time it was demonstrated that the simulation and a correct methodology were crucial for validation purposes.

6. NEOS vs other closure rate methodologies

6.1. Two cameras methodology

It is a method based on the tracking of just one mark using two cameras [1].

Advantages and disadvantages are presented with respect to the closure rate calculated using NEOS:

- Generates the 3D trajectory of one local point in the receiver meanwhile NEOS generates the relative position of the geometric center of the receiver
- Does not produce Euler angles
- Does not need to know the 3D positions of the selected mark in the receiver reference system
- Two camera positioning and calibration

6.2. One camera, 1-D methodology

It is a method based on the tracking of just one mark using one camera [2].

Advantages and disadvantages are presented with respect to the closure rate calculated using NEOS:

- Does not generate receiver trajectory
- Does not produce Euler angles
- Does not need to know the 3D positions of the selected mark in the receiver reference system
- Does not allow trajectory validation using the bounding box over the camera image
- Not camera positioning and calibration
- Not robust to lateral/vertical relative movements

7. Conclusions

This paper presents the methodology used for the closure rate calculation between the A400M and the helicopters. It also details the onboard camera installed in the tanker used for the photogrammetry algorithms.

The methodology is based on the safe separation internal tool to generate the receiver trajectory and angles in tanker reference system adding a last step to calculate the relative speed from this trajectory.

Virtual testing and empirical statistical accuracy study were used to validate the overall process.

Respect to other methodologies it is more complete and robust but on the other hand it needs information from the receiver model.

8. Acknowledgement

I would like to thank Francisca Coll Herrero for her support. I would also like to thank Moisés González Martín for giving me the opportunity to present this methodology.

9. References

[1] I. Lopez, F. Coll, A400M PARACHUTISTS TRAJECTORY CALCULATION, SFTE EC 2016

[2] F.Coll, I. Lopez, Optical Methodes to Calculate Relative Distances and Approach Speed during Refuelling Manoeuvres, SFTE EC 2016

[3] Camera Calibration Toolbox for Matlab, http://www.vision.caltech.edu/bouguetj/calib_doc, June 2008

[4] solvePnP, https://en.wikipedia.org/wiki/Perspective-n-Point

[5] Euler angles, https://en.wikipedia.org/wiki/Euler_angles

[6] Rotation Matrix to Euler Angles, https://learnopencv.com/rotation-matrix-to-euler-angles/

[7] Butterworth filter https://docs.scipy.org/doc/scipy/reference/generated/scipy.signal.butter.html

10. Glossary

AAR: Air to Air Refuelling

FTI: Flight Test Instrumentation

NEOS: New Safe Separation tool

STD: Standard Deviation

DOI 10.5162/ettc2022/5.3

Automated Registration of Large Assemblies with Robot Guided 3D Sensors and CAD-based Planning

Steffen Sauer[1], Daniel Sopauschke[1], Thomas Dunker[1], Michael Heizmann[2], Dirk Berndt[1]
[1] Fraunhofer Institute for Factory Operation and Automation IFF, Magdeburg, Germany,
[2] Karlsruhe Institute of Technology (KIT), Karlsruhe, Germany
steffen.sauer@iff.fraunhofer.de

Abstract:

We address the problem of automated inspection of rivets and brackets in aircraft fuselage shells with a robot guided 3D-sensor. High variety of such assemblies requires that an inspection automatically compares acquired 3D data to the CAD model representing the assembly. For this purpose, a precise sensor pose with respect to the fuselage shell coordinate system is needed. In this industrial context, the current set-up can deviate from the model by few centimeters which is too much for inspection. We present an automated registration method, which does not need further sensors for tracking. This method reduces the deviation between measured points and the CAD model to few tenth of a millimeter in regions with no assembly defect. Therefore, we find automatically measurement positions for registration which cover all degrees of freedom. The algorithm for registering the 3D points to the CAD model avoids the assignment of points to faces which cannot be reached by the sensor, and parts to be inspected. In addition, local registration can deal with slight deformation of the fuselage shell.

Key words: robot guided inspection, CAD model, automated viewpoint selection, point cloud registration, simulation

Motivation

We consider inspection of rivets and brackets inside an aircraft fuselage shell. As assembly errors may cause high costs in downstream processes or could lead to dangerous malfunctions, a reliable and automated inspection solution is preferred to the frequent visual inspection by a second person. Such solution must be able to inspect new part configurations without time consuming preparation effort. Digital models of assembly and work shop equipment provide necessary information for model-based inspection. Robot guided sensors assure the needed flexible acquisition of camera images and 3D point clouds.

CAD-based approaches to this inspection task need an estimate of the sensor position with respect to the coordinate system of the CAD model in order to compare an image or point cloud to the nominal model. Using the estimated sensor position, one can map the acquired data to the model. The remaining deviation between model and data of error free parts should be much smaller than the smallest deviations caused by assembly defects.

Fig. 1: Robot guided sensor inspecting a fuselage shell

We use a 3D-sensor with a measurement volume of about 160 x 100 x 110 mm^3 and a working distance of 160 mm, see Fig. 1. A hand-eye calibration showed a sufficiently small 6D uncertainty of the robot deviation on the target below one millimeter. The robot is able to inspect a volume of about 2.8 x 2.5 x 2.5 m^3, which is only a part of the entire fuselage shell. Whenever the fuselage shell position changes with respect to the robot, a local registration of the reachable region of the fuselage shell is needed. This can be achieved by registering the point cloud from four measurements in the corners of the inspection volume. This approach of reusing the inspection sensor saves e.g. further wide-angle cameras for tracking like in [1]. Besides the skin, we need to capture stringers and frames in order to bind all 6 degrees of freedom. There are two challenges: Well suited measurement positions binding all 6 degrees of freedom need to be generated automatically. The point cloud registration to the CAD model, representing mostly metal sheet parts, should not assign points to false faces that cannot be reached by the sensor.

Because of its own weight, the fuselage shell, which is held by the processing fixture, may be slightly deformed compared to the CAD model. That is why an additional local registration of single inspection measurements may be necessary.

Summarizing, our contributions presented in the sequel are:

- A solution for a viewpoint selection problem using rendering-based measurement simulation and an objective function including analysis of the surface normal distribution and
- a fast point cloud to CAD model (triangle mesh) registration using acquisition direction and surface orientation in order to avoid finding the closest point on a surface not visible for the sensor.

Related work

Survey [2] gives an overview of early work in the domain of CAD-based inspection. The papers [3, 4] discuss methods to compare camera images to rendered CAD data.

It appears natural to combine this CAD based approach with flexible robot guided image [5] and point cloud [1] acquisition by choosing viewpoints which allow to distinguish assembly errors from correct assemblies best. For reviews on viewpoint selection see [6, 7]. A recent technique to find good viewpoints is to simulate the measurement and feed it to an objective function, which measures the “goodness”. An optimization algorithm samples over the feasible viewpoints, see e.g. [5] for rendering and [8] for ray tracing.

The registration between a measured point cloud and a corresponding CAD model is usually performed with the Iterative Closest Point (ICP) algorithm [9, 10]. This algorithms is based on the detection of nearest neighbors of the points on the CAD model and the subsequent computation of a rigid transformation [11], which reduces the distances between the correspondences. This two-step process is repeated until it converges to a local optimum. In order to perform the ICP efficiently, a fast, spatial filtering technique for the point cloud is required to accelerate the costly nearest neighbor searches. The most common data structures for this purpose are the Octree [12, 13] and the k-d tree [14, 15]. Both employ a recursive, spatial subdivision method to significantly reduce the number of candidates for the nearest neighbor. Our work focuses on the k-d tree, since it enables efficient nearest neighbor searches [16] and can be implemented using a favorable memory layout [17], which is utilized in our approach.

Numerous extensions to the original ICP algorithm exist, which improve the matching procedure and increase the chance of reaching the global optimum. The correspondence detection can be extended from simple geometric distances to more sophisticated compatibility measurements [18], that take additional point cloud features into account. Common choices are intensity values obtained from 3D-scanners [19], colors [20], or surface features and contour lines [21]. Taking the normal vectors of the sampled surface into consideration helps to avoid local optima, where local surface orientations are not compatible, see [22].

Sensor simulation and view point selection

The global sensor registration is based on matching measured 3D points towards a CAD model of the given assembly. As the typically used ICP algorithm is vulnerable to local minima, the acquired 3D points must cover all six degrees of freedom in order to reach a global maximum. Thus, for the use of automatic inspection systems it is important to know well suited target locations that should be used to acquire registration data. One can see easily that a maximum spread of 3D point locations within the measuring range is not sufficient. Instead the underlying surface orientation has a major impact on the ICP algorithm result.

Therefore, we propose a new optimization technique to automatically find good sensor poses, which selects poses such that resulting 3D points are acquired from the most orthogonal surfaces around a target location. We call the evaluation criterium *orientation coverage*. It denotes the ability to cover all six degrees of freedom within a 3D point cloud.

This method uses a simulation which was already introduced in [23]. Based on sensor parameters and an assembly CAD model, the simulation framework is able to compute an approximately expected 3D point cloud generated by a fringe projection system (see Fig. 2). For a given target coordinate on the surface of an assembly, we wish to compute a sensor pose that maximizes the orientation coverage. The algorithm follows a generate and test strategy [24] and performs the following steps:

1. Generate equally distributed poses on a sphere using a radius equal to the sensor working distance.
2. Eliminate those poses that cannot be reached by the sensor due to robot movement limitations.
3. Eliminate those poses which would cause collision between sensor and assembly or robot and assembly.
4. For the remaining poses perform a sensor simulation and evaluate the orientation coverage.
5. Select the pose resulting in the highest coverage.

The number of initially generated poses depends very much on the assembly complexity. In the airplane shell scenario, we started using 4.000 poses which were typically reduced to a third, caused by collisions and robot limitations.

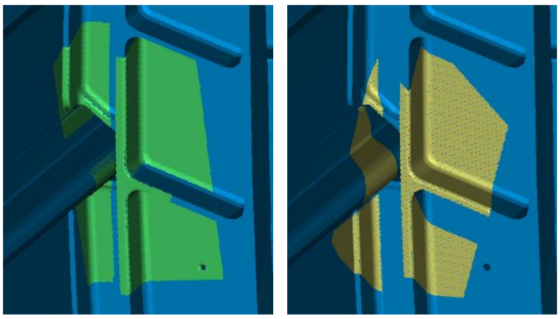

Fig. 2: Simulated point clouds. Left: a poor simulation covering only two space axes, right: more sophisticated points, covering all three axes.

To compute the *orientation coverage*, we use the surface normals within a simulated 3D view. Given a set of simulated 3D points $\boldsymbol{P}$, we call $\boldsymbol{N} = \{\boldsymbol{n}_1 \ldots \boldsymbol{n}_m\}$ the set of normals that correspond to each coordinate of $\boldsymbol{P}$. The normal can be derived from the CAD model during simulation. By visualizing $\boldsymbol{N}$ as coordinates on a unit sphere, we see a characteristic distribution depending on the scene geometry (see Fig. 3).

Furthermore, the set $\widetilde{\boldsymbol{N}} = \{\boldsymbol{n}_1 \ldots \boldsymbol{n}_m, -\boldsymbol{n}_1 \ldots -\boldsymbol{n}_m\}$ describes the set $\boldsymbol{N}$ united with the inverse of $\boldsymbol{N}$. Thus, using a principal component analysis (PCA), we can estimate the normal principal axes and their variance. As the mean of $\widetilde{\boldsymbol{N}}$ is $(0,0,0)^T$ the variance indicates the density of normals with respect to each axis.

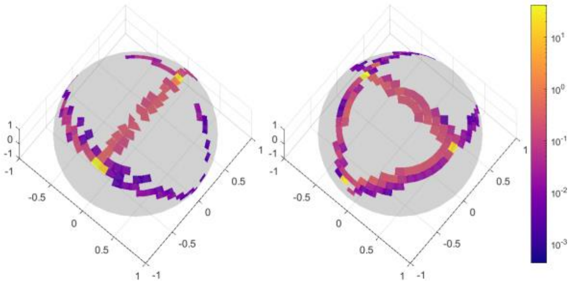

Fig. 3: Density of binned simulated surface normals on a unit sphere: left and right results from point clouds shown in Fig. 2.

Given $\widetilde{\boldsymbol{N}}$, the covariance matrix $\Sigma_{\widetilde{\boldsymbol{N}}}$ is defined as

$$\Sigma_{\widetilde{\boldsymbol{N}}} = \begin{bmatrix} cov(x,x) & cov(x,y) & cov(x,z) \\ cov(y,x) & cov(y,y) & cov(y,z) \\ cov(z,x) & cov(z,y) & cov(z,z) \end{bmatrix}. \quad (1)$$

The Eigenvalues λ_k of $\Sigma_{\widetilde{\boldsymbol{N}}}$ can be computed by solving

$$(\Sigma_{\widetilde{\boldsymbol{N}}} - \lambda_{\mathrm{k}}\boldsymbol{I})\boldsymbol{v}_{\mathrm{k}} = 0, \ \ \mathrm{k} = 1 \ldots 3. \quad (2)$$

Furthermore, let $F(\widetilde{\boldsymbol{N}})$ be a function which selects the smallest Eigenvalue of $\Sigma_{\widetilde{\boldsymbol{N}}}$:

$$\mathrm{F}(\widetilde{\boldsymbol{N}}) = \min \mathrm{eig}(\Sigma_{\widetilde{\boldsymbol{N}}}). \quad (3)$$

The smallest Eigenvalue is used as an indicator for the orientation coverage. Fig. 4 visualizes $\mathrm{F}(\widetilde{\boldsymbol{N}})$ for a set of sensor pose candidates:

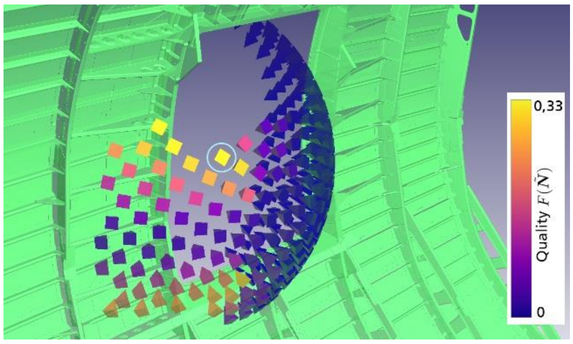

Fig. 4: Thinned result of a generate and test simulation. Evaluated sensors positions are shown as pyramids directed to a target on the surface. The color encoding visualizes each test quality. The best pose is highlighted.

Given sets of simulated normals from different sensor poses $\boldsymbol{N}_i, i = 1 \ldots n$, we finally select the dataset of index i^* that maximizes $F(\widetilde{\boldsymbol{N}}_i)$:

$$i^* = \arg\max_i F(\widetilde{\boldsymbol{N}}_i). \quad (4)$$

Based on the candidates shown in Fig. 4, the automatically selected sensor pose is visualized in Fig. 5.

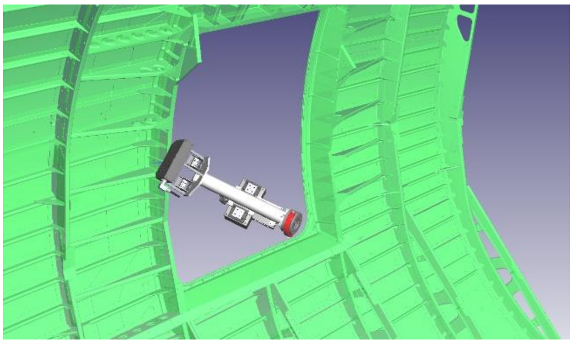

Fig. 5: A final sensor position, which is selected by using the best orientation coverage.

This method is very independent of the assembly shape itself and can be applied to arbitrary target points on the object surface. Fig. 6 shows the results of a systematic sampling of an airplane shell at distances of 100 mm. As expected the resulting qualities between the frames are extremely low, as the geometry in those regions is almost completely flat. However, in more complex areas and especially at stringer frame crossings, the expected quality reaches its maximum.

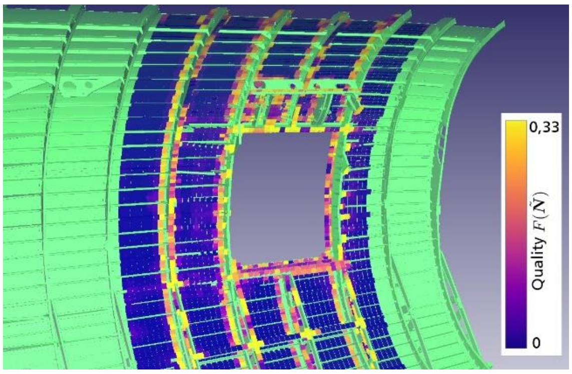

Fig. 6: Systematic surface sampling and evaluation of referencing areas. Flat areas result in low qualities whereas strongly structured geometries provide almost ideal results.

Point cloud registration

The measured point clouds are recorded in the sensor coordinate system and need to be transformed and aligned to the aircraft CAD model in order to analyze them. Usually this is done by computing a registration using the ICP algorithm. However, a direct application of this strategy is not feasible in our use case.

Since the aircraft shell is very thin the ICP, which is based on iterative nearest neighbor detections, could assign a point of the measured point cloud to the backside of the CAD model. This could result in a transformation that places the entire scan on the backside of the model, which complicates further analysis steps. Secondly, the CAD model of the aircraft does not represent the real-world situation accurately. We found out that the shell is slightly deformed, due to its own weight and supporting mounting frame. Furthermore, brackets or other parts of the shell might be missing or are mounted incorrectly, which also distracts the ICP.

To address these challenges, we subdivide the registration process into two parts: In the first step a coarse registration is computed, that aligns measurements at the corners of the inspection area with the aircraft shell as a whole. The computed transformation is used as an initial alignment afterwards, which is refined by the second registration step. This step aligns each scan individually to its local surroundings and handles the challenges created by missing or misplaced parts, while the first step ignores these issues.

Different strategies can be applied to solve the thin shell challenge. One could remove all triangles facing in the opposite direction prior to the registration. However, this approach is not feasible on larger scales, as it requires a view dependent adaption of the triangle mesh, which results in a much more complex data handling. We use a modified ICP variant, that incorporates information from normal vectors into its nearest neighbor search procedure. Only neighboring triangles, for which the scalar product between their normal vector and the one of the search point is larger than a threshold, are considered during the registration. Therefore, measurement points cannot find neighbors on the backside of the shell. This strategy only works reliably if the initial alignment of the two objects does not contain very large deviations.

Since this normal compatible alignment strategy is performed in both registration steps, computing the normal vectors of a point cloud is a vital step of the processing pipeline that should be performed with high speed. The common naïve approach (see [25]) did not fit these requirements. We therefore propose a new method for computing normal vectors of point clouds in an approximation fashion that results in low latencies while preserving enough quality to not interfere with subsequent steps.

The basic idea of our method is to extract a density dependent subset of the whole point cloud and only compute normal vectors for this subset. Afterwards, the normal vectors of this set are distributed to their local neighborhood. As a result, small patches of the point cloud will share the same normal vectors. If these patches are small enough, the subsequent steps are not or only imperceptibly impaired.

Our method is based on a k-d tree, whose structure was presented in detail in [17]. To be most efficient, our method utilizes the specific node types of the tree and their memory layout, which are shown in Fig. 7.

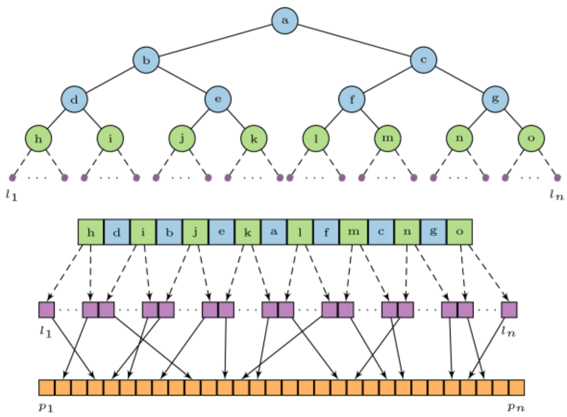

Fig. 7: Top: tree structure and node types (internal blue, pre-leaf green, leaf purple), bottom: memory layout with 3 arrays (internal and pre-leaf nodes, leaf nodes and points)

The tree consists of internal, pre-leaf and leaf nodes, whereby the internal and pre-leaf nodes are stored contiguously in an array in their in-order traversal order. The leaf nodes and actual points are stored in separate arrays.

We use the internal nodes of a specific tree level as the subset of points, for which the normal vectors are computed. This selection satisfies all requirements: Since the underlying k-d tree is constructed using a recursive median of the longest axis splitting method, the corresponding points are spread across the whole point cloud and their distribution reflects the local densities. The size of the subset grows quadratically with each tree level, so the degree of approximation can be tuned with a simple parameter.

After collecting the subset, its k-nearest neighbors of each point of the set are found. The k-d tree is used to perform this search efficiently. Afterwards a plane is fitted into the neighbor set using a least squares approximation method. The normal vector of the plane is used as the point normal.

The normal vectors of the subset are distributed to all of their children as shown in Fig. 8. Due to the special memory layout of the k-d tree, collecting the relevant child nodes can be performed very efficiently. For each subset point the leftmost leaf node of the leftmost child and the rightmost leaf node of the rightmost child are determined. These leaf nodes form a contiguous range, with all leaf nodes in between belonging to the original subset point. Traversing the tree to determine these leaf nodes isn't really required, since the leftmost and rightmost internal node can be determined by subtracting or adding an offset in the internal nodes array. Furthermore, the required computations can be performed in parallel since all subset points and their children are completely independent from another.

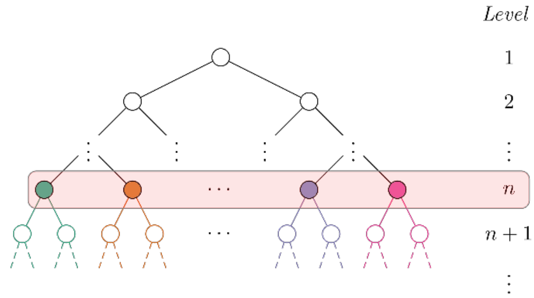

Fig. 8: Approximated normal vector distribution

After the normal vectors have been computed and distributed, a consistent alignment must be ensured, since the least squares plane fitting results in inconsistent normal vector directions. In some scenarios this inconsistency might be ignored, but our workflow relies on correctly oriented normal vectors to perform the described modified ICP algorithm. Different approaches exist to solve this issue, either by modifying the underlying eigenvector computation directly like in [26, 27], or by trying to recreate consistent alignment afterwards by propagating aligned directions through the point cloud [25, 28, 29]. However, our scenario allows to employ a simpler and faster solution. The points are measured in sensor coordinates and only points located on surfaces pointing towards the sensor have been generated. Therefore, a simple dot product test between the computed normal vector and the direction vector towards the sensor origin is enough to realign the normal vectors consistently across the point cloud.

The first coarse alignment step uses the approximated normal vectors to perform the modified ICP. It first collects the corner measurements and combines them into a single point cloud, taking the information about their corresponding robot orientation into account to preserve their relative positions and orientations. This cloud is registered against the CAD model as a whole, supported by an initial guess of its orientation. The modified ICP ensures that the cloud is aligned to the front side of the model.

Again, a k-d tree is used to speed up the nearest neighbor searches, performed by the ICP. The k-d tree uses the same structure as described before, but stores triangles instead. We found that a preprocessing of the triangle mesh of the CAD model was necessary to achieve acceptable processing speeds. The CAD model contains very long triangles, that can span

DOI 10.5162/ettc2022/5.3

almost the entire length of the aircraft shell. These elongated triangles prevent the k-d tree from creating tight bounding volumes, which otherwise account for the fast neighbor detection. Therefore, we subdivide all triangles recursively until all edges are shorter than a threshold value of 200 mm. This increases the total number of triangles by a significant amount, but nevertheless leads to an improved performance due to tighter bounding volumes.

After performing the coarse registration there are two main sources contributing to the remaining alignment error. Due to the uncertainty of the robot positions, the relative positions of the corner measurements contain a small error. The second is the deviation between CAD model and the deformed real aircraft shell, which cannot be eliminated as the cloud is transformed as a whole. The measurement uncertainty of the 3D sensor of about 50 µm can be neglected.

To reduce the remaining error, a second alignment step is performed. This fine registration is applied to each scan individually, to account for local conditions. Again, the ICP with the compatible normal nearest neighbor search is employed, to ensure that the current alignment to the front side of the aircraft shell is retained. In contrast to the coarse registration, the fine registration is performed against a simulated point cloud. Using an artificial reference cloud has several advantages. The nearest neighbor searches can be performed at higher speeds, as only a relatively small point cloud has to be searched instead of the triangle mesh of the whole CAD model. Secondly the registration is focused on the relevant parts of the model, which leaves fewer opportunities for misalignments.

Only the so-called background of the scene is simulated. No points are simulated on brackets or other parts, whose existence and placement should be checked in a following analysis. Without this exclusion the ICP could transform points of a misplaced bracket to its actual position on the CAD model. A following analysis then might overlook this assembly error due to its close alignment. Computing a registration against the background implies that a maximum distance for the nearest neighbor search of the ICP has to be defined, so only background points of the measurement are used during the alignment. Since the coarse registration ensures a decent initial alignment, enough background points are close to the CAD model and a tight threshold can be chosen.

Results

Our new method for computing approximated normal vectors can be applied to any kind of point cloud, therefore we tested it on generic data sets as well as measurements from the aircraft scenario. The results are shown in Fig. 9 and Fig. 10. The blue line depicts the runtime, displayed is the median over 10 runs. Each step of the x-axis corresponds to a specific level of nodes in the k-d tree, that results in a distribution of one computed normal to 2^x points. The red line shows the median of the overall normal quality, measured as dot product between the ground-truth normal and the approximated one. The shaded red areas display quantile ranges of the normal quality.

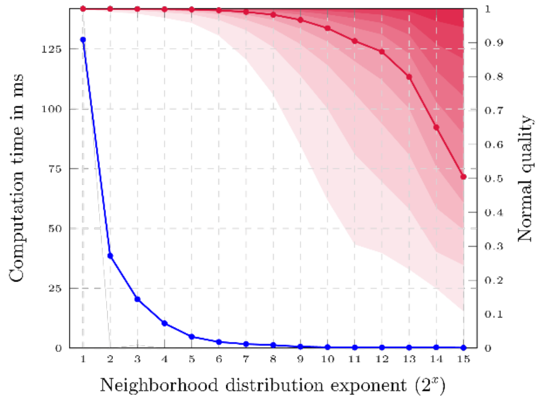

Fig. 9: Results of the approximated normal vectors computation for a generic point cloud; runtime in blue; quality of normal vectors in red; red areas show quantile boundaries in 10% steps

The runtime decreases almost quadratically with each level. The large reduction between the first two steps is explained by an implementation artifact, as the approximation is only used when a normal is distributed to more than two points. The first measurement therefore represents the base runtime with no approximation.

The quality of normal vectors remains very high and stable for the first exponents. Up to an exponent of 6, which corresponds to a distribution of one normal to 128 points, more than 90% of the points have a normal quality of 0.9 or more. The distribution patches remain small and localized enough to not impair the overall normal quality significantly. Afterwards the quality starts to drop faster with each level. The aircraft shell showed even better results, since more points retain a good normal quality for higher exponents. This is explained by the large number of flat or gently curved parts of the shell, in which a normal is very similar to its neighboring ones. Only if the distribution patches cover larger surface areas, the normal quality starts to drop significantly.

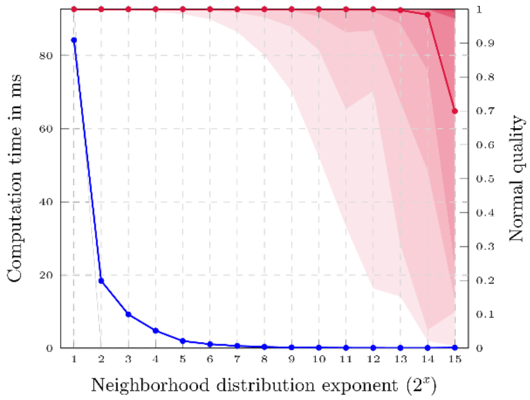

Fig. 10: Results of the approximated normal vectors computations for a point cloud from the airplane shell

In summary, choosing an exponent of four or five seems to represent a good tradeoff between high processing speeds, with reductions to 8% resp. 4% of the original runtime, and preserving a high quality of the resulting normal vectors.

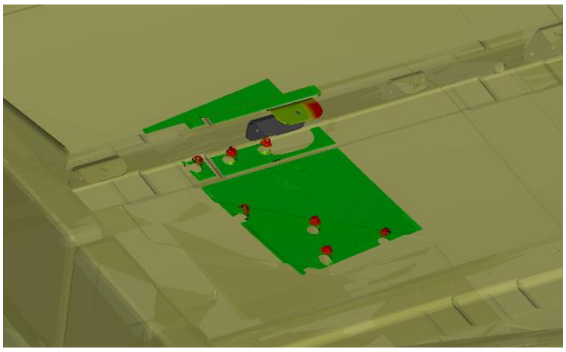

Fig. 11: Fine registration result with a misplaced bracket, colors represent distances to CAD model

The two-step registration process results in stable and close alignments of the measured point clouds with the CAD model. Due to the faster normal vector computation the overall registration time can be reduced, too. Deviations of the scans from the real CAD model are distributed across all scans.

The fine registration is able to eliminate the remaining deviations and aligns the scans very closely to the model. Especially the registration against a simulated background point cloud proves to be beneficial. Fig. 11 shows the alignment result of a misplaced bracket. A registration against the whole mesh would have resulted in a translation that places the bracket at is actual model position, making it challenging to detect this assembly error afterwards.

Summary

In this article we presented a novel, innovative approach for the automatic registration of 3D point clouds in challenging inspection tasks. Therefore, we use a CAD model based, two step registration. In the first step, we compute a coarse registration which estimates a 3D sensor location roughly. Suitable sensor poses for the required data acquisition are computed in preface by simulation and automatic view point selection. In the second step, a fine registration is performed that accounts for local deviations from the CAD model and improves the prior alignment. Both registration computations use a modified ICP algorithm, which registers measured 3D point clouds to simulated point clouds efficiently.

References

[1] H.B. Abdallah, J.-J. Orteu, B. Dolives, and I. Jovančević, 3D point cloud analysis for automatic inspection of aeronautical mechanical assemblies, *Fourteenth International Conference on Quality Control by Artificial Vision*, 209–217 (2019), doi: 10.1117/12.2521715.

[2] T.S. Newman and A.K. Jain, A Survey of Automated Visual Inspection, *Computer Vision and Image Understanding* 61 (2), 231–262 (1995), doi: 10.1006/cviu.1995.1017.

[3] I. Viana, J.-J. Orteu, N. Cornille, and F. Bugarin, Inspection of aeronautical mechanical parts with a pan-tilt-zoom camera: an approach guided by the computer-aided design model, *J. Electron. Imaging* 24 (6), 61118 (2015), doi: 10.1117/1.JEI.24.6.061118.

[4] S. Sauer, E. Trostmann, D. Berndt, and G. Holtmann, Optische Messsimulation zur flexiblen, automatischen Montageprüfung, *19. Anwendungsbezogener Workshop zur Erfassung, Modellierung, Verarbeitung und Auswertung von 3D-Daten (3D-NordOst 2016)*, 123–132 (2016).

[5] H. Ben Abdallah, I. Jovančević, J.-J. Orteu, and L. Brèthes, Automatic Inspection of Aeronautical Mechanical Assemblies by Matching the 3D CAD Model and Real 2D Images, *Journal of Imaging* 5 (10), 81 (2019), doi: 10.3390/jimaging5100081.

[6] S. Chen, Y. Li, and N.M. Kwok, Active vision in robotic systems: A survey of recent developments, *The International Journal of Robotics Research* 30 (11), 1343–1377 (2011), doi: 10.1177/0278364911410755.

[7] R. Zeng, Y. Wen, W. Zhao, and Y.-J. Liu, View planning in robot active vision: A survey of systems, algorithms, and applications, *Comp. Visual Media* 6 (3), 225–245 (2020), doi: 10.1007/s41095-020-0179-3.

[8] T. Kot, Z. Bobovský, D. Heczko, A. Vysocký, I. Virgala, and E. Prada, Using Virtual Scanning to Find Optimal Configuration of a 3D Scanner Turntable for Scanning of Mechanical Parts, *Sensors (Basel, Switzerland)* 21 (16), 5343 (2021), doi: 10.3390/s21165343.

[9] P.J. Besl and N.D. McKay, Method for registration of 3-D shapes, *Sensor fusion IV: control paradigms and data structures*, 586–606 (1992), doi: 10.1117/12.57955.

[10] Y. Chen and G. Medioni, Object modelling by registration of multiple range images, *Image and Vision Computing* 10 (3), 145–155 (1992), doi: 10.1016/0262-8856(92)90066-C.

[11] W. Kabsch, A solution for the best rotation to relate two sets of vectors, *Acta Cryst A* 32 (5),

922–923 (1976), doi: 10.1107/S0567739476001873.
[12] D. Meagher, Geometric modeling using octree encoding, *Computer Graphics and Image Processing* 19 (1), 85 (1982), doi: 10.1016/0146-664x(82)90128-9.
[13] M. Schütz, S. Ohrhallinger, and M. Wimmer, Fast Out-of-Core Octree Generation for Massive Point Clouds, *Computer Graphics Forum* 39 (7), 155–167 (2020), doi: 10.1111/cgf.14134.
[14] J.L. Bentley, Multidimensional binary search trees used for associative searching, *Commun. ACM* 18 (9), 509–517 (1975), doi: 10.1145/361002.361007.
[15] R.A. Brown, Building a Balanced k-d Tree in O(kn log n) Time, *Journal of Computer Graphics Techniques (JCGT)* 4 (1), 50–68 (2015), doi: 10.48550/arXiv.1410.5420.
[16] J.H. Friedman, J.L. Bentley, and R.A. Finkel, An Algorithm for Finding Best Matches in Logarithmic Expected Time, *ACM Trans. Math. Softw.* 3 (3), 209–226 (1977), doi: 10.1145/355744.355745.
[17] D. Sopauschke, C. Teutsch, E. Trostmann, and D. Berndt, A parallel memory efficient outlier detection algorithm for large unstructured point clouds, *Optical Measurement Systems for Industrial Inspection XII. 21-25 June 2021, online only, Germany*, 68 (2021), doi: 10.1117/12.2592299.
[18] S. Rusinkiewicz and M. Levoy, Efficient variants of the ICP algorithm, *Proceedings Third International Conference on 3-D Digital Imaging and Modeling* (null), doi: 10.1109/im.2001.924423.
[19] G. Godin, M. Rioux, and R. Baribeau, Three-dimensional registration using range and intensity information, *Videometrics III*, 279–290 (1994), doi: 10.1117/12.189139.
[20] M. Korn, M. Holzkothen, and J. Pauli, Color Supported Generalized-ICP, *Proceedings of the 9th International Conference on Computer Vision Theory and Applications* (2014), doi: 10.5220/0004692805920599.
[21] J. Fan, L. Ma, and Z. Zou, A method of registering point cloud with CAD model based on line contour matching, *Optics and Photonics for Information Processing XIV*, 55–64 (2020), doi: 10.1117/12.2570494.
[22] K. Pulli, Multiview registration for large data sets, *Proceedings / Second International Conference on 3-D Digital Imaging and Modeling, October 4 - 8, 1999, Ottawa, Ontario, Canada*, 160–168 (1999), doi: 10.1109/IM.1999.805346.
[23] S. Sauer, T. Dunker, and M. Heizmann, Ein Framework zur Simulation optischer Sensoren, *20. GMA/ITG-Fachtagung. Sensoren und Messsysteme 2019*, 35–42 (2019), doi: 10.5162/sensoren2019/1.1.1.
[24] K.W. Khawaja, A.A. Maciejewski, D. Tretter, and C.A. Bouman, Camera and light placement for automated assembly inspection, *Proceedings 1996 IEEE International Conference on Robotics and Automation*, 3246–3252 (1996), doi: 10.1109/ROBOT.1996.509207.
[25] H. Hoppe, T. DeRose, T. Duchamp, J. McDonald, and W. Stuetzle, Surface reconstruction from unorganized points, *Proceedings of the 19th annual conference on Computer graphics and interactive techniques*, 71–78 (1992), doi: 10.1145/133994.134011.
[26] R. Bro, E. Acar, and T.G. Kolda, Resolving the sign ambiguity in the singular value decomposition, *J. Chemometrics* 22 (2), 135–140 (2008), doi: 10.1002/cem.1122.
[27] F. Tombari, S. Salti, and L. Di Stefano, Unique Signatures of Histograms for Local Surface Description, 356–369 (2010), doi: 10.1007/978-3-642-15558-1_26.
[28] H. Xie, J. Wang, J. Hua, H. Qin, and A. Kaufman, Piecewise C/sup 1/ continuous surface reconstruction of noisy point clouds via local implicit quadric regression, *IEEE Visualization 2003. Seattle, Washington, October 19 - 24, 2003; VIS 2003; proceedings*, 91–98 (2003), doi: 10.1109/VISUAL.2003.1250359.
[29] N. Schertler, B. Savchynskyy, and S. Gumhold, Towards Globally Optimal Normal Orientations for Large Point Clouds, *Computer Graphics Forum* 36 (1), 197–208 (2017), doi: 10.1111/cgf.12795.

DOI 10.5162/ettc2022/5.4

Utilising an Autonomous Video Kit for Launcher to Video Deployment of the James Webb Space Telescope

Diarmuid Corry[1], Danny Gleeson[1], Michael Martin[1], James Murphy[1], Peter O'Connor[1], Aaron O'Grady[1], Peter Reynolds[1], John E Ward[1]
[1] Réaltra Space Systems Engineering Ltd., Dublin, D17 H262, Ireland
dcorry@realtra.space

Abstract:
This paper describes the elements of a video kit comprised of terrestrial COTS equipment, modified and re-qualified for the space environment and supplied as a complete self-contained system with minimal interfaces to the host launcher. The video system was used to capture, compress and downlink the HD video images of the James Webb Telescope being deployed after launch on 25th of December 2021, and provided mankind's last direct view of the telescope as it headed on its mission. The video system provided the world's first HD video images broadcast from orbit. The paper describes the components of the video kit and the process of development, integration and qualification that led to the capture of those iconic images..

Key words: Video, Space, Telemetry, JWST, COTS.

Introduction

The use of real-time video imagery on launchers is still relatively rare. While SpaceX has led the way (using COTS equipment as early as 2011 [1]), other launcher manufacturers have been slow to follow. This is because providing a reliable video kit for a launcher is not a trivial task, and there are many challenges to overcome. Apart from the normal technical constraints of limited on-board processing power for compression and restricted bandwidth for telemetry of the images, there are the additional constraints of weight, size, shock and vibration which are critical in a launcher environment. In addition, thermal management becomes difficult once the spacecraft leaves the earth's atmosphere. Finally, since a functional video system is not mission critical for most launches, the system must in no way affect the reliable operation of the launcher or any of its on-board systems which greatly constrains the type of electrical interfaces which can be supported. From a commercial point of view, the system needs to be cost-effective in the highly competitive launcher market.

The autonomous Video Kit (VIKI) was conceived and developed by Réaltra Space Systems Engineering Ltd. (www.realtra.space) as a solution to meet these onerous requirements. The system is a complete telemetry kit consisting of cameras, data concentration unit, power distribution unit, battery, RF transmitters and antenna. While initially developed for use on a different launch mission the VIKI system was reconfigured for installation on the Ariane5 and had its maiden voyage on launch VA-256 on December 25th 2021 for the historic launch of the James Webb Space Telescope (JWST)..

Using COTS in a Space Environment

VIKI progressed from concept to qualified flight model in approximately two years. This relatively rapid development was made possible by using Commercial Off The Shelf (COTS) equipment designed for terrestrial applications and modified it for space use, coupled with a nimble development process that involved close co-engineering between all the stakeholders over the entire program life.

COTS in this context refers to complete sub-systems (as opposed to using COTS components in "New Space" design applications). Réaltra has developed a four stage process for qualifying COTS for the space environment. First, terrestrial electronics are characterised to assess their suitability for use in orbit, then the mission requirements are mapped in detail. Next, the technology is adapted so that it can function reliably in the harsh environment of space before being put through its paces in specialist test facilities ahead of launch. This is the process that was followed to develop VIKI.

Requirements Synthesis

Functional

The primary function of VIKI is to capture and telemeter HD video in real-time from the launcher during the launch mission. From an operational point of view, the key constraint is the limited link budget. In addition, the available budget changes through the course of the mission as the spacecraft travels further from the ground stations. The system therefore has to adapt to the various stages of the mission. This adaptation must occur autonomously as there is no uplink available for control.

In order to meet this operational requirement several key requirements were identified:

- A need for efficient on-board video compression. H.265 compression was selected as it offers the highest efficiency currently available in a hardware implementation
- Dynamic control of the compression algorithm to permit the system to adjust to available bandwidth, using a constant bit rate (CBR).
- Some on-board intelligence is required, both to monitor system performance and to implement configuration changes during the course of the mission
- Compliance with open video standards is required to enable the transmitted video to be processed and broadcast using common tools

Environmental

The VIKI system is designed to be installed in the equipment bay of the Upper Stage of a launcher. In this location the equipment may experience severe vibration during take-off, coupled with extreme shock when the fairings are explosively jettisoned. The envelope for the vibration and shock qualification exceeded that of the COTS elements used in the system, so these requirements had to be considered and modifications to the COTS units were implemented to mitigate the effects.

The thermal environment experienced by the unit was also challenging. On the ground, the equipment experiences high humidity and temperatures up to 40C, but during launch the temperatures quickly drop as the launcher escapes the atmosphere. Once in a vacuum, there is no longer any heat convection and localised hot-spots can quickly develop around devices such as MOSFETS, FPGAs and processors. A detailed thermal model of the unit had to be developed and validated during a campaign of ground testing in a thermal vacuum chamber. Once identified, the COTS units had to be modified to mitigate the effects of hot spats and ensure the component thermal junction temperature limits were not exceeded.

The EMC/EMI environment of a launcher can also present problems since the usual EMC profile contains “notches” in which there is very little tolerance of emitted radiation. Further modification of the power and wiring interfaces were implemented.

Radiation

The short duration of a launch mission means that long-term radiation effects (Total Ionisation Dose) are not normally a concern. However, single event upsets (SEUs) are and an SEU could lead to a part of the system failing. A detailed analysis of radiation susceptibility was performed. The distributed nature of the processing and system operation reduces the chances of an SEU causing a total failure. In addition, fault detection and mitigation was built-in to the power distribution unit and the control processor to provide a macro level of recovery.

Interfaces

The Ariane5 is an extremely reliable launcher, with a 95.5% success rate out of 111 launches. There has been only one partial failure in the 98 launches since April 2003 [2]. Given its track history and reliability, it was a necessary requirement that adding VIKI could not in any way compromise the safety, capacity or reliability of the host spacecraft. This is accomplished by minimising the interfaces between the existing spacecraft systems and VIKI. In effect the unit had to be stand-alone.

In the end, the spacecraft electrical interfaces were reduced to just five:

- 1 dry-loop (relay) for on/off control
- 1 dry-loop (relay) for on/off control
- 1 dry-loop (relay) for system reset
- 2 RF interfaces from the transmitter to antennae that were already installed on the spacecraft

In addition to the electrical interfaces the mechanical mounting required some adaptation of the spacecraft to provide mounting points for the VIKI equipment. The same mechanical interfaces provided the thermal conduction path for the equipment once in orbit. Mass is a critical parameter for launcher performance, so there was a requirement to provide the system functionality at the lowest mass possible. This presented a significant challenge since the mass constraint had to be traded off against the shock, vibration and thermal constraints.

DOI 10.5162/ettc2022/5.4

System Overview

Complete System

The VIKI system is an Ethernet system built around the KAM-500 Data acquisition Unit from Curtiss-Wright Corp [3] which acts as the VIKI Data Controller Unit (VDCU). A full system block diagram is shown in Figure 1 while the network topology is shown in Figure 2.

Each element of the system is a COTS part, designed and manufactured for a terrestrial aerospace environment, with the exception of the Power Distribution and Control Unit (PDCU) which was an existing space qualified design that was modified for the VIKI requirements.

While the VIKI system can support up to six cameras, just two were installed for the JWST launch.

The principal of operation is that the cameras are IP cameras, streaming video into the network architecture hosted in the VDCU. The video streams eventually end up in IP Switch 1 where they are combined with system health information and made available to the Electrical Ground Support Equipment (EGSE) while on the launch pad, and the CCSDS encoder for telemetry when in flight.

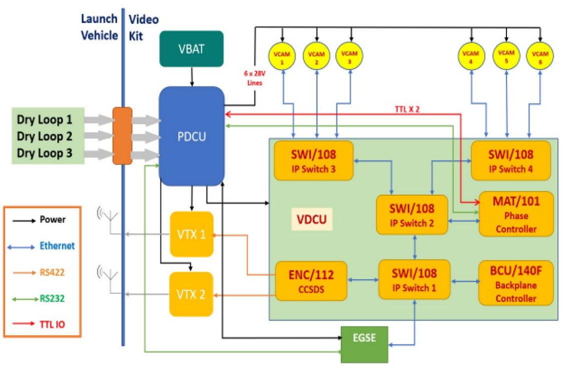

VIKI Block Diagram

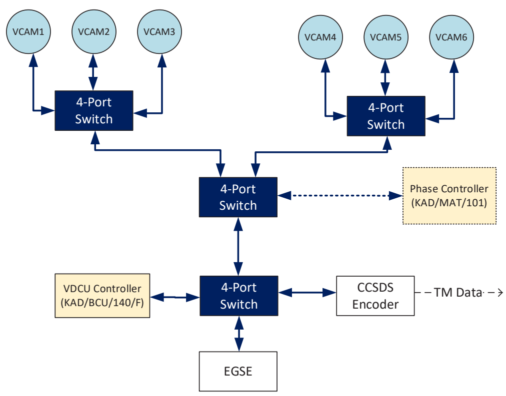

VIKI Network Topology

The CCSDS encoder can filter and process the IP data for encapsulation in CCSDS transmission frames. These frames are then sent via two independent and redundant RS-422 outputs to two independent transmitters. The transmitters send the RF data to the antennae for transmission to ground.

Camera operations are dynamically controlled by the phase controller based on sequenced inputs from the dry-loops. The dry loops are also used to power the entire system on or off and to reset it to a known initial state

Data Concentrator Unit

The VDCU is based around the KAM-500 Data Acquisition system from Curtiss-Wright. The COTS KAM-500 was selected as the base unit because of its space heritage and relatively small size, mass and power footprint [4], [5].

Réaltra developed a 9-user slot space grade version of the KAM-500 chassis which acts as a host for COTS modules from the KAM-500 family.

The VDCU runs from 28V and is powered by the PDCU. It acts as the main controller and data management centre for the VIKI system. It implements several discrete functions as follows:

1. Implementation of the VIKI network via a number of 4-port network switches. The switches (manufacturer part number KAD/SWI/108) are cross-bar switches designed to be live at power up. They provide data filtering capability and support IEEE1588 time protocols. Their fixed, preconfigurable capability makes them ideally suited for this launcher application where all aspects of the network need to be deterministic and pre-configurable. Being fully FPGA based increased their tolerance to radiation upsets.
2. Operational Phase control of the entire VIKI system via an integrated micro-processor (manufacturer's part number KAD/MAT/101). The module is fed conditioned versions of the dry-loop inputs from the spacecraft over TTL. Based on the input the module selects a pre-configured state from a mission table that determines the configuration and power status of each element of the system. The module can communicate with both the PDCU and the cameras to implement the desired configuration. This allows the mission controller to control both the power utilisation and the bandwidth utilisation of the VIKI system and tailor it for different phases of the mission. The software to manage the phases was developed by Réaltra and is designed for robust operation as an

autonomous system, with built-in protections against loss of state in the event of an unexpected event. Configuration information (such as the mission state table) is stored in triplicate in non-volatile memory and uses voting techniques to detect and mitigate against radiation induced bit errors.

3. Encapsulating the IP data streams from the cameras in a CCSDS frame for transmission to the RF encoders. This is performed by a dedicated encoder (manufacturer part number KAD/ENC/112) which outputs two identical data streams for redundancy. The KAD/ENC/112 was developed by Curtiss-Wright specifically for launcher applications and was part funded by the ESA FLPP office. The encoder captures the camera data packets, along with system housekeeping packets created by the VDCU itself, and creates a CCSDS bit stream. The source cameras and the transmission bit-rate can be changed as the mission progresses to optimise data trasnfer to the available link budget.

VIKI System showing (left to right): PDCU, VDCU and two VCAM cameras

Cameras

The VCAM is based on the HDC-430 IP Camera from Curtiss-Wright. This camera was selected based on its use in aerospace applications, integrated H.265 compression, support for standard C-mount lenses and ease of control and configuration over standard IP protocols. The camera has integrated H.265 compression and can provide HD video at bit rates from 128kbps to 5Mbps. Video is output as H.265 frames embedded in an MPEG2 transport stream.

The camera required significant re-engineering to meet the shock and thermal environment encountered by the camera. A custom housing was developed to provide both protection and support for the lenses, as well as enhanced thermal conduction. The housing also integrated IR filtering and anti-fog measures. For interior mounting, an LED unit was mounted on the housing to provide illumination of the payload while the fairings were closed.

Power Distribution and Control Unit

The PDCU was provided by Evoleo Technologies (Portugal), designed specifically for VIKI but as an evolution of an existing design.

The PDCU provides all the power management of the system. It accepts 28V from the battery, and distributes it to up to ten devices. Each output channel can be turned on or off under RS-232 control. The unit provides over-current monitoring and can autonomously power down an output in the event of an over-current condition.

Battery

The battery was developed for VIKI by Réaltra utilising military grade Li-MnO2 battery cells from SAFT. Two variants were developed (42Ah and 63Ah) to provide for different mission durations. The harsh shock and vibration environment presented a particular challenge for the battery design, but the unit that was eventually qualified meets all safety and environmental requirements. The battery is intended for use as a non-rechargeable primary battery.

The battery has mounting locations for the RF transmitters, one on each side. While simplifying installation, they also allows the battery, which has a large thermal mass, to act as an effective heatsink for those high power devices.

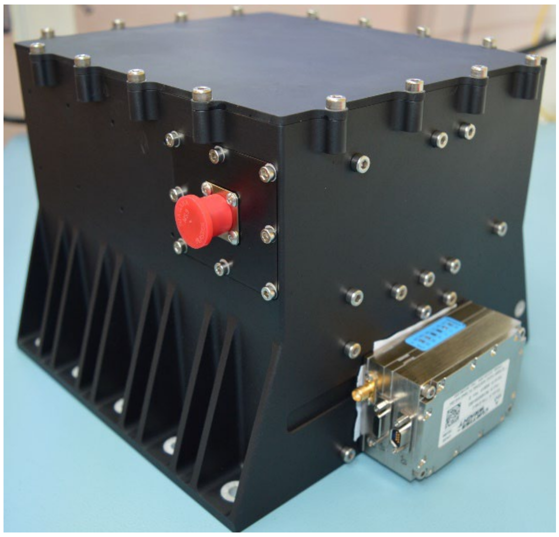

VBAT Battery for VIKI with RF Transmitter

Transmitters

The RF transmitters are COTS devices from Curtiss-Wright, model number TTS-5749. This is an S-Band transmitter ruggedised for Aerospace environments, with a power capability up to 10W. The transmitter interfaces to existing Antennae on the spacecraft.

Electrical Ground Support Equipment

An EGSE was developed to meet the needs of VIKI during testing, qualification, integration and pre-flight configuration and was supplied by Celestia-STS (Netherlands).

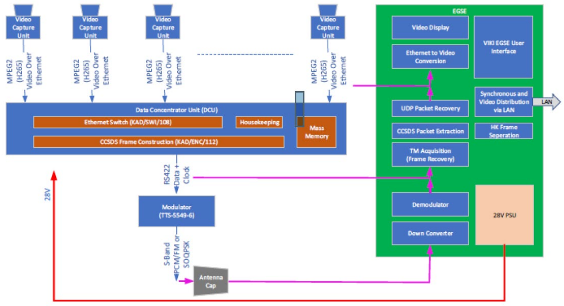

EGSE Block Diagram

EGSE Unit

Réaltra developed additional ground support harnesses and dry-loop emulators for the test phase.

The EGSE consists of a standard 19” rack unit with an integrated laptop and a combination of standard equipment including a down convertor, and demodulator. Software developed by Réaltra builds on the Celestia STS provided interfaces to create a user-friendly interface that permits detailed control of the EGSE, and examination of the data streams from the VIKI unit both at a raw binary level and as a fully decompressed video output.

The EGSE is used for system test and configuration, and for pre-checks before launch.

Integration and Qualification

During the design and integration phase extensive analysis of the COTS units was performed. A lack of detailed information from the manufacturers meant that some critical performance parameters had to be determined empirically through development testing. A series of analyses were produced to determine worst case performances, failure modes, thermal and mechanical performance. In addition radiation effects on the COTS parts were analysed and a detailed Reliability, Availability, Maintainability and Safety (RAMS) analysis was performed.

Integration of the VIKI system took place in Réaltra’s premises in Dublin. A three model philosophy was adopted:

- Electrical Mock-up (EM): A functionally representative system both mechanically and electrically.
- Qualification Model (QM): A system that is fully representative of the flight model, used for the qualification campaign
- Flight Model (FM): The model intended for installation and flight

These models were then subjected to a sequence of tests to build up a dataset that proved the systems capabilities for operation in the mission environment (Table 1). Where possible, testing was carried out in-house by Réaltra personnel, but where specialist test equipment or facilities were required the testing was out-sourced.

Test	EM	QM	FM
Screening	X	X	X
Physical Properties	X	X	X
Full Functional Performance	X	X	X
Resonance Search		X	X
Sine Vibration		X	
Random Vibration		X	X
Mechanical Shock		X	
Thermal Cycling		X	X
Thermal Vacuum		X	
Thermal Shock		X	
EMC/EMI		X	
ESD		X	
Full Functional Performance	X	X	X

Table 1: Test Sequence

The test campaign was planned to take place at the test facilities in DLR Bremen under supervision of Réaltra personnel in early 2020. The emergence of the world-wide Covid-19 pandemic meant that travel to test facilities was prohibited, so a few hectic weeks were spent re-configuring the test plans and writing a series of software tools that would permit DLR personnel to perform the tests under remote supervision. The first series of tests were successfully performed in this way.

For the subsequent series of tests, all testing was performed on the island of Ireland once in country travel was permitted. Several test facilities undertook to upgrade their capabilities to meet the demanding requirements, and a thermal vacuum test facility was commissioned in Dublin. With the assistance of these partners, and under the guidance of Réaltra personnel, the test campaign was completed within schedule and a successful Qualification Review was held early in 2021 which enabled the system to be approved for installation on the Ariane5 for the JWST launch. This marked the first time a space system was qualified wholly on the island of Ireland.

In parallel with the system qualification, the installation plan for the equipment on the launcher was created. Once installation locations were finalised, a final thermal analysis was performed to ensure that the conduction paths were sufficient to keep the unit within functional thermal limits. This was especially critical for the cameras which were mounted on a raised framework.

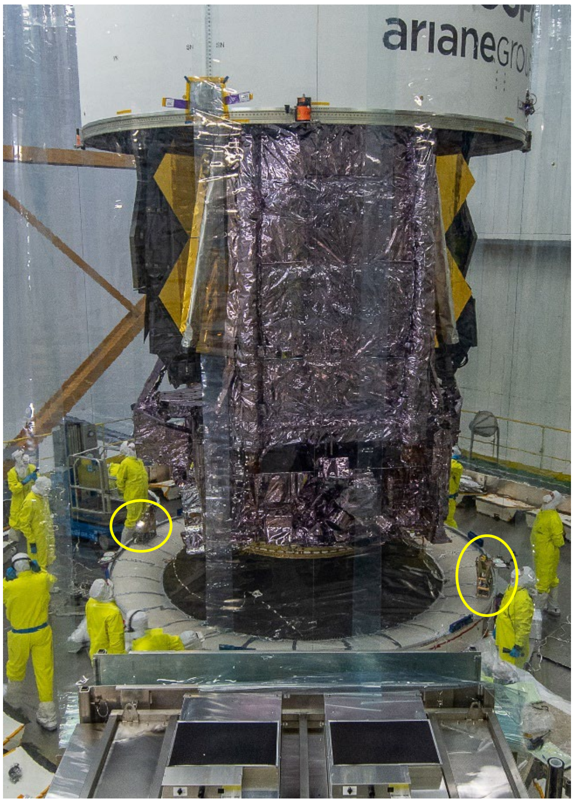

Fairing being lowered over JWST. VIKI cameras visible on left and right - left camera LED is on.

Installation and Commissioning

The VIKI unit shipped from Dublin, Ireland in Q2 of 2021 to ArianeSpace in Bremen where it was installed in the equipment bay of the Ariane5 upper stage in preparation for transportation to the launch site in Kourou, French Guiana.

Once at the launch site, ArianeSpace personnel performed pre-flight checks and evaluations during launcher preparation. This included a complete test with RF being transmitted from VIKI to the ground station and video images recorded successfully. All testing and checks were completed before the payload (JWST) was lowered onto the upper stage and attached. The VIKI cameras were used to observe the process of lowering the fairings over the JWST. The margins were very tight due to the telescope's large size [6].

Performance

VA-256 launched at 12:20 UTC on December 25th 2021. The camera was configured to capture HD video (1920px x 1080px), compress and transfer it to the VDCU for encapsulation and transmission. The transmission rate was adjusted during the course of the mission.

The VIKI system was operating from before take-off and successfully recorded and transmitted conditions in the upper stage during the entire launch; before, during and after payload deployment. While most of this recording is proprietary, several key segments were shown during the live broadcast – a brief view of the JWST in-situ on the upper stage shortly after the fairings had been jettisoned (using both cameras to provide a view from each side) and the, now famous, view of the JWST being deployed from the upper stage and moving majestically away. This segment is publicly available at https://www.esa.int/ESA_Multimedia/Videos/2021/12/Webb_separation_from_Ariane_5 and demonstrates the excellent performance of the VIKI system, the first time HD video has been broadcast from space.

Conclusion

The hostile environment of a launcher, coupled with the relatively low volumes required, makes the development of a bespoke video system for launchers prohibitively expensive. However, adapting COTS equipment for the same environment is a challenging exercise which involves a series of engineering trade-offs and some degree of modification and adaption of the COTS equipment. Nevertheless, the VIKI system demonstrates that achieving a cost-effective balance of cost and performance is possible.

To create VIKI, Réaltra took a variety of COTS equipment from different suppliers and modified them to meet the mission requirements of their customer. The modified systems were then integrated and put through a rigorous qualification campaign to ensure that the overall system would perform as expected during the mission.

The entire project was completed in less than two years, and culminated in an astonishing and iconic video that gave mankind our last view of the JWST departing on its historic mission to reveal the deepest secrets of the beginnings of our universe.

Acknowledgements

The development, integration and qualification of VIKI was a complex task completed in a relatively short time. This would not have been possible without the enthusiastic and dedicated support of partners and suppliers. Réaltra would like to acknowledge the following individuals and corporations without whom VIKI would not have been possible.

Réaltra VIKI Team: Graham Buckley, Diarmuid Corry, Jim Davenport, Ronan Flanagan, Danny Gleeson, Michael Martin, Oxin McKittrick, James Murphy, Sophie Nolan, Peter O'Connor, Aaron O'Grady, Peter Reynolds, John E Ward, Paddy White, Paul White, Aidan Wilson, Mark Wylie, Saoirse Corry.

ArianeSpace VIKI Team: Jesus Aspas-Puertolas, Florian Bouvay, Laurent Mazo, Celen Nil, Brice Pinta, Philippe Rello, Francois Tourreuil

Realtime Technologies Space Manufacturing Team: Agita Branka, Brendan Chapweteka, Yesudas Devassy (Daz), Luke Hall, Danny Murphy, Liam Murphy, Peter O'Kane,

COTS and supporting equipment was supplied by Curtiss-Wright Corp. (www.curtisswrightds.com), Evoleo (www.evoleotech.com), SAFT (www.saftbatteries.com), Schneider (www.schneiderkreuznach.com) and Celestia STS (www.celestia-sts.com).

Testing and qualification services were provided by Resonate Testing Ltd. (www.resonatetesting.com), Compliance Engineering Ireland Ltd. (www.cei.ie), DLR (Bremen) (www.dlr.de) and EnBio (www.enbio.eu).

Support provided by the European Space Agency and Enterprise Ireland.

.

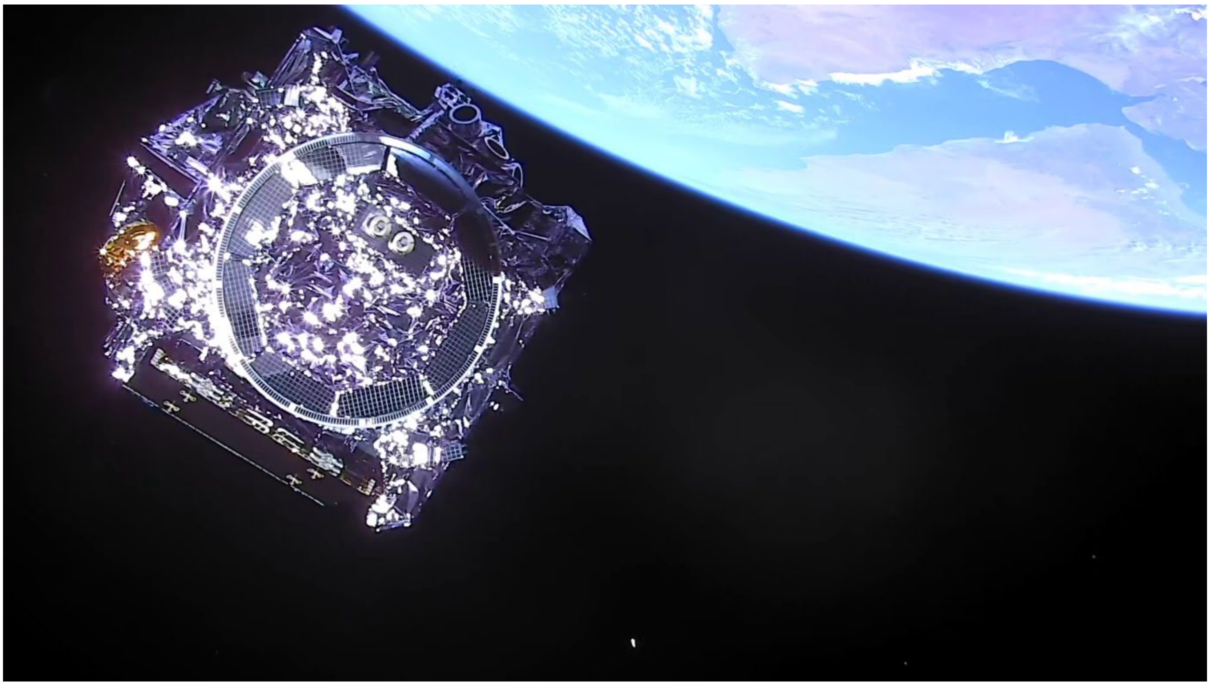

.Goodbye JWST...an image from VIKI © ArianeSpace, ESA, NASA

References

[1] N. Heffernan, Curtiss Wright, 2011. [Online]. Available: https://www.curtisswrightds.com/infocenter/case-studies/spacex-records-video-and-high-speed-sensors.html. [Accessed 11 January 2022].

[2] “Ariane 5 Datasheet,” 25 December 2021. [Online]. Available: https://www.spacelaunchreport.com/ariane5.html#log. [Accessed 11 January 2022].

[3] “Space Data Acquisition Units,” Curtiss Wright Corp, [Online]. Available: https://www.curtisswrightds.com/products/flight-test/space/. [Accessed 11 January 2022].

[4] D. Corry, “Data Acquisition Blasts Off - Space Flight Testing,” in International Telemetering Conference Proceedings, 2009.

[5] D. Gleeson, M. Panighini and M. Melicher, “COTS ETHERNET BASED TELEMETRY SUBSYSTEM FOR THE INTERMEDIATE EXPERIMENTAL VEHICLE (IXV),” in International Astronautical Foundation, 2012.

[6] ESA, “Webb and Ariane 5 - A fit made perfect,” 1 6 2021. [Online]. Available: https://www.esa.int/ESA_Multimedia/Images/2021/06/Webb_and_Ariane_5_a_fit_made_perfect. [Accessed 11 4 2022].

DOI 10.5162/ettc2022/6.1

Encryption Techniques for Test Data

Malcolm Weir[1]
[1] *Ampex Data Systems Corporation, Hayward, CA, USA,*
mweir@ampex.com

Abstract:

The ubiquitous need for *data security / information assurance* in test applications is no longer remotely controversial. But there exists significant confusion in the marketplace regarding the virtues and values of the various techniques and technologies. This paper discusses the standards and certifications used to protect data and explores the cost/benefit analysis of various approaches, including both traditional government-sponsored devices and commercial alternatives.

There are many overlapping *standards* for encryption, both for data in transit and data at rest. While this paper mostly focusses on data at rest applications, there are many commonalities with data communications security problems.

A key source of market confusion is the overlapping terms and acronyms, including AES, FIPS, Common Criteria, etc. This paper seeks to clarify these labels and explores the suitability of the various approaches to specific test and telemetry requirements.

Key words: Encryption, information assurance, standards, data at rest, data in transit.

Background

Data encryption has always been a desired feature for a subset of test applications, especially for military applications. Historically, when a program requires that data be encrypted, the supplier and the customer / end user are engaged in the provision of the appropriate technology e.g. “Government Off The Shelf” (GOTS) encryptors.

This is now changing in two key regards: first, for reasons that will be discussed later, encryption has become the “best practice” for all applications, regardless of who the end user happens to be, and secondly the suitability of GOTS solutions is not universal, again for a number of reasons.

With the increased demand for these technologies, there is an increased level of confusion in the industry as to what, precisely, is available and required to meet the needs of a program. This confusion leads to the critical problem that they very technology that is being deployed to protect data may not, in fact, be well suited to the task.

This paper attempts to demystify some of the terminology and processes around data encryption standards.

Introduction

It is sometimes noted that it’s very easy to invent a cipher. The only challenges are (1) to ensure that it can run in the hardware resources available at the performance required, and (2) to prove it isn’t easily cracked (defined as deciphered without the appropriate key or keys).

Obviously, those two factors are linked: there’s no point in having an uncrackable cipher that takes too long to use, nor having an extremely efficient but weak one. But as a general rule, consumers of this technology care most about the cipher’s “strength”[1], and work around the performance issues. This paper is mostly concerned with issues of “strength”.

Why Encrypt?

The benefits of encrypting data sets can be described as confidentiality, authenticity, and sometimes integrity. The first is obvious: without the key, unauthorized access requires cracking the cipher or exhaustively trying keys, both of which are (hopefully) hard. But the information

[1] *Technically, in this context “strength” is a function of key size and algorithm, but common usage tends to ignore the former on the basis that comparisons assume equivalent key lengths, and thus the algorithm is the determining factor.*

assurance benefits of encryption are sometimes overlooked: because only those with the correct key can create the expected data sets, accidentally or maliciously falsified data cannot be introduced between the source and destination. And integrity – the assurance that chunks of the data set are not missing or corrupted, for example – can come about in the much the same way by using encryption schemes that “chain” blocks together, so a single corrupted word will cause a ripple effect that will be easier to detect. Of the three benefits, confidentiality has been the driving rationale for test data sets.

Traditionally, the apparent need for encryption was frequently avoided by the use of physical security – vaults of tapes and dedicated, isolated telephone circuits. But by the mid-1970s, the financial services sector had started to implement distributed systems (for cash dispenser devices / “Automated Teller Machines”); these networks required technical means to make eavesdropping unproductive.

And as the world became more connected and more digital, the consequences of data leaks became more significant. Previously, the data on a misplaced reel of tape was reasonably safe from disclosure, because of the rarity of suitable drives to read the media as well as the obscurity of most data formats meant it unlikely that accidental loss would represent a significant risk. Today, though, an accidentally lost dataset or a malicious exfiltrated one are quite likely to end up in “the wrong hands”, which has lead to a recognition that data previously thought mundane (such as accounting or stock control records) or data that is confidential but of very limited interest (e.g. health information) may have economic value on a “black market” sale.

As the (real or imagined) value of purloined (or misplaced) data has grown, so has the default posture: it is now “best practice” to assume that data will leak, and therefore the appropriate posture is to encrypt everything to protect the underlying information.

General Types of Encryption

Broadly speaking, encryption applications relevant to test data can be broken down into two types: data-at-rest (DaR), and data-in-transit (DiT). In terms of encryption technology, the differences can sometimes be ignored, although the implementations have different characteristics and requirements. For example, with a DaR implementation, an attacker may be assumed to have a large volume of ciphertext to work against, while with a DiT system attention must be given to prevent compromising the system with “side-band” leaks (such as Radio Frequency leaks or power consumption monitoring).

As well as DaR and DiT applications, encryption algorithms can be summarized as either symmetric or asymmetric; the former is defined as using the same key to encrypt as you use for decryption, while the latter uses different keys for each operation. The vast majority of DaR applications use symmetric algorithms, while the modern internet is based on asymmetric protocols (HTTPS, SSL, etc). (The principle virtue of asymmetric algorithms is that it allows for a model where the sender and receiver need not know each other’s secrets, so, for example, members of the public can communicate securely with an online store without having to be given the store’s private encryption key).

While asymmetric ciphers are exceedingly useful, most test applications do not require them; about the only obvious exception are remote “phone home” telemetry systems, where widely deployed devices report to a central “mothership”. While the following sections focus on symmetric “block” ciphers (as required by DaR, but also applicable to DiT), the use of asymmetric algorithms should not be completely ignored.

The First Encryption Standard

With the possible exception of Julius Caesar’s cipher, the DES standard was the first openly published encryption standard. Invented by IBM and codified as the US National Institute for Standards and Technology’s (NIST’s) Federal Information Processing Standard (FIPS) Publication 46 (FIPS 46) in 1977, it has since been withdrawn because it is too insecure for contemporary use: with only a 56-bit key, all possible keys can be tried in a reasonable time. It also illustrates a risk in algorithm design: the rationale for some of the design decisions was opaque, leading to suspicions that the algorithm was built with a ‘backdoor’ known only to the designers.

One of the criticisms of the standard is that it is explicitly forbidden for use with classified information, fueling the suspicions of a backdoor – a deliberate vulnerability that would allow the National Security Agency (NSA) to read any encrypted material. It is now believed that, in fact, there was no backdoor -- to the contrary, the reason for seemingly nefarious decisions about its architecture was to protect it against a new type of attack threat which the government cryptanalysts understood but which was not at the time common knowledge – although the US Government did indeed weaken the algorithm by reducing the key size from 64 bits to 56.

To compensate for the short key size in DES, the 3rd version of the FIPS standard (FIPS 46-3 [1]) was released in 1999. This introduced a method whereby the data was looped through the DES algorithm three times, each time with a different key, making the overall key length 168 bits. This might appear to triple the strength of the encryption, but in fact, due to a specific type of cryptographic attack, it really only doubles the strength.

While technologically obsolete, Triple DES as TDEA is also known is still approved for protecting sensitive but unclassified US government data (although not recommended for new applications!).

The Advanced Encryption Standard (AES)

The workhorse of the current state-of-the-art in encryption is AES. It was the result of an open, international contest conducted by the NIST between 1997-2001. Fifteen algorithm designs were considered and evaluated for cryptographic security and performance in a variety of implementations (software, FPGA, and so on). Three technical conferences were held in the USA and Europe, involving more than 180 people from 23 countries, and featured voting by the cryptographers on the candidate algorithms.

The winner of this process was an algorithm designed by two Belgian cryptographers, a subset of their Rijndael family of ciphers – the name is derived from the surnames of the inventors. Three Rijndael ciphers make up the AES standard. Each takes a block of 128 bits of data and uses key lengths of 128, 192 and 256 bits, respectively. In the twenty years since it was published, the best technique for breaking into it has improved the number of keys one needs to “brute force” from 2256 to “just” 2252, so this is an interesting result, but not particularly useful for reading the ciphertext.

AES is the only block cipher in the Commercial National Security Algorithm Suite (which replaced the former “Suite B”) list. As such it is listed by the NSA as being suitable, when used with 256-bit keys, to protect up to TOP SECRET information (although this list says nothing about the implementation, only the algorithm; see the next section on FIPS 197 [2]).

All AES algorithms operate on a block of 128 bits, that is 16 bytes; to encrypt larger quantities of data, the algorithm must be applied to successive 16-byte pieces. This creates a new problem: if you use the same key for each piece, then the output ciphertext will show where those 16-byte pieces are duplicated (even if you don’t know what the plain text actually is), which can provide a lot of information about the plaintext. To address this, AES features several “modes”, the simplest of which is the “electronic code book” (ECB) mode, where you use the same key for each block. This can yield the unfortunate results shown in the picture in Figure 1. A straightforward enhancement is to include a counter merged into the process, so that each block is encrypted with different settings (the AES CTR mode). Other modes use different ways to perturb the process; which one is “best” depends entirely on the application. For data at rest encryption two modes are often used: CBC (Cipher Block Chaining) and XTS (Xor–encrypt–Xor-based tweaked-codebook mode with ciphertext stealing), the latter using two equal-sized keys[2].

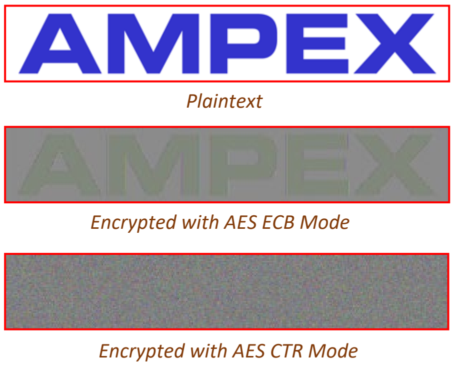

Figure 1 AES Modes

Compared to other algorithms, one significant advantage of AES is that modern CPUs often contain either special instructions or complete special-purpose subsystems to perform (or assist with) the operation. Examples include Intel’s “AES-NI” instructions and NXP’s “AES Execution Unit”. These hardware features not only improve performance but make it harder for an attacker to perform “side-channel” or “timing” attacks where information about the process can be deduced by monitoring the operation: the special hardware subsystems act as “black boxes” which conceal the details of the operation.

It should be remembered that these modes are mechanisms for applying the AES algorithm, which itself always remains the same: a “black box” that takes the same 128 bits of data and a

[2] *The use of two keys is not to increase the strength of the encryption per se, rather it makes it very hard to extract any information even given a huge amount of encrypted data. Using the two 256-bit keys provides no more than the strength of one 257-bit key: if it takes a certain time to try 2^{256} possibilities to get the first key, then it will take the same amount of time to guess the second, and $2^{256} + 2^{256} = 2^{257}$!*

key of 128, 192 or 256 bits in length and produces a 128-bit encrypted output.

FIPS Publication 197 (FIPS 197)

The document that codifies AES encryption – that is, defines the algorithm is FIPS 197. Related to the publication, certifications assuring compliance with FIPS 197 are issued via the Cryptographic Algorithm Validation Program (CAVP). While it is possible to implement an AES architecture, one can only be deemed "certified" after having gone through the CAVP process and awarded a FIPS 197 certificate.

While FIPS 197 improved upon its predecessor, DES, it is likely the FIPS 197 standard will be updated in the future with changes in how AES is used or implemented to increase the strength of the protection. This is not unlike how FIPS 46-3 introduced Triple DES.

In normal usage, when an algorithm is referred to as FIPS 197, the implication is that the algorithm has been certified by an accredited laboratory to conform to the standard. NIST has a Cryptographic Algorithm Validation Program (CAVP) that defines the test suite that an implementation of AES must pass, and then the certified implementation will be recorded on the NIST website. So, for example, certificate "AES 2408" was issued to Intelliprop, Inc. for their AES-XTS implementation (an FPGA core), and the NIST website indicates their implementation is FIPS 197 certified for key lengths of 128 and 256 bits (but evidently not 192 bits).

In terms of a hierarchy of quality, it is perfectly possible to have an AES implementation that works and is functionally correct, but without a NIST certification one cannot be objectively confident of that correctness; in effect, the certification is objective proof that the implementation is a correct interpretation of the standard.

FIPS Publication 140 (FIPS 140, FIPS 140-2, FIPS 140-3)[3]

Complimentary to FIPS 197, FIPS Publication 140 "Security Requirements for Cryptographic Modules" (FIPS 140) [3] covers the pieces surrounding the actual encryption. When working together as sub-component of a system, these pieces are often referred to as a "module" and consists of things like a micro-controller, encryptors, and a supporting storage on the same circuit board, or a software library with clearly defined interfaces.

In this broader context, a FIPS 140 module includes some very straightforward concepts and some more abstract ideas. The straightforward concepts include physical security requirements like "how can attempts to physically interfere with the module be detected?" and "how can accidental or deliberate interference result in the module 'failing safe' and refusing to function?" The more abstract ideas are things like the characterization of the interfaces into the module and the functional roles, services and authentication provided. In general, these concepts pull in other standards, so while the FIPS 140 document is quite short, by the time the rest has been incorporated, it becomes a very extensive standard.

To understand this better, a brief description of how encryption modules tend to be architected is in order. It is common to consider the DaR encryption on storage devices as matching the illustration in Figure 2: unencrypted ("plaintext") data is fed into an algorithm, together with a suitable key, and the resulting encrypted data is stored on the device. As similar approach can of course be used for DiT.

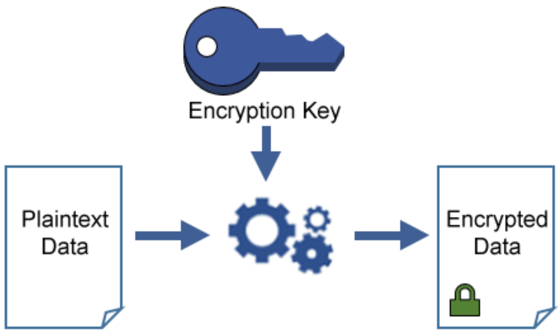

Figure 2 Simple Encryption

This is, of course, perfectly functional, and usable, but it has limitations; probably most significant of those is the fact that one, and only one, key can decrypt the data. This may sound like a good idea, until one realizes that it means that every authorized user must have that one single key, which becomes problematic when there's a need to revoke access to just one of those users or the key gets compromised: the only option is to decrypt all the data with the original key and then re-encrypt it with a new one.

[3] *Note: the "dash" after a FIPS publication number is the major version indicator, so "FIPS 140-2" is the se9cond major version of the standard, and "140-3" is the third. There are also minor revisions within version, so there are three revisions of FIPS 140-2, usually indicated by the publication date.*

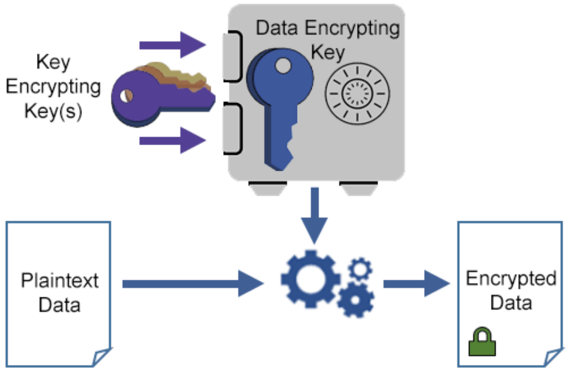

Figure 3 Key Encrypting Keys

But there is a straightforward alternative: instead of the user passing in the key used to encrypt the data, they pass in a key that is used to unlock the key that's protecting it, as illustrated in Figure 3. In this arrangement, multiple copies of the "data encrypting key" (DEK) can be stored on the storage device, with each copy encrypted with its own "key encrypting key" (KEK). Any one of the KEKs can be used to access a copy of the DEK, and the DEK is then used to access the data.

In this way, if one KEK gets compromised or lost, an administrator can simply erase the copy of the DEK that is encrypted with that particular KEK, leaving the rest untouched. And of course, an outdated KEK can be updated by simply decrypting the DEK using the old KEK, and then re-encrypting it using a new one – a simple operation involving a few bytes instead of gigabytes!

An additional benefit of this approach is that the DEK – the key that is protecting the user's data – need never leave the storage device. This means that "multi-factor" arrangements, in which you need two or more distinct and independent KEKs to unlock the DEK, and each KEK is provided by a different mechanism or "factor", can be crafted so that unless both factors (i.e., both KEKs) are simultaneously compromised, the data remains safe – and the pieces only come together within the controlled environment of the storage device protecting the integrity of the separate "factors"!

A slight variant of this idea is that, instead of the DEK being stored in the storage device, one or more KEKs are, and then the encrypted DEK is provided to be decrypted by the KEK(s) within the device. This approach ensures that the storage device cannot be "tricked" into giving up the DEK (as it simply doesn't have it), yet security is preserved as the DEK isn't usable unless it's "correctly" encrypted by the KEK(s) in the storage device.

So, getting back to FIPS 140: where a KEK/DEK architecture (Figure 3) is being used, the DEK must be generated using an appropriately random "deterministic random number generator" (DRNG) algorithm, an approved list of which is provided (FIPS 140, Annex C, which calls out NIST SP800-90B [4], amongst others). Next the approved modes of AES operation are detailed (NIST SP800-38E [5], for example, defining how AES-XTS must be used).

Then there are algorithms (key derivation functions, KDF's) that convert weak (human-grade) passwords into acceptably strong keys. The idea here is that although it is straightforward to "brute force" a short text password, it is also easy to lock the module after a certain number of failed attempts – and that lockdown can be either temporary, preventing additional efforts for some period, or irretrievably permanent, by destroying the hidden DEK. Instead, if the password is first converted into a strong key, then backdoor attacks that nullify the password-checking logic (i.e. make any password appear to be "correct") will be useless: one would still need the key that was created by applying the password together with some fixed (but hidden) constants through the KDF algorithm.

There is also another very significant capability associated with a FIPS 140 certification: the use of "message authentication" services ("HMAC": Keyed-Hash Message Authentication Code). These provide a mechanism by which the system can validate that a particular arbitrary-sized stream of bytes (a "message") has not been tampered with. The fundamental idea is that one can use a "hash algorithm" (e.g., "SHA-256") that creates a checksum of the message, and then cryptographically signs it using the private part of a public key cryptography key pair, so that any change to the message will change the checksum and it is impossible to update the signature without the secret, private key. This approach is used in the Ampex TSEM FIPS 140 module to validate the contents of the memories storing the FIPS 197 FPGA bitstream using firmware code in a secure microcontroller that is itself "signed" in the same way.

Both the hash algorithm and the HMAC are defined by their own FIPS standards: FIPS 180-4 "Secure Hash Standard (SHS)" [6] and FIPS 186-4 "Digital Signature Standard (DSS)" [7], respectively. And the digital signature standard defines the specifics of the acceptable public key cryptography schemes.

Since "one size rarely fits all", FIPS 140 defines levels of increasing security, with "Level 3" is theoretically more secure than "Level 2". It is important to note that these levels are not related to the version “dash” number, so that it is appropriate to comment that FIPS 140-2 Level 2 is the most common certified level! As is usually the case with these types of collections of disparate requirements, many implementations might qualify for a higher level in some areas but are “held back” in others. So, for example, the logical protection mechanisms (e.g., code-signing) might warrant a higher level, but the physical anti-tamper protections might not. It should be noted that some anti-tamper methods are reasonably easy to achieve but impose consequences for the product development; Level 3 physical security can be achieved by “potting” all the hardware in epoxy!

One important characteristic of a module’s certification is how and where the boundary between it and the rest of the system is drawn. A very tightly drawn boundary reduces the elements that must be certified (and so potentially reduces the overall security / value of the module), while a broad brush will include pieces (of software, usually) that become subject to the restrictions of certification, so that any updates to that software will require updating the certificate.

A cautionary tale as to why FIPS 140 certification (or equivalent) can be valuable comes from security researchers who created attacks that defeated the encryption on several non-FIPS commodity storage devices (Meijer & van Gastel, 2019 [8]). Their attacks included loading modified firmware into the target devices, having instrumented them to identify how the firmware was intended to work. So, for example, they created firmware that would always believe the supplied password was correct, no matter what. It is possibly tempting fate to assert that, had the drives been FIPS 140 certified, their attacks would have failed, but it is certainly true that it would have been much harder to gain access to the data.

Common Criteria Certification (CC, NIAP)

While the FIPS 140 certification process provides assurance of a solid solution for many applications, it is intrinsically an American (USA and Canada) framework. To put another way, the only authorities issuing certificates are the US and the Canadian governments.

This introduces obvious issues for non-American applications: does using the FIPS approach implicate exportability (ITAR, etc)? How can a non-American user (particularly sovereign users) be assured that there was no interference with the evaluation? (And regardless of the likelihood of that happening, the issue is the ability to assert that it could not have happened; certification is always trying for absolute assurance, not just reasonable conclusions).

The solution for both American and non-American users lies with the Common Criteria for Information Technology Security Evaluation (referred to as Common Criteria or CC). This is an international framework for providing security certification a system. In the USA, the responsible body for CC efforts is the National Information Assurance Partnership (NIAP), which is operated by the NSA.

The international members of the framework are (currently) a total of 31 countries, slightly more than half of which are “certificate producers” with the rest being “certificate consumers”. Producer nations run a full scheme including certifying labs to evaluate products. Consumer nations agree to accept certificates from the “producing” nations. A program based in a “consumer” country that wants a certified product would simply outsource the certification to a producer nation (Indonesia outsourcing to Australia, for example).

Common Criteria stands in contrast with FIPS 140, as the latter is concerned solely with cryptographic systems, while CC can be applied to any type of system. The two schemes are very closely related, and indeed up until 140-2 the FIPS standard explicitly called out requirements from the Common Criteria standard (those requirements haven’t gone away but are now separately and explicitly listed in FIPS 140-3).

Common Criteria is concerned with the security functions of a product as a whole, which obviously includes cryptography (overlapping with FIPS 140), auditing and logging, access controls, administrative roles, and so on. For a data storage device, there is a lot of commonality between the CC DaR and the FIPS 140 requirements, but enough variability (e.g., on the drawing of a FIPS 140 boundary) to keep CC separate from the FIPS certification.

For DaR applications, there are five potentially relevant CC protection profiles (PP): two for full-disk encryption, two for file-based encryption, and one for USB flash drives. The two full-disk encryption protection profiles boast a “collaborative” tag – they are collaborative PPs (cPPs), not just PPs – indicating that they’ve been developed with a larger group of contributors than just the US government. The two full-disk cPPs are for the “Encryption Engine” (the module that does the encryption) and then for the “Authorization Acquisition”, which handles key management.[4]

The Encryption Engine cPP [9] defines how the data must be encrypted; slightly bizarrely, it references the ISO/IEC standard (18033-3) [10] for AES rather than FIPS 197, even though the NSA’s CNSA list references the latter! The Authorization Acquisition cPP [11] is significant mostly because it is an entirely separate standard, allowing the two functions to be separated and even provided by two distinct suppliers.

One of the ramifications of the CC authentication certification for DaR is that it *must* contain the totality of the key lifecycle, from key generation through key transport to loading the key into the encryption engine. This leads to the somewhat paradoxical situation that a gold-standard, NSA-generated secret key *cannot* be used in CC (or in related standards, such as CSfC).

In the context of DaR and DiT, a standalone CC certification is rarely required, as FIPS 140 provides a similar level of assurance in a more narrowly focused standard; of course, when dealing with other security accreditations, CC is more commonly mandated. The value of the CC DaR/DiT certification is not inherent in the validation itself, but because the “next layer” (e.g. CSfC, see below) uses CC certificates as building blocks to practical, approved solutions.

Commercial Solutions for Classified (CSfC)

CSfC is a program run by the NSA which uses a pair of layered, Common Criteria certified encryption products to create a solution that may be used to secure National Security Information. The stated rationale for using two products, with the second encrypting the output of the first, is that this mitigates deficiencies that might exist in the implementation of either. However, one might recall the aforementioned “triple DES” exists to provide a security boost over regular DES, so it is not unreasonable to assume that the layering provides some additional security, even if that isn’t the public rationale for it.

Unlike FIPS 140 and CC in isolation, CSfC is specifically designed to secure data at the levels needed for the most sensitive of information and is recognized by the US government for that purpose; unlike “Type 1”, it is also designed for non-governmental use, such as by finance or healthcare organizations.

CSfC provides requirements for solutions via Capability Packages (CPs). The “Data-at-Rest CP” [12] defines several implementation architectures, such as a software layer on top of a hardware one, or two full-disk software layers, or file-based software on top of full-disk, and so on. The most recent version of the DaR CP also supports solutions using two hardware designs.

To help ensure that the same vulnerability does not exist in both layers, the CSfC philosophy requires that each layer must be produced by different vendors (or, in the case of corporate mergers and acquisitions, demonstrably different teams within the same company). Under this principle of diversity, there must be at least two, and possibly three, organizations involved in a CSfC solution: one each to produce the encryption implementations, and optionally a third to serve as an integrator of the other two.

From a functional standpoint, CSfC solutions are as good as the traditional US Government “Type 1” approach, but with significantly increased versatility. First, CSfC implementations are not “controlled cryptographic items (CCI)”, which facilitates (and reduces the cost of) logistics and handling and particularly international/export applications. Second, key handling concepts can be tailored to the specific application and mission requirements.

Key handling with legacy “Type 1” systems is based entirely on the NSA’s “one size fits all” model: all keys are generated by the NSA, and distributed through the appropriate secure channels, before being loaded into the encryption device, typically using a “Secure Key Loader”. This approach is fine when being used within the US/NSA sphere of influence, it is naturally impractical for commercial and sovereign international customers.

By contrast, with a CSfC device, keys must be “organically” created within the device (or the ecosystem for the device). This inherently creates significant flexibility for the design of mechanisms to deliver keys to the encryptors.

[4] Prior to 2010, CC evaluated products according to Evaluation Assurance Levels (EALs), of which there are 7. The lower four (EAL1 through EAL4) were process-based evaluations, meaning most any system could be evaluated and certified whether or not it met a particular function or purpose (which were termed “robustness” evaluations). While this obviously has value, it is at odds with the sponsoring governments’ goal of qualifying functionally similar products in a comparable and repeatable manner. The revised approach (since 2010) substitutes the old robustness evaluations with strict compliance with defined protection profiles for the lower four levels, and then retained the semiformal and formal design analysis for the upper levels only once a protection profile has been validated.

Over a longer term, by contrast with "Type 1" solutions, CSfC requires periodic recertification through the NSA (or equivalent), and there is always the possibility that, during that process, new or modified requirements may become mandated with possible budget implications. While this may appear a significant and justifiable concern, real-world cybersecurity – obviously including cryptography – demands regular software / firmware updates to protect against newly identified vulnerabilities. The old model, where a single product certification survives the life of the program, cannot be sustained in the contemporary "connected world"; the well-publicized attacks on certain Intel CPUs ("Meltdown"[5] and "Spectre"[6]) are examples of unexpected problems that cannot be ignored.

The value of the CSfC program can be summarized by the following: at least one foreign government has used the CSfC "recipe" (that is, the CP) together with products locally certified to Common Criteria PP standards.

The integrity of CSfC can be illustrated by noting that, using a properly certified and structured CSfC solution, the NSA will approve the use of industry standard WiFi network and internet bridges to carry US Top Secret information.

Test Data Applications

Several features common to many test applications lend themselves to the use of FIPS or Common Criteria.

First, test articles are frequently heavily constrained in terms of Size, Weight and Power (SWaP). This can pose insurmountable challenges with integrating GOTS / legacy devices with the required capabilities. By contrast, FIPS/CC solutions can include software implementations, which can be scaled to fit the physical constraints of the application.

Second, test applications tend to involve numerically small numbers of systems: the largest pools of flight test recorders number in the scale of a few dozen units, which makes the time and expense of a "from the ground up" encryption solution much harder to justify. But if the virtues of certification can be obtained by judicious selection of key components (e.g. by using a FIPS 140 certified SSD in place of an uncertified one), then the cost differential becomes marginal and the schedule impact trivial.

Third, it is sometimes said (partially in jest) that "encryption is easy, but key handling is a challenge". Using GOTS solutions or similar tends to include a rigid key handling policy, deviation from which (e.g. to using "test keys") has unknown consequences: if the test keys all have the form '123456', then it's fair to say that security will be compromised! More seriously, because open certification processes like those of FIPS and Common Criteria allow system designers to make informed, intelligent decisions about the consequences of changes to the expected application. As an example, it is possible that a designer of a DiT solution might conclude that only FIPS 197 is required on the test article, with the other parts that would make up a FIPS 140 system being distributed to ground-support equipment or other certification efforts.

Conclusion

With the maturation of programs like FIPS and Common Criteria, the commercial and international market can have confidence that "government quality" (i.e. US Government quality) solutions can be implemented without recourse in cost, confidentiality, or schedule to independent developers and integrators, and end users can have confidence that their solutions really do provide the features and benefits that they expect.

References

[1] National Institute of Standards and Technology,FIPS PUB 46-3 "Data Encryption Standard (DES)", 25 October 1999. [Online]. Available: https://csrc.nist.gov/csrc/media/publications/fips/46/3/archive/1999-10-25/documents/fips46-3.pdf

[2] National Institute of Standards and Technology,FIPS PUB 197 "Advanced Encryption Standard (AES)", 26 November 2001. [Online]. Available: https://doi.org/10.6028/NIST.FIPS.197

[3] National Institute of Standards and Technology,FIPS PUB 140-3 "Security Requirements for Cryptographic Modules", 22 March 2019. [Online]. Available: https://doi.org/10.6028/NIST.FIPS.140-3

[4] M. Turan, E. Barker, J. Kelsey, K. McKay, M. Baish and M. Boyle,SP 800-90B "Recommendation for the Entropy Sources Used for Random Bit Generation", January 2018. [Online]. Available: https://doi.org/10.6028/NIST.SP.800-90B

[5] CVE-2017-5754 is the official reference to Meltdown. CVE is the Standard for Information Security Vulnerability Names maintained by MITRE.

[6] CVE-2017-5753 and CVE-2017-5715 are the official references to Spectre. CVE is the Standard for Information Security Vulnerability Names maintained by MITRE.

[5] M. Dworkin,SP 800-38E “Recommendation for Block Cipher Modes of Operation: the XTS-AES Mode for Confidentiality on Storage Devices”, January 2010. [Online]. Available: https://doi.org/10.6028/NIST.SP.800-38E

[6] National Institute of Standards and Technology,FIPS PUB 180-4 “Secure Hash Standard (SHS)”, August 2015. [Online]. Available: https://doi.org/10.6028/NIST.FIPS.180-4

[7] National Institute of Standards and Technology,FIPS PUB 186-4 “Digital Signature Standard (DSS)”, July 2013. [Online]. Available: https://doi.org/10.6028/NIST.FIPS.186-4

[8] C. Meijer and B. van Gastel, “Self-Encrypting Deception: Weaknesses in the Encryption of Solid State Drives”, in *IEEE Symposium on Security and Privacy*, San Francisco, CA, USA, 2019. Available: https://doi.org/10.1109/SP.2019.00088

[9] National Information Assurance Partnership, “collaborative Protection Profile for Full Drive Encryption - Encryption Engine”, 1 February 2019. [Online]. Available: https://www.niap-ccevs.org/MMO/PP/CPP_FDE_EE_V2.0E.pdf

[10] International Standards Organization,ISO/IEC 18033-3:2005 “Information technology - Security techniques - Encryption algorithms - Part 3: Block ciphers”, July 2005. [Online]. Available: https://www.iso.org/standard/37972.html

[11] National Information Assurance Partnership, “collaborative Protection Profile for Full Drive Encryption - Authorization Acquisition”, 1 February 2019. [Online]. Available: https://www.niap-ccevs.org/MMO/PP/CPP_FDE_AA_V2.0E.pdf

[12] National Security Agency Central Security Service, „Data-at-Rest Capability Package V5.0“,18 November 2020. [Online]. Available: https://www.nsa.gov/Portals/75/documents/resources/everyone/csfc/capability-packages/Data-at-Rest%20Capability%20Package%20v5.0.pdf

DOI 10.5162/ettc2022/6.2

EUROCAE ED247 (VISTAS) Rev B On the way evolutions ettc2022

CHRISTIAN HERBEPIN,
United Electronic Industries, Inc, 249 Vanderbilt Avenue, Norwood, MA 02062, USA,
cherbepin@ueidaq.com

Abstract:
Since 2018, each year, a few papers on EUROCAE standard ED247 (aka VISTAS) have already been presented in the frame of the ETTC. This standard defines a light and efficient way to virtualize avionic signals and digital buses on a standard communication bus like Ethernet in the frame of full simulation or hybrid benches.

After a brief summary of the standard main concepts and benefits associated, the presentation will be focused on the new functionalities and performance improvements that are currently discussed for the next release of the standard (Rev B) which include:

- New channel types like ARINC 708,
- New transport protocols like DDS, RDMA in addition to the UDP current one,
- ED247 components command and control,
- State machine & time management,
- Virtual components internal data monitoring,
- Failure injection and data overwriting limited to data exchanged between virtual components,
- Health monitoring.

Key words: ED-247, VISTAS, Virtual testing, Test Bench, Simulation.

Introduction

The purpose of this paper is to focus on currently discussed evolutions of the EUROCAE standard ED-247 (aka VISTAS) in the frame of the Rev.B

The paper first recalls the main outlines of the EUROCAE standard ED-247:

- History,
- Working Group Members,
- Main principles,
- Use cases,

Next, the paper presents the “on the way” evolutions of the standard, focused on the following topics:

- ED-247 State machine description,
- Command&Control generic mechanism,
- Instrumentation,
- Health Monitoring,
- New transport protocols in addition to Ethernet UDP,
- New type of signal taken into account.

ED-247: History

The EUROCAE Workgroup 97 in charge of ED-247 was founded in 2013.

The first release of the standard was published in November 2017 including the virtualization of AFDX, Arinc 429, CAN Bus, DISCRETE, ANALOG and Non avionic data.

In March 2020, the release A was published bringing a bunch of clarifications and additional signals virtualization: serial line, MIL-STD-1553, voice and video.

The release B is now planned for Q2 2023. It will include additional capabilities like Control & Command mechanism, Instrumentation, Definition of the virtual component delivery format and additional transport protocols.

These additional capabilities will be described in detail in the following paragraphs.

DOI 10.5162/ettc2022/6.2

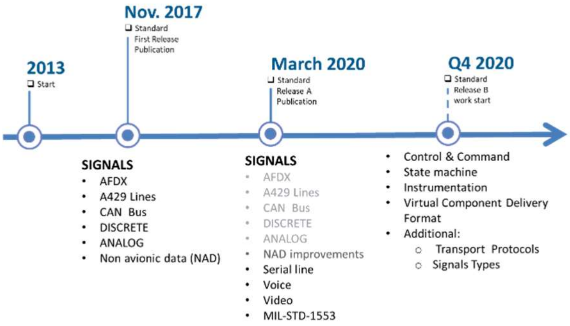

Fig. 1. ED-247 history.

ED-247: Working Group Members

Members within ED-247 Working Group are representing names in the aerospace (such as AIRBUS, DASSAULT or BOEING) along with key instrumentation and flight simulator suppliers.

ED-247: Standard in a nutshell

ED-247, also called VISTAS (Virtual Interoperable Simulation for Tests of Avionics Systems) is defined under the umbrella of the EUROCAE organization in the frame of the Working Group 97.

The main objective of the standard is to improve the integration test process, by reducing drastically the associated costs and delays and by starting this process as soon as possible during the development cycle.

To achieve this target, the standard proposes a way to share easily models between the different actors, to use these models in the frame of full simulations or hybrid ones mixing real or virtual components not necessarily collocated and to virtualize the communication exchanges between the different elements on an IT network.

The standard provides a way to transport all the information exchanged between equipment, not any more through multiple wirings (discrete, analog, bus) but through an IT network (Cf. *Fig. 2*).

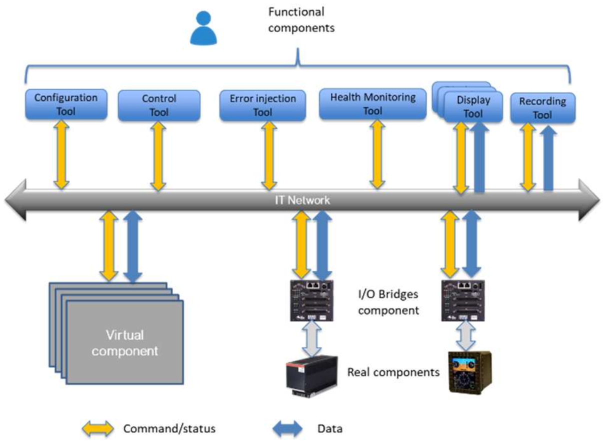

Fig. 2. ED-247: High level architecture and components.

These information are acquired, timestamped, multiplexed and stored into data packets sent on the network with the following constraints:

- Minimizing the latency introduced by the virtualization as far as possible,
- Limiting the CPU, Memory, Bandwidth usage,
- Reproducing with a high accuracy the timing of the original signal.

For the releases "-" and "A", the transport protocol used is Ethernet UDP.

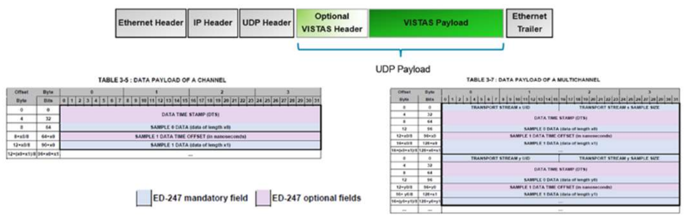

ED-247: Use cases

The ED-247 is usable on both sides of the V development cycle:

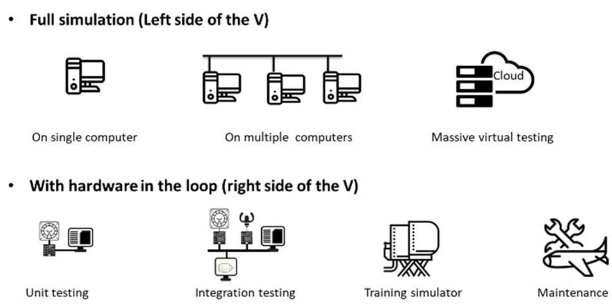

ED-247 Rev. B: Working groups process

The ED-247 Rev. B work began in the end of 2020.

The release B is planned for Q2 2023.

DOI 10.5162/ettc2022/6.2

In the meantime, the working group (split in different sub-groups for different topics) is meeting periodically to discuss the different subjects.

The following paragraphs summarize the actual status of the main improvements introduced by the rev B:

- ED-247 State machine description,
- Command & control generic mechanism,
- Instrumentation,
- Health Monitoring,
- New transport protocols in addition to Ethernet UDP,
- New type of signal taken into account.

Warning: The following paragraphs reflect the current state of the working group's discussions. As the release "B" document is still under construction the final document might be slightly different.

ED-247 Rev. B: State machine

A simplified version of the State machine is described below:

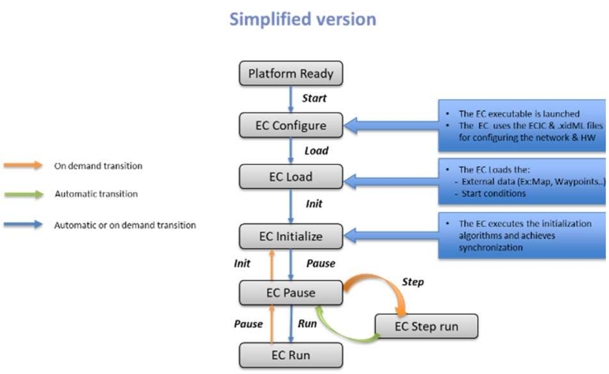

ED-247 Rev. B: Command and Control

<u>Applicability:</u>

The same generic Command-and-Control mechanism/Protocol will be used for all the topics where commands are defined by the standard:

- Load and configure the EC component,
- Request state machine transition,
- Instrumentation commands (Inspection request, Failure & Overwriting demand),
- Asynchronous Health monitoring request (TBC),
- Power supply management (TBC),
- Time management (TBC),
- Functional, Virtual or Bridge components specific command.

<u>Command & response Block structure</u>

Different solutions have been studied:

- Binary structure like defined in Rev "-"
- XML using a schema derived from the one used by XML-RPC,
- JSON with an ED-247 proprietary schema,
- JSON using a schema like the one used by the JSON-RPC.

The last solution appears to be the preferred one (TBC) due to its compacity, flexibility and compatibility with the execution of multiple command in parallel.

```
{
    "jsonrpc": "2.0",
    "ID" : "132" ,
    "method": "Monitoring.New",
    "params": [
        {"name": "Variable_Id", "type": "array", "value": [
            {"type": "int", "value": 7},
            {"type": "int", "value": 1247},
            {"type": "int", "value": 91},
            {"type": "int", "value": 42}
        ]}
    ],
}
```

<u>Multiple steps response</u>

As the execution of some commands could take time, the standard will allow two different types of response mechanism: One step or N steps

One Step: The response is sent immediately with an error description if the command is detected as not valid or after the command execution, with the results, if the command is valid.

N Steps: The first step is sent immediately to mention that the command is well received (command valid or not). The intermediate steps are reporting the progress of the command execution. The ultimate step is reporting the command termination and the result.

The First step answer could be used by the sender to secure the transmission thanks to a timeout if the transport protocol in not 100% safe.

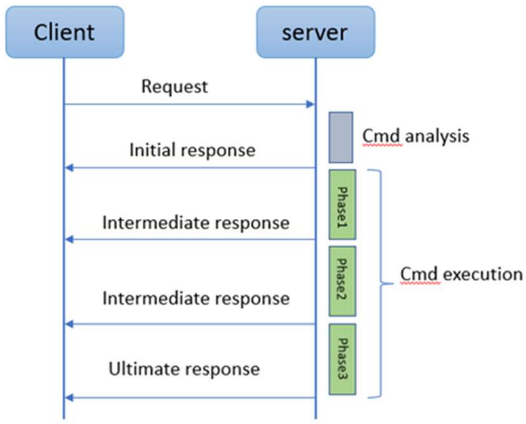

Transport protocol

Different protocol could be used:

- HTTP: in this case, if the format of the command block is in line with the .xml schema presented, the implementation is fully the XML-RPC with some additional constraints,
- TCP: The packet lost management will be done through the protocol itself,
- UDP: The latency will be reduced and the multicast command allowed but the good reception must be managed thanks to the first step response
- QUIC (Quick UDP Internet Connections) on the top of UDP which bring better performance, multiple exchange through the same connection and crypto basically mandatory but extension can be used to make it optional,
- HTTP/3 which run over QUIC,
- Web Sockets.

Due to its simplicity and efficiency, UDP is the one that will probably be retained for at least the release B.

ED-247 Rev. B: Instrumentation

The instrumentation part covers two different functionalities.

Regarding the data monitoring: The standard will provide mechanisms allowing the inspection of internal variables of all the ED-247 components (real or virtual) with exactly the same operating modes.

Virtual Component Real Component

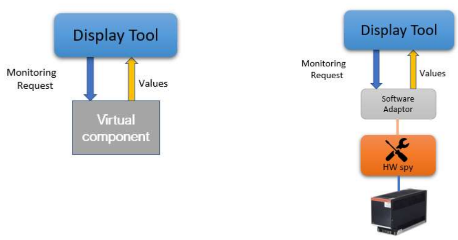

The corresponding values could be received only once or periodically.

Regarding the failure Injection: The standard will provide mechanism allowing the perturbation of data exchanged between the components. This perturbation could be applied at the source or at the destination. The failure injection of component internal variables is out of the scope of the rev B.

ED-247 Rev. B: Health monitoring

The role of the health monitoring part of the standard will be to specify:

- ED-247 component heartbeat mechanism and format. This Heartbeat will provide the global status of the component but potentially also the one of its visible subparts.
- The error logging process, format and associated command if any (like the one requesting the level of detail requested).

ED-247 Rev. B: EC delivery format

In order to facilitate the exchanges of virtual components between organizations, the delivery format will be defined in the Rev B specification. It will be based on a .zip file with a predefined structure.

ED-247 Rev. B: Additional Transport protocols

In order to improve the performances and the functionalities of the virtualization process, different transport candidates have been proposed:

- RDMA: Reduces the latency and the packet lost probability,
- TSN: Brings deterministic capability,
- DDS: Procures some cybersecurity aspects and abstraction of the physical transport layer.

The figure below presents the main benefit of RDMA vs UDP:

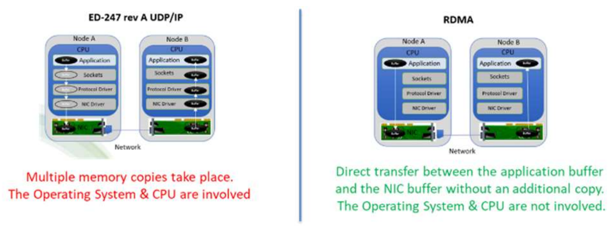

The main targeted benefits of this protocol are:

- A strong latency reduction (the Lowest latency reachable on Ethernet up to less than 1.3 µs),
- A significant latency jitter reduction,

DOI 10.5162/ettc2022/6.2

- An ultra-low CPU overhead,
- A packet lost reduction,
- A capability to offer light multicast message transfer,
- An efficient usage of the existing network infrastructure,
- A message routing capability over WAN.

ED-247 Rev. B: New signal type introduced

ARINC 708 is a standard used by airborne pulse Doppler weather radar systems on commercial aircraft. It is based on a 1600 bits data frame, composed of a 64 bits header followed by a data section consisting of 512 bins of 3bits each.

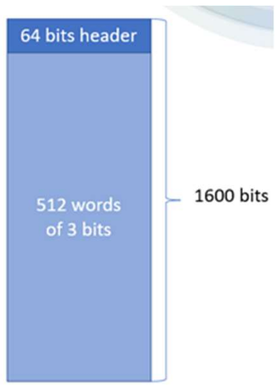

The A708 Packet structure proposal is described below:

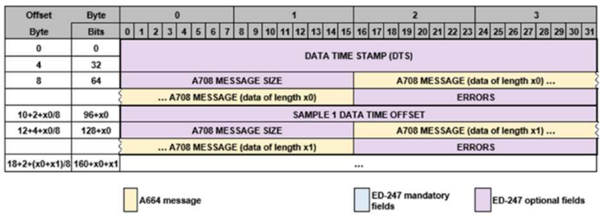

Conclusion

The ED-247 standard Rev. A, published in March 2021, achieves a maturity level compatible with operational implementation. It has already demonstrated its capacity to reduce the development cycle costs and delays.

The Rev B that will be published Q2 2023 will bring:

- Additional functionalities: Component Control & Command, access to internal variables of the virtual/real components, error injection and value overwriting, standardization of the virtual component delivery format, virtualization of the ARINC 708.
- Performance improvements especially in terms of latency thanks to the introduction of new transport protocols.

References

[1] ED-247A - Technical Standard for Virtual Interoperable Simulation for Tests of Aircraft Systems in Virtual or Hybrid Bench.

https://eshop.eurocae.net/eurocae-documents-and-reports/ed-247a/

DOI 10.5162/ettc2022/7.1

Evolution of Data Exporting

Fatih HACIÖMEROĞLU[1], Egemen GÜÇLÜ[1], Mehmet KEKEÇ[1], Raşit UZUN[1]
[1] Helicopter Flight Test Instrumentation, Turkish Aerospace, ANKARA

Abstract:
This paper summarizes the data exporting methods and their evolution in the Helicopter Division in Turkish Aerospace. Initially, we could get away with using the utilities, which are provided by FTI System Supplier (Curtiss-Wright). These utilities helped to sustain data export process in first period of the project. However, along with increasing data export tasks, improvements in data exporting demands were eventually becoming inevitable. First, a utility is developed to exploit the batch process capability of the IADS Server license ("*Data Manager*" tool) in a multi-tasking fashion. This custom Data Export tool accelerated the exporting task and saved the day in the tight schedule of the T625 Project, even though it has its own substantial shortcomings namely creating a huge set of regular files without security or redundancy and not being a searchable database. In the meantime, a novel platform (named as "Optimus") is being developed in-house and is now starting to gain popularity among data clients.

Keywords: multiprocessing, multitasking, data export

Introduction

Before the T625 Project, the data export requests were not considerable and we used to utilize either the software suite of KAM-500 Data Acquisition System ("kFlashCard" of "KSM-500" software suite) or the GUI interface of the data conversion and visualization software ("IADS" of Curtiss-Wright) for data exporting. However, the requests in T625 Project, along with both the size of the collected data and the number of manoeuvers and data type combinations, forced us to look for a solution.

We decided to take advantage of a utility in IADS software suite, namely "IADS Data Manager Tool", which can be run from a terminal to export data, without opening an IADS Client session. A custom Data Export tool is developed to exploit this "batch processing" capability and run multiple data export processes in parallel. This solution, despite decreasing considerably the data export times, is by no means an "ideal" data sharing solution. It enabled us to keep up with project deadlines. The main shortcoming is that the data is not kept in a database through which one can query. Being able to make a query, which covers all flight data, is a must and can only be addressed by a dedicated platform, our Data Export Tool is an interim utility to accelerate export process. Other crucial areas which are not in the scope of our tool are data redundancy and data security issues.

Nevertheless, the Data Export Tool relieved time schedule pressure, enabled the continuation of the Project and more importantly from our point of view, increased consciousness for the necessity of a "Data Platform". In the time gained, a novel data platform (named as "Optimus") has been under development by the Artificial Intelligence Group. Here we only present the Data Export Tool in detail, as for Optimus, we provide solely a glimpse.

In the next section, we briefly describe the FTI System employed in T625 Project to provide an understanding about the scale of the FTI System which required novel solutions for data exporting. Then we mention about the problem faced in data exporting emerged by a flooding growth of data volume. Next we provide details about the developed tool which makes the most of the batch process capabilities of "IADS Data Manager" utility. Finally a glimpse into the Optimus platform is provided, which is getting popular and to which new capabilities are being added.

FTI System in T625

The Data Acquisition System in T625 comprises 8 KAM/500 DAQ's, 2 Ethernet Switches, 1 Ethernet Recorder and 2 Rotating DAQ Systems with contactless slip rings (for rotor & blade measurements).

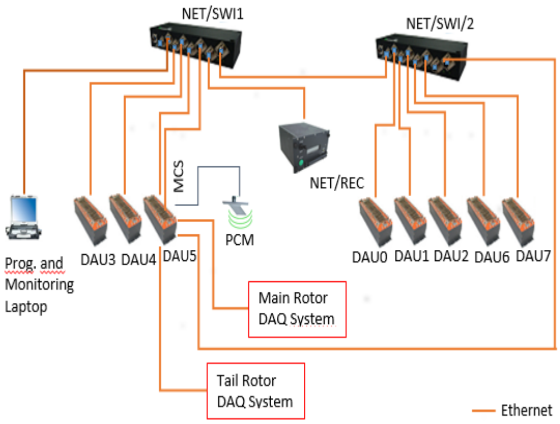

Figure 1 Instrumentation Architecture in T625

There are about 6000 raw parameters defined in the FTI System, about 1000 of them are for analog measurements (among which 150 of them are from rotating systems). We telemeter around 3200 out of the total 6000 raw parameters while the on-board recording rate of Ethernet packets is about 50 Mbps.

Raw parameters are sent from DAU's. The receiving side is responsible to perform the Engineering Unit derivations.

Issues in Data Exporting

Each test, either Ground or Flight Test, contains numerous "TestPoints" and collected data is grouped into numerous "DataGroups".

"*TestPoint*" (or Test Operation) is the name given to the maneouvre of interest which is marked with a start time and an end time. In other words it is a time slot in the whole test duration whose start and stop times are used to slice the data to indicate an interested section of test. Typical examples can be given as "Level Flight at 70 kts at 3000 ft AGL", "Deceleration from 70 kts to 40 kts at 3000 ft AGL", "Taxi 20 kts", "Left Coordinated Turn at 70 kts at 3000 ft AGL", etc. In addition to the executed testpoints, we define an enclosing TestPoint to slice all the time from beginning of Engine Start upto end of Engine power off, the aim of this enclosing testpoint is mark the region for data to be used for fatigue calculations.

"DataGroup" is the name given to the datasets containing parameters originated from same type of source and have same sample rate. Some typical examples can be given as "Pressure Parameters sampled at 256 Hz", "Pressure Parameters sampled at 4096 Hz", "Thermocouple Parameters sampled at 8 Hz", "RTD Parameters sampled at 8 Hz", "Arinc-429 Messages from ADC-1 sampled at 128 Hz", etc. Each one is a distinct DataGroup (note that the distinction comes both from data source type and also from the sample rate). There are over 100 DataGroups defined in T625 Project.

We are required to export data for each TestPoint and DataGroup combination as separate text file (Designers and Analyzers, who are the data customers, prefer the exported data to be in a text file such as "csv" format rather than in binary format). Using typical per flight quantities of 30 TestPoints and 100 DataGroups, it makes 3000 distinct TestPoint-DataGroup pairs and hence 3000 files to export.

IADS software is used for real time data monitoring during ground and flight tests. IADS uses its own data format (with extension "*iadsData*") in order to handle the demanding real time data processing feature. To obtain required csv files, we have been using IADS's export functionality available in an IADS Client or IADS RTStation licenses. They work great for small scale tests but they fall short when there are 3000 csv files to export. Since, to export data from an IADS Client, it is required to playback the IADS's test session, select the DataGroup and select the TestPoint manually. After a data group exported for all test points, another data group needs to be selected manually, which necessiates a user to wait in front on an IADS session during all the process and use the GUI.

On the other hand, IADS's Server Licence provides a Data Manager Utility, with which one does not need to re-open (playback) a test session in IADS in order to export data. It is only needed to provide the configuration file in test session (the file named as "*pfConfig*" file) and Data Manager can use it to export data in desired format. What makes Data Manager worthy in our application is that it can also be run from command line. This batch capability was the enabler in the creation of the custom export tool. Our Data Export tool only needed to form a queue of the the Data Manager commands (one for each TestPoint and DataGroup) and call them in parallel, consecutively, until the exhaustion.

Custom Data Export Tool

First attempt was to write an application in Python which opened a new thread for each Data Export task (i.e. TestPoint-DataGroup pair). User can select the TestPoints and DataGroups and once exporting is started, the program was keeping track of the threads in order not to exhaust the CPU (obviously starting 2500 threads at once is a sure way to crash the operating system. Our CPU consists of 24 cores). This first program used the low-level thread functions of Python. For instance if alive thread number is set to be 10, the program would initiate first 10 threads and then keeps monitoring their execution, as soon as one thread finishes, the 11th export is initiated. Keeping track of active threads was a considerable part of the code. Each thread used to call an “os.system()” call in Python which creates a separate process. Therefore, our multithread application was actually running as a multiprocess application (Multiple threads can be run in a single core, so that user thinks that they are running simultaneously but in fact there is a fast switching undergoing. On the other hand, multiple processes are run in different cores so that the tasks are running simultaneously in the true meaning of the term). The code was difficult to maintain.

As the second version, we wanted to resort to Python’s built-in modules to handle multitasking (instead of keeping track of alive tasks ourselves). We chose ***“concurrent.futures”*** module in which a “pool” is created and all the export tasks are sent into this pool. We only have to adjust the pool size (a.k.a worker size) to determine how many simultaneous tasks we want the computer to run in separate cores. Our IADS Server computer has a 24 core processor, we generally used 12 as pool size. Using a high-level library such as “concurrent.futures” leads to cleaner code. As for the GUI, **“Qt5”** module is preferred (over “**tkinter**” module which was used in the first version).

The GUI has 4 toolbar buttons that have to be run in order, which is imposed by the program by activating and deactivating them as required.

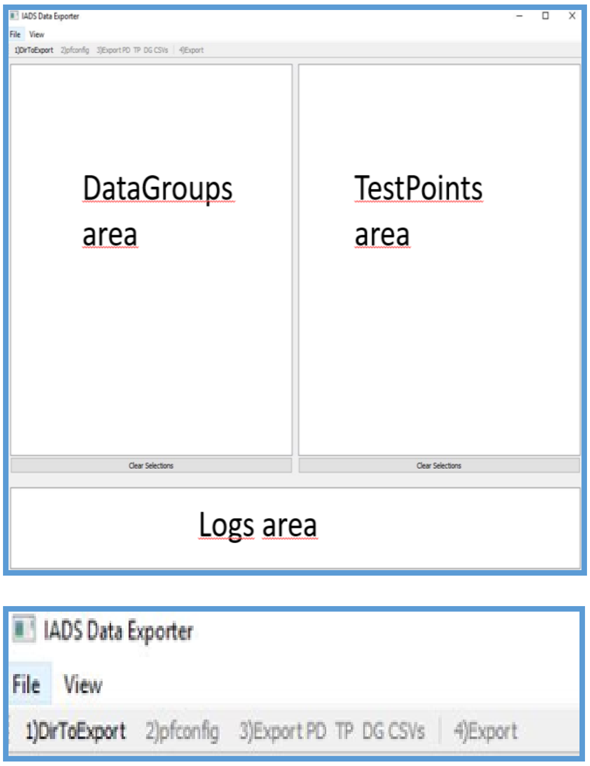

Figure 2 The Data Exporter GUI (top) Toolbar buttons (bottom)

STEP 1) “DirToExport” Button: First user selects the destination directory. A confirmation is presented in the Log area. The destination directory can be a local folder or it can be a folder which is in the intranet of the Company.

STEP 2) “pfconfig” Button: Then user selects the configuration file within the folder where IADS Session related to the test resides.

STEP 3) Export TP DG PDs Button: Pressing this button issues commands to Data Manager to export DataGroups file, TestPoints file and ParameterDefaults file (a fancy name of IADS used to refer to formulas (EU derivations)) to the export folder, as well as population of the DataGroups area and TestPoints area (as in Figure 3). User can select/deselect TestPoints and DataGroups to narrow down the export tasks if desired.

DOI 10.5162/ettc2022/7.1

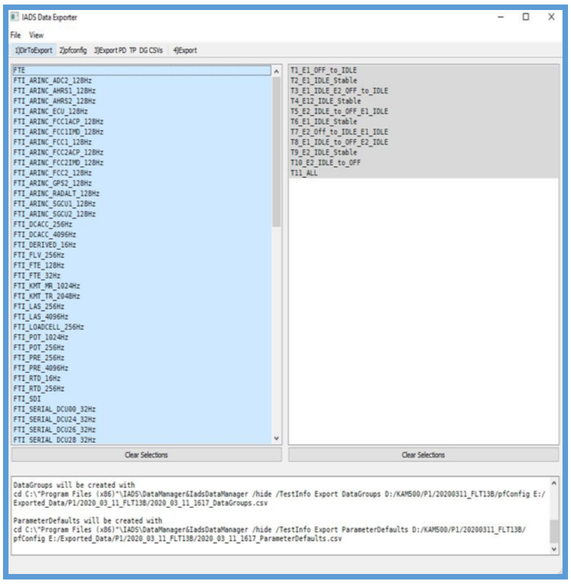

Figure 3 An example view after TestPoints and DataGroups are listed (from a very short test)

STEP 4) "Export" Button: This is the final step, where program starts running processes in parallel.

User can determine the number of processes that will run in parallel (i.e. number of workers). Generally, we use 12 workers, because using more would saturate CPU. In fact, this depends on the export location choice, which is another setting user can make. We named two distinct methods for export methods.

Export Method 1) Export each file directly to the destination folder in intranet.

Export Method 2) Export to a local temporary folder first and at the end copy all data to the destination folder in intranet.

For instance, if Method 1 is chosen, the copying of the file to intranet slows down and choosing a worker size of 12 would make the CPU to work at 50%. (Network speed bounds the CPU usage.) However if Method 2 is chosen, since writing to local drive is much faster than sending over Ethernet, the processes run faster and CPU utilization increases to about 80%, during the export process. Depending on the network speed and whether or not we have some other task to do in the Computer, user has the flexibility to choose worker size and export method.

During the execution, a log file is filled with information regarding the individual export tasks (as in Figure 4), such as the number of parameters in the DataGroup, the TestPoint time slot duration. There is also a metric showing how much we gained from parallelism. In this example, the parallel exporting process took about 10 times less than the time it would have taken, had all the exports been taken consecutively (without parallelism).

TAIDERIVED_XMS_2048Hz (96 params)	T8_ECS_BLEED_ON (42 sec)	2020_02_18_2000	2020_02_18_2007	7.5 min. (~2 MBps)
TAIDERIVED_XMS_2048Hz (96 params)	T14_ECS_BLEED_OFF (12 sec)	2020_02_18_2006	2020_02_18_2008	2.4 min. (~2 MBps)
TAIDERIVED_ROT2_2048Hz (230 params)	T4_E1_E2_IDLE_Stable (88 sec)	2020_02_18_1925	2020_02_18_2009	43.9 min. (~2 MBps)
TAIDERIVED_XMS_2048Hz (96 params)	T4_E1_E2_IDLE_Stable (88 sec)	2020_02_18_1954	2020_02_18_2010	15.5 min. (~2 MBps)
TAIDERIVED_XMS_2048Hz (96 params)	T13_ECS1_Valve_CB_ON (36 sec)	2020_02_18_2005	2020_02_18_2011	6.2 min. (~2 MBps)
TAIDERIVED_XMS_2048Hz (96 params)	T15_E1_EMRG_OFF (29 sec)	2020_02_18_2007	2020_02_18_2011	4.8 min. (~2 MBps)
TAIDERIVED_XMS_2048Hz (96 params)	T5_ECS_BLEED_ON (90 sec)	2020_02_18_1956	2020_02_18_2012	15.6 min. (~2 MBps)
TAIDERIVED_XMS_2048Hz (96 params)	T16_E2_EMRG_OFF (33 sec)	2020_02_18_2007	2020_02_18_2012	4.8 min. (~2 MBps)
TAIDERIVED_ROT2_2048Hz (230 params)	T5_ECS_BLEED_ON (90 sec)	2020_02_18_1929	2020_02_18_2013	43.8 min. (~2 MBps)
TAIDERIVED_XMS_2048Hz (96 params)	T6_ECS_BLEED_ON_Stable (393 sec)	2020_02_18_1957	2020_02_18_2033	35.9 min. (~1 MBps)
TAIDERIVED_ROT1_2048Hz (201 params)	T6_ECS_BLEED_ON_Stable (393 sec)	2020_02_18_1900	2020_02_18_2058	118.5 min. (~2 MBps)
TAIDERIVED_FUS_2048Hz (351 params)	T6_ECS_BLEED_ON_Stable (393 sec)	2020_02_18_1822	2020_02_18_2106	164.5 min. (~2 MBps)
TAIDERIVED_ROT2_2048Hz (230 params)	T6_ECS_BLEED_ON_Stable (393 sec)	2020_02_18_1932	2020_02_18_2111	98.7 min. (~1 MBps)
S U M O F A L L	R E P O R T E D E X P O R T			2323.3 min.
T O T A L	E X P O R T D U R A T I O N	2020_02_18_1713	2020_02_18_2111	238.4 min. (9.7 times faster)

Figure 4 An example Log file, providing details of each export task.

DOI 10.5162/ettc2022/7.1

Glimpse into the New Platform

The Optimus Platform, being developed by the Artificial Intelligence Group, saves the raw data (pcap files) in a computational cluster (providing built-in redundancy and security) and uses parallel processing techniques to perform EU conversions on the fly. Having saved only the raw data provides substantial storage area savings. This data storage and on-demand data conversion platform is aimed to be equipped with analysis functionalities.

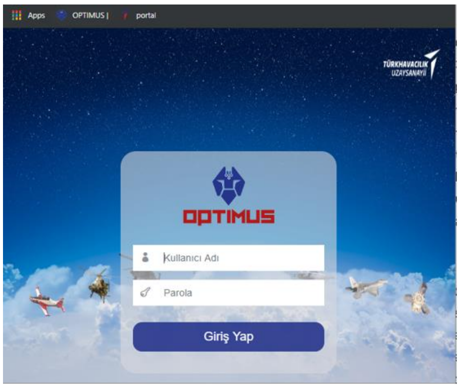

Figure 5 Login Screen of Optimus

Besides, basic statistics (such as minimum, maximum, average for each minute) about all parameters are stored in a separate database in Optimus (it is the first database (in the true sense of the word) used for flight data). This enables users to have a look at the data (as in Figure 6) and also more importantly to query flight data. This is especially worthy since the query can span over multiple flights, i.e. search is not limited to one flight. To illustrate, to investigate if some parameters exceeded some thresholds in all of the prototype flights can be almost instantly obtained by means of Optimus.

Figure 6 Example view of search capability in Optimus (Many flights are detected, user can plot the parameter (along with exceedance criteria)

Conclusion

A Data Export Tool is developed to overcome the increasing data export requests, where conventional methods based on Supplier utilities was getting insufficient. The created tool makes use of the batch processing capability of the IADS software using parallel processing techniques provided in Python. We have successfully used the tool in T625 Project. Nevertheless increasing frequency of the flights necessitated novel computer science techniques for data storage and processing, which led to development of a new platform. Without the Data Export Tool, we would not be able to meet the data expectations and we would not have time to have Optimus developed in parallel.

References

[1] www.xidml.org

[2] www.qt.io

[3] www.curtisswrightds.com

DOI 10.5162/ettc2022/7.2

TENA, JMETC, and BDA TOOLS FOR TELEMETRY

Gene Hudgins and Juana Secondine
TENA Software Development Activity (SDA)
Niceville, FL, 32578
gene.hudgins@tena-sda.org and juana.secondine@tena-sda.org

ABSTRACT

TM often requires operators on location with receive system(s) or at a remote console, resulting in TDY for operators and possibly a shortage of operators to support all scheduled operations. A remote-control capability along with centralized data collection could eliminate existing personnel requirements at both the local system antenna site as well as the control facility, greatly reducing operational costs and providing insight to system status. TENA provides for real-time system interoperability, as well as interfacing existing range assets, C4ISR systems, and simulations; fostering reuse of range assets and future software systems. JMETC is a distributed, LVC capability using a hybrid network solution for all classifications and cyber. TENA and JMETC in conjunction with BDA tools and techniques, allow for the most efficient use of current and future TM range resources via range resource integration, critical to validate system performance in a highly cost-effective manner.

Key Words: TENA, JMETC, BDA, multi-site, multi-domain

TRMC SOLUTIONS FOR the Telemetry Community

As in the past, present telemetry (TM) support requires operators to be on location with the TM receive system or at a remote TM console (with a remote TM antenna control unit). This often results in temporary duty (TDY) for operators and potentially an insufficient number of operators to support all scheduled operations. The capability to remotely operate the telemetry system (i.e., perform status monitoring, data distribution, and/or command and control from a centrally-located, manned site) greatly reduces operational costs of TDY to remote TM sites. A remote control capability could altogether eliminate the existing requirement for personnel at both the local TM system antenna site as well as the TM control facility, alleviating previous manpower issues (Figure 1).

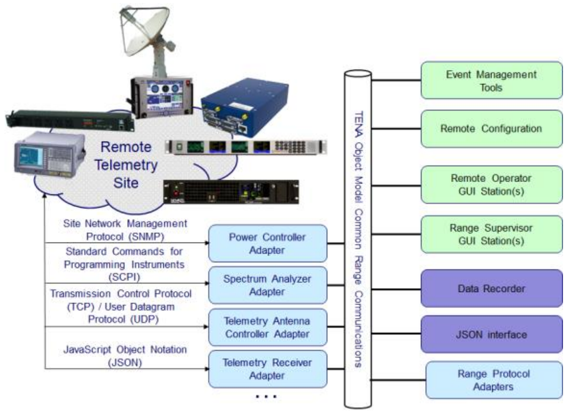

Figure 1 Architecture to a Remote TM Site.

The original design of the DoD test and training range infrastructure was not intended to be interoperable, and rapidly became inadequate in this new era of warfare. The cost-effective integration of range data and telemetry resources is critical to ensuring the war-worthiness of today's advanced weapon systems and platforms which populate the air, land, sea, and cyber areas of operations. To ensure the advantages of range interoperability are available across the DoD, the OSD Test Resource Management Center (TRMC) Central Test and Evaluation Program (CTEIP) developed and is constantly refining the Test and Training Enabling Architecture (TENA).

TENA is a common architecture providing real-time software system interoperability and the capability to interface existing range assets, systems, and simulations at distributed facilities. Government-owned and free for anyone to use, TENA allows the most efficient use of current and future range resources via range resource integration. This integration invariably fosters interoperability and reuse within the test and training communities – critical in validating system performance in a highly cost-effective manner.

TENA provides a middleware software component and can be used on any internet protocol (IP)-based range or distributed network, such as the Joint Mission Environment Test Capability (JMETC) networks and the Joint Staff (JS) J7 Deputy Director Joint Training (DDJT) Joint Training Enterprise Network (JTEN).

Upgrading an existing range system to TENA can be achieved in a drastically shorter time frame than traditional software integration efforts. Additional benefits include the cost-effective replacement of unique range protocols, enhanced exchange of mission data, and organic TENA-compliant capabilities at sites which can be leveraged for future events, enhancing both reuse and interoperability.

The JMETC Secret Network (JSN), which leverages the Secret Defense Research and Engineering Network (SDREN) for connectivity, is the test and evaluation (T&E) enterprise network solution for secret testing. SDREN is a network established to support research, development, testing and evaluation, and science and technology activities in the DoD. The persistent JSN infrastructure includes sites at Defense industrial facilities and peering with sites on other DoD networks at like classification such as the Secret Internet Protocol Router Network (SIPRNet).

JMETC also offers a network capability to its customers with a requirement for higher-than-secret classifications of distributed testing, cyber testing, or unique requirements that don't fit the JMETC JSN model. The JMETC Multiple Independent Levels of Security (MILS) Network (JMN) is the enterprise network solution for higher test event classifications, as well as those which are cyber-specific.

The primary product of T&E is the data and knowledge gained through the collection of information about a system or item under test. The amount of information needed to acquire this knowledge is growing exponentially due to more complex systems needing to operate in System of Systems (SoS), Family of Systems (FoS), Joint, and Coalition environments. With many DoD tools and methods remaining largely the same for decades, the T&E infrastructure necessary to collect and analyze this information has not evolved alongside this increased complexity, becoming increasingly deficient and ineffective. By contrast, corporations have dramatically changed their methodologies – modernizing their analytics capabilities to keep up with the massive influx of data.

To properly test and evaluate today's advanced military systems, the T&E community must leverage new algorithms using the equivalent processing power of many computers in parallel to effectively analyze large amounts of data. This process is called "big data analytics (BDA)" and the Test Resource Management Center is taking the initiative to develop better tools and techniques to empower DoD analysts to make better and faster decisions using more of the collected data than was previously usable.

CURRENT TELEMETRY APPLICATIONS

Automatic Dependent Surveillance-Broadcast (ADS-B) Adapter: Starting January 1, 2020, aircraft must be equipped with an air traffic control "Automatic Dependent Surveillance-Broadcast (ADS-B) Out" to fly in most controlled airspace. ADS-B is a surveillance technology in which an aircraft determines its position via satellite navigation, and periodically broadcasts position (and other information), enabling it to be tracked. The TRMC is creating a library of software products called Range System Adapters which present a common distributed communication mechanism for the remote configuration, monitoring, and control of range systems. As such, the TENA Software Development Activity (SDA) has developed an ADS-B Adapter – a software application designed to expose a common communication interface to an existing range system by wrapping the system's custom external interface.

The ADS-B Adapter is a computer process separate from the software running an existing system. By "wrapping" the existing ADS-B system, there is no modification of the existing system, allowing use on legacy systems that cannot be updated or have limited communication capabilities. The ADS-B Adapter translates identification and position information sent by aircraft and interfaces an application called a dump1090 server (Transmission Control Protocol (TCP)/Internet Protocol (IP) connection), which translates signals received by the Software Defined Radio (SDR) to a data stream that makes it available via a TCP service.

The TRMC-developed ADS-B Adapter provides a low-cost solution to acquire live/local aircraft information: an SDR radio and antenna costs >$100 and the dump1090 server software is freely available, open-source software and works with a variety of SDRs and antennas. The ADS-B Adapter is free, government-off-the-shelf (GOTS) software and when used in conjunction with the TENA Data Collection System (TDCS), captures/replays repeatable and realistic local air traffic scenarios in simulated environments (Figure 2).

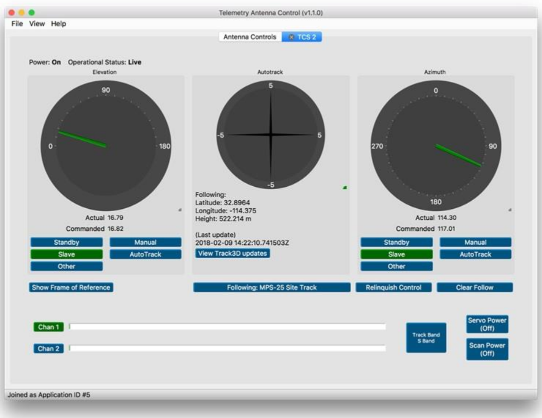

Figure 2 TENA ADS-B Adapter Telemetry Antenna Control Display.

TENA Plugin for SIMDIS: SIMDIS is a Naval Research Laboratory (NRL) set of software tools that provide two and three-dimensional interactive graphical and video display of live and post-processed simulation, test, and operational data. SIMDIS has evolved from an NRL display tool for the output of missile models, to a premier GOTS product for advanced situational awareness and visual analysis (Figure 3). The TENA plugin for SIMDIS allows a set of TENA Stateful Distributed Objects (SDOs) and messages to be used in SIMDIS (e.g. SIMDIS can be used in conjunction with the TENA ADS-B Adapter to provide a display of local aircraft identification and position).

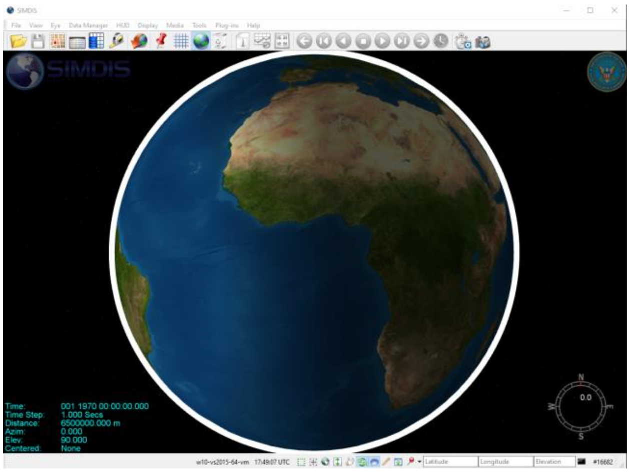

Figure 3 SIMDIS Graphical User Interface (GUI) Display.

TENA Interface for Yuma Proving Ground (YPG) TCS Antenna: YPG, located in Yuma, Arizona has chosen to add a TENA interface to their TCS Antenna Control Unit (ACU) model M1 used on their TM pedestals. The Antenna Control System SDOs created by the ACU adapters are visible on SIMDIS and the Instrument System Assignment Tool (ISAT), where SIMDIS shows the system with a beam indicating where it is pointed and ISAT allows users to select a Track SDO to send cueing data to the ACU. The operator then uses the data to point the system. Operational testing is currently underway on the remote monitoring and control capabilities of the telemetry antenna system using TENA.

Cloud Hybrid Edge-to-Enterprise Evaluation & Test Analysis Suite (CHEETAS) Tool: The TRMC has developed and successfully demonstrated a rapid Knowledge Management/Big Data Analysis capability to support hypersonic flight test. During a recent high-priority hypersonic test mission at Edwards Air Force Base, CA, post-test data processing (download, conversion, and validation – all necessary steps that must occur prior to data analysis) took approximately ten hours using existing capabilities. Working with the 419th Flight Test Squadron the following week, the TRMC team processed the same raw mission data with the CHEETAS tool in less than 15 minutes. Using CHEETAS cut the time required to get the test data into the hands of analysts by over 95%.

The CHEETAS framework provides a common tool suite for building evaluation infrastructure for disparate acquisition portfolios. Developed and supported by TRMC, CHEETAS is provided to the test community for free and is currently in use at multiple locations throughout the test community. CHEETAS is vendor- and hardware-agnostic, and can run on anything from a laptop to a full GPU-enabled, hyper-converged cluster, to a commercial cloud environment. CHEETAS is providing game-changing knowledge management and big data analysis capability both pre-flight and post-mission to support the testing of hypersonic boost-glideweapons and other systems requiring large-scale test data collection.

Data Processing Timeline: Traditional Software vs. CHEETAS

Description	Traditional Software *(what was used for ARRW mission)*	TRMC CHEETAS GOTS Software *(evaluated week after ARRW mission)*
Data Size	57 GB DTD X 3 DTDs	*57 GB DTD X 3 DTDs*
Dataset Used	BIMDAS Data Collection Memory Modules	BIMDAS Data Collection Memory Modules
Ingestion Equipment Capacity	Single RMM Reader *(serial process)*	8 RMM Read Simultaneously *(parallel process utilizing multi-cartridge reader)*
Data Ingestion Time 1 Module	55 minutes	3 minutes 7 seconds
Data Conversion Time 1 Module	9 hours 39 seconds	11 minutes 4 seconds *(included data validation)*
Data Available for Analyst Use	Approx. 10+ hours post-test	Approx. 15 minutes post-test
Computer System	Data Ingestion Workstation	Spare 4-year-old High Performance Desktop

CHEETAS Enables Timely Delivery of Validated Data to Analysts for Future Tests

Figure 4 CHEETAS Data Processing Timeline.

PAST TM USES OF TENA

Eglin Gulf Test Range (EGTR) Gulf Range Enhancement (GRE) Program: As in the past, present telemetry Theater Missile Defense (TMD) missile systems are designated to provide regional defenses against present and future conventional, chemical, biological, or nuclear ballistic, cruise, or air-to-surface guided missiles that can endanger deployed U.S. forces as well as U.S. friends and allies throughout the world. Eglin Air Force Base (AFB) in Florida is enhancing the capability of the EGTR to conduct TMD programs via the GRE program. This development includes the selection and construction of land-launch facilities; the modification of land, sea, and air safety zones; and the subsequent conduct of TMD missile system test and training flights within the enhanced EGTR. When complete, this expansion will allow launched target missiles to be halted by interceptor missiles with the intercepts occurring in the airspace over the Gulf of Mexico.

The EGTR expansion will provide greater flexibility in test scenarios than is possible using other ranges, and permits more realistic testing of TMD interceptor systems. This next-generation architecture is expected to be completely remote controlled when classification allows.

To make this happen, GRE engineers met with representatives of the TENA Software Development Activity (SDA) concerning the many TENA capabilities which would benefit this new architecture. TENA, chosen for the command and control (C2) portion of the GRE plan, will support remote operations of numerous Joint Gulf Range Complex test assets. TM equipment currently identified to be accessed via TENA adapters and controlled by TENA interfaces include the following: Antenna Control Units (ACU), digital switches, Time to Live (TTL) splitters, data link test set / Bit Error Rate Test (BERT), monitoring systems, spectrum analyzers, Global Positioning System (GPS) receivers, oscilloscopes, TM receivers, telemetry recorders, power strips, dehydrators, IP cameras, and uninterruptible power supplies (UPS). The long-term plan is for all GRE devices to be retrofitted with TENA adapters and interfaces.

Naval Air Station (NAS) Patuxent River, MD (Pax River) Atlantic Test Range (ATR): The Pax River ATR is another excellent example of how beneficial TENA can be for TM control. Before work began to develop and field an enterprise approach to remotely monitor and operate all components of remote ATR ground telemetry systems, Pax River was faced with four major, and incredibly common, TM range issues: operator proximity, lights-out operations, a generalized interface, and Information Assurance (IA) requirements.

The existing approach at Pax required TM operators to be on location with the TM ACU during missions. Any near-term remote operations concepts required a one-to-one correlation between the remote ACU and remote TM Antenna, and no sub systems were supported. They also had no ability to fully power-on, configure, operate, or obtain the status of their remote Auto-Tracking Telemetry System (ATAS) and Mobile Telemetry Acquisition System (MTAS) systems, therefore requiring personnel on-site to perform power-on and to configure all systems with no distributed status available from TM system components.

Vendor-specific interfaces and data models were used, which meant operators had to gain proficiency on each system component. This generalized interface prohibited uniform operator consoles, and limited the ability to easily access and share relevant metrics and engineering data. Furthering the problem was that Pax River had a limited ability to meet evolving IA requirements and Security Technical Implementation Guides (STIG) on system components.

Working alongside members of the TENA SDA, NAS Pax River developed an enterprise approach to remotely manage and operate all components of remote ground telemetry systems. This method provides a common architecture (TENA) which interfaces system components, regardless of system manufacturer. Upon completion, this effort now provides for single operator control of several remote TM systems, therefore reducing travel and manning requirements at remote sites. It also allows TM status information, setup, and control to be distributed to appropriate destinations for system verification and operations.

Additional Applications: Other TM applications of TENA are ongoing at White Sands Missile Range (WSMR) in New Mexico and Vandenberg AFB in California. WSMR reached out to the TENA SDA seeking a TENA-capable range interface unit (RIU) for existing radars; a TENA-capable Telemetry Tracker pointing data interface (as a modification to the existing RIU); and a persistent, distributed TENA capability through WSMR's Inter Range Control Center (IRCC). TENA is currently being used to connect FPS-16 radars, telemetry systems, and optics systems. Future plans at WSMR include the use of TENA for Real-Time Data Processing (RTDPS). Redstone Test Center also used TENA to pull real-time Time, Space, Position Information (TSPI) data via a "Data Adapter Tool" which fused other real-time TSPI sources. The Data Adapter Tool allows operators at RTC to now transport data via TENA using the Standard platform object model.

Understanding TENA

Understanding composability is the ability to rapidly assemble, initialize, test, and execute a system from members of a pool of reusable, interoperable elements, the TENA architecture is a technical blueprint for achieving an interoperable, composable set of geographically distributed range resources (both live and simulated) that can be rapidly combined to meet new testing and training missions in a realistic manner. TENA is made up of several components, including a domain-specific object model that supports information transfer throughout the event lifecycle, common real-time and non-real-time software infrastructures for manipulating objects, as well as standards, protocols, rules, supporting software, and other key components.

The TENA Middleware (currently at Release 6.0.8 and available for free download at the TRMC web site: https://www.trmc.osd.mil) combines distributed anonymous publish-subscribe and model-driven, distributed, and object-oriented programming paradigms into a single distributed middleware system. This unique combination of high-level programming abstractions yields a powerful middleware system that enables TENA middleware users to rapidly develop complex yet reliable distributed applications.

The TENA object model consists of those object/data definitions derived from range instrumentation or other sources, which are used in a given execution to meet the immediate needs and requirements of a specific user for a specific range event. The object model is shared by all TENA resource applications in an execution. It may contain elements of the standard TENA object model although it is not required to do so. Each execution is semantically bound together by its object model.

Therefore, defining an object model for a particular execution is the most important task to be performed to integrate the separate range resource applications into a single event. In order to support the formal definition of TENA object models, a standard metamodel has been developed to specify the modeling constructs that are supported by TENA. This model is formally specified by the Extensible Markup Language (XML) Metadata Interchange standard and can be represented by Universal Markup Language (UML). Standards for representing metamodels are being developed under the Object Management Group Model Driven Architecture activities. The TENA Object Model Compiler is based on the formal representation of this metamodel, and TENA user-submitted object models are verified against the metamodel. However, it is important to recognize the difference between the TENA metamodel and a particular TENA object model. The object captures the formal definition of the particular object / data elements that are shared between TENA applications participating in a particular execution, while the object model is constrained by the features supported by the metamodel.

Another significant benefit for TENA users is auto-code generation. The TENA Middleware is designed to enable the rapid development of distributed applications which exchange data using the publish-subscribe paradigm. While many publish-subscribe systems exist, few possess the high-level programming abstractions presented by the TENA Middleware. The TENA Middleware provides these high-level abstractions by using auto-code generation to create complex applications, and these higher-level programming abstractions (combined with a framework designed to reduce programming errors) enable users to quickly and correctly express the concepts of their applications. Re-usable standardized object interfaces and implementations further simplify the application development process.

Through the use of auto code generation, other utilities, and a growing number of common tools, TENA provides an enhanced capability to accomplish the routine tasks performed on the test and training ranges in support of exercises. The steps in many of the tasks are automated, and thanks to the enhanced software interoperability provided by TENA, the information flow is streamlined between tools and the common infrastructure components.

TENA utilities facilitate the creation of TENA-compliant software and the installing, integrating, and testing of the software at each designated range. This complex task falls to the Range Developer who, in this phase, performs the detailed activities described in the requirement definitions and event planning, as well as the event construction, setup, and rehearsal activities of the range's Concept of Operations. While some manual exercise and event setup is required at ranges, TENA tools, as they are developed and become accepted across the range community, make exercise pre-event management easier.

SUPPORT FOR TENA USERS

The TENA SDA has developed a website that provides a wide range of support for the TENA user, including an easy process to download the Middleware, free of charge. The website also offers a helpdesk and user forums that will address any problems with the Middleware download and implementation. The TENA SDA is very aware of the need to inform range managers and train TENA users, and the TENA SDA presents regular training classes that are designed to meet attendees' needs; from an overview or technical introduction of TENA, all the way to a hands-on, computer lab class on the TENA Middleware.

TENA's continuing evolution in its support of the test and training range community is managed by an organization of users and developers. TENA is maintained according to a consensus of its users, which assemble as the JMETC Configuration Review Board (JCRB). These meetings are generally held at technical exchanges JMETC holds each year called the JMETC Technical Exchange (JTEX). At these meetings, users are updated on TENA usage, problems, and advancements. Although the agenda involves briefings, it is open to wide-ranging discussions. This ensures the users' concerns and inputs are understood, recorded, and action items are made if necessary. Of equal importance, TENA developers and management have had a long and mutually beneficial relationship with the Range Commanders Council.

CONCLUSION

Although it was a technological and software evolution that was the impetus for TENA's growth in its enabling of range interoperability and resource reuse, the Middleware found its needed validation on DoD test and training ranges. On these ranges, the U.S. Military evaluates the warfighting equipment, personnel, and concepts that are deployed in support of ongoing missions around the globe. Unfortunately, test and training events only provide the opportunity for evaluation. It is the data collection and analysis that determines the war-worthiness of the equipment or concept; this data can quickly and definitively illuminate any necessary improvements needed to ensure effective and safe weapon system operation and training. TRMC TENA, JMETC, and Big Data Knowledge Management are time-tested, proven, integral parts of that equation.

JMETC reduces the time and cost to plan and prepare for distributed events by providing a persistent, readily-available network, and the TENA common integration software is easily-integrated into telemetry environments and applications. Even the remote control capability alone alleviates previous manpower issues and greatly reduces operating costs for the telemetry community.

The TRMC is constantly building on a DoD T&E data management and analysis capability that leverages commercial big data analytic and cloud computing technologies to improve evaluation quality, reduce decision-making time, and reduce T&E cost. This vision encompasses a big data architecture framework – its supporting resources, methodologies, and guidance – to properly address the current and future data needs of weapon systems testing.

Transforming the current T&E data infrastructure to one employing a Big Data approach will support both current warfighter T&E needs and the developmental and operational testing of future weapon platforms. The T&E community will be able to realize improvements in cost avoidance and cost reductions, in faster and more accurate T&E responses, and in overall T&E capabilities. Using TENA, JMETC, and BDA, Test Directors can put their focus back where it needs to be – on the warfighter and the task at hand.

For more information, contact Ryan Norman, Chief Data Officer and Lead, Joint Mission Environments, E-mail: jmetc-feedback@trmc.osd.mil or tena-feedback@trmc.osd.mil. For the Unclassified, Controlled Unclassified Information (CUI), U.S. Government / Contractor website, go to https://www.trmc.osd.mil; for Distribution A, non-U.S. Government / Contractors, please visit https://www.tena-sda.org.

DOI 10.5162/ettc2022/7.3

Optimizing PCM Bandwidth Usage in Flight Test by Real-time Data Analysis During Flight

Patrick Quinn

Aerospace Instrumentation
Curtiss-Wright
Unit 5, Richview Office Park, Clonskeagh, Dublin 14, Ireland
pquinn@curtisswright.com

Abstract:

There is an ever-increasing demand for more data to be captured during flight test applications, placing more demand on the limited bandwidth available for PCM data transmission. Some strategies can help, such as performing analysis on the platform itself. For example, by performing Fast Fourier Transform (FFT) analysis in the air and sending just the results down over PCM in real-time, the PCM bandwidth usage can be optimized, saving the users time and reducing the overall cost of ownership.

This paper discusses data analysis methods, specifically FFT analysis on accelerometer data in real-time during flight, that can be used without additional flight test instrumentation hardware onboard the aircraft.

Keywords: Big Data, real-time data analyses, Data Reduction, Bandwidth Optimisation

1. Introduction

During flight test applications, it is critical to understand and quantify the vibration frequencies experienced by the airframe during an actual flight. The vibration data is compared to flight qualification random vibration test standards and are typically substantially lower than the random vibration test curves.

Traditionally, the vibration measurements are taken using ICP type accelerometers positioned on the aircraft's control surfaces, sampled at a high rate, and transmitted to the ground over PCM for real-time FFT processing. However, as many FTI engineers will attest, PCM is not impervious to drop-outs and interference, and high sample rate accelerometer measurements can take up huge amounts of the available PCM bandwidth.

There has been a trend to attempt to move the analysis to onboard the aircraft and send only the FFT results over the PCM stream. This should speed up the data analysis and free up the PCM bandwidth for other data, thereby reducing the number of flights required for the test campaign and the program's overall cost. This approach, up to now, has required separate data analysis computers to be onboard the aircraft, increasing the complexity and size of the FTI installation.

This paper discusses some of the issues, challenges and trade-offs that must be made when considering performing FFT analysis in real-time onboard the aircraft. It proposes an approach where data acquisition units conduct the FFT analysis in real-time, and both the raw data and FFT results are available to the user, with the raw data recorded onboard and the FFT results sent over PCM, highlighting the bandwidth savings that are possible.

2. Considerations for Measuring Vibration in Flight Test

One of the first steps when measuring vibration is to calculate the expected vibration frequency range of the control surface under test during all stages of flight and then ensure your sensor has the bandwidth to measure the expected vibration.

Following that, data acquisition units must be selected that meet the required bandwidth, taking into account the filtering applied by the data acquisition modules to ensure all the signal frequencies are captured. Then, as part of the full FTI system architecture, especially the telemetry bandwidth available on the test range, a PCM frame structure is selected that allows sampling of all the required data sources at the required rates. This PCM frame structure usually defines the limits of available sampling rates for the accelerometer channels.

3. FFT Analysis, the Balancing Act

There are multiple factors to consider and trade-offs to be made when performing FFT analysis; these will be discussed in detail below:

For this discussion, we will consider the example of the NASA F-15B/ Flight Test fixture II Test Bed. On this airframe, the power spectral density (PSD) of accelerometer flight data was required to be analyzed to quantify the in-flight vibration environment from a frequency of 15 Hz to 1,325 Hz[1].

3.1 Channel Sample Rate and Filter Cut-off

To meet the above bandwidth requirements, the accelerometer modules in the data acquisition units must have a bandwidth available greater than 1325 Hz after filtering is applied. Considering this, sampling at 8,192 Hz with FC set to FS/4 gives us a bandwidth of 2,048 Hz,

DOI 10.5162/ettc2022/7.3

easily meeting the bandwidth requirements of the program.

3.2 Max detectable FFT Frequency

FFT maths tells us that the maximum detectable frequency in an FFT analysis is driven by the number of FFT points or BINs and the resolution of the FFT. The number of FFT points or BINs of intestest is half the FFT block size due to the Nyquist theorem:

FFT BINs = No of FFT Samples / 2

The resolution of the FFT points is driven by the sample rate of the raw samples and the number of FFT samples:

FFT Resolution = Sample Rate / # FFT Samples

The Maximum detectable FFT frequency is the frequency contained in the final FFT BIN of your FFT analysis. It is important to ensure that the number of FFT samples and the sample rate of the channels results in a Maximum detectable FFT frequency that is greater than the expected frequency range required to be analyzed.

Relating this back to the NASA F-15B example:
For a sample rate of 4,986 Hz and an FFT block size of 16,384, there would be 8,192 frequency BINs, and the maximum detectable frequency would be 2,047.75 Hz.

For a sample rate of 8,192 Hz and an FFT block size of 32,768, there would be 16,384 frequency BINs, and the maximum detectable frequency would be 4,095.75 Hz.

3.3 Number of FFT Samples

Following on from the previous section, the number of FFT samples must be large enough to give both the resolution required and cover the frequency range required.

3.4 FFT Resolution

FFT resolution is a critical consideration; if the frequencies required to be analyzed are all close together, the highest possible resolution is required; lower resolutions may be acceptable if spaced apart.

Relating this back to the NASA F-15B example:
An FFT Block size of 16,384 at a sample rate of 4,096 Hz will result in an FFT resolution of 0.25Hz. Doubling the sample rate to 8,192 Hz decreases the resolution to 0.5 Hz.

3.5 Time to gather FFT Samples

Considering the sampling rate and the number of FFT samples required, the FFT results can only update once the required number of samples have been gathered. Large FFT sample blocks at lower sample rates can take considerable time to gather the samples. Higher sample rates obviously gather faster, but at the trade-off of resolution.

Looking at all of the above and considering the NASA F-15B example:

- Sample rate of 8,192Hz, max required frequency 1,325Hz.
- An FFT block size of 8,192 samples will give us a resolution of 1Hz, and 4,096 FFT Points, with a max detectable frequency of 4,095 Hz, and will take 1 second to gather the samples.
- Changing this to a block size of 16,384, improves the resolution to 0.5 Hz per BIN and will take 2 seconds to gather the data.
- Doubling the block size to 32K samples improves the resolution to 0.25 Hz per BIN, but will take 4 seconds to gather the samples.

3.6 FFT Windowing Function

FFT transforms of a pure sinewave signal assumes that the data is one period of a periodic signal. For the FFT, both the time domain and the frequency domain are circular topologies, so the two endpoints of the time waveform are interpreted as though they were connected. When the measured signal is periodic and an integer number of periods fill the acquisition time interval, the FFT turns out fine as it matches this assumption. However, in reality, the measured signal is not an integer number of periods, not a pure sinewave, and this introduces discontinuities in the signal that appear as spectrum leakage, visible in the FFT results as magnitude spread both sides of the main peak.. These can be reduced by applying "windowing" functions to the FFT analysis. Many windowing functions are available in FFT analysis, but Hann and rectangular windows are most common. Hann windows are better for detecting frequencies that are closer together, where higher spectral resolution is required. Rectangular windows are better where the amplitude accuracy is the important factor.

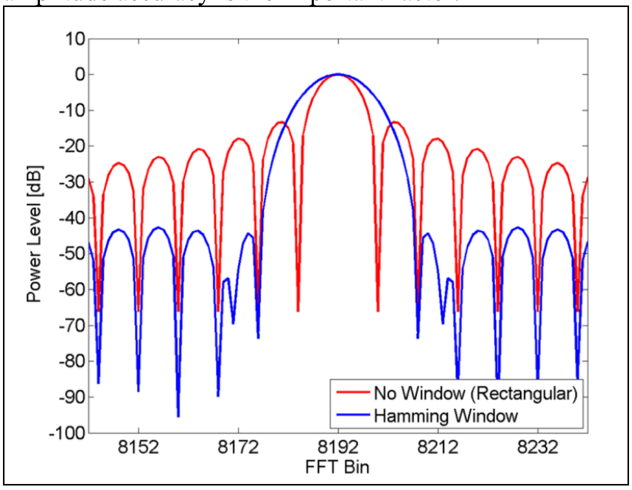

Figure 1: Rectangular vs Hann Window[2]

3.7 FFT Frequency Spread

Typically, vibration signals are not pure sinewave signals, where all the signal's power is concentrated into a single

DOI 10.5162/ettc2022/7.3

frequency point in the spectrum. It is more common that the true power of a specific frequency is spread across a number of points, all close together.
To this end, reading the power at a single frequency BIN may not accurately reflect the power seen. It may be more beneficial to read the power across several sequential BINs and average the reading across those points.
Breaking the FFT results into clusters or groups and calculating the power seen on that group can give a more accurate result, provided that the members of said group are close together. Groups of 3 or 4 give good average power readings.

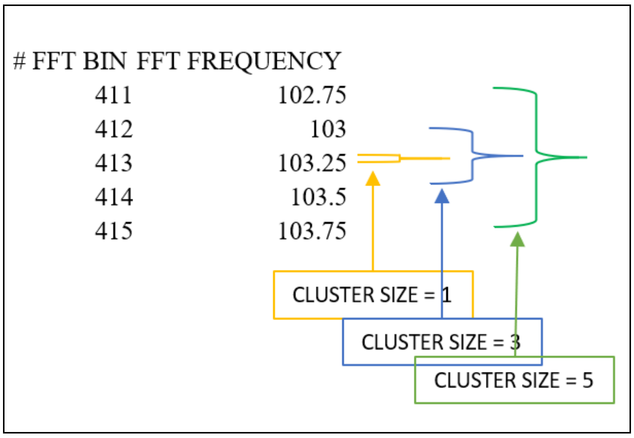

Figure 2: Cluster Sizes

3.8 Challenges of Designing in FFT analysis into Data Acquisition Modules

As stated at the outset of this paper, we will discuss an approach whereby the FFT analysis is done as part of the normal data acquisition, not in a separate box on board the aircraft. To that end, some of the challenges in achieving this are discussed below.

3.8.1 Raw Sample Storage / Buffering

ICP modules typically sample at high rates. Balancing this alongside channel density can be a challenge. For multiple channels at high rates, large buffers are required to store the data prior to processing; not only that, but the buffer also needs to store the next set of samples while the 1st set is being processed.

3.8.2 DC Offset Removal

One of the highest frequency components of any signal is a zero frequency component of a DC signal. This can have the undesirable effect of making it look like the largest frequency component is 0 Hz, washing out the actual frequencies of interest. Correcting this can be done by either applying a high pass filter to the signal or subtracting the mean from the original signal. However, applying a high pass filter increases filter delay; therefore, subtracting the mean is better.

3.8.3 Timestamping of the FFT Blocks

It can often be critical to know when the block of interest started and ended to correlate the FFT results back to the raw data. To this end, the timestamp at the start of the block must be tracked and available to the user.

3.8.4 FFT Windowing & Processing

The windowing function must be applied to the raw buffered FFT samples before passing them to the FFT IP for FFT processing.
The FFT processing itself must be balanced against the time taken to process multiple channels as the buffering requirements of storing the data while the FFT is being processed.
The cluster size selected must also be applied to the results to calculate a siding average of the power seen at each frequency BIN.

3.8.5 Power Consumption

All of the above can increase power consumption and, therefore, the overall temperature of the data acquisition unit. Care must be taken to ensure the processing time and data buffering is not so high that larger buffers are required and, therefore, excessive power is used.

3.9 How to Present the Results to the User

As can be deduced from the above, running an FFT creates a massive amount of possible data results that may be of interest to the user. An FFT block size of 32,768 results in 16,384 frequency measurements with 16,384 corresponding RMS Voltage measurements, per channel. From the point of view of PCM bandwidth saving, presenting all 16K frequency and 16K corresponding power measurements per channel would easily defeat the purpose of saving space in your PCM frame.
To this end, there are two possible approaches discussed here:

3.9.1 Peak Detect

Based on the idea that the user wants to know the most significant frequencies being seen in the FFT, the results, after DC offset removal, can be sorted into a list ordered by most significant power first and then offered as a fixed list of frequency and power pairs. Typically, the top 32 frequency and power pair results will cover most of the required data as after that, the powers seen are so low those frequency components are insignificant.

3.9.1 User Defined Frequencies of Interest

Based on the idea that the user knows which specific frequencies they expect to see in the results, the ability to define a set of user-defined frequencies of interest (FOI) and only get the RMS voltages seen at those specific points is sufficient.

4. PCM Bandwidth Saving Examples

At this point, we have discussed the challenges and trade-offs that must be made when considering performing an FFT in real-time during flight test; now we will highlight the potential bandwidth savings in real-time telemetry that is possible by taking such an approach, whereby, instead

of flooding the entire PCM bandwidth with the raw samples, the FFT results are transmitted instead.
Taking an extreme example, based on the IRIG-106 Chapter 4 PCM rules.[3]

IRIG-106 2020, Chapter 4 Section 4.3.2 a.1 allows for 16,384 bits per minor frame (Class II), and section b.1 allows for a max of 256 minor frames per major frame. At 16 bits per word, this gives us a major frame that is 1,024 words wide and 256 minor frames deep.
In such a frame, after accounting for Sync words and Subframe ID there would be 261,376 sample locations in the PCM frame

Sampling 16-bit ICP channels into such a frame at 8,192 Hz, in keeping with the NASA F-15B example above, each channel would require 1,024 PCM sample locations, assuming an 8 Hz major frame rate. This allows us to have 253 ICP channels, each with 4:1 commutation. This would take up 99.12% of the available PCM bandwidth for 253 ICP channels.

Now, using an FFT block size of 32K and a sample rate of 8,192 Hz and in peak detect mode, using the top 32 frequency and power pairs, that is 64 parameters per channel, each updating at 8 Hz rate, we would have a resolution of 0.25 Hz and only require 16,192 of the available sample locations in that frame for the same 253 channels, that is a total bandwidth usage of 6.19%, a 92.93% saving.
Switching this to user defined frequencies, and defining 8 specific FOI, and just transmitting 8 RMS voltage readings per channel, we would require only 0.77% of the available PCM sample locations.

Under a more realistic example, 12 ICP channels sampled at 8,192Hz inside a 100-word wide minor frame with 256 minor frames per 16 Hz major frame takes up 12.18% of the available PCM frame.

Figure 3: 12 ICP Channels Sampled Raw at 8192Hz

Changing that to just the top 32 FFT frequencies and respective powers per channel takes up only 1.52% of the available PCM space.

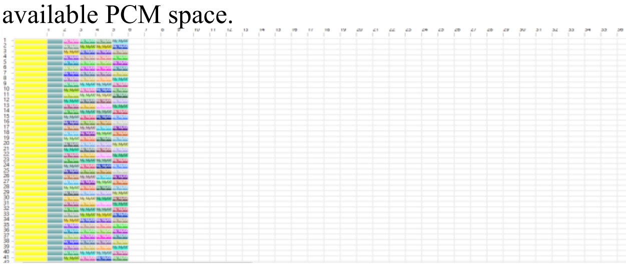

Figure 4: 12 ICP FFT Results Only

5. Conclusions

This paper has discussed the increasing demand for more data in flight test applications and the associated problems for transmission? bandwidth. It has been shown that by conducting FFT analysis in real-time in the relevant data acquisition modules, significant bandwidth savings can be achieved.

References:

[1] In-Flight Vibration Environment of the NASA F-15B Flight Test Fixture:- Stephen Corda, Russell J. Franz, James N. Blanton, M. Jake Vachon, and James B. DeBoer NASA Dryden Flight Research Center Edwards, California
[2] Realistic Extended Target Model for Track Before Detect in Maritime Surveillance:- Borja Errasti-Alcala, Walter Fuscaldo, Paolo Braca & Gemine Vivone
[3] IRIG-106 2020, Chapter 4, Section 4.3.2, Sections a.1 & b.1
This document was reviewed on 29/04/2022 and does not contain technical data

DOI 10.5162/ettc2022/7.4

Big Data Tooling and Usage Perspectives in the Airbus Helicopters Test Center

N. Brisset
Airbus Helicopters, Marignane, France
nicolas.brisset@airbus.com

Abstract

In the past years, Airbus Group has been investing into Big Data by developing and setting up infrastructures and backends which have already been presented in various papers. The platform has now reached sufficient maturity to be usable for concrete work and while work is continuing on the backends to improve performance and features, the emphasis is gradually shifting towards end-user tools and operational use cases, among others in the testing domain. New possibilities are appearing, but it also requires some changes in mindsets as commonly used approaches and habits need to be challenged.

This paper will discuss these aspects, focusing on tests performed during development and covering in particular:

- Typical types and volume of data generated during testing
- The need for appropriate data retention policies
- New opportunities brought by big data
- An overview of the palette of tools now available for Airbus Helicopters testers – and SDRs alike – as well as the different use cases it covers
- How some historic data analysis and plotting tools like Sandra can be connected to the big data infrastructure
- Some discussion on challenges and ideas to achieve digital continuity through all test means, from simulation through rigs to flight tests.

Key words: big data, digital continuity, timeseries, test configuration, data retention policies.

Data Generated During Testing

The test center at Airbus Helicopters (AH) is focusing on system-level testing more than software-level testing, but this paper will try to cover both as the boundaries are not always so clear and there are very many commonalities between these two areas anyway.

For vehicle testing the situation is similar: in spite of some quite significant differences in terms of data types and rates, the technical approaches and data strategy seen at a global scale are fairly similar and many challenges are shared with this area.

In terms of data types, during test execution we usually produce a mix of:

- **Raw data** as time series or individual samples, which can vary greatly in terms of frequency, range, amount of parameters or signal types
- **Still images** like for instance screenshots of various displays
- **Videos** (image sequences), either recorded directly at the output of an equipment, or acquired through a camera installed specifically inside the aircraft or sometimes outside the aircraft (e.g. for icing tests)
- **Audio** signals, such as alarms or cockpit conversations.

Based on a subset of all produced data, the tester generates a test result (FAILED or PASSED), which is captured and put into a test report. This test report can be directly produced as proof of compliance (MoC 4: "Lab Test Means"), or provided to a metier specialist who is then in charge of analyzing all test results and producing the final substantiation data (MoC 2: "Analysis").

<u>Note</u>: the amount of data generated by collecting customer data can reach considerable volumes due to the very large number of flights, which compensate for the far smaller number of available parameters per flight. This qualifies

DOI 10.5162/ettc2022/7.4

analysis of customer data during operations as very interesting application field for big data technology, but this paper intentionally focuses primarily on data generated during development phases, which have somewhat ironically seen a slower adoption of big data technology at AH.

The table below gives some orders of magnitude of the kind and amount of data generated (not necessarily recorded!) during system testing. When the system contains video signals, particularly ARINC 818, the figures can become so high that it warrants special consideration. Note that the table does not consider the volume that permanent video recording would generate: it assumes only extracts are generated for those parts that can't be analyzed using only still images, and which are run in automatic mode.

Table 1: Typical Generated Data Volumes during System Testing

Data type	Generated volume
	~ 5000 to 15000 1 to 10 Go
	~ 100 to 500 10 to 100 Go (only snapshots)
	~ 100 to 1000 < 1 Go
010110 101100 0101111	150 A429 15 RS 2 CAN 650 discretes 200 analogues 1 Ethernet network ~ 35 Mb/s (15 Go/h)

Data Recorded During System Tests

In recent years, AH has not had the means to store systematically all data produced on system rigs and has usually retained only high-level test result evidence: the PASSED / FAILED status. The situation has naturally evolved with the introduction of test automation, which executes automatically during nights and week-ends and produces data that the human operator will need to look at during a post-processing phase. For that to become possible, obviously more data needs to be recorded compared with the situation where the tester is visualizing the data live during the test.

However, for practical reasons (i.e. the lack of efficient storage means compared with the amount of produced data) the bulk of data collected during these automated test runs is "still", ie a snapshot of a given state during execution but not complete time series. Furthermore, data actually collected usually represents only a small fraction of all that is available.

The test reports are managed in version-controlled environments (typically DOORS) and contain high-level test results, but not the complete associated data. With the advent of big data infrastructures, this is now becoming a viable option, opening new perspectives which we want to discuss in this paper.

Data Recorded During Vehicle Tests

Vehicle tests (i.e. essentially tests of mechanical parts and dynamic assemblies) are performed in the same department as system tests at AH. Though quite different from avionics system tests due to the nature of the system under test and physical phenomena to observe, there are some interesting facts to share about them. We could sort these tests into four somewhat arbitrary categories using different means:

- *Rotor testing*, which is usually split into different campaigns typically focusing on performance or dynamic behavior
- *Gearbox testing*, which is very specific to these critical parts and for which AH is currently building a whole new rig that will be dedicated to gearbox testing during development phases
- *Iron bird testing*, where we basically put a complete helicopter into a dedicated building and let it run for many hours, either to derisk/reduce test flights or for endurance tests
- *Fatigue, load and environmental testing*, which is a very varied activity where various parts are tested to determine their mechanical characteristics when submitted to environments constraints representative of the most extreme cases that may be encountered during in-service life – and often even beyond to determine margins.

The table below gives some orders of magnitude of the volume and types of data generated during recent campaigns, which are currently stored in data filers under the native recording format, not really suitable for large-scale analysis. For future helicopters, even if we try to contain the increase

DOI 10.5162/ettc2022/7.4

of data recording requests, it is clear that at least as much data will be generated, probably even significantly more. Therefore it has to be expected that the current challenges in storing and above all efficiently analyzing these data will only increase.

Table 2: Orders of Magnitude of Vehicle Testing Data Recording Volumes

Test type	Recorded data
Rotor tests	Dynamic tests: 62 runs 45 h 115 sensors Max frequency 5 kHz ⇨ 100 Go (≈ 2Go / h) Performance 66 runs 37 h 60 sensors Max frequency 5 kHz ⇨ 80 Go data ⇨ 30 Go video
Gearbox tests	50 campaigns / year Max frequency 100 kHz Up to 1 To / campaign ⇨ 300 Go / campaign
Iron bird tests	250 h over 3 years (dev) 350 h in 3 months (endur.) ⇨ 3 To (≈ 5 Go / h)
Fatigue, loads & env.	Multiple smaller tests, less standardized. But not dimensioning overall

Data Retention Policies

Even though in the initial stages of big data introduction many engineers tended to think that there are no limits on storage capacity, nothing comes for free and it is obviously not good practice to accumulate large amounts of data without a clear purpose, and without a clear associated configuration.

Testing during engineering phases, especially when considering the whole palette of possible means from simulation to rigs to real aircraft, can produce very substantial amounts of data. Therefore to avoid filling up the data lake with useless data, following criteria are proposed to be considered for the preliminary definition of retention policies:

- Data recorded during **formal sessions** used to demonstrate compliance should be archived for as long as the tested configuration is in use by customers
- Data pertaining to the demonstration of **safety-critical** functions should be archived for the very long term (e.g. the lifespan of the considered product)
- Data recorded during sessions where an **unexpected event occurred** should be archived until the event if fully understood and resolved, unless any major technical hurdle makes it impossible to leverage the data
- Data recorded during **engineering test sessions** where nothing special happened should be archived until certification is completed
- Finally, in the **absence** of accurate **configuration data** for some archived test results, the interest of keeping time series data should be questioned.

Expected Benefits of Large-Scale Test Data Recording

There are a number of scenarios in which systematic data storage during development phases can be quite critical to optimize efficiency:

- **Unexpected events** can happen during testing. Sometimes they can't be analyzed on the spot, or even worse: reproduced. In such cases, systematic recording of the data can turn out to be precious to enable analyzing the event after the test session, without the need for repeated test sessions and without the risk of missing out on an important event
- **Comparing with a past configuration** can be very useful when a given test starts failing while it used to work a few weeks or months before. Coming back to the root cause of the difference can be extremely costly or even impossible, and if no data is available for in-depth analysis then the risk is high that the complete root cause remains only partially understood
- **Looking for already performed test points**, be it in simulation, a rig or in flight is expected to bring very significant savings over a full test campaign. It is still too early to give figures, but we do know that sometimes a flight or test for a specific test point is simply redone because it is currently too time consuming to determine whether it has already been done and/or to find the corresponding data. However, in order to bring any real-world benefit the big data

approach must deliver on its performance promise: finding any event through a substantial number of tests shall not take longer than a few minutes! And as highlighted below in the section about challenges, proper configuration data must be associated to the raw data in way that makes it convenient to query

- **Faster data access** even for routine tasks that we perform daily (like plotting curves for test data analysis) can bring very interesting benefits, even though it is more a collateral benefit than the essential reason why we introduce big data. Considering Sandra for instance with a few hundred active users including some people who use it for a few hours every day, the productivity boost they will gain from almost instantaneous access to the data they need can scale up to quite significant savings…

Big Data Tool Palette

We have seen that data volumes generated during testing phases increase constantly, and that big data will largely determine our ability and efficiency in coping with this huge amount of data. But for that we will clearly need some specific tools, and not only for data storage.

Big data is a rather simple concept that turns out to be very complex in terms of implementation, and it often requires specific non-trivial tools, adding to the complexity of already demanding test environments. This complexity is impacting users and especially difficult to manage, as the technology is still evolving at a very fast pace and tools are far from mature in this field.

In this context the introduction of new tools must be considered with caution, balancing the benefits of integrating already existing tools with big data technology against the introduction of new specialized tools. The following picture illustrates various types of tools needed for efficient big data usage. They can be broken up into various categories:

- **Data ingestion** tools that allow efficient data pre-processing and ingestion
- **Storage and processing infrastructure** ("data lake") that holds the data in an efficient way, making it possible to retrieve it in a massively parallel and very quick way
- **APIs** that allow accessing the data from a large variety of tools and languages
- **Specialized/metier tools** that are used to develop and run complex dedicated algorithms
- **General-purpose data analysis and plotting tools** that can be tuned either for time series, or for statistical analysis of discrete events

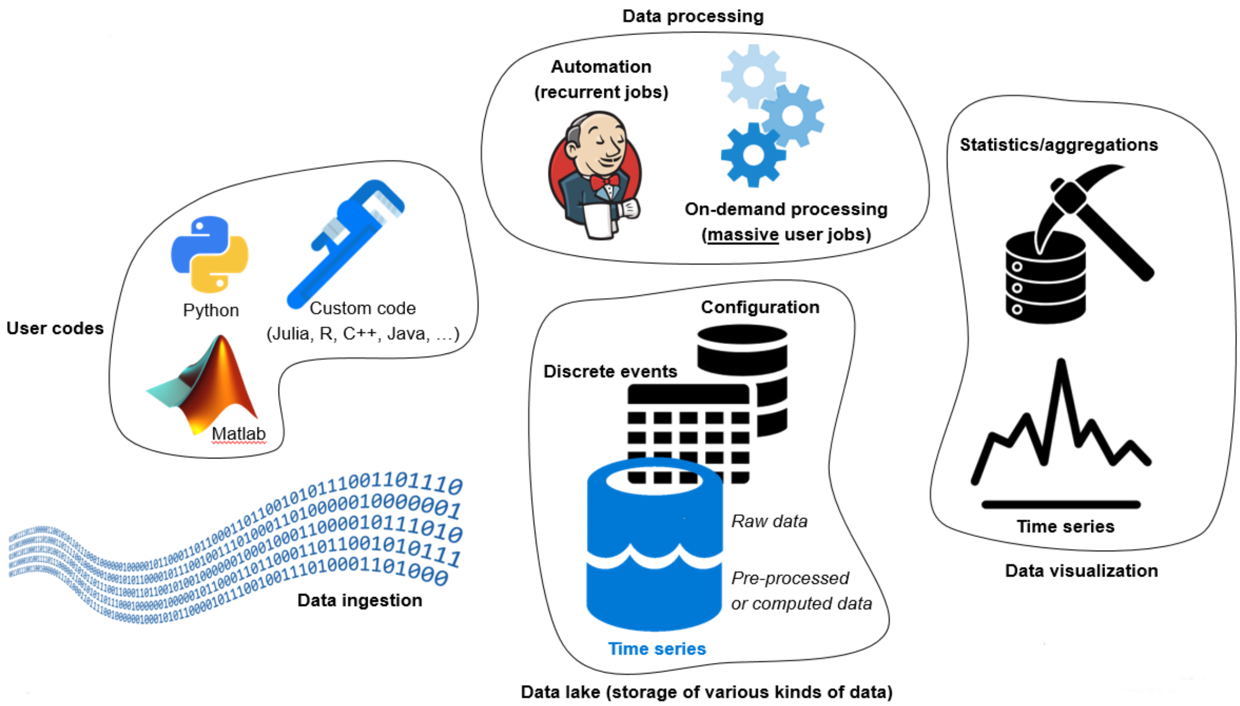

Figure 1: Big Data Tool Palette (Generic)

Current Tooling Landscape at AH

Big data is still in its early stages at AH, especially when it comes to development test results. There is an extensive on-premises platform which is used for a number of use cases but not yet for the storage and processing of time series. The various components described in a generic way in the previous paragraph are currently supported as follows:

- **Data ingestion** is performed in mutliple steps: data is transferred either as CSV (fleet data) or in a HDF5 container (prototype test data), then turned into AVRO buffers and ingested into HBase
- **Storage** components are offered by the TSAS infrastructure, which provides the "data lake" component in the form of a **timeseries** database working together with another database dedicated to the storage of other kinds of data like **events**
- **Massive processing** can be achieved thanks to TSAS.processing, a spark-based engine with a user-friendly web interface for the configuration of search jobs
- **Job automation** can be setup in order to launch data tagging (e.g. Flight Regime Recognition) or data check routines (e.g. CheckFTI)
- **Parameter management and queries** are done thanks to the combination of a specific database, along with a dedicated TSAS.search web front-end
- **REST APIs** are at the core of TSAS and allow accessing the data from a large variety of tools and languages: Matlab, python (PyTSAS), curl, etc…
- **Specialized/metier tools** that are used to develop and run complex dedicated algorithms
- **Time series analysis and visualization** can be done using either TSAS.plot (in the browser, stateless no-install usage) or using the well-established Sandra tool, that requires an installation but offers many more capabilities and ubiquity (same tool for all sources)
- **Data statistics, aggregations and event analysis** are preferably performed using Tibco Spotfire, which is the standard tool selected for that kind of task. It can be connected to the event database and leverage all pre-processing done using the TSAS ecosystem
- A generic platform for the user-triggered deployment of **user web apps** built using Dash

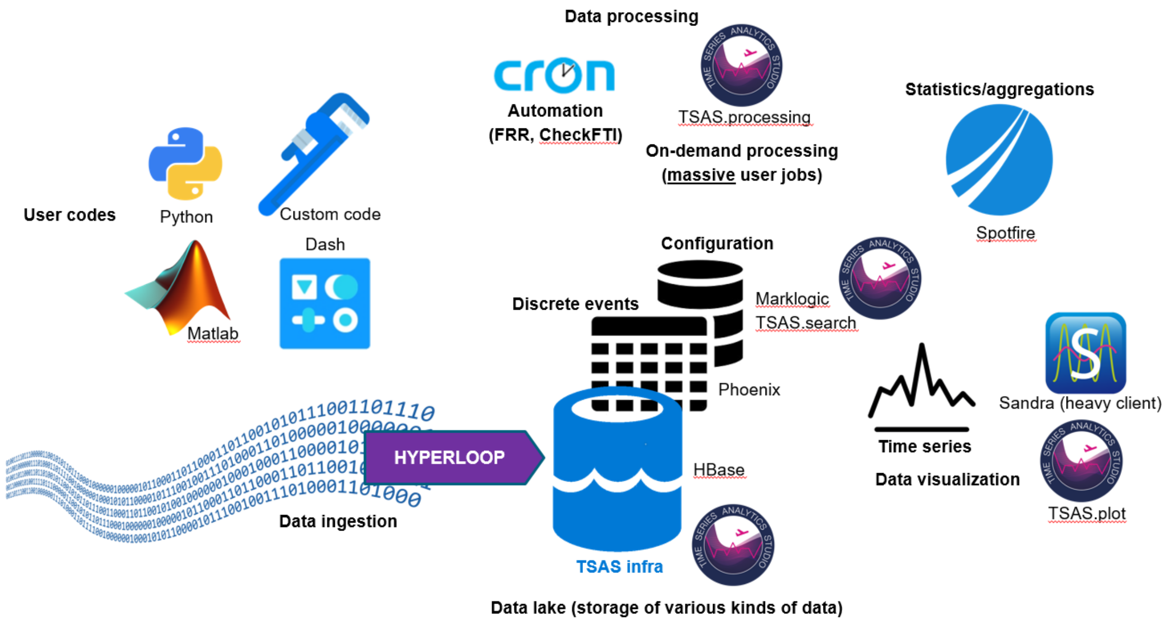

Figure 2: Current Big Data Tools at AH

Timeline

Big data experiments are already quite numerous at AH, but we are nonetheless still in the early stages. There are currently more use cases developed on data types other than time series and with data from other sources than development tests (i.e. the focus is rather on customer data). But it will undoubtedly come as the company digitalizes itself and strives for increased efficiency.

Without taking the risk of giving dates that are still quite uncertain, we can estimate that it will take years until big data is fully integrated into daily routine for all areas of the company. Many plans will probably need to be revisited along the way, but we can try to outline the natural steps through which we will have to go until full production deployment. This is what the next picture attempts to do.

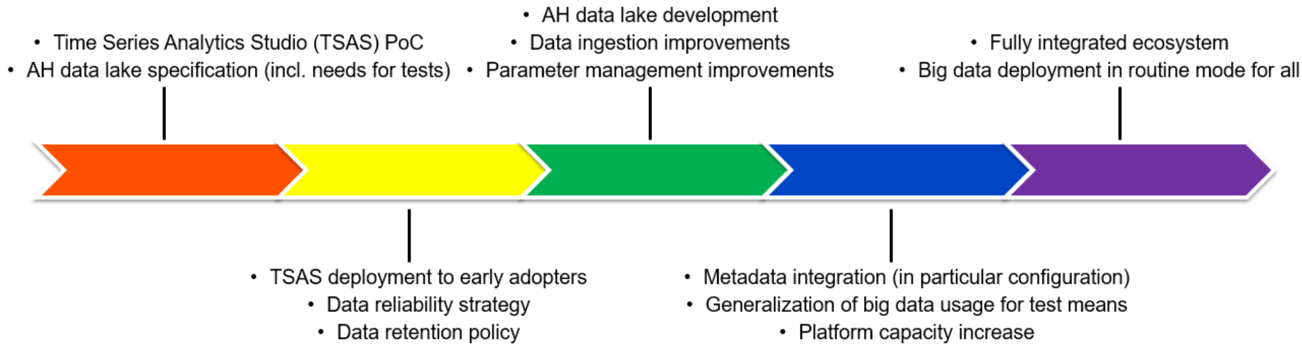

Figure 3: Big Data for Tests: Deployment Outline

Challenges, Present and Future

A number of unique challenges will come from the massive introduction of big data into testing routine. They are listed below, with some hints as to how they could be addressed in a journey that is only starting.

- **Data security and compliance** will be an essential element, probably one of the main driving factors in terms of technological choices as addressed in previous papers like [1]. The constraints in terms of data protection are likely to force some major big data editors to develop extensive on-premises solutions, or to force companies like Airbus to invest into cloud technologies which are not necessarily their primary area of expertise
- **Configuration data** must absolutely be considered as a very high priority. As challenging as collecting huge amounts of timeseries may be, there are solutions to this problem. But maintaining a consistent, up-to-date, accessible, relevant and reliable configuration index associated with the raw data may prove to be even more of a challenge considering the complexity of current products and industrial processes undergoing a major digitalization effort!
- **Data reliability** is likely to be one of the hardest parts in this endeavour. When people look at data directly, it is realistic to assume that any error in the data will get noticed and be corrected. But what will happen when we start running massively parallelized and unsupervised queries to analyze the data for us, in order to define potentially safety-critical part sizing or maintenance intervals? Tomorrow's design office engineers will have direct and efficient access to enormous amounts of data on his/her own, but how can we ensure that it cannot be misleading?
- **Digital continuity across means** will play an increasingly important role when our new efficiency targets command that our testing fully leverages a large palette of testing means ranging from simulation to real aircraft over all kinds of rigs. Not only will configuration data be key, but data continuity will be adding a substantial amount of complexity to the approach. If a given parameter or data cannot be correlated between the different means, a large part of the benefit (and the ability to rely more on simulation in the future) will be lost
- **Easy to use & learn tools** will be a prerequisite to reap the full benefits of the introduction of big data. Preliminary experience shows that while a small number of highly-skilled, motivated and IT-oriented engineers might be ready to learn a new programming language or a complex new tool, it is by far not given that the majority will find time and/or motivation to do that. It will therefore be of paramount importance to develop easy-to-use and well-integrated tools for the end users, carefully designed to fit their workflows
- **Management of parameter lifecycle** during the whole service life of our aircraft is already a challenge, but it will become even more difficult as we collect and keep data over long periods of time. Flight Test Installations are fairly complex, some sensors age and must be recalibrated, requests change permanently thereby calling for adjustments in the installations. This makes digital continuity even more

challenging, but also more necessary than ever as we will likely be using more and more data thanks to the new possibilities

- **Data volumes** (especially with the development of automatic testing) will drastically increase. The ability to store large amounts of data will likely turn into a form of obligation to store data. The seemingly huge datalakes of today will probably run full much faster than expected, and what happens next is easy to imagine: even larger storage volumes, soaring costs and substantial difficulties in maintaining data consistency and integrity over time. A dangerous factor is also that the cloud is something intangible (unlike manipulating physical media), blurring the perception of actual data volumes being stored. Data acquisition and retention policies will certainly need to be developed, but pruning and cleaning up petabytes of accumulated data will never be an easy task! Not to add the fact that storage formats will probably evolve, and some (typically proprietary formats) may prove to be a deadly trap
- **Obsolescence** will strike, as in any other field of technology. Or possibly even faster considering the relative immaturity of big data technological bricks, from hardware all the way to software components. We have to make choices today to advance on the path that unlocks the most interesting use cases. But having to run before we can walk and developing using agile and incremental approaches makes us prone to errors and the need to rework and refactor. It is therefore critical to carefully lay down the foundations of our future environments! One particularly acute issue will be data formats, because it is likely that these will continue evolving.
- Therefore **open-source or at least fully documented formats must be preferred** to proprietary formats for sustainability
- **Video** is a topic that calls for specific attention because although any modern smartphone can record in 4K at 60 fps or even more, leading to people expecting any video in the professional world to be recorded in 4K at least, this kind of data can represent very massive volumes that take their toll on any infrastructure in terms of processing power, storage size, etc… On top of that, videos can be compressed in many different ways and will most of the time require dedicated tools for their in-depth (automated) analysis, tools that may be sensitive to compression and formats
- Finally, the **mindsets** of engineers in our companies must evolve. Some may believe that the young generation of digital natives is better prepared and that their increasing presence over the coming years will ease the transition. It may be true, but others may argue that having grown up in a world of unlimited storage, bandwidth and computing power may push them down a dangerous path. We will need to pay attention to training and support for all the new users, and make them aware of the most important challenges to guarantee efficient usage and sustainability of big data in the testing area.

Conclusion

Even though the previous chapter on challenges may sound scary, it is not the intention of this paper to paint a grim picture of the future of testing in a big data enabled world!

On the contrary, the advent of big data in our development environments opens up very interesting perspectives in terms of being able to detect previously unseen phenomena, catching rare events and generally optimizing testing during development phases. It will most certainly be a pillar of our future efficiency.

Before jumping head first into the data lake at the risk of drowning in it, it is crucial to address all the listed challenges and to ensure that we take the most promising and future-proof paths. And even doing so, we must be ready to adapt as we progress along this exciting and fast-changing path.

References

[1] L. Peltiers, Data storage landscape: which solution for which purpose ?, *ETTC'21*, Proceedings p. 101

[2] A. Miguel Arevalo Nogales, Embracing new generation data access and processing methodologies in Flight Test, ETTC'21, Proceedings p. 123

DOI 10.5162/ettc2022/7.5

OASIS: a big data platform for satellite testing

A. Charcosset[1], F. Morel[1], J. Siega[1]
[1] Airbus Defence and Space SAS, 31 rue des Cosmonautes, 31400 FRANCE,
anais.charcosset@airbus.com, fanny.morel@airbus.com, julien.siega@airbus.com

Abstract:
Airbus Defence and Space (ADS) has developed a big data platform named OASIS for Open Analytic Services for Satellites. Since 2020, this big data platform is in charge of real-time telemetry ingestion, analytics and visualization for a wide and global ADS Satellite Fleet Supervision. It is used all along the satellite lifetime, from design and test to in-orbit support. The supervised fleet is now composed of 55 satellites and the platform aggregates 300Gb per day.

In particular, OASIS is used in the satellite Assembly Integration and Test (AIT) context, where the final satellites platforms and payloads are assembled and validated on various test benches. The OASIS capabilities to store, index, analyze test data, alert in case of anomaly during tests are vital.

To cover the challenging platform requirements (scalability, high availability, data persistency, security, easy maintenance), OASIS is virtualized on a cloud environment. The architecture offers COTS as well as internal big data analysis applications. Combined with the huge telemetry data available on the platform, they intend to offer Artificial Intelligence (AI) solutions, such as automatic failure detection and predictive maintenance. They represent a huge benefit especially for testing applications, where automatization is the key of future ways of working.

Key words: Satellites, real-time telemetry, Assembly Integration and Test, Artificial Intelligence, Big Data.

Glossary

ADS: Airbus Defence & Space

AI: Artificial Intelligence

AIT: Assembly Integration and Tests

OASIS: Open Analytic Services for Satellites

TM: TeleMetry

TC: TeleCommand

Introduction

Since its entry into service in 2020, the OASIS platform is ingesting, storing, and making available test & operational satellite data for business and engineering exploitation purposes. Today, the OASIS usage is mainly ADS centric. In particular, the platform is a key enabler of satellite testing in the AIT context, from simple data exploration to validation checks automatization and more complex investigation. Decision-making solutions built on Artificial Intelligence capacities are part of the next OASIS challenges. Some AIT use cases involving automatic anomaly detection are currently under development, taking advantage of the data accessibility on the platform and of its computation capabilities.

OASIS platform presentation

The OASIS big data platform creation is part of the global ADS digital transformation plan. By gathering all sort of satellite data, it enables data continuity and breaks data silos within the company. By moving to a data centric way of working, it increases productivity and improves Airbus efficiency. By offering new digital services, it increases customer satisfaction and business outcomes. By creating new analytics products, it enables the company to target larger and more complex systems, such as satellite constellations. For all these reasons, the OASIS adventure has been launched and pushed forward by ADS since 2018 and the platform is in service since June 2020.

OASIS is based on four strong innovation levers: data continuity & persistence, standardized data analytics toolset, optimized data visualization and centralized product lifecycle. To achieve these innovation objectives, the OASIS solution is relying on a centralized platform architecture, which supports every operation on satellite data: ingestion, storage, visualization and exploitation. The platform is used all along the satellite lifetime, from design and test to in-orbit support, gathering a large range of different space data. In particular, real-time telemetry from 55 under-development or in-orbit satellites is daily supervised thanks to the OASIS platform, which aggregates 300Gb per day.

The figure 1 illustrates the OASIS platform situation and data exchanges within ADS and with external interfaces.

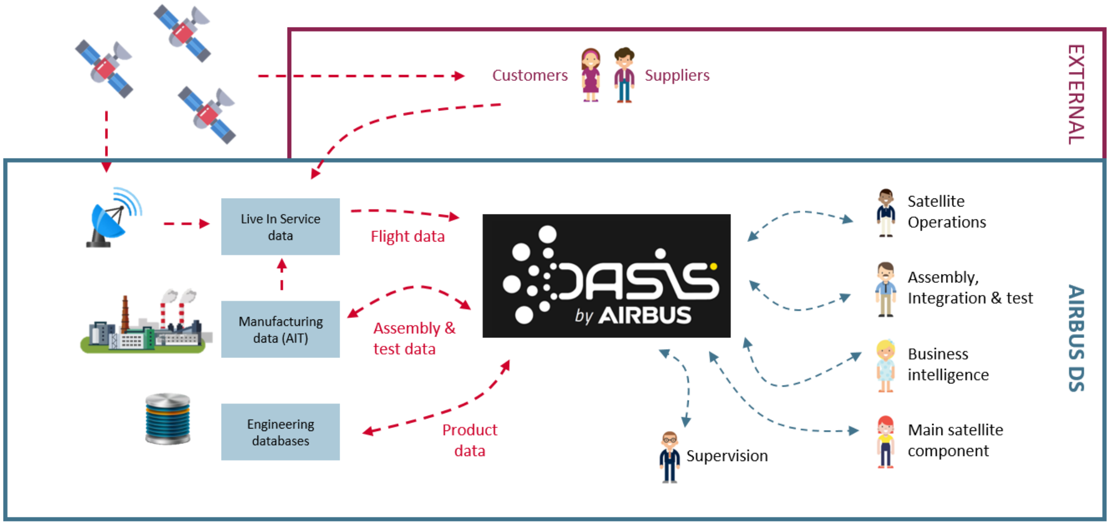

Fig. 1. OASIS platform situation plan.

Within the ADS ecosystem, the OASIS platform is receiving multiple satellite data, mainly satellite telemetries (TM), but also satellite telecommands (TC) and events logs. These various data, either simulated or real ones, come from different data sources all along the satellite lifecycle:

- Product data from engineering databases,
- Test data from ground manufacturing databases and test benches,
- Flight data from live in service data centres. Flight data are either real-time telemetry from in-orbit satellites sensors, or business data from external customers and suppliers.

Different ADS users have access to the platform. Their data usage (from simple visualisation to deeper analysis) is depending on their needs, roles and responsibilities. In-flight satellite operators, Assembly-Integration-Test (AIT) engineers, development engineers, marketing managers… are typical OASIS users. Their access to OASIS is finely managed so that their user experience is maximized and the platform & data security is ensured.

The OASIS platform is supervised daily in order to ensure service continuity to every user.

The data flow between OASIS and its data providers or between OASIS and its data users are not unidirectional. Beyond its data lake role, the platform is indeed also providing data computing and data analytics resources. The resulting added-value is then spread into the entire OASIS community: users as well as data providers can take advantage of this bidirectional communication flow.

Future OASIS improvements will give to the platform a wider dimension, as it will be open to external entities, customers and suppliers. Data governance and right access management are already major OASIS strengths. They will be at the heart of this OASIS next chapter.

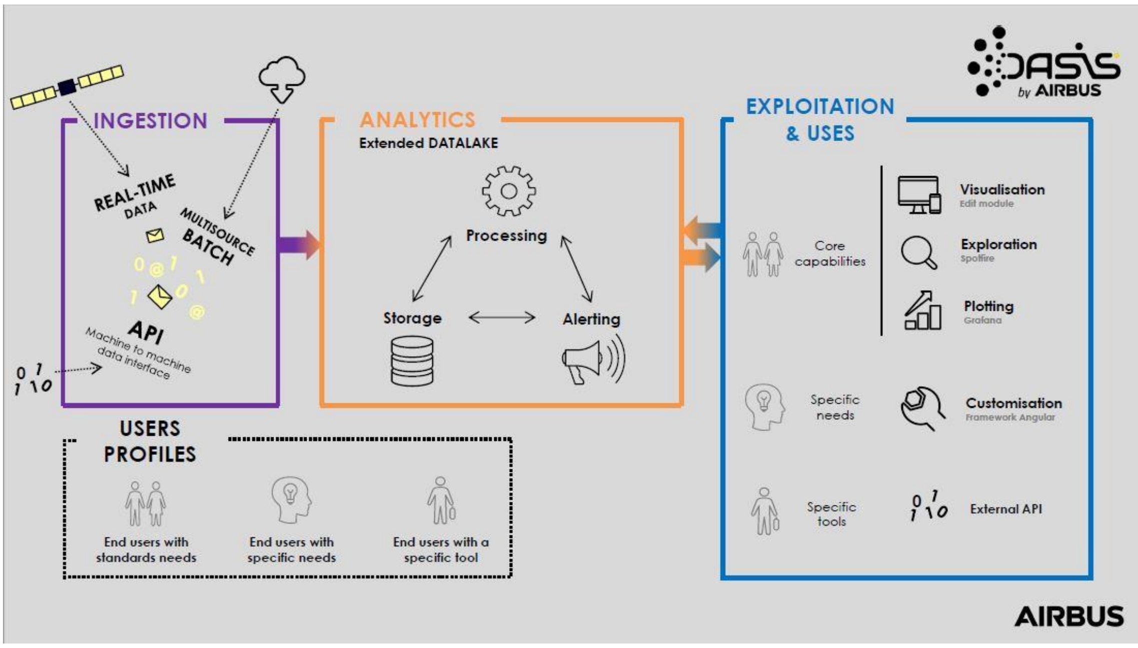

Fig. 2. OASIS three functional pillars.

As shown in figure 2, the OASIS engine is based on three pillars, which are the three main OASIS functionalities:

Ingestion: OASIS is gathering satellite data from different business sources, not only internal (e.g. Airbus ground test data) but also external (e.g. satellite positioning data from the North American Aerospace Defense Command NORAD public source). All ingestions are conducted automatically, in parallel, with multi batch capacities and real-time processing. Application programming Interfaces (APIs) are also used for machine-to-machine communication.

Analytics: once ingested, data are stored on several databases and database instances. The capabilities of this data lake are extended to analytics functionalities, thanks to centralized analytics tools. Once stored, raw data are transformed into gold data, making them ready for consumption. They can be analysed either through basic data analysis algorithms or through elaborated machine learning solutions. Anomalies or specific alerts are then raised to OASIS users when relevant.

Exploitation & uses: OASIS users have the capacity to fully exploit their data through:

- Visualisation and edition: access to the information of interest for the user (in read and/or write mode according to the user's right access) and to digital products via a web based user interface.
- Exploration: Via the Spotfire COTS, data that are not time stamped can be easily manipulated and explored.
- Plotting: Via Grafana, times-series data can be visualised through dedicated dashboards.
- Specific customisation: For specific user needs, the OASIS framework can be customised, so that specific visualisation or analytics requests are satisfied.
- Specific tools: Users can make their own tools compatible with the OASIS platform thanks to dedicated API, taking advantage of the OASIS data management capabilities.

Since its entry into service, the OASIS platform has covered around 20 major use cases. The ones involving AIT will be presented in the following chapter.

AIT use cases

During spacecraft tests and validation phases, OASIS is becoming a true enabler to follow, monitor and validate test sessions.

In its primary role of big data lake, data coming from ground test benches as well as data from the spacecraft itself (being from the service module i.e. platform part, from the communication module i.e. payload part, or from the overall spacecraft) are daily gathered and stored in OASIS platform. AIT engineers and architects thus can have access quickly and in one place to numerous data, including TM, TC, events or logs, both from simulations and real tests. It allows then to monitor their tests in real time, but also to perform investigation on dedicated past time periods thanks to archive data stored in the OASIS databases. These monitoring and investigation tasks are enabled using Grafana dashboards, which are thoroughly prepared to display relevant time series data through status or numerical plots.

With its high configurability, the tool offers functionalities, such as transformations to easily compute derived parameters. These transformations are helpful to derive the balancing between battery cells for instance, but also counters to get the exact life duration or total count of equipment activations since beginning of tests.

On top of this, an alerting system allows to get instantly notified by email or text message when an issue occurs. This is particularly very useful in case of loss of the data link between the spacecraft and OASIS, during thermal vacuum test phase (see figure 3).

Fig. 3. Example of OASIS Grafana dashboard for live TM monitoring.

Aside from parameter live monitoring, detailed descriptions of test sessions, named AsRun, are also sent to OASIS by batch multiple times a day. These AsRun files, along with their associated metadata (source, dates, duration, test status to name a few), are collected in structured databases and linked together with related test sessions and satellite.

This relational structure allows to seamlessly explore the 200,000 AsRun today available, as well as other test data, thanks to dedicated Spotfire dashboards, as shown in figure 4.

The wide field of customization possibilities, including multiple visualization types, filters or buttons, enables to quickly navigate among the various data available, and lead to insightful data-driven decisions.

For example, specific dashboards are used to analyze trends of equipment behaviours during the distinct testing phases (ambient, pre-vacuum, hot plateau, etc.) and to compare Airbus test values with respect to tests data coming from manufacturers.

Other dashboards are also being implemented to validate test results, before making them approved and signed off by the different people in charge, namely subsystem architect, AIT leader and even customer.

DOI 10.5162/ettc2022/7.5

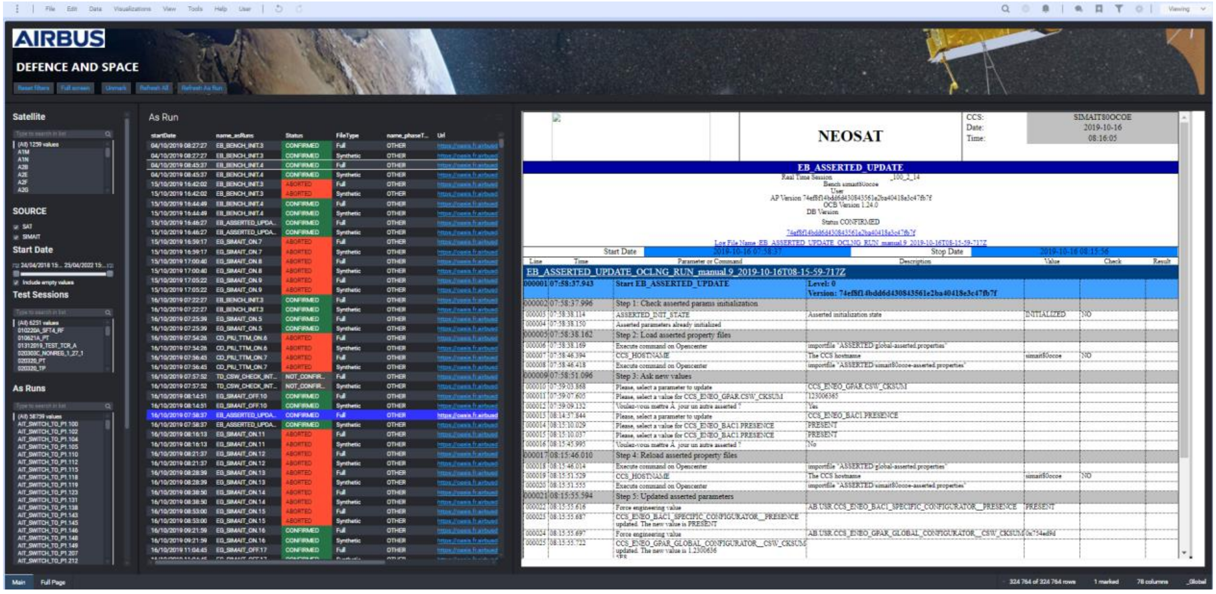

Fig. 4. Example of OASIS Spotfire dashboard for AsRun exploration.

Another important feature more and more used for AIT purposes, is the analytics capability, offered by a development environment made accessible for all the OASIS users. In this perspective, algorithms, from basic analyses to complex and smart solutions, can be developed and deployed so as to leverage the wide amount of data available.

In tests context, processings have been implemented to check that configuration of the spacecraft complies with predefined criteria evaluated within reference periods, either during thermal vacuum or mechanical tests.

Another algorithm has been developed to monitor nominal relay on-off transitions and ensure thermal groups validation. A third one has for objective to verify that all numerical and discrete TM and TC have been successfully tested on all functional chains, so as to demonstrate a proper TM/TC coverage and the end-to-end consistency with spacecraft hardware.

These algorithms can be scheduled to run automatically on a user-defined frequency, but it is also possible to launch them on demand, via a specific widget allowing the user to choose the right satellite, phase, time period, and other input parameters. As displayed in figure 5, this algorithm widget has been specifically designed to offer genericity and flexibility to the users, while keeping simplicity.

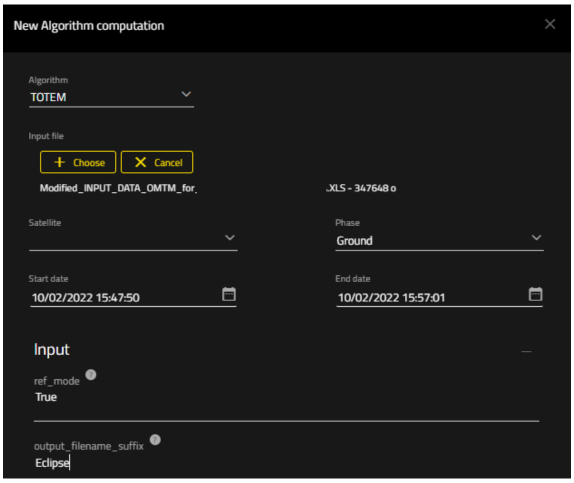

Fig. 5. OASIS Algorithm widget.

Through these various examples, it is shown that exploring and manipulating data is made easily accessible via such digital tools, which is key to ensure good execution and follow-up of spacecraft test phases.

OASIS next challenges: towards decision-making enablers

The OASIS system intends to offer Artificial Intelligence solutions as decision-support enablers. In the ADS ecosystem, possible application fields are numerous:

- In-flight or in-test satellite operators assistance for daily tasks and automated anomaly detection,

DOI 10.5162/ettc2022/7.5

- Automatic reconfiguration proposal in case of failure,
- Failure origin determination assistance for complex and multimodal systems,
- Reconfiguration proposal for complex and multimodal systems,
- Predictive maintenance
- etc.

To address these challenges, the OASIS solution takes advantages of two constituent components of the cloud platform: first, easy access to a large amount of different satellite data and second, easy access to suitable analytics tools.

Today, the supervised in-development, in-test or in-flight satellite fleet is composed of 55 satellites, ingesting continuously their flow of telemetry. Each day, 300 Gb of TM data are thus aggregated by the OASIS platform, and are made available for further analyses. The archived TM of about 20 satellites are also stored since beginning of life. This huge data volume is a strength for the development of AI algorithms, especially for the algorithm training phase.

As seen in previous chapters, OASIS data sources are multiple: real-time or archived, in-flight or on-ground satellite telemetry, manufacturing and test AsRun files, satellite identity cards, etc. All these kinds of data come from Telecommunication satellites, as well as Earth observation, Navigation and Science (ENS) ones. About 800 users can visualise, or even edit, these data, depending naturally on their access permissions. Some key figures on OASIS data are presented in figure 5.

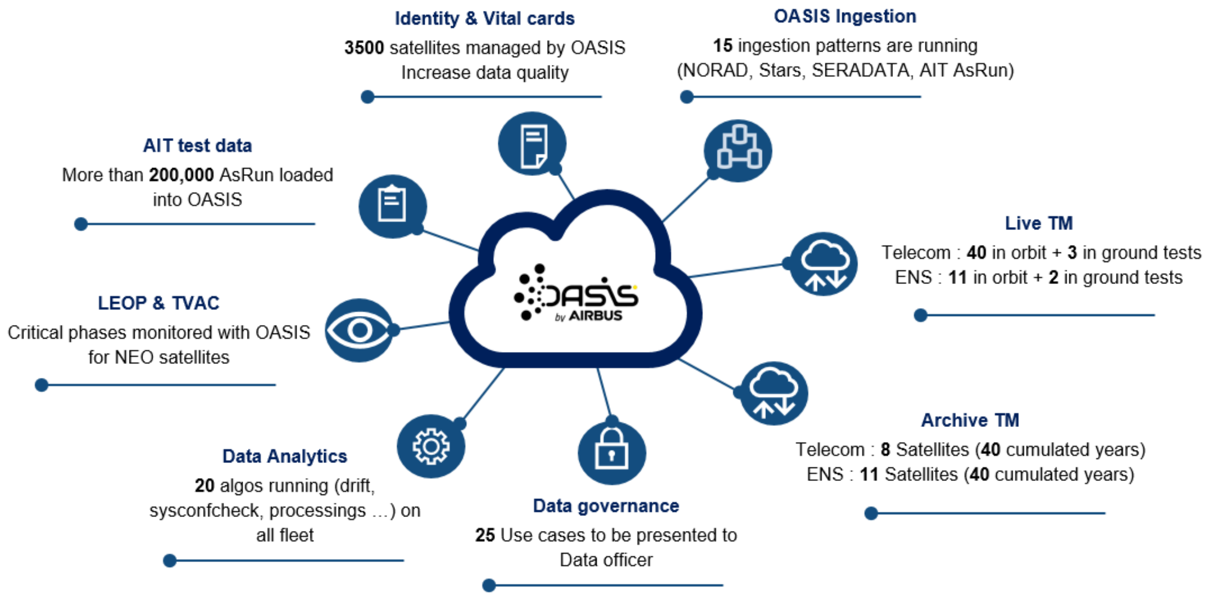

Fig. 5. Key figures on the data aggregated by the OASIS platform.

Despite their diversity, data are ingested, stored and organized the same way (database storage) and using the same technical solutions (InfluxDB for time series data, MongoDB for relational non-time series ones and Hadoop Distributed File System for unstructured and voluminous ones). Doing so, analytics studies can be conducted on every available data, independently of their nature or origin. This enables transversal analyses. An AI algorithm can indeed be developed, trained and validated on a large variety of satellite data, making links between different use cases. Furthermore, one algorithm solution developed in the frame of one particular use case can be easily adapted to another situation, assuming that associated data are available.

The OASIS platform is virtualized on a cloud environment, which offers the following advantages for analytics studies:

- Layer design approach: the OASIS platform architecture is built on a four layers pattern in order to isolate web user interface, data access, data processing and business logic. In that way, main functionalities and in particular analytics functions are independent and can be updated according to specific analytics needs.

DOI 10.5162/ettc2022/7.5

The four layers design approach is presented in figure 6.

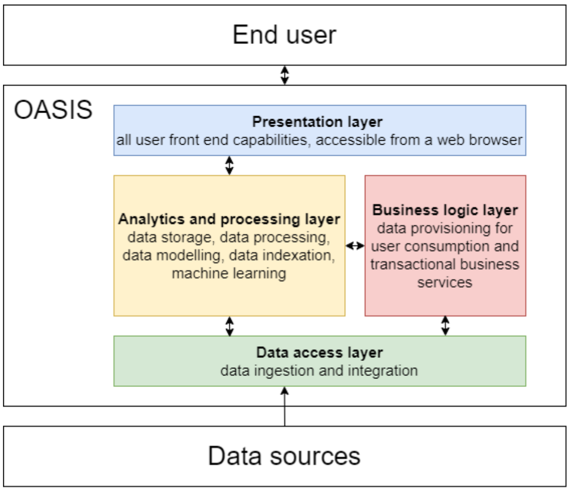

Fig. 6. OASIS high-level functional architecture.

- On-demand resources allocation: the cloud architecture offers the capacity to allocate the right resources amount to each service that is running on the platform, according to its effective needs. The resources allocation is done via Kubernetes resources management.
- Centralized security management: the four layers described above are supported by a set of basic and centralized support functions that ensure data security (through authentication management, data governance process) and data confidentiality.

Huge data amount availability and flexible cloud environment are two key enablers for the development of data-driven solutions on OASIS satellite data. One Airbus AIT use case can illustrate this statement.

For the test campaign of two new Airbus satellites, the OASIS data scientist team is asked to develop a novelty detection solution in order to automatically detect abnormal behaviours in telemetry test data. The ambition is to highlight upstream abnormal events during the test phases thanks to an exploratory methodology. The first version of the study focuses on satellite electrical and power subsystems. This detection intends to assist and complete manual anomaly detection operations, which are time-consuming and, above all, non-thorough.

A non-supervised study based on correlation analysis is performed. The anomaly identification is done without any a-priori on the data (unsupervised study), but using contextual data (i.e. relying on correlation analysis), so that found abnormal behaviours can be explained and, as a future improvement, further reinjected in the algorithm training process.

As in-service data linked to the two targeted satellites is not available on OASIS yet, the algorithm is experimented on substitution data from another similar Airbus satellite with the same avionics, on a few days of recorded telemetry.

After data cleaning, data that are relevant from a functional point of view are selected for the study. The correlation matrix between all TM and all contextual status is then computed. Data are classified (clustered) according to this matrix, and telemetries with similar behaviours are linked together. In that way, the established data groups (clusters) are correlated to known contextual status and can be further analysed. The different clusters are presented in figure 7.

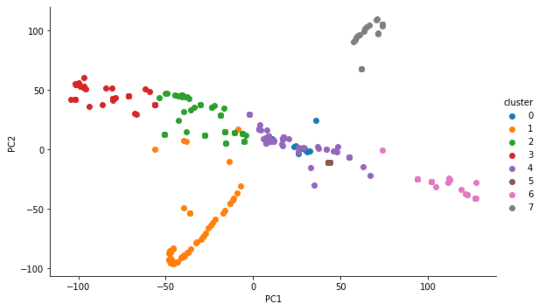

Fig. 7. TM clusters represented according to 2 Principal Components (PC) values.

For each cluster, a “break” detection is then conducted using unsupervised machine learning algorithms. Breaks are dates for which the TM behaviour significantly and abnormally changes. The algorithms give good results in detecting the breaks and in providing context allowing the user to identify their root causes, thanks to the clustering previous operation.

The main advantage of this unsupervised approach is its strong reusability: it can be applied to all TM regardless of the subsystem. An expertise analysis (supervised approach) is nevertheless needed in order to better identify breaks root causes. That is why an hybrid solution taking into account user feedback and strong contextualization is recommended for this AIT use case. This hybrid solution is still under development on the OASIS platform, and will be part of the next platform improvements.

DOI 10.5162/ettc2022/7.5

Conclusion

As digital transformation is becoming widespread in Airbus daily tasks, it is more and more needed to have the right tools to easily manipulate and visualize data, while benefitting from the precious value they can bring. OASIS has been designed to answer this purpose.

Throughout the whole satellite lifecycle, from satellite prospects to end of life, and going through ground tests, launch pad and in-orbit phases, hundreds of gigabytes are daily gathered in this centralized platform for a common objective: towards more and more automation and data-oriented decisions. Given storage, analytics, dashboarding, alerting and other capabilities, a large number of use cases have already proven their values, and in particular in tests and validation context.

One of the main assets of this big data platform is its generic and transverse capability, enabling to create synergies between the diverse business entities. But despite the generic aspect, OASIS also provides a wide range of customization possibilities, to perform automatic data processing and visualization dashboards suitable for each user need. Last but not least, all the infrastructure is relying on a fine-grained data segregation to ensure security requirements about data classification and sensitivity.

Nonetheless, there is still room for improvement, and that is why smart and hybrid approaches are being further studied to enhance AI predictions, while technical optimizations are conducted to improve performance. All this to answer the continuously growing data volume and help bringing data-driven solutions for the challenges of tomorrow.

Platform extension beyond Airbus Space Systems is one of these major challenges, as OASIS is being adapted to integrate Military Aircraft data, but it is also being sold to external customers, in particular as their new payload monitoring tool.

DOI 10.5162/ettc2022/8.1

Evaluation of Solar-based Energy Harvesting for Indoor IoT Applications

Leander B. Hörmann[1], Thomas Hölzl[1], Christian Kastl[1], Peter Priller[2], Hans-Peter Bernhard[3], Philipp Peterseil[4], Andreas Springer[4]
[1] Linz Center of Mechatronics GmbH, Altenberger Straße 69, 4040 Linz, Austria,
[2] AVL List GmbH, 8020 Graz, Hans-List-Platz 1, Austria,
[3] Silicon Austria Labs GmbH, Altenberger Straße 69, 4040 Linz, Austria,
[4] Institute for Communications Engineering and RF-Systems, Johannes Kepler University Linz, Altenberger Straße 69, Austria, 4040 Linz
Leander.Hoermann@lcm.at

Abstract:
Internet-of-Things (IoT) devices and other embedded devices are more and more used to measure different conditions inside of buildings and industrial facilities as well as to monitoring machines or industrial processes. IoT sensors communicate wirelessly and are typically supplied by batteries. Energy harvesting can be used to extend their operational time or enable self-sufficient supply of them. Energy from the environment is converted into electrical energy by energy harvesting devices (EHDs), for example solar cells or thermo-generators. However, the available output power of the EHDs is highly dependent on the mounting location as well as on environmental conditions and may vary greatly over time. Therefore, it is meaningful to evaluate the EHDs at the location of use over a certain period of time in order to characterize them in real world scenarios. This paper presents the evaluation setup and the results of the characterization of four different solar cells at different locations in an office building and at different weather conditions. Furthermore, a method is presented to estimate the possibility to supply embedded device using energy harvesting. The results can be used to simplify the selection of a suitable EHD and the design process of an energy management system. The method is applied on two different use cases to estimate the needed size of the solar cells to enable a continuous supply.

Key words: Internet-of-Things, wireless communication, energy harvesting, self-sufficient.

Introduction

In the last years, Internet-of-Things (IoT) spreads rapidly and reached more and more new application areas. The advances in ultra-low power electronics and wireless communication are key enabling technologies for this development. The IoT connects wireless embedded devices to the internet. Such devices could be sensors or actuators and application areas reach from smart buildings and home automation over smart farming to industrial application where they are often referred as industrial IoT (IIoT). Especially, sensors are predestinated to be implemented as IoT or IIoT devices since a lot of them could be used to monitor the surrounding inside a smart building or industrial machines and processes. They are than often called “sensor nodes”, measure physical quantities, and transmit them wirelessly towards a gateway using a certain communication protocol [1], [2]. These sensor nodes should be powered without a wired connection to reduce cost, enhance the flexibility and handling, enable an easy encapsulation for e.g., water tightness, and to reach application areas where cabling is not possible. Thus, they can be powered in two different ways, by batteries and by energy harvesting [3]. Using batteries, the needed energy is supplied with the installation of the sensor nodes and operational time is limited but guaranteed. In this paper, we focus on the second possibility. Using energy harvesting devices (EHDs), the needed power to supply the sensor nodes is converted from power available in the environment, e.g., solar or artificial light or temperature gradients. By using energy harvesting, the theoretical operational time of the embedded devices is not limited. However, the harvestable electrical power of the environment is highly variable [4], [5]. Therefore, an energy storage is needed to provide a continuous supply of the wireless sensor node, e.g., rechargeable batteries or supercapacitors. If the capacity is well dimensioned, a perpetual operation is achievable [6].

Illumination-based environmental power sources are typically available in office buildings and factories since they are regularly used by humans. Natural sunlight is available on a daily base but

DOI 10.5162/ettc2022/8.1

varies with weather and season. Artificial light is available only during the regular working time which is often on a weekly base. Furthermore, the convertible power depends also on the location inside a building. To characterize the convertible power of EHDs directly on location over a certain period of time, we have developed a characterization instrument which we have presented in [7] and evaluated in [8]. This paper presents the results of measurement campaign for indoor scenarios focusing on solar-based energy harvesting at different locations. These results can be used to estimate the available energy for different application scenarios.

The rest of the paper is organized as follows: First, this paper gives an overview of the measurement system, second, it describes the measurement campaign including the location dependent and the time dependent evaluation, and third, it discusses the applicability of the measurement results on two different use cases. Finally, it concludes the paper and outlines directions for future work.

Measurement System for the Characterization of Energy Harvesting Devices

The measurement system is designed to characterize EHDs automatically and autonomously. Thus, it can be used to characterize EHDs directly on site. The characterization is based on a cyclic acquisition of the current-voltage characteristics of the connected EHDs. The measurement interval and the number of measurement points to be recorded can be configured. The characterization results are transmitted wirelessly towards a base station using a mesh network. The autonomous measurement device is shown in Fig. 1.

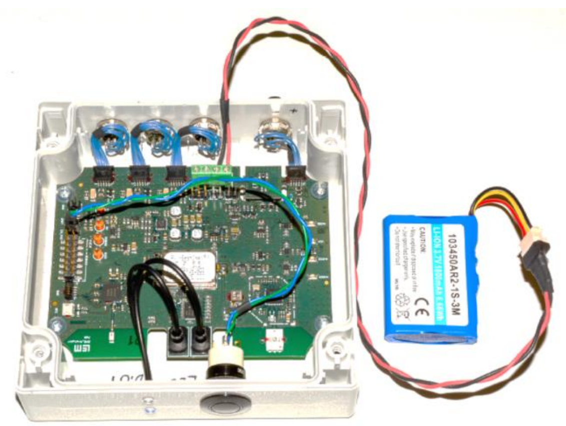

Fig. 1: Autonomous characterization instrument for energy harvesting devices.

The main parts of the measurement device are the nRF52840 system-on-chip containing a microcontroller and a transceiver circuitry for wireless communication, a power supply circuitry including the Lithium-Ion rechargeable battery, and the measurement circuitry. The measurement circuitry characterizes the EHDs using a variable load for setting different operating points. The voltage for each operating point is set by the microcontroller and a digital-to-analog converter. The resulting voltages and currents at the EHD are measured using an analog-to-digital converter. The supported voltage ranges from below 1 mV up to 24 V in two measurement ranges. The supported current ranges from below 1 µA up to 1 A in three measurement ranges which are automatically selected using an analog comparator circuit. A detailed analysis of the mode of operation and achieved accuracies is given in [8].

Measurement Campaign

The measurement campaign was performed inside an office building in Linz, Austria with the coordinates N 48.335902 and E 14.322516. The campaign consists of different short-term measurements at different location in two different rooms (one south aligned, and one north aligned) and on different days in the summer (between 22nd and 26th of July 2021) with different weather conditions (sunny and foggy days). A rough ground floor plan of the relevant part of the office building including the two rooms are shown in Fig. 2.

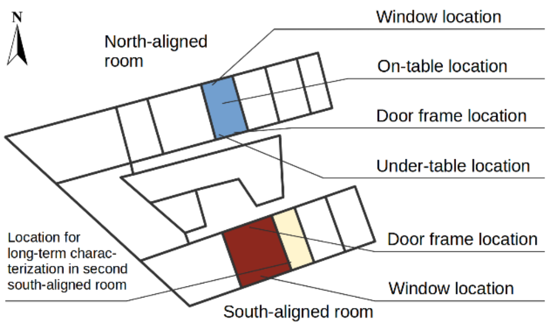

Fig. 2: Floor plan of the relevant part of the building showing the orientation of the rooms and indicating the locations of the measurements.

At all locations, four different solar cells have been evaluated: YH-46x76 from Conrad components with an active area of 11.78 cm² [9], YH-57x65 from Conrad components with an active area of 30.87 cm² [10], SM141K10LV from IXYS with an active area of 16.2 cm² [11], and SM141K09L from IXYS with an active area of 14.49 cm² [12]. Due to insufficient output power at locations with bad illumination conditions, not all solar cells could be characterized at all locations and at all weather conditions. The results are shown in the following section.

Location Dependent Evaluation

The location dependent evaluation was performed at two different locations at the south aligned room and at four different locations at the north aligned room. Fig. 3 shows the power density of the solar cells placed directly on the window facing outwards at the south aligned room.

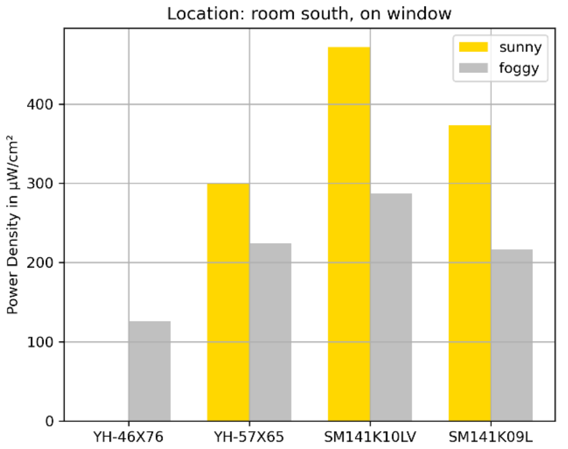

Fig. 3: Power density of the solar cells placed on the window at the south aligned room.

Fig. 4 shows the power density of the solar cells placed on the doorframe on the opposite side of the windows facing to the windows at the south aligned room.

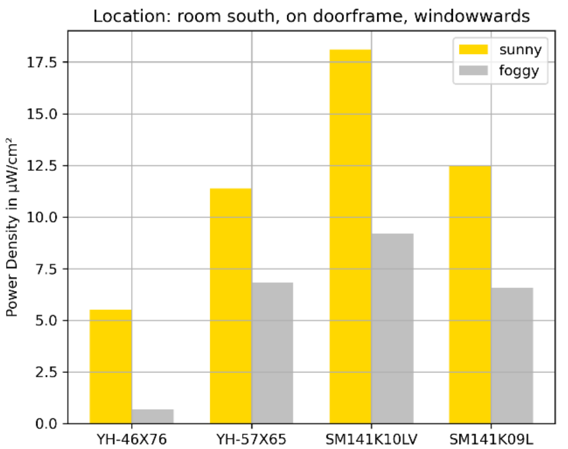

Fig. 4: Power density of the solar cells placed on the doorframe at the south aligned room.

Fig. 5 shows the power density of the solar cells placed directly on the window facing out-wards at the north aligned room.

Fig. 6 shows the power density of the solar cells placed on the doorframe on the opposite side of the windows facing to the windows at the north aligned room.

Fig. 7 shows the power density of the solar cells placed on a table in the middle of the north aligned room facing upwards.

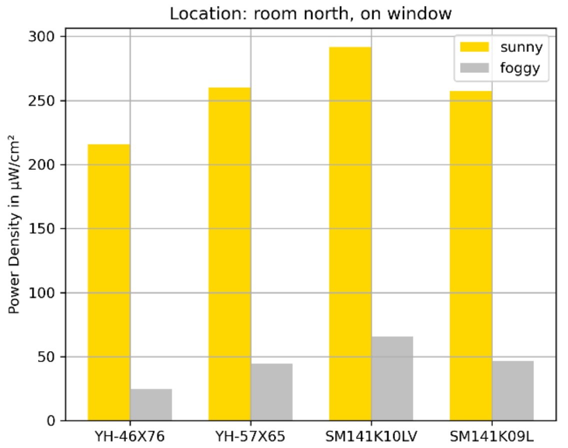

Fig. 5: Power density of the solar cells placed on the window at the north aligned room.

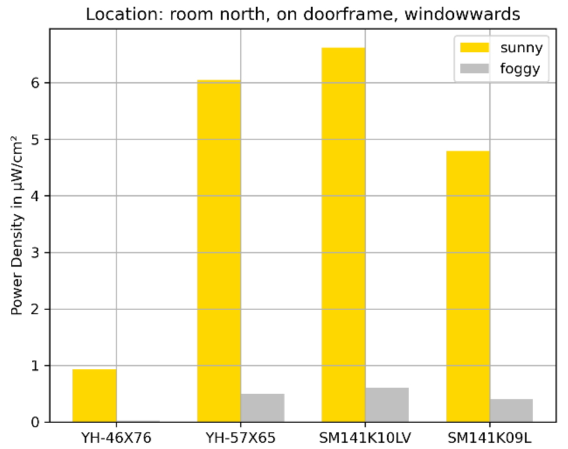

Fig. 6: Power density of the solar cells placed on the doorframe at the north aligned room.

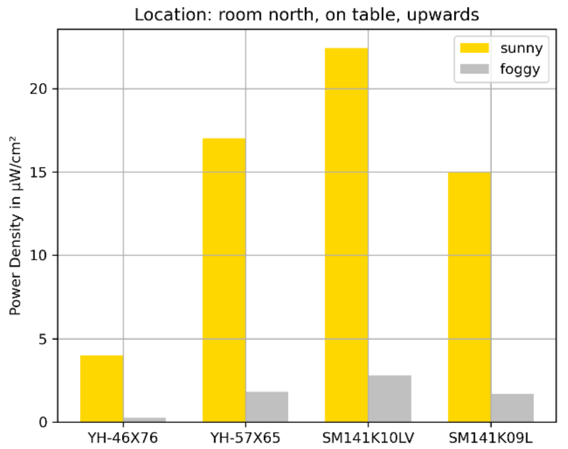

Fig. 7: Power density of the solar cells placed on a table in the middle of the north aligned room.

Fig. 8 shows the power density of the solar cells placed on the floor under a table on the opposite side of the windows of the north aligned room facing upwards. A measurement at foggy conditions was not possible due to insufficient power output of the solar cells.

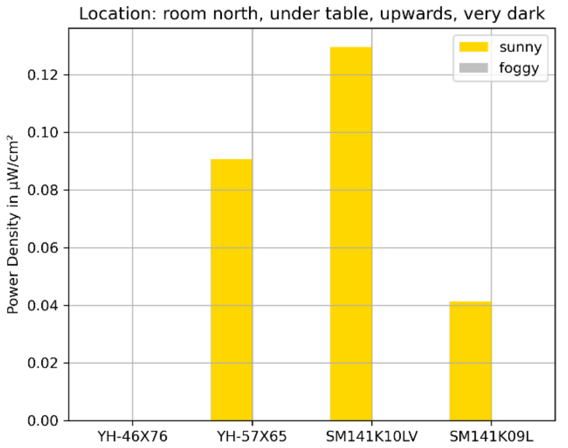

Fig. 8: Power density of the solar cells placed under a table in the north aligned room.

The results are summarized for the best performing solar cell (SM141K10LV) and compared in Tab. 1. The given percentage refers to the maximum achievable power (obviously at the window) for each room. It depends mainly on the geometry, the window placement, and the interior of the room. There is a big difference between the best placement for energy harvesting at the window and the opposite side of the room with a factor of 26.1 to 44.1. At very dark locations (e.g., in a dark corner under the table), the power density is again significantly reduced by a factor of 50.9 compared to the location at the doorframe resulting in a total factor of 2245 compared to the optimal window location. This factor can be seen as a location dependent inter-room factor.

Tab. 1: Power density of the best performing solar cell SM141K10LV at different locations.

Location	Power density in µW/cm²	Percentage referring to maximum in room
South, window	472.04	100 %
South, doorframe	18.11	3.84 %
North, window	291.85	100 %
North, doorframe	6.62	2.27 %
North, on table	22.44	7.69 %
North, under table	0.13	0.045 %

Time Dependent Evaluation

The time dependent evaluation focuses on the determination of the daily change of harvestable power and total harvestable energy over a day. Therefore, the solar cell AM-1815CA from Sanyo with an active area of 26.22 cm² [13] is placed at the wall beside the window (on the side wall of the room) of the south aligned room. Fig. 9 shows the harvestable power of the solar cell during a sunny day (13th of April 2022, 12.2 hours of sun). During this day, the harvestable energy sums up to 45.24 J which corresponds to an average harvestable power of 523.6 µW or 19.97 µW/cm².

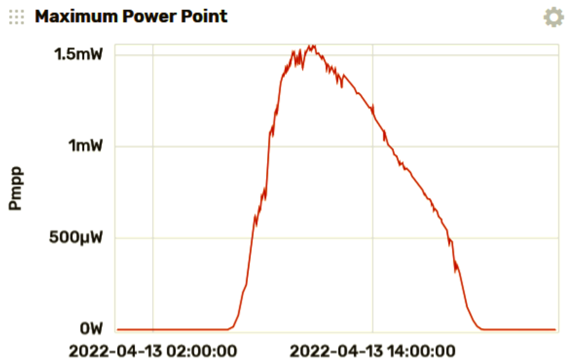

Fig. 9: Harvestable power of the solar cell AM-1815CA over a sunny day.

Fig. 10 shows the harvestable power of the same solar cell during a day without sun (22nd of April 2022, 0 hours of sun). During this day, the harvestable energy sums up to 18.75 J which corresponds to an average harvestable power of 278.25 µW or 10.61 µW/cm². This results in a weather dependent factor of 41.4 % compared to sunny weather conditions. However, the measurement period must be extended to a whole year and a detailed analysis regarding the seasonal weather variations has to be done.

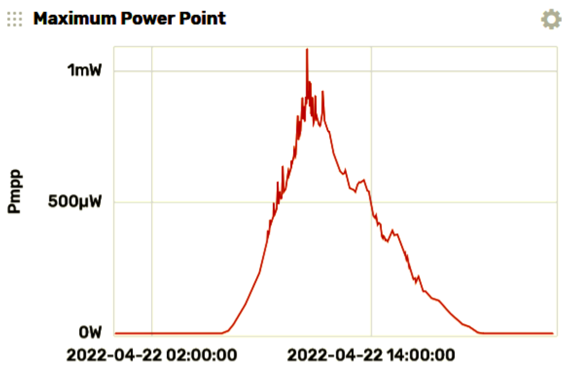

Fig. 10: Harvestable power of the solar cell AM-1815CA over day without sun.

Fig. 11 shows the harvestable power of the solar cell during a 13-day period with different weather conditions (from 12th to 24th of April 2022). During this period, the harvestable energy sums up to 422.18 J which corresponds to an average harvestable power of 375.9 µW or 14.34 µW/cm². It can be seen that the weather dependent variation is orders of magnitude smaller than the location dependent variation inside a room. From previous measurements with a different measurement hardware presented in [3] the seasonal dependent factor ranges approximately from 16.7% to 26.7% between sunny weather condition in summer and winter.

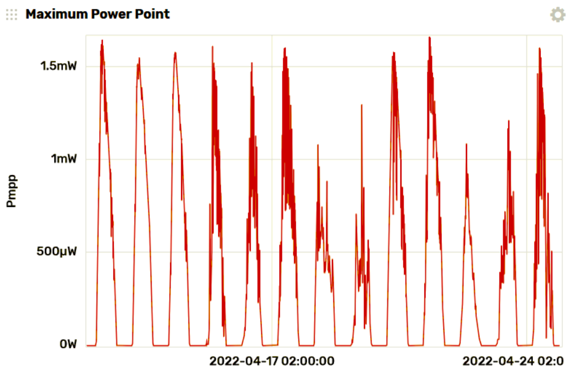

Fig. 11: Harvestable power of the solar cell AM-1815CA during a 13-day period (from 12th to 24th of April 2022).

Supply Possibility Analysis by Means of Energy Harvesting

To analyze the possibility to supply an embedded device using energy harvesting, the following information must be known as also presented in [14]: the trace of the harvestable power P_{EH}, the trace of the consumed power of the embedded device P_{SUP}, the capacity of the energy storage device in terms of energy $E_{BAT,max}$, and the amount of energy stored in the energy storage device $E_{BAT,0}$ at time step $n=0$. Starting from time step $n=1$, the energy stored in the energy storage device for the next time step $E_{BAT,n}$ is calculated. For this purpose, the stored energy of the last time step $E_{BAT,n-1}$, the measured input power in this time step $P_{EH,n}$ and the expected output power in this time step $P_{SUP,n}$ are taken into account as shown in (1).

$$E_n = E_{BAT,n-1} + \left(P_{EH,n} \cdot \eta - P_{SUP,n}\right) \cdot \Delta t \quad (1)$$

The factor η describes the efficiency of the energy harvesting circuit since losses occur during the DC-DC conversion and storage of the electrical energy. Furthermore, the calculated energy must be limited to the maximum capacity of the energy storage $E_{BAT,max}$ as shown in (2).

$$E_{BAT,n} = \min\left[E_{BAT,max}\ ,\ E_n\right] \quad (2)$$

For each time step $n > 0$ this energy must be greater than 0 as shown in (3).

$$E_{BAT,n} > 0 \qquad for\ n = 1,2,\ldots \quad (3)$$

Not considered here is the self-discharge of the energy storage device. The energy stored in the energy storage device is calculated iteratively for each time step n. If the calculated energy is greater than 0, then continuous operation till this time step n is possible.

Based on equation (1), it can be seen that if the second term is greater zero, the energy stored in the energy storage device will never run out of energy and a perpetual operation is possible. Simplifying this by using the average harvestable power $P_{EH,avg}$ and the average consumed power $P_{SUP,avg}$, and considering enough energy storage capacity, it can be reduced to the equation shown in (4).

$$P_{EH,avg} \cdot \eta > P_{SUP,avg} \quad (4)$$

Use Case Automotive Testing

Academic and industrial research have demonstrated the benefits of using IoT in industrial applications [15] [16]. Use cases in mobility, industrial, and smart city domains, for example, clearly benefit from wireless connectivity, which allows dynamic placement, saves cost and weight of cables, and often allows even tighter integration into components.

Automotive test factories provide good examples for a particularly worthwhile, but also challenging use case, and have been studied in more detail in [2]. Such facilities are widely used across the automotive industry for research, development and quality control accompanying production. Test factories for batteries in electrical vehicles, for example, are used to explore the relevant properties of battery cells, modules, or racks, in order to improve and validate their design. Powertrain test beds allow to analyze engines (E-Motor or ICE) and transmissions to study and improve efficiency, performance, vibration (comfort), degradation patterns, and aging. Other examples include full vehicle testbeds to develop advanced driving assistance systems (ADAS) and automated driving functionalities (AD), or component test beds used for example to optimize the thermal system in a vehicle.

These use cases typically deploy a wide range of sensors, which need to be placed on, or even integrated into the systems under test (SUT). Using wireless sensor networks (WSNs) to instrument SUTs has demonstrated clear cost advantages due to a significant reduction of the time required for installation and configuration. In addition, typical sources of failures, like poor connectors or miswiring issues, are eliminated, further contributing to improved productivity in test fields operations.

A critical part however is adequate energy supply of the nodes. The desired operational time of an IoT node might vary from hours to weeks. Some test sequences allow the node to power down between phases. Others require continuous 24x7 operation, resulting for example in 720 hours runtime per month. Some current solutions rely on batteries to power nodes locally; in combination with highly energy-efficient communication protocols and ultra-low power hardware design, batteries provide sufficient operating time for a subset of scenarios. Energy supply must be ensured for the full time an SUT is deployed in the test scenario, as power failure would likely lead to a loss of experimental data, rendering the whole test worthless. A change of batteries is often impossible due to operational needs. The promise of continuous energy supply for nodes using EHDs is therefore highly welcome. Many test cells are typically well-lit laboratory environments, with levels of luminous intensity comparable with or even exceeding typical indoor office conditions.

However, it is necessary that the IoT nodes are based on ultra-low power electronics and are wirelessly connected using an energy efficient communication protocol. In [2] we have introduced an Energy and Power Efficient SynchrOnous wireless Sensor network (EPHESOS) protocol. This protocol is especially designed for wireless sensor networks requiring on average low power and at the same time defined latency. Low power consumption is achieved by using a time division multiple access (TDMA) protocol which enables tightly synchronized wireless sensor nodes. Thus, the transmission and reception times with powered transceiver circuitry of each individual sensor nodes can be minimized. The TDMA structure is based on a frame called superframe (SF) with pre-allocated time slots for each sensor node to transmit sensor data and one time slot used by the base station addressed as wireless network processor (WNP) to transmit a beacon to all sensor nodes. This beacon time slot is one timeslot per SF in which the sensor nodes are receiving data synchronously. The individual sensor node time slots are used for transmitting sensor data. The nodes remain in sleep mode whenever they are not receiving or transmitting. The communication protocol supports two different modes, which are briefly explained below: First, the sporadic transmission mode, EPhESOS-S, is responsible for network commissioning, integration of new nodes, initial synchronization, node configuration and maintenance. Second, the continuous transmission mode, EPhESOS-C, is used to transmit measurement data from the nodes towards the WNP in their own time slots. If a packet is lost, the incorrectly received or missing value is added to the next packet and sent again in the following SF.

We have designed and implemented wireless sensor nodes based on an nRF52840 system-on-chip (SoC) which integrates a processing unit and a wireless transceiver for 2.4 GHz radio frequency (RF) communication. It uses the EPhESOS communication protocol for wireless communication. Furthermore, the sensor node contains an analogue-to-digital converter with an associated analogue circuit. The analogue circuitry is designed to support Pt100, Pt1000 and thermocouple temperature sensors as described in [17]. Fig. 12 shows the average power consumption of the wireless sensor node at different measurement modes and temperatures.

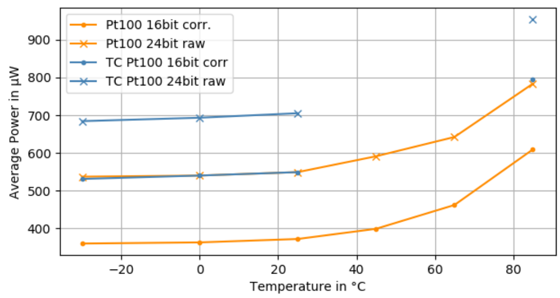

Fig. 12: Average power consumption of the wireless sensor node at different measurements modes and different temperatures.

For a further estimation of the ability to supply the wireless sensor node using energy harvesting, we will use the average power consumption of the measurement mode “Pt100 24bit raw” at 25°C which is 549 µW. In this mode, a Pt100 sensor is sampled with 10 Hz and the results are transmitted with 1 Hz. Considering further a supply a table conditions in a south-aligned room. The average harvestable power can be estimated by multiplying the optimal harvestable power density in this room ($S_{EH,opt}$ = 472.04 µW/cm²) with the location dependent factor (f_{Loc} = 0.0769) and the weather dependent factor ($f_{Weather}$ = 0.414) as shown in (5). Since the measured harvestable power is given per square centimeter, it is a power density and the symbol *S* will be used instead of the symbol *P*.

$$S_{EH} = S_{EH,opt} \cdot f_{Loc} \cdot f_{Weather} = 15.03\ \frac{\mu W}{cm^2} \quad (5)$$

Considering an energy conversion efficiency of η = 80% and an operation only during daytime, the needed solar cell area is calculated as in (6).

$$A_{Solar} = \frac{P_{SUP,avg}}{S_{EH} \cdot \eta} = 45.7 cm^2 \quad (6)$$

The resulting area is not that small but can be reduced by reducing the sample frequency or enhancing the illumination conditions. However, this result shows, that under reasonable conditions the power supply of a wireless sensor node can solely rely on energy harvesting based on solar cells.

DOI 10.5162/ettc2022/8.1

Use Case User Tracking and Access Authentication

Localization and tracking of persons and assets are services with a huge application potential. Localization systems based on radar or LIDAR (Light detection and ranging) demand large amounts of power, are usually costly, but have a high localization precision. If precision in the millimeter-range is not required, low-power and low-cost wireless localization systems, usually based on Time of flight (ToF), are preferred. During the last years, Ultra-Wideband (UWB) devices have been adopted in many localization systems due to their relatively high ranging precision and low cost. The high bandwidth of UWB enables time of flight measurements with high resolution [18] and thus makes high precision indoor localization possible. UWB impulse radio (IR) enables the implementation of low complexity and low-power transceivers, which translates into low-cost devices.

For access authentication of users, one wants to combine conventional user authentication by means of a cryptographic method with the location of the user. E.g. a cryptographically authenticated user is only granted access to a restricted area if the user in within a certain area to prevent relaying attacks. UWB IRs can be applied here also, because with their ranging capabilities so-called distance bounding (DB) protocols can be executed. DB protocols are employed such that a verifier node (V) can authenticate a prover node (P) with cryptographic methods and at the same time ensure that P is close enough to V by setting an upper bound to its distance to the verifier [19].

We have developed wireless sensor nodes (Fig. 13) based on the DWM1001C UWB-module (1.) which consists of a Bluetooth Low Energy (BLE) capable Nordic nRF52832 microcontroller, a Qorvo DW1000 UWB transceiver and antennas for both standards.

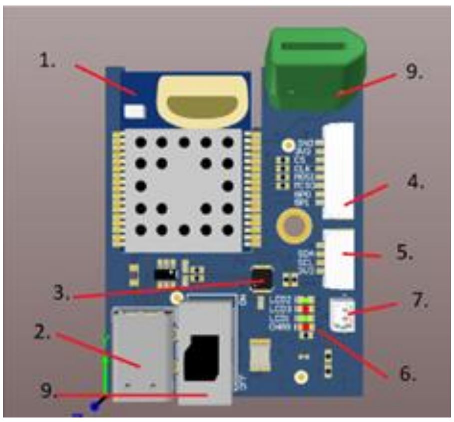

Fig. 13: Wireless sensor node.

Our sensor nodes provide the supply voltage via USB-C (2.) as well as a virtual COM-port (VCP) interface (3.). The extension connectors (4.) and (5.) allow to connect external peripherals via I²C and SPI. With these wireless sensor nodes, UWB-based ranging and DB protocols can be executed and in addition data can be transmitted to base stations or other nodes via BLE. To figure out if a wireless localization and tracking system can be operated solely based on energy harvesting, we performed power measurements. To this end we conducted so-called double-sided two-way ranging (DS-TWR) rounds between two nodes. In an operational localization system, one node would be an anchor, i.e. a node with known position, and the other node would be the tag, which the systems wants to localize by performing ranging with a set of anchors. In a DS-TWR round, the tag transmits a short packet, receives the answer from the anchor, and transmits again. From the two received packets, the anchor estimates the distance and transmits the result back to the tag. In our implementation, such a DS-TWR round has a duration of 11.15 ms and consumes 3.22 mWs of energy at the tag if operated at 3 V. Most energy is consumed during the reception mode of the tag with an average power consumption of approx. 450 mW for 3.5 ms. According to the data sheet of the DWM1001C module [20], the minimum achievable current consumption in the sleep mode is only 12 µA which will be used in further estimation. However, one needs to consider, that both, our design of the node and also the firmware which implements the DS-TWR procedure is currently not optimized for low power. By triggering this procedure using the integrated accelerometer, the average ranging frequency can be reduced and thus, also the power consumption. We will use here the same assumption about the location as at the previous use case and use the power density S_{EH} = 15.03 µW/cm². By assuming a full DS-TWR round every 30 seconds to four anchor nodes, the average power consumption is 465.28 µW. Considering an energy conversion efficiency of η = 80% and an operation only during day, the needed solar cell area is calculated as shown in (7).

$$A_{Solar} = \frac{P_{SUP,avg}}{S_{EH} \cdot \eta} = 38.7 cm^2 \qquad (7)$$

Considering, that neither node hardware nor DS-TWR protocol is optimized for low-power operation, this result clearly shows that under reasonable conditions the power supply of a tag of a UWB-based localization system can solely rely on energy harvesting based on solar cells.

Conclusion

This paper presented the evaluation of four different solar cells as energy harvesting devices in a real-world environment at different locations in two different rooms of an office building. The results can be used to estimate the location-based influence on the harvestable energy. Furthermore, an evaluation of several days at one specific location has been used to estimate the weather-based influence on the harvestable energy. The paper also presented a methodology to analyze the possibility to supply embedded devices using energy harvesting systems. This methodology has been used to estimate the needed solar cell size for a continuous supply using energy harvesting at two different use cases. Future work will target the evaluation of further locations focusing also on industrial facilities and the long-term evaluation of energy harvesting devices.

Acknowledgement

This work has been supported in part by the COMET-K2 Center of the Linz Center of Mechatronics (LCM) funded by the Austrian federal government and the federal state of Upper Austria, and the InSecTT project. InSecTT (www.insectt.eu) has received funding from the ECSEL Joint Undertaking (JU) under grant agreement No 876038. The JU receives support from the European Union's Horizon 2020 research and innovation programme and Austria, Sweden, Spain, Italy, France, Portugal, Ireland, Finland, Slovenia, Poland, Netherlands, Turkey. The document reflects only the author's view and the Commission is not responsible for any use that may be made of the information it contains.

References

[1] M. Bal, Industrial applications of collaborative wireless sensor networks: A survey, 2014 IEEE 23rd International Symposium on Industrial Electronics (ISIE), June 2014, pp. 1463–1468; doi: 10.1109/ISIE.2014.6864830

[2] H.-P. Bernhard, A. Springer, A. Berger, and P. Priller, "Life cycle of wireless sensor nodes in industrial environments," in 13th IEEE Int. Workshop Factory Commun. Sys., Trondheim, Nor-way, May 2017; doi: 10.1109/WFCS.2017.7991943

[3] L. B. Hörmann, T. Buchegger, and C. Steger, Optimizing the Energy Supply of Autonomous Wireless Sensor Nodes, Microelectronic Systems Symposium (MESS 2014), 2014, pp. 1–6; doi: 10.1109/MESS.2014.7010257

[4] A. Janek, C. Trummer, C. Steger, R. Weiss, J. Preishuber-Pfluegl, and M. Pistauer, Simulation based Verification of Energy Storage Architectures for Higher Class Tags Supported by Energy Harvesting Devices, 10th Euromicro Conference on Digital System Design Architectures, Methods and Tools (DSD 2007), Lubeck, 2007, pp. 463-462.; doi: 10.1109/DSD.2007.4341510

[5] L.B. Hörmann, A. Berger, A. Pötsch, P. Priller, and A. Springer, "Estimation of the harvestable power on wireless sensor nodes," IEEE International Workshop on Measurements and Networking (MN 2015), 2015, 1-6; doi: 0.1109/IWMN.2015.7322964

[6] A. Kansal, D. Potter, and M. B. Srivastava, "Performance Aware Tasking for Environmentally Powered Sensor Networks", Proceedings of the joint international conference on Measurement and modeling of computer systems, ser. SIGMETRICS '04/Performance '04, 2004, pp. 223–234; doi: 10.1145/1005686

[7] T. Hölzl, "Drahtloses Messsystem für die Charakterisierung von Energy Harvesting Devices," master thesis, Institute for Communications Engineering and RF-Systems, Johannes Kepler University Linz, Austria, 2019.

[8] L. B. Hörmann, T. Hölzl, C. Kastl, P. Priller, and A. Springer, "Evaluation of Energy Harvesting Devices for Industrial Applications", Proceedings of the European Test and Telemetry Conference 2020 (ettc2020), 2020, pp. 31-37, doi: 10.5162/ettc2020/1.2

[9] Conrad Components SE, "Data Sheet – Solar cell 0.5V/400mA", Version 02/08, Item no. 19 12 81, https://asset.conrad.com/media10/add/160267 /c1/-/gl/000191281DS01/datasheet-191281-conrad-components-yh-46x76-solar-panel.pdf, retrieved April 2022.

[10] Conrad Components SE, "Product Specification – Solar Cell Module Type YH-57X65", https://asset.conrad.com/media10/add/160267/c1/-/en/000 191321DS01/datasheet-191321-conrad-compone nts-yh-57x65-solar-panel.pdf, retrieved April 2022.

[11] IXYS KOREA LTD, "SM141K10LV – IXOLAR™ High Efficiency SolarMD", Rev. Sep. 2018, https://ixapps.ixys.com/DataSheet/SM141K10LV. pdf, retrieved April 2022.

[12] IXYS KOREA LTD, "SM141K09L – IXOLAR™ High Efficiency SolarMD", Rev. Sep. 2018, https://ixapps.ixys.com/DataSheet/SM141K09L.p df, retrieved April 2022.

[13] SANYO Semiconductor Co., Ltd., "Amorphous Silicon Solar Cells / Amorphous Photosensors", Version 2007-11, https://media.digikey.com/pdf/Data%20Sheets/Sanyo%20Energy/Amorphous_Br.pdf, retrieved April 2022.

[14] L.B. Hörmann, T. Hölzl, C. Kastl, P. Priller, A. Springer, "Methode zur Evaluierung der Versorgungssicherheit von autarken Sensorknoten für industrielle Anwendungen", Automation 2020: Shaping Automation for our Future, VDI Verlag GmbH, 2020, doi: 10.51202/9783181023754

[15] Dependable Wireless Infrastructure, European Research project 2013-2017, http://www.dewiproject.eu

[16] Secure, connected and trustable things, European Research project 2017-2020, https://scottproject.eu/

[17] L. B. Hörmann, T. Hölzl, P. Priller, W. Neuwirth, H.-P. Bernhard, A. Springer, “Autarke Sensorknoten für industrielle IoT Anwendungen mit Multi-Sensor-Unterstützung,” in Innovation Messtechnik 2019, Linz, Austria, May 2019.

[18] S. Gezici, Z. Tian, G. Giannakis, H. Kobayashi, A. Molisch, H. Poor, and Z. Sahinoglu, “Localization via ultra-wideband radios: A look at positioning aspects for future sensor networks,” IEEE Signal Processing Magazine, vol. 22, pp. 70–84, 08 2005

[19] G. Avoine, M. Bingol, I. Boureanu, S. Capkun, G. Hancke, S. Kardas, C. Kim, C. Lauradoux, B. Martin, J. Munilla, et al., “Security of distance-bounding: A survey,” ACM Computing Surveys, 2017

[20] QUORVO, “DWM1001 Data Sheet”, https://www.decawave.com/dwm1001/datasheet/, retrieved April 2022

DOI 10.5162/ettc2022/8.2

Simplified and reliable channel modeling for Aerospace, Defence and 5G

Karen von Hünerbein,
Lange-Electronic GmbH, Germany

Abstract:
Currently, a lot of new, high performance communication radio links are being developed and implemented. In the military and in safety-critical missions mesh radios are used in the VHF and UHF region. In the civilian domain new mobile phone frequencies and transmission technology are being developed such as 5 G, which is going to be used in safety critical applications such as autonomous driving. These safety critical applications require new and better test approaches, than have been available so far. In addition, there are more and more satellite communication links for ground-satellite and satellite ground communication. Creating a robust RF test plan for tactical and other mission critical radio systems requires specialized techniques. The standard RF channel modeling used in typical cellular and Wi-Fi tests can fall short. Mission critical devices encounter higher Doppler, lower frequency ranges, multiple device-to-device paths and other challenges that make standard channel models and test approaches unsuitable. This paper will examine the unique aspects of tactical and other mission critical mesh radio systems and their impacts on propagation.

Key words: satellite communication, 5G, channel modeling, fading

Introduction

In recent years, there has been more and more communication traffic wirelessly transmitted on different Radio Frequency bands. Both the number of services and the data volume have increased. Mobile phone usage and diversity of apps have exploded, and new technologies are being developed all the time both in the military and in the civilian domain. More and more small satellites are being launched to Low Earth Orbit LEO, contributing to an ever increasing RF communication data stream from ground-to-satellite and from satellite-to-ground. In the satellite case challenges are high Doppler shifts due to high velocity of satellites and sometimes significant signal delays due to long distance of signal propagation. In the military domain, lower RF frequencies are used in mesh networks, to enable communication between multiple participants on the ground, from ground-to-flight, and from coast to marine vessels and back. Challenges are safety and robustness, interference mitigation and obscuration, e.g. when using hand-held radios in uneven terrain, behind rocks and in forests, or near buildings.

Nowadays the military is also looking at 5-G in C5ISR Command, Control, Computers, Communication, Cyber, Intelligence, Surveillance, Reconnaissance, Systems, for discovering, selecting, organizing, filtering and sharing information to achieve ultimate situational awareness during field operations.

In summary, this means, that data transmission via radio channels at different frequencies and especially at 5G is becoming increasingly important, and in many cases human lives depend on it. Thus, it needs to be robust and reliable for safe, secure and trustworthy operations and data transmission. This can be ensured and improved with proper testing before deployment in the field.

Radio Channels

Signal propagation takes place between the transmitter and the receiver over the air or over parts of space outside the atmosphere and the air and thus always needs to cross the atmosphere. On its path, it is subject to many atmospheric effects and disturbing factors, that will impact and attenuate the signals. “The signal propagation over the radio channel is affected by free-space loss, ionosphere, troposphere, fading, multi-path, shadowing and interference” [2]. In the atmosphere, radio signals will be delayed, attenuated and phase-shifted, e.g. by charged ions in the ionosphere [1,2]. Distance plays a major role, as “every doubling of the distance cuts the received power by a factor of four”. [3] Radio signals can and will interact with each other, resulting in constructive and destructive interference, and sometimes create signal energy at frequencies other than the original frequency, leading to new peaks in other bands, different from the original transmission frequencies. “Sources on different frequencies could be creating harmonics or spurious noise that appear in our band”[3] Such effects are called intermodulation effects.[7] Anything in the environment can cause reflections. The reflections “typically arrive with different delays and power levels and from various angles of arrival. Even in the simplest case, where we have an unobstructed line of sight, there are still ground reflections that arrive at the receiving antenna in-phase or out-of-phase with the primary signal and thereby cause higher or lower received power levels. Some obstructions may block signals entirely, while others may partially absorb RF energy. Barriers, such as structures, weapon systems and armored vehicles have a wide variety of reflectivity and absorption characteristics, which may also vary considerably depending on frequency” [3].

RF Signals can and will also be affected by Interference and noise. There are many different potential sources. Another radio system may be operating on a nearby frequency, such as WiFi routers or IoT devices. [3]. Non-wireless electronic devices in the area can create RF emissions, such as computers, on-boards devices or weapon systems.[3]

“Movement also causes highly variable fading: even at low speeds and over short distances, a receiver experiences widely fluctuating power levels as the phasing of reflections add up constructively or destructively. When endpoints are moving at higher speeds, Doppler effects come into play and shift the frequency of the received signals” [3,4].

Testing

Since, there are all these different effects, which delay, attenuate, and degrade the propagated radio signals, it is essential to properly test the devices against radio channels before installation and operation in the field. These tests can be performed in the laboratory in a repeatable and controlled way, with automation, enabling much faster and less expensive radio channel validation and thus leading to greater reliability and quality of the communication later in the field. In this paper, we will describe some use cases, which are demonstrating these advantages.

Bench Testing with Basic Channel fading

“Two of the most fundamental characteristics of RF channels that transceivers must cope with are the wide change in received power levels, as the distance increases, and the multitude of multi-path signals as a result of reflection, refraction and scattering. Both conditions can be modeled easily and inexpensively with a tapped delay line.” Multi-path propagation, for instance, “results in numerous copies of the original signal, each arriving at the receiving antenna at slightly different times and with different power levels. The tapped delay line starts with the original signal, and then adds some delay and phase offsets with attenuation to create a second copy of the signal, simulating a reflection. By adding successive stages of delay and attenuation, a power delay profile is created that mimics multipath behavior.” [3]

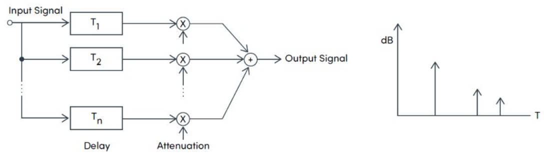

Fig. 1. A tapped delay line uses stages of delay and attenuation to model Multi-path reflections [3].

“The tapped delay line can be built from readily available components and at a relatively small cost. By simulating distance vs. power effects and simple multi-path effects,” it is possible to ”test the basic sensitivity and range of” the receiver and establish the best-case link throughput data rate. The setup gives a way to rapidly iterate on a design, as it is highly repeatable and easily available.” [3] However there is also a drawback, as the test set-up is not realistic. It does not represent all error conditions and environmental effects and is not able to “meet the complexity of modern systems such as 5G that use many (dozens or more) RF channels simultaneously.” [3]

Bench Testing with Channel Modeling and Emulation

To move beyond simple channel power and delay characteristics, requires complex mathematical models. “Channel models are mathematical descriptions of radio signal propagation”. [3] They cannot be described in a deterministic way, as this would involve solving the Maxwell equations in a non-ambiguous way, which is not possible. Another way of dealing with the effects described above, is by representing them as a series of impulse responses. “Channel modeling can be used to describe” signal propagation in time, frequency and space. Modern channel models can use antenna embedding, i.e. 3 D radiation patterns can be included in spatial characterization of the propagation. These effects can be combined to create complete scenarios, such as urban and rural models.” [3]

A channel emulator will execute these models. “at its simplest, a channel emulator takes in an RF signal, uses digital signal processing to implement the mathematics of a channel model and applies it to the input signal, and outputs the resulting signal.” [3] The signals are not interpreted or decoded. Thus, the channel emulator is agnostic to codes and modulation and can deal with any signal in the specified frequency range.

In the last few years, the mathematical modeling of conditions and scenarios has gotten more sophisticated. ”Frequency dependent fading, complex multi-antenna-element phasing for beam forming and beam tracking, and arbitrarily complex motion paths can all be modeled mathematically.” In addition, “the power of the channel emulator hardware has vastly improved. Today’s channel emulators can operate over a broad range of radio frequencies (from VHF Very High Frequencies to millimeter wave), employ state of the art DSP (Digital Signal Processing) and FPGAs to implement complex channel models, and can support large numbers of connections to simulate multiple endpoint scenarios. “ [3]

Fig. 2. A channel emulator creates a simulation environment for real RF signals [3].

“A benchtop setup with state-of-the-art channel emulator is a hardware-in-the-loop-environment for modern radio systems. It is capable of emulating urban, rural, indoor and custom propagation model. It can model ground-to-ground RF channels as well as ground-to-air and air-to-air-channels. It allows the user to simulate macro-cell (large radius, high power) and micro-cell (small radius, low power) architectures, with antenna placements at arbitrary heights. It can implement frequency dependent fading effects that are especially important in wide bandwidth and frequency hopping channels. It can simulate the Doppler effects of high speed motion, with user-defined motion paths for transmitters, receivers and reflectors. And it can handle peer-to-peer and mesh network scenarios, where a dozen or more endpoints are communicating with each other, each with a different propagation model comprising” all sorts of different effects, as described above. [3]

VERTEX Channel emulator

Here, we present an example for a channel emulator, the Spirent VERTEX Channel emulator, executing the radio channel emulation in a wide range of frequencies of 30 MHz to 5925 MHZ. This frequency range can be extended to higher frequencies from 6 GHz up to 47.5 GHz with a High frequency converter. Thus, it can operate in mm Wave range, and support military and public safety bands and bandwidth, for instance 5G, LTE, WiFi and military mesh network communication links. It is a modular and scalable system with 2-32 RF Outputs and up to 256 internal digital links. Radio channel bandwidth is 200 MHz. There is the option to concatenate several channels to achieve 1 GHz bandwidth or more. The VERTEX channel emulator enables real-time and I/Q playback channel emulation and is provided with Extensive channel model and connection setup libraries. Channel models can also be modified and defined by the user. Field measured channel models can be loaded and applied [8].

Fig. 3. VERTEX channel emulator

To facilitate scenario creation including movement of receivers and transmitters there is an Advanced Channel Modeling Software (ACM). It supports circular, linear, orbital and static motion. After input of the user settings, it automatically “creates and downloads channel samples to the VERTEX Channel emulator.” [5] With a Plugin “Array Modeling Tool” it is possible to visualize antenna array theoretical performance. [6] Virtual Drive Test (VDT) solutions allow field measurement conversions and dynamic emulation engine (DEE) enables dynamic scenarios.

The following conditions can be modeled:

* Urban, long-distance, indoor and custom propagation models
* ground-to-ground, ground-to-air, air-to-air..

* Antenna heights and ground effects
* Angle spread clusters and 3 D geometry
* Phased Array antennas for MIMO
  and beamforming
* High-speed device motion
* complex motion paths
* Blockers and moving blockers
* Multiple nodes and each with distinct models

A channel emulator can support the following major types of tests

- Conformance Tests to check if a user device conforms to a certain standard such as 3-GPP standards (3-GPP: Third Generation Partnership Program) [12]
- Performance Tests
- Field to Lab: to find out how well does a user device operate in different environments

And it supports simulated drive fly routes for development, performance tuning, trouble shooting and regression and manufacturing parametric validation.

Use Cases

A great variety of 5G civilian use cases can be tested and supported: such as acceleration of 5G development and replacement of field testing for 5G Cellular Vehicle-to-Everything (V2X) chipset validation. A North American OEM used Vertex for assuring 5G chipset performance, and enabling early 5G launch by fast validation of mm Wave communication in an Over the Air Test Setup. In all these cases, a VERTEX test setup has been successfully used to accelerate testing and thus save time.

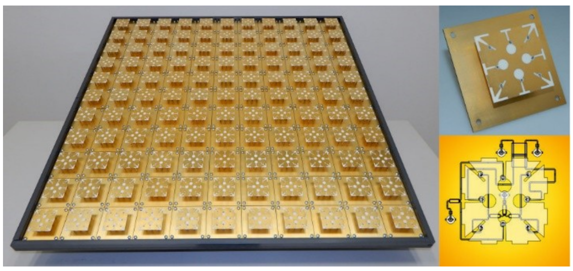

Fig. 4. Multi Mode Massive MIMO Antena Array, by www.hft.uni-hannover.de

Other challenging 5 G use cases, which can be addressed with this technology, are MIMO (Multiple Input, multiple Output) over the Air Testing, massive MIMO with a large amount of antenna elements, mm Wave for fast video communication with high throughput of data, and beamforming [9,10,11].

The spatial channel models of the VERTEX channel emulator were validated in 2021 for 3GPP FR2 (upper Frequency Range of 24.25 GHz – 40 GHz) MIMO Over the Air Tests, for metrics such as Doppler Autocorrelation, Power Delay profile, Vertical to Horizontal Power Ratio and Power Angular Spectrum Similarity Percentage [13].

A test setup for conductive MIMO testing for a network equipment manufacturer was implemented comprising four VERTEX units connected to each other, each with 18 I/O Ports and a sum of 72 I/O Ports. In addition there is a VERTEX Baseband Synchronizer. This complex system was delivered to one of the world's largest network equipment manufacturers.

One major oil and gas company managed to successfully test their own network base station and their high-powered devices before installation in the field with a VERTEX RF channel emulation platform, and thus assured Device Connectivity for specialized Devices and Spectrum.

5G is also considered by the military for applications such as Smart Command Centers, Enhanced Intelligence, Surveillance and Reconnaissance, unmanned operations, smart warehouse and logistics and health and supply monitoring. In every case, controlled and repeatable testing will make a big difference in reliability and quality and robustness of communication in field operation under real conditions.

Traditional military use cases are usually characterized by lower frequencies, higher velocity, mesh networks and complex ground-to-air radio channels. Some Examples: Testing has been performed for handheld radios in the field with obscuration by rocks and forests and also for verification of mesh network design with testing multiple radios simultaneously under a variety of channels, network configurations and implementations. [15]

In the Aircraft field, a Military contractor needed to simulate high-speed beamforming scenarios for several flight to ground applications, where a beam from the base station needed to track the flight. They were able to test their beamforming performance with a VERTEX system plus a Live Streaming Dynamic Environment Emulation. [15]

Satellite-to-ground and ground to satellite radio channels can suffer from long delays of up to 1-2 seconds and a very high Doppler shift, due to the high speed of satellites in orbit. The above test system was used to simulate satellite to ground connectivity with dynamic scenarios including moving vehicles. [13]

Conclusion

Data transmission via radio channels at different frequencies and especially at 5G is increasingly important, and needs to be robust and reliable for safe, secure and trustworthy operations, in all sorts of communication applications, both military and civilian, ground-to-ground as well as air-to-ground, satellite-to-ground and vice versa, and many more.

Radio channel modeling is a way to represent environmental conditions, fading, attenuation and different types of potential errors.

Here we present a versatile tool to test all sorts of communication signals' fading, by applying channel models to them, across a very wide frequency range. The signals are not interpreted or decoded, which results in the possibility to test fading with any type of signal.

We have also shown a wide range of use cases, in 5G communication, in aircraft and satellite communication and in the military domain, where this type of testing has been successfully implemented and used.

Acknowledgements

Special thanks go to Jukka-Pekka Nuutinen for sharing his expertise.

References

[1] P. Kintner, T. Humphreys, J.Hinks, GNSS and Ionospheric Scintillation – How to Survive the Next Solar Maximum, 2009. Inside GNSS 22- 29 (July/August 2009). http://www.insidegnss.com/wp-content/uploads/2018/01/julyaug09-kintner.pdf

[2] Jahn, A. Propagation Considerations and Fading Countermeasures for Mobile Multimedia Services. 2001. International Journal of Satellite Communications, 19, 223-250 2001. doi:10.1002/sat.699

[3] Spirent Whitepaper. Speed up Radio System Development for Defence Application. 2022

[4] Yacoub, Michel Daoud. Foundations of Mobile Radio Engineering. 1993. CRC Press, Inc. Boca Raton, Florida, USA. pp. 92-96.

[5] Bhargav, N., da Silva, C. R. N., Cotton, S. L., Sofotasios, P. C., & Yacoub, M. D. Double Shadowing the Rician Fading Model. 2018. IEEE Wireless Communications Letters. https://doi.org/10.1109/LWC.2018.2871677

[6] Spirent Brochure, Spirent Advanced Channel Modeling Software. 2020

[7] https://www.analog.com/en/analog-dialogue/articles/passive-intermodulation-effects-in-base-stations-understanding-the-challenges-and-solutions.html

[8] Spirent Brochure. Spirent Vertex Channel Emulation Solution for Defense & Aerospace. 2021

[9] Doug Reed, Alfonso Rodriguez-Herrera: 'Emulating a Moving Cluster in a Massive MIMO OTA Test Scenario', 2017 Asia-Pacific Conference of Antennas and Propagation, Xi'an, China, 2017

[10] Doug Reed, Alfonso Rodriguez-Herrera, Jukka-Pekka Nuutinen: 'Massive MIMO Array Testing using a Programmable Phase Matrix and Channel Emulator', 2017 European Conference of Antennas and Propagation, Paris, France, 2017

[11] Doug Reed, Alfonso Rodriguez-Herrera, Jukka-Pekka Nuutinen: ' Comparing Options for 5G MIMO OTA Testing for Frequency Range One', 2019 European Conference of Antennas and Propagation, Cracow, Poland, 2019

[12] https://www.3gpp.org/

[13] Alfonso Rodriguez-Herrera, Doug Reed, Jukka-Pekka Nuutinen: 'Spatial Channel Model Validation for 3GPP FR2 MIMO OTA', 2021 European Conference of Antennas and Propagation, Virtual Conference, 2021;,

[14] Jukka-Pekka Nuutinen, Doug Reed, and Alfonso Rodriguez-Herrera, '5G MIMO OTA Testing on Frequency Range 2 (FR2)', URSI GASS 2020, Rome, Italy, 29 August - 5 September 2020.

[15] Spirent Communications. Use Case Presentation. 2021.

[16] Jukka-Pekka Nuutinen, Doug Reed, Alfonso Rodriguez-Herrera,' Supporting FR2 channel models with a small scale UE chamber, 2021 European Conference of Antennas and Propagation, Virtual Conference, 2021

[17] Doug Reed, Alfonso Rodriguez-Herrera, Jukka-Pekka Nuutinen: ' Spatial Channel Model Validation for 3GPP FR2 MIMO OTA', 2021 European Conference of Antennas and Propagation, Virtual Conference, 2021

[18] Jukka-Pekka Nuutinen, Doug Reed, Alfonso Rodriguez-Herrera,' Large DUT Testing in FR2 MIMO OTA', 2022 European Conference of Antennas and Propagation, Madrid, Spain 28 March – 1 April, 2022

[19] Doug Reed, Alfonso Rodriguez-Herrera, Jukka-Pekka Nuutinen: ' Polarization of BS Array in FR2 Deployments', 2022 European Conference of Antennas and Propagation, Madrid, Spain 28 March – 1 April, 2022

DOI 10.5162/ettc2022/8.3

Alternate benefit of Forward Error Correction

First Author Paul Cook   Presented by Brandon Rosso
Institution or company, Curtiss Wright Corporation Newtown Pennsylvania USA
Corresponding PCook@curtisswight.com
Phone number +1 267.352.2018   Cell: +1 609.694.0344

Abstract

The use of Forward Error Correction not only increases the link performance in a high noise environment but also provides an alternate solution for thermal management. A paper was presented in 2020 on a tri-band transmitter that briefly discussed thermal management. It was not obvious then that the use of forward error correction could be used to manage the thermal heating of the unit while still maintaining the RF link margin. This concept of using the benefit of coding gain to reduce the RF dissipation is applicable to many use cases that are prone to overheating. This paper explores the practicality around transmitter thermal management and some test results of using FEC as a possible alternate thermal control mechanism.

Keywords
Forward Error Correction, thermal management, LDPC, Transmitter, Link margin

Introduction

Forward Error Correction has been used in telemetry applications for many years. With the publication of the latest technology in the IRIG-106 standard, provided the opportunity to implement and test the algorithm over a number of transmitter products that Teletronics Technology (TTC-CW) produces. Throughout the many bit error rate tests over the months of performance corner cases with good and consistent results, the question arose, what else could we use LDPC for?

Background information

It's becoming problematic for end user to deal with the dissipation requirements for modern transmitters with all of the features that the industry has developed. The features require high speed FPGA implementations to obtain the performance and spectral purity required to compete in this industry. These devices operate at higher speeds dissipating greater heat, raising the transmitter temperature. If heat transfer properties are ignored by the end user, it will create a good chance of overheating the transmitter. Thermal management for the high performance transmitter of today is a concerned when used on aircraft, missile, and hypersonic vehicles based on the availability of adequate mounting surfaces as well as the overall environmental conditions that these platforms operate in.

Heat flow in transmitters

As a rule for many years, the highest heat dissipator is the power amplifier section with the modulator section being smaller of the two. Typical modulators dissipate 5 watts where the PA section dissipates 20 watts or more depending on the RF power rating of the transmitter. The modern transmitter provides efficient RF conversion percentages with the modulator taking 12-14% of the overall power use; the PA is a healthy 58-60%, and the remaining 28% of power is transferred out the RF connector to the antenna as radiated energy.

The transmitter is normally configured with the PA section close to the mounting surface to allow the heat to be transferred efficiently through the bottom cover to the chassis of the system. This has worked well for many years until lately with the modern vehicles using structures with reduce thermal properties with limited heat transfer characteristics.

As the technology has advanced in the RF product requirements and product offering the percentage of power usage is increasing. The modern FPGAs and DSPs operate at a much higher clock rate with many features that are required today to stay competitive with the advancing feature list. Most or all of the modern modulator designs, use the higher dissipation FPGAs resulting in a shift in a higher percentage of power, or dissipation in the modulator section. Since all of the transmitter vendors box configuration for packaging has the modulator on top and the PA on the bottom, the increased heat in the

DOI 10.5162/ettc2022/8.3

modulator now impacts the temperature rise of the transmitter increasing the risk of overheating.

Dissipation techniques

Some of the RF Vendors use a fan accessory to create airflow to remove the heat the new transmitter dissipates. Airflow works well and TTC-CW has provided several telemetry products with integrated heat sinks to assist in the removal the excess heat. Unfortunately airflow is good for ground applications but in practice, there is rarely enough airflow to make it the solution for all use cases. Other systems use a cold plate which work very well with high power dissipating systems. Not all aircraft have the facility to support a cold plate to keep their electronics cool to within its rated temperature which ultimately leads to early failure and reduced reliability.

Over-heating protection

There have been several occasions where overheating events have happened in the past with fielded TTC-CW Transmitters. The damage was caused by exceeding the chassis rated temperature of 85^0C. TTC-CW also provide a temperature sensor on the side of the Transmitter to indicate a maximum chassis temperature exposure. Case temperatures above 93^0C typically degrades functionality of several RF devices within the transmitter. This happens when the end user does not understand the heat flow characteristics of these modern transmitters and their required installation. Over-heating protection varies by application and the priority of the data over the hardware. Meaning, in some applications the Transmitter should be allowed to over-heat if the data that it is transmitting is more important than turning the unit off when temperature exceeds its maximum safe level. But on the other hand, there are applications where, saving the hardware when in a over heating condition is more important than the data. For these various applications, modern transmitters offer a temperature control function that when enabled will automatically reduce the RF output level when the internal temperature exceeds a preset value in an attempt to regulate the chassis temperature. This control mechanism saves the hardware but results in a potential link margin risk with the reducing RF output levels and is warranted for application where loosing the link is not critical to the success of the test.

Additional over-heating mitigation include external cooling whether forced air or a cold plate which have been successfully implemented on many programs when available on the test platforms and in lab test applications. Unfortunately this is not the case for all applications most missile, launch, long range weapon systems still suffer the risk of over heating when there is poor heat flow or insufficient heat sinking.

The ultimate solution is reducing the self-heating of the transmitter and until the chip manufacturers can increase the RF efficiency over what the RF devices provide today, there is not much came done on the electrical design, to reduce the dissipation requirements for the Telemetry Transmitter for the near term.

RF link margin background

Telemetry link margins are calculated based on the maximum transmission distances that involves counting the system losses from the transmitter output, through the cabling, filters, isolators, and other devices the system engineers add in line with the transmitter to be compliant to the local transmission standards. Unfortunately the RF loss of those items incur reduces the RF energy that propagates through the air to the dish antenna on the ground to complete the link. Forward Error Correction provides coding gain which adds to the link margin when used in the operational range of the receiving equipment. FEC increases the data rate and resulting modulation bandwidth by the “overhead” or the additional data that the FEC algorithm requires. The increased bandwidth has always been a debate over using FEC and the value it provides. In fact the ½ rate LDPC algorithm increased the data rate by 2.0625 times which equates to a loss of 3dB of link margin. Due to the high coding gain of the ½ rate LDPC, the 3dB is only a fraction (20%) of the overall link improvement that the LDPC ½ rate provides.

$$\mathbf{IFBWdb=20*(Log(2*data\ rate))} \quad (1)$$

Forward Error Correction (FEC) Types, performance, and correction

Convolutional Encoding has been used for many years in Telemetry and much of the earlier Bit Synchronizers had an option for a Viterbi™ decoder. This coding scheme provided several dB of coding gain and was standardized almost 40 years ago for use in flight test telemetry. Developments in Turbo codes lead to the most current variant in the IRIG-106 standard Low Density Parity Check or LDPC and offers higher coding gains than some of the earlier version of FEC used in streaming telemetry.

The practical performance of these LDPC algorithms is very much dependent on the receiver, de-modulator, and decoder performance was well as the test setup to include high isolation of the transmitting device and the LDPC receiver. The author has tested four of the leading vendor's receiving equipment and found very good consistency in the test results with all of the vendors products

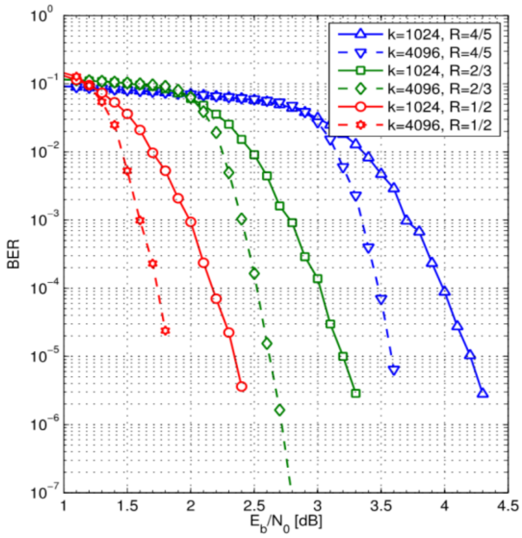

Figure 1 IRIG-1060029 Figure D-11. LDPC Detection Performance with Symbol-by-Symbol Demodulator [1]

when performed in a lab environment in use of a noise interference test set. The combination of the receiver sensitivity and coding gains may the higher gain algorithms more of a test challenge for consistent results when varying the RF power into the receiver over adding noise to the IF path using the noise interference test set.

Why would we consider using FEC to reduce the transmitter dissipation?

Reducing the level of RF output power of a transmitter reduces its dissipation. The gains provided with the new FEC algorithms allows for the link to be closed with lower RF Transmitter power. As an example, a typical 10 watt transmitter outputs 40 dBm and draws 1.25 amperes and dissipates 25 watts that is required to be properly heat sunk to maintain its case temperature below the absolute maximum of $+85^0$C. Applying $4/5^{th}$ LDPC provides a minimum of 8 dB of coding gain. A 5 watt transmitter output is 37 dBm, draws 0.9 amperes, and dissipates 20 watts, 20% less than the 10 watt transmitter. Applying the $4/5^{th}$ LDPC FEC to the 5 watt transmitter, the resulting BER performance equates to the non-FEC 10 watt transmitter but at a lower dissipation.

- 10 watt transmitter, outputs 40 dBm, Eb/N_0 level for 1E-6 BER is measured at 13 dB and dissipates 25 watts.
- 5 watt transmitter, outputs 37 dBm, Eb./N_0 level for 1E-6 BER in using 4.5^{th} LDPC now at 11 dB and dissipates 20 watt or 20% less.
- Note the increased BW of the $4/5^{th}$ LDPC FEC contributes 3 dB more noise.

Test results and conclusions

Testing this concept in a lab environment resulted in several surprises. The test configuration is critical to obtain reliable results. Using today's highly sensitive receivers combined with coding gains that are achieved in using LDPC creates a challenge to provide enough isolation between the receiver to the RF cabling to avoid having the cable leakage mask the true algorithm performance. The use of a Noise Interference Test set that operates at the IF level into the receiver and avoids much of the complexity of attempting to measure the combined gains.

Testing the coding gains provide a pleasant surprise with consistent improved BER performance with all three variants of the LDPC algorithms. The results measured in the lab setup were with in a 1 dB of the Eb/No plots provided above. In additional the increased coding gains of 2/3 and 1/2 rates over the $4/5^{ths}$ rate operated at Eb/No performances below 3 dB demonstrating the algorithm performance. The tests demonstrated BER rates of approximately 1E-6 rate at very low signal to noise levels consistency across all of the FEC variants.

Table 1 4/5th FEC BER 10vs5 watts

LDPC	RF Watts	I total amps	Eb/No	BER
None	10	1.25	13	1.2e-6
¾ 1024	5	0.9	7	1.8e-6
¾ 4096	5	0.9	5	1e-6

The Transmitter included in the tests offers variable RF output power, and performed closely to the expected results were the reduction of the RF output to reduce the power dissipation and used the coding gain to restore the BER performance back to the Non-FEC rate at 1E-6.

Between the three variants though, the recovery time from a significant fade from the receiver perspective indicated the higher gain algorithms (2/3 and 1/2 rates) were slower to respond than the lower gain from that 4/5ths algorithm demonstrated good response to deep fades.

Summary.

The use of FEC for reducing the dissipation of the transmitter was proven with the evaluation and test process described here in. The result of using the 4/5ths algorithm as the best performer over the two higher coding gain variant to reduce the dissipation with consistent results. The use of Forward Error Correction is not design for all applications but certain does provide an unique solution to reduce a transmitters dissipation and maybe consider when the traditional methods of heat sinking is not enough to keep the product from overheating.

References:

[1] IRIG-106-20, Range Commanders Council, IRIG-1050029 Figure D-11

DOI 10.5162/ettc2022/9.1

VeDAS Vehicle Data Acquisition System

Martin Bussas
Trout GmbH, Parkstraße 28, 34119 Kassel
m.bussas@trout-gmbh.de

Abstract

Predictive maintenance with machine learning is a new challenge for the automotive industry. Depending on the level of vehicle use and the load on components beyond predefined limits, the detection and elimination of systematic faults and the introduction of demand-oriented maintenance helps increase efficiency and reduce costs.

With this in mind, TROUT has developed VeDAS, a self-sufficient system that can be easily adapted to different vehicles. It is used for the automatic acquisition of vehicle data, which is evaluated with machine learning. Fast and secure communication to the downstream evaluation system is ensured via mobile storage media or wireless communication.

Collected data includes position, acceleration and vibration of the vehicle, as well as speed and distance travelled. In order to take possible environmental influences into account, temperature and humidity are also determined. A structure-borne sound microphone provides information about the operating status of the monitored vehicle. Further data provided by an engine control unit can be accessed via CAN bus interface.

In addition to data acquisition, VeDAS also provides a logbook function for documenting maintenance activities. Maintenance intervals and deadlines are determined for all entered vehicle assemblies. The selected method of condition monitoring specifies maintenance intervals and ensures the availability of the vehicle. Expanded functions include determining when an engine oil change is due.

Key words: machine learning, structure-borne sound microphone, vehicle data acquisition, predictive maintenance

Fig.1 VeDAS Box

Structure of the Evaluation Software

Data from the VeDAS box is transferred via USB connection to the evaluation software, which runs on a laptop computer. Tabs give access to the collected data and the calculation functions.

- Vehicle data: Creation and modification of vehicle master data, summary of all vehicle data.
- Vehicle usage profile: Evaluation of the data after a selectable period according to terrain and environmental data.
- Graphical representation: Route of the vehicle, structure-borne noise, nick and gear rates, acceleration and speed, shock diagram.
- Assemblies: Organization of the condition-monitored components
- Settings: language, directories, export properties, time zone, definition of limit values and correction factors.
- VeDAS data transfer: Configuration of data import from the VeDAS Box.
- VIN: Vehicle-specific identification numbers and identifiers as well as the date for the last maintenance, the next maintenance and the last data import can be found here.

The data is used for further training and for remodeling the intelligent evaluation module using various Machine Learning methods.

The trained network is then made available within a software update to the evaluation PCs.

Shock Diagram

The diagram shows the number of shocks for the respective load range.

The user can choose between two forms of visualization. The bar chart and a cumulative sum chart. The cumulative sum is formed starting from the highest g-values (here > 2g). The lowest value in the graph, here > 0.2 g, thus indicates the total number of shocks. The user determines in the settings from which g-limit value a measured value is assessed as a shock.

If the number of shocks in a certain range (in the example below >2 g) exceeds the limit value, maintenance is required.

The user defines the limit values for this in the settings.

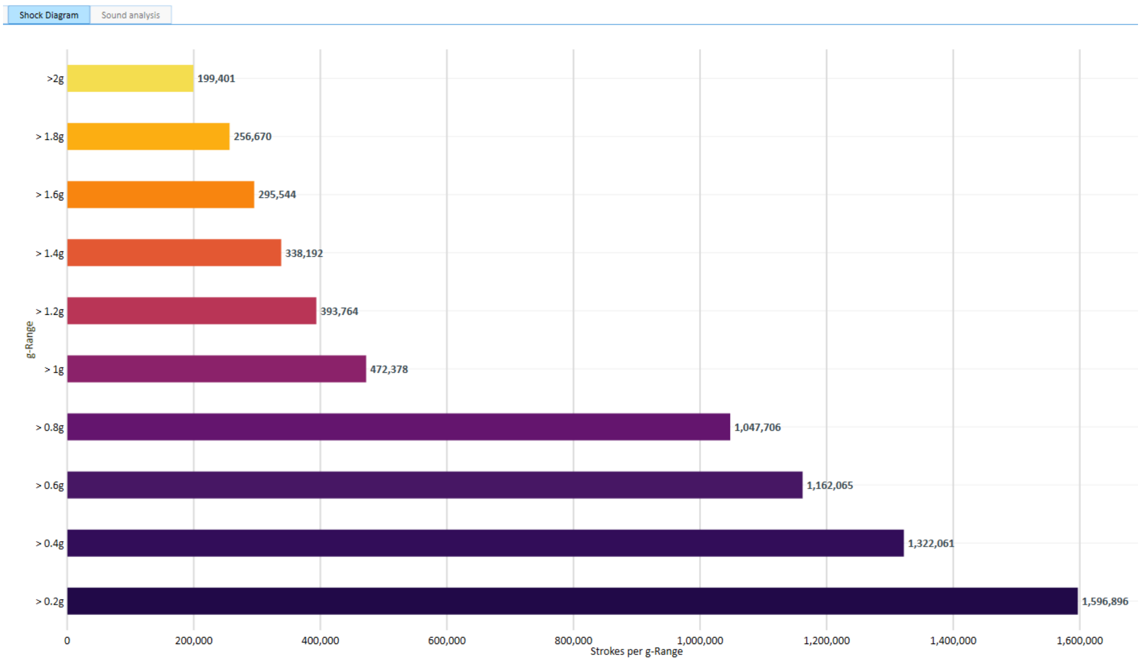

Fig. 2 Shock Diagram, cumulative sum chart

Acceleration and Speed

The shocks in the chapter above are measured via built-in acceleration sensors. In addition, the accelerations for the 3-space axes can be displayed. The speed of the system/vehicle is determined via GNSS. If there is a connection to the vehicle CAN bus, the speed can also be obtained from there. (diagram overleaf)

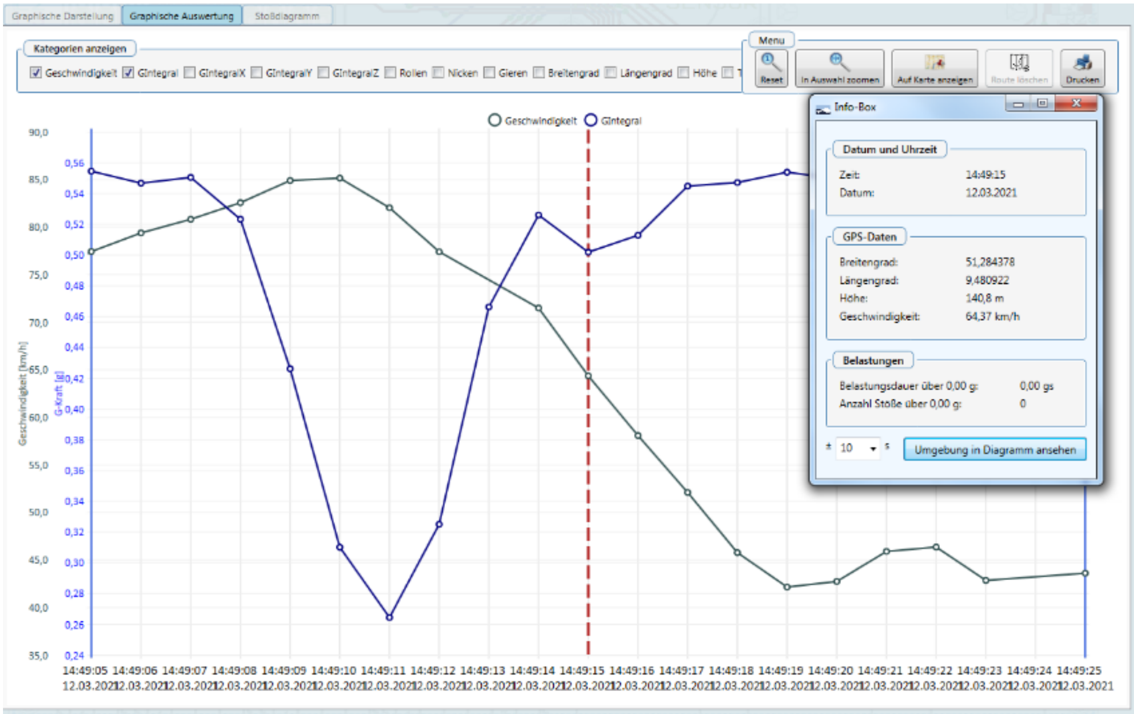

Fig. 3 Acceleration and Speed

Nick and Gear Rates

In addition to the experienced accelerations, the spatial position of the system is recorded. The system shows the deviation from the configured zero position for the parameters roll, pitch and yaw.

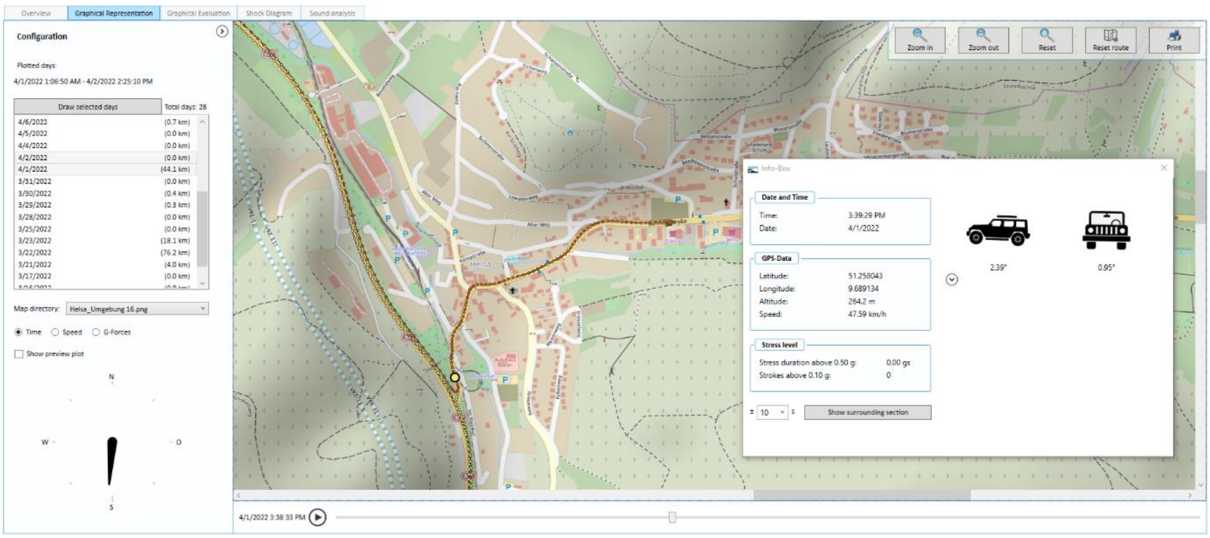

Fig. 4 Nick and Gear Rates

Usage Profile of Vehicle

The evaluation module provides information about the usage profile of the vehicle. The terrain sections are calculated as well as the kilometers driven on the road. The temperature and humidity are also recorded. A velocity profile is presented in tabular and graphical form. (diagram overleaf)

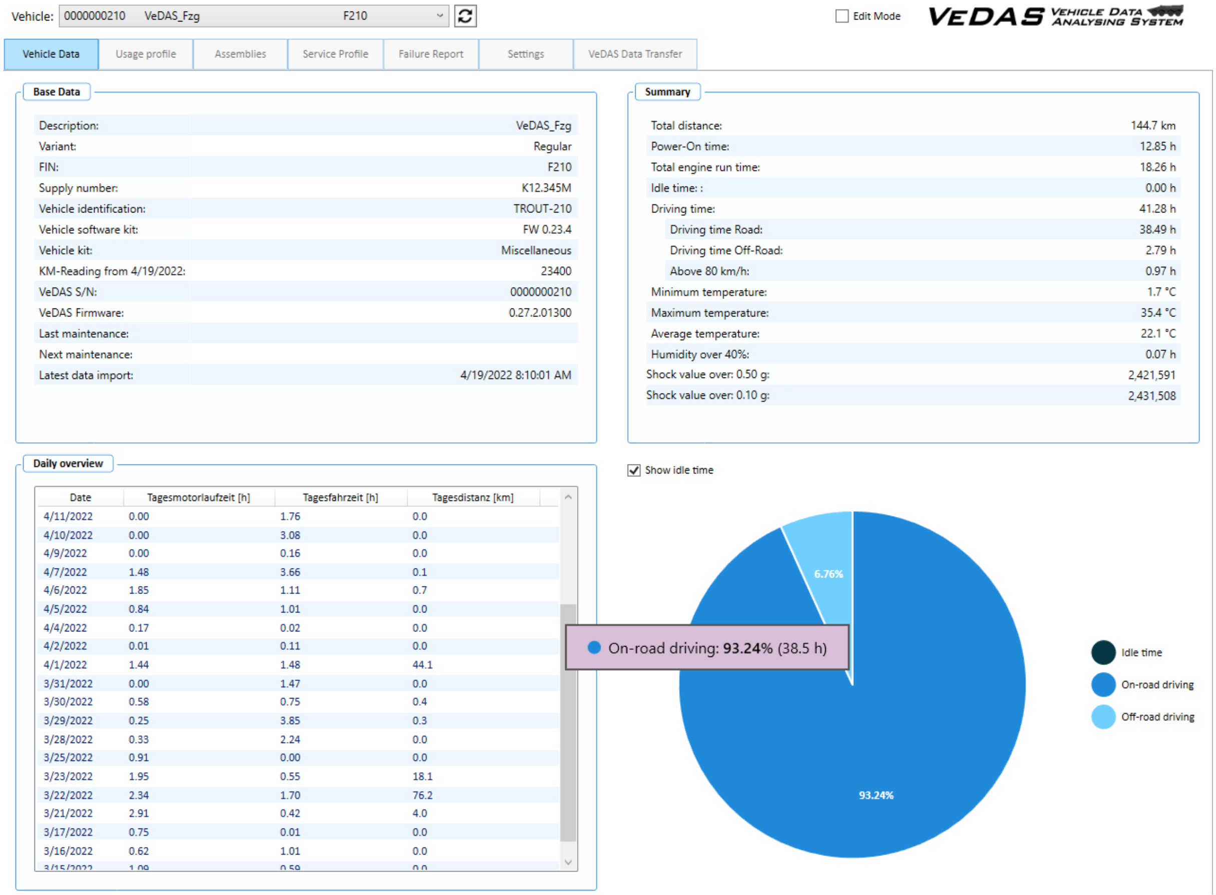

Fig. 5 Usage Profile of Vehicle

Structure-borne Noise

The recorded structure-borne sound [1];[2] can be output directly (green graph). Furthermore, individual frequency components can be displayed (yellow graph). The aim is to assign changes in frequency and amplitude to a defect in the vehicle by means of intelligent evaluation via Machine Learning. [3].

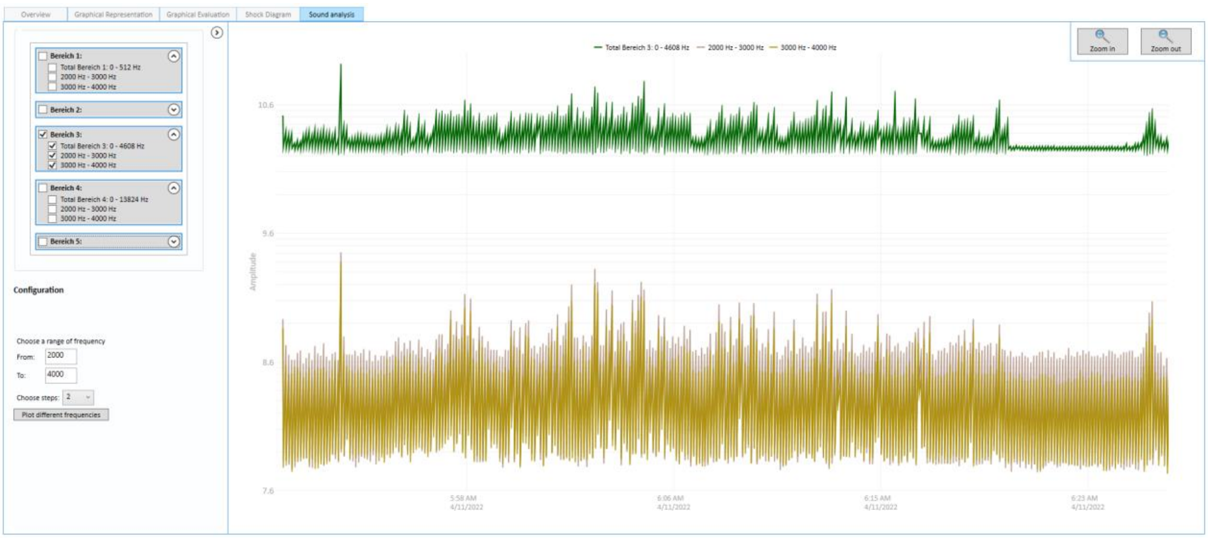

Fig. 6 Structure-born Noise

DOI 10.5162/ettc2022/9.1

Data Process Chain

Vehicle data from the CAN bus and sensors connected to the VeDAS Box are written to a ring memory after filtering with data reduction and a plausibility check. The capacity of the ring memory includes measurement data of several months.

The data can be exported from the ring memory to a database on a PC/laptop at any desired time. There, the data can be evaluated and visualized via a pre-installed artificial intelligence module. In particular, statements are made about maintenance work that is likely to be necessary and the oil quality

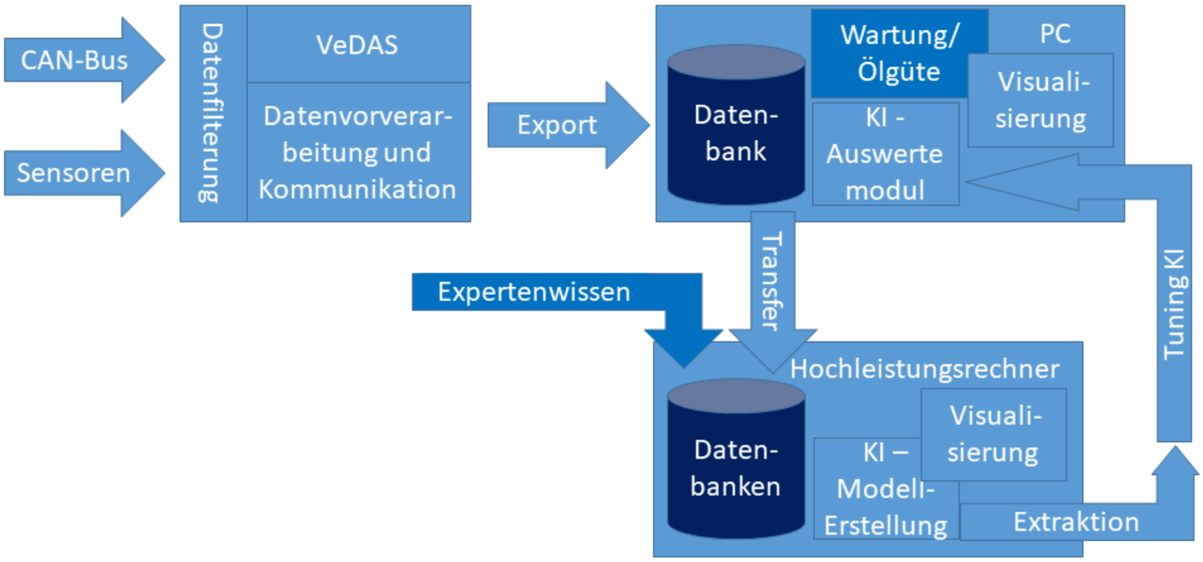

Fig. 7 Process Chain

The data is transferred to a high-performance computer system for further training and for remodeling the intelligent evaluation module using various Machine Learning methods. There, further training of the artificial neural networks takes place with the involvement of expert knowledge. The trained network is then made available within a software update to the evaluation PCs.

In further processing, an additional software component can be used to establish a relationship between the parameters operating hours, engine speed, oil pressure, oil temperature, water temperature, oil pressure profile and a key figure for the oil quality for a specific vehicle type and a specific type of oil. Start is with a default parameterization.

The procedure for calculating potentially required maintenance work on vehicle components is analogous. An evaluation of the measured structure-borne noise spectrum is also included here. The frequency range from 20 Hz to 60 kHz is considered.

Measuring the entire frequency range in one measurement would generate a very large amount of data, since a long period of time would be required to measure low frequencies. It therefore makes sense to carry out several measurements for different frequency ranges, in which the amount of data can still be evaluated.

The initial configuration of the sensor consists of a set of three frequencies and three measuring intervals. (Duration of measurement TM1, TM2, TM3 and measurement frequency MF1, MF2, MF3).

The sensor carries out the configured measurements in a loop:

1. Measuring with TM1, MF1

2. Evaluate data and send to the main processor for storage

Step 1 and 2 are repeated with TM2, MF2 and TM3, MF3. The AI evaluation is then used to search for patterns of sound characteristics of incipient defects in vehicle parts in order to plan an exchange at an early stage if necessary.

Predictive maintenance is the logical continuation of condition monitoring, which has long been integrated into many vehicles as a further development of the classic recording of operating hours. While condition monitoring only enables the detection of a state of wear, with predictive maintenance a maintenance appointment can ideally be scheduled well in advance. As a consequence, this results in higher availability and reduced costs.

Reduce of costs and increase performance

All relevant information is available via the vehicle data from the CAN bus communication plus the data from an additional sensor box in order to recognize whether the vehicle is in the best technical condition or that there are imminent defects. Maintenance can then be planned in advance, vehicle downtimes reduced and breakdowns avoided. This lowers costs, increases performance and extends the service life of the vehicle.

Especially if a special vehicle is used in comparatively small numbers but distributed worldwide, the expense of an additional sensor box with downstream evaluation of the parameters combined with the CAN bus data via machine learning processes pays off. Because, firstly, good predictive maintenance makes some visits by a service technician unnecessary. Second, the vehicle is only serviced when wear and tear requires it. And finally, thirdly: If a technician has to travel, then he knows in advance where the fault lies and, if necessary, which spare parts he needs on site.

Predictive maintenance is particularly attractive in scenarios in which a small malfunction or intervention that is too late can cause extremely high damage.

If the status data is evaluated regularly, the predictive maintenance system sounds an alarm before system failures occur. Then costly consequences can usually be avoided.

Predictive maintenance thrives on the leading system evaluating sensor data and drawing conclusions about the actual wear and tear of the respective component and its remaining service life. The effect of a predictive maintenance model is greater, the more sensors deliver data. And: The more precisely the system works, the more precisely it can be determined when which component should be replaced - in good time before a failure, but also only when it is actually necessary.

To do this, the prediction model must constantly adapt to the circumstances. This means that the measurement data collected must be interpreted continually, and the interpretation should increasingly approximate actual requirements.

This is exactly the function of machine learning algorithms. With their help, functional relationships can be derived from the data, which allow a reliable diagnosis of the status of the monitored system and reliable forecasts. The first goal is therefore to predict the Remaining Useful Life (RUL) of vehicles and components as accurately as possible. The second goal is the already mentioned learning effect. This is because the algorithms not only automate predictive maintenance. They also deliver adequate results and, if necessary, recommendations for action if there are changes in the behavior of the vehicles, but also in the general conditions.

On this basis, maintenance processes, intervals and stocking of spare parts can be optimally adapted to the current conditions. And the model helps to identify deviations before the vehicle is no longer fully functional or major damage occurs. Incidentally, this can also be used for lubricants and consumables. Their condition and wear can also be monitored and the optimal maintenance and replacement times can be derived from this.

For a predictive maintenance project using machine learning, the database must first be examined carefully. It is good if the vehicles to be integrated were already equipped with sensors and these can be read out via log books and log files.

The first step is to view and evaluate the data. What is particularly interesting here is which status or measurement data is collected from vehicles at specific times and since when. Unstructured data such as audio signals/structure-borne noise data can also be viewed and evaluated using additional sensors, such as those available via VeDAS. Not to forget static data such as the Vehicle Identification Number VIN, date of manufacture, supply number, vehicle identification, vehicle software kit and conversion kit.

The next step, the processing, is crucial: the data records have to be cleaned up, wrong values deleted, missing values filled in. At the same time, it is important to develop an understanding of which data was collected, how and under what circumstances.

Conclusion: Companies that pursue ambitious goals with predictive maintenance must integrate artificial intelligence or machine learning. Because only with AI can the value creation potential of predictive maintenance be optimally exploited.

References

[1] Michael Möser, Wolfgang Kropp, Körperschall Physikalische Grundlagen und technische Anwendungen, 2010 ISBN: 978-3-540-49048-7

[2] Michael Möser, Körperschall-Messtechnik, 2018 ISBN: 978-3-662-56621-3

[3] Bernd Orend & Ingo Meyer Schadensfrüherkennung mittels Körperschall, 2009 MTZ - Motortechnische Zeitschrift volume 70, pages 386–391

DOI 10.5162/ettc2022/9.3

Aircraft Maneuver Prediction with Machine Learning Applications

Emir ÇAKICI[1], *Onur YÖRÜK*[1]
[1] *Turkish Aerospace, Kahramankazan Ankara Turkey,*
muhammedemir.cakici@tai.com.tr, *oyoruk@tai.com.tr*

Abstract:
The flight tests are an important phase of aircraft development programs. Currently, parameters of manned or unmanned test flights are analyzed by the test engineers. Maybe the process is still best choice for the reliability concerns, but on the other hand it is time consuming. So we want to propose flight maneuver predictor with using Machine Learning techniques. For this purpose, a collected dataset of a fixed-wing propeller aircraft is used. A machine learning model was created that can predict seven different maneuvers using the gathered data. During flight test every test maneuver's start and stop time tagged and labeled as test points by the flight test engineers. These labels are Takeoff, Landing, LSS, Phugoid, Loop, Wind Up Turn, and Aileron Roll. After gathering data, preprocessing is performed such as fixing row size of all attributes by timestamps. Also some other attributes which had less frequent data than the others reproduced. For the creation of prediction model, support vector machine (SVM) applied. Overall prediction score of the model is 0.90.

Key words: aircraft, maneuver prediction, machine learning, support vector machines

1. Introduction

The aerial vehicles are one of the biggest innovations in human history. After the development of plane and other aerial vehicles, humans rapidly started to use them in many areas such as surveillance, rescue, transportation, military etc. Along with these developments, flight test phases began to play a major role in the development of aircraft. During the flight test phase even the high-tech and other vehicles need some traditional methods to achieve completely success; therefore, the main problem starts with the test process. In aerospace every aircraft should be validated by professionals to be acceptable to fly [1]. Also some discrepancies of the aircraft can't be observed by bare-eyes even that the observer is professional. Thus, the flight test engineers must rely on the parameters displayed by the software and analyze those parameters. Flight tests are performed on varying flight conditions in order to address possible discrepancies. Furthermore, some of the test conditions need to be repeated over and over to evaluate the aircraft. Flight tests generally runs in campaigns. There are different types of flight test campaign such as experimental, certification, product delivery. In experimental flight tests, the engineers create a campaign that requires necessary maneuvers. After conducting maneuvers, analyses are performed by different aspects. Flight test phase of an aircraft can be a challenging issue for all types of aerial vehicles due to its risk of injury or worse possibilities. Risk management has to be done and flight tests must be performed in the safest way with the minimum number of sorties. To improve efficiency, automatic recognition of maneuver is crucial to recognize the maneuver and determine its accuracy. In the literature, many methods have been proposed for flight trajectory estimation, although they do not fully overlap with this issue. Most of this methods used for predicting trajectories of commercial aircrafts. To the best of our knowledge, there is no specific study on this subject in the literature. Machine learning, deep learning methods are proposed [2], [3] to predict the trajectory of the aircraft. In the past, the mathematical methods were used to predict the trajectory but with the growing effect of machine learning and deep learning methods, mathematical methods lost their place and they became complementary factors in deep learning and machine learning methods. The main motivation of the paper is related to solve the problem of predicting maneuvers. We want to contribute test phase of the aerial vehicles by using machine learning that predicts maneuvers automatically. By applying this, the results of the predictions will give the researchers new perspective of test scenarios and help them to complete the flight test campaign much faster.

In this study, we propose a novel Machine Learning based maneuver prediction method that can predict the maneuver between 7 different maneuver set, which are Takeoff, Landing, LSS, Phugoid, Loop, Wind Up Turn, and Aileron Roll. Another difficulty in this article is that the maneuvers we are trying to predict are acrobatic, complex so they are difficult to predict. As mentioned earlier in this article, the maneuvers we are trying to predict are those with acrobatic features rather than the maneuvers has stable parameter changes such as climbing, cruise, or descending maneuvers.

The rest of the paper is organized as follows. In the section 2, the related works are given. In the section 3, the maneuvers and data preparations are described. In section 4, we introduced the flight maneuvers prediction. In section 5, experimental setup and results are given. Finally, section 6 concludes the report by listing future directions.

2. Related Works

This section presents the related works that used in the aerial vehicles. Even there are similar studies, we would like to inform readers that there is no maneuver prediction study that aim to predict maneuvers in flight test processes. Moreover, we would like to remind you that the data was also gathered from a real propeller fixed wing aircraft.

The related works are generally stand for the classification of the maneuvers type. For example, NC. Oza et al. [4] used classification of aircraft maneuvers that was used for fault detection. Their main aim is to find automated fault detection approach. To apply this, they used method which is present mismatch between the current flight maneuver being performed and the result of prediction that consists classifier. Their dataset is collected under a controlled test environment. The detailed description of dataset is not given.

Another work which was released by M Al Mansour et al.[5],[6] tried to classify maneuver of moving vehicle by using logistic regression technique and analytical algorithm. In the first study, the researchers dealt with the problem using on-board MEMS IMU's data (three accelerometers and three rate gyros). The classification of the data is separated under the either discrete or continuous. The test data consists mixed between the simulation and real experiments of an UAV. The second study is a modified adaptive analytical algorithm that predict heading and attitude estimation. Different from the first study, their dataset consists fusion of IMU, magnetometers and the velocity data from GPS. They didn't use extra filter like Kalman Filter [7] to prevent noisy data.

Wang et al. [7] propose a pattern-recognition model to find a way of loads analysis from operational flight data for advanced aircraft. In the experiments actual F16, F18 flight data records are used. They firstly extract the maneuver from the flight data and determine the characteristics of maneuvers with a rule based application. After determining the maneuver they check the maneuver with the ones in the database. If the maneuver matches the maneuver from database then the output is successful. According to results, if there is enough number of identified maneuvers in the same type at database, new maneuvers can be determined after same preprocessing steps that used in the identified maneuvers.

3. Preliminaries of Flight Maneuvers Type and Dataset Preparation

This section presents maneuvers analyzing and dataset preparation which are needed for better understanding the whole dataset.

3.1 Maneuvers

Takeoff maneuver is the first maneuver of the flight. The aircrafts's landing gears and wheels are on the ground before maneuver. After engine got the power the take off, aircraft increases air speed rapidly. Also, Pitch angle will be increased after the wheels are on the air. The takeoff can be performed only once per flight. [9]

Landing maneuver is the last maneuver of the flight. In the landing maneuver, aircrafts ground speed decreases to zero. In addition, Pitch angle will be decreases until the limit. When the vehicle approaches the ground, pitch angle firstly has a small positive change then the pitch angle come close to zero. The land can be performed only once per flight.

The phugoid maneuver is a rippling movement in which kinetic and potential energy are traded. Each move takes about one minute. As the the altitude increases the airspeed decreases, and as the altitude decrease the airspeed increases. There is, however, little or no change in the load factor if the aircraft has a neutral pitch stability. (see Fig 1.) and this motion depends on the characteristics of the aircraft.

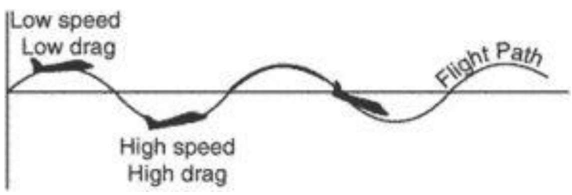

Fig 1. Phugoid Maneuver.

The loop maneuver is achieved by having the pilot pull the aircraft up and continue the pulling motion until a 360° turn is completed. (see Fig 2.). At the apex of this maneuver, the pilot will be upside down.

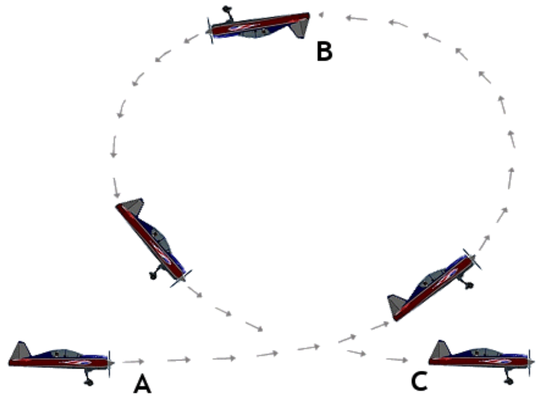

Fig 2. Loop Maneuver.

The Windup Turn maneuver is a mostly constant altitude turn with increasing angle of attack or increasing normal acceleration. During this maneuver, the steepness of the bank transfers some of the lift toward the direction of the turn. During this maneuver, the aircraft moves to the center of the earth and its weight remains the same, while the pilot increases the angle of attack to prevent the aircraft from falling [11].

The stability of an airplane in the longitudinal, or pitching, plane under constant flying conditions is known as longitudinal static stability. This quality is critical in deciding whether a human pilot can control the aircraft in a pitching plane without demanding undue concentration or strength. If an aircraft is longitudinally balanced, a modest increase in angle of attack will result in a negative (nose-down) pitching moment, lowering the angle of attack. A modest drop in angle of attack, on the other hand, will result in a positive (nose-up) pitching moment, causing the angle of attack to increase. In the LSS maneuver, the pilot gives command to change the aircraft's angle of attack in a negative or positive direction and tests whether the aircraft has stabilized [12].

An aileron roll is a constant 360° roll about the aircraft's longitudinal axis. When properly executed, there is no visible change in altitude, and the aircraft finishes the maneuver on the same heading as when it entered. In the Aileron roll maneuver, the pilot starts from steady flight and steers the aircraft's horizon to a slight climb of about 10 to 30 degrees. When the aircraft begins maneuvering, it begins to lose lift. When the wings become upright, only a slight lift is generated from the fuselage and tends to lose altitude. The short ascent at the beginning will compensate for this loss and will enable it to reach the initial altitude. When the airplane is fully inverted, the increased pitching results in a greater angle of attack and allows the inverted wing to generate lift. After completing the roll, the pilot will need to ascend to return to level flight [13].

3.2 Dataset

In Turkish Aerospace flight test processes, flights are made for many maneuvers within the flight test campaigns for each aircraft. The maneuver data we obtained was created with the maneuvers selected from these flight test campaigns. The whole flights are performed under control of the skilled pilots and powerfull ground telemetry systems. Data grounded by telemetry over a real aircraft were used. Each of our maneuvers is labeled by flight test engineers. Thanks to our telemetry engineers and flight test engineers we didn't need to label the data after we gathered it. There are lots of different parameters in an aircraft with FTI configuration in it. We needed to select the specific ones in nearly 15000 parameters. We narrowed it down to 17 parameters to prevent overfitting and making model too complex than it should be. Because every flight has some characteristic values, if we use all attributes on the train part, the test part and results would be really unacceptable. These parameters are the accelerations, rates etc. We didn't use the GPS data to prevent model to learn the GPS coordinates for a maneuver and make wrong predictions. We used 50 samples for each maneuver in training and 8 samples for each maneuver in test. In total 350 sample for training and 56 sample for test.

3.3 Preprocessing the Dataset

In the preprocessing phase, our aim is to reduce dataset with the related ones. In addition to this, we reproduce the missing and insufficient data that produced in low frequency. After trying different approaches, we chose augmenting the data. After augmentation we fix the row size of the dataset. After the fixing row size of dataset, we added 7 binary columns as target columns.

At first sight the data was noisy and had different sample rates for each different files that the sensors made. We needed to resample the data to a fixed sample rate. Some of the files had 49000 rows and some of the files had only 250 rows. That was a major problem for our situation but it's always a problem that the people who works with sensor data to solve. The final solution to solve this problem was the interpolation. But before that we tried to solve this problem by hand and try to avoid the rounding problems that interpolation gives. In the end due to the timestamp problems we solve this sample rate problem with interpolation. After interpolation, as can be seen in the Fig. 3 and Fig. 4 the output that the sensors give did no change. As can be seen at Fig. 3 to Fig. 4 the interpolation made just slight changes at the data that we can ignore while working on our project.

Fig 3. Not augmented data gathered direct from the sensors

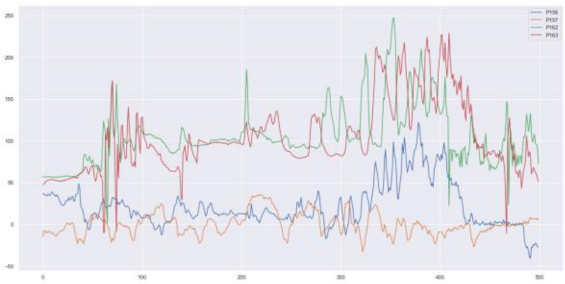

Fig 4. Augmented data.

After this we finally had a dataset we can work on but with slight problems. The dataset was spread over 400 different files. We concatenated the dataset into per maneuver and add the binary classifier as takeoff or landing or any other class.

4. Flight Maneuver Prediction

In this section, evolution of our model is presented.

After preprocessing stage of the data finished, we had nearly 400 different files that each one has the all data from one particular maneuver. To predict the maneuver of aircraft we use SVM One-Vs-Rest classifier [14]. Originally SVM only works for binary classification problems but in our situation we had 7 different maneuvers to predict. To predict that we use the One-Vs-Rest classifier. Before starting to work with the files first we need to fix some other problems like scaling and vectorising the data [15]. The data is splitted according to the flight numbers and the maneuvers. Firstly we interpolate the data that distributed in different files. Reason of this interpolation was that the row number of each maneuver tag must be equal when we fed data to model. If row numbers are not equal then one has the most row number will probably dominate the model and made model memorize itself rather than learn. To do so we did the interpolation and set the row size to 500 for each maneuver. After interpolation there was one last thing to do before send data to train. We used MinMaxScaler to scale the interpolated data. With that we shrink the range of data between 0 and 1. The advantage of using this scaler was mostly we don't want the information loss in the data and we want to make all parameters in dataset in the same range to prevent one parameter to dominate the other ones. After scaling we send the data to train. In the training phase firstly we vectorized every single different maneuver. We did that because we need to use SVM and to use SVM with time series data needs reshaping. Before reshaping we have nearly 400 different files with 17 columns and 500 rows. After reshaping and vectorising, the shape of the data changes as in Fig. 5. After this we had a data frame for each maneuver –in our case this maneuvers are "Takeoff", "Landing", "LSS", "Phugoid", "Loop", "Aileron Roll", "Wind Up Turn" -contains 50 rows –this rows stands for each flight- and 8500 –to get this size 500*17- data in each row. While vectorising data we split the data and target matrix.

After doing all interpolation, scaling, normalization and vectorization operations the data is ready to train. As we mentioned before we used SVM as model and "One Vs RestClassifier" as approach. We use 50 samples per maneuver as train and 8 samples

Fig 5. The reshaping process of the data

per maneuver as test data. The results are quite convincing and good for a predict like this as you can see in Experimental results. Table 1.

5. Experimental Results

At the beginning of the experience, experimental results are generally close to 1.0 overall score. This problem indicated to overfitting problem. We were using almost every attribute of the flights. Thus, we had to move our model to a more generalized one. Then we wanted to catch the sweet-point of the obtained attributes. With generalization and feature engineering phases we finally find the sweet point that doesn't overfit and gives us the pretty good results.

Experimental Result(ER)	Accuracy	Presicion	Recall
ER-1	0.90	0.90	0.91
ER-2	0.89	0.89	0.91
ER-3	0.89	0.90	0.90
ER-4	0.87	0.88	0.88

Table 1. Model Experimental Result Values.

As can be seen in Table 1, each experimental result gives pretty close results to each other. Four different ER refers to four different test datasets of maneuvers.

6. Conclusion and Future Directions

In this paper, a new technique for flight test data processing is introduced. This work present the opportunities on the test field in the many areas of flight test phases by using Machine Learning techniques to validate system. The results show the success of the method.

As a result of this paper, we have seen that machine learning methods can help both test engineers and developers in every field during and after flight tests. By using these methods, the accuracy of the maneuvers made in the tests can be validated, it can be determined whether the test has been successful or not, or the outputs of the method we recommend can be used in the analysis after the test.

In the following process, our first goal will be to increase the number of maneuvers in the model and turn the model into a machine learning model that detects which maneuver the aircraft is in from among more maneuvers. As the number of maneuvers checked in the SVM method increases, SVM models slowing down will be a problem for us. We plan to overcome this problem by using hybrid systems or by switching to deep learning methods. Our long term goal is to create a model that can predict which maneuver the aircraft is in during the test by making this model prepared for real time prediction. With the help of this method we are aim to create a learning model that can create a virtual pilot with the abilities to do the predicted maneuvers and reduce the workload on the pilot in flight.

References

[1] Kate M Pavlock. Aerospace engineering handbook chapter 2 (v): Flight test engineering. Technical report, NASA Technical Reports Server.

[2] Esther Calvo Fern´andez, Jos´e Manuel Cordero, George Vouros, Nikos Pelekis, Theocharis Kravaris, Harris Georgiou, Georg Fuchs, Natalya Andrienko, Gennady Andrienko, Enrique Casado, et al. Dart: a machine-learning approach to trajectory prediction and demand-capacity balancing. SESAR Innovation Days, Belgrade, pages 28–30, 2017.M. Mouse, D. Duck, The Beagle Boys for President, *Journal of Applied Nonsense* 13, 123-134 (2011); doi: 10.1234/s10000

[3] Zhengmao Chen, Dongyue Guo, and Yi Lin. A deep gaussian process-based flight trajectory prediction approach and its application on conflict detection. Algorithms, 13(11):293, 2020

[4] Nikunj C Oza, Kagan Tumer, Irem Y Tumer, and Edward M Huff. Classification of aircraft maneuvers for fault detection. In International Workshop on Multiple Classifier Systems, pages 375–384. Springer, 2003.

[5] Mehyar Al Mansour, Ibrahim Chouaib, and Asef Jafar. Maneuver classification of a moving vehicle with six degrees of freedom using logistic regression technique. Gyroscopy and Navigation, 9(3):207–217,2018.

[6] Mehyar Al Mansour, Ibrahim Chouaib, Assef Jafar, and AA Potapov. Analytical algorithm for attitude and heading estimation aided by maneuver classification. Gyroscopy and Navigation, 10(2):77–89, 2019.

[7] Greg Welch, Gary Bishop, et al. An introduction to the kalman filter. 1995

[8] Yongjun Wang, Jiang Dong, Xiaodong Liu, and Lixin Zhang. Identification and standardization of maneuvers based upon operational flight data. Chinese Journal of Aeronautics, 28(1):133–140, 2015.

[9] Federal Aviation Administration. Airplane Flying Handbook (FAA-H-8083-3A). Skyhorse Publishing Inc., 2011.

[10] Neil Williams. Aerobatics. Crowood, 2014

[11] Ralph B Roncoli. A flight test maneuver autopilot for a highly manueverable aircraft. In AIAA region 6 32nd Ann. Student Conf., number NAS 1.15: 81372, 1982.

[12] Irving, F.G. An Introduction to the Longitudinal Static Stability of Low-Speed Aircraft, Pergamon Press, Oxford, UK., 1966

[13] Ward; et al. (2006). Introduction to Flight Test Engineering (3rd ed.). New York: Kendall Hunt.

[14] Rifkin, R. and Klautau, A., 2004. In defense of one-vs-all classification. Journal of machine learning research, 5(Jan), pp.101-141.

[15] Juszczak, P., Tax, D. and Duin, R.P., 2002, May. Feature scaling in support vector data description. In Proc. asci (pp. 95-102). Citeseer.

DOI 10.5162/ettc2022/9.4

TABAI. Test Assistant Based on Artificial Intelligence

Francisca Coll Herrero[1], Pedro Rubio Alvarez[1]
[1] Airbus Defense and Space, Av John Lennon s/n, Madrid, Spain
Francisca.Coll@airbus.com
Pedro.R.Rubio@airbus.com

Abstract:
An Artificial intelligence (AI) is the simulation of human intelligence processes by machines, especially computer systems.
AI include expert systems, natural language processing, speech recognition, machine vision, pattern recognition, etc.
Artificial intelligence has been used in Test for several years specifically in the field of Computer Vision - for example in safe separation (store trajectory calculation), aerial delivery (paratrooper's trajectory calculation), and refuelling manoeuvres (approach speed calculation).
Also other projects where a prototype in which we have already developed or there is an interest in its study and evaluation, such as: pattern recognition based on wavelets for automatic manoeuvre detection (BMAD), real time object detection (basket detection, relative position, approach speed…), measuring pilots workload (eyes, head and hand movement) and FTI validation (Parameters anomaly detection, bad calibrated sensors, failure prediction).
This paper will describe a project called TABAI which consists of a Test assistant based on artificial intelligence.
TABAI is an assistant like Alexa or Siri to help in the Test activities. Using TABAI it will be possible to access to all the Test information that currently is available in a database or in documents or stored in data files.
The potential of TABAI is enormous, from obtaining the maximum value of a flight parameter to become the entry point for many test tools.

Key words: TABAI: Test Assistant Based on AI, Chatbot, AI: Artificial Intelligence, NPL: Natural Language Processing, LM: language Model, FTPR: Flight Test Program Requirements, TPKEY: Test Point Key

1 Introduction

The Airbus Defense and Space organization has grown a lot in recent years, so it is increasingly difficult to access required information quickly and efficiently.

This is the reason why **TABAI has been envisaged to be develop.**

TABAI is a Text Assistant based on Artificial Intelligence with the objective to help Test activities such as plotting Test parameters corresponding to a specific Test, to check the status of a program, to find documents using key-words, etcetera.

The interface of **TABAI** is a Chatbot that interprets the user's requirements using Natural Language Processing,

Fuzzy String searching that interprets the request and a server who finds the information and sends it to the Chatbot.

In the Figure 1 you can see the workflow of **TABAI.**

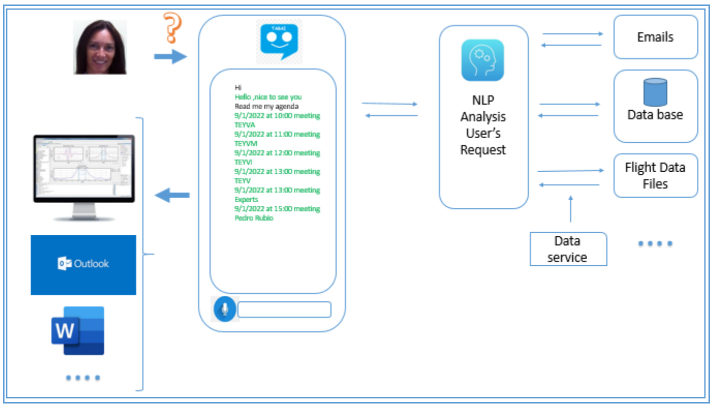

Figure 1.TABAI Workflow

This information is of origin Airbus Defense and Space/Spain and does not contain any export controlled information.

DOI 10.5162/ettc2022/9.4

2 TABAI components

TABAI consists of a Chatbot-like interface with a multiple of utilities such as accessing Test information contained in databases, Test data files, Test document files, Test video files, running analysis tools , read out emails and finally a server that finds and provides the information required by the user.

2.1 TABAI tool

The interface is a Chatbot developed in Python [Ref.1].

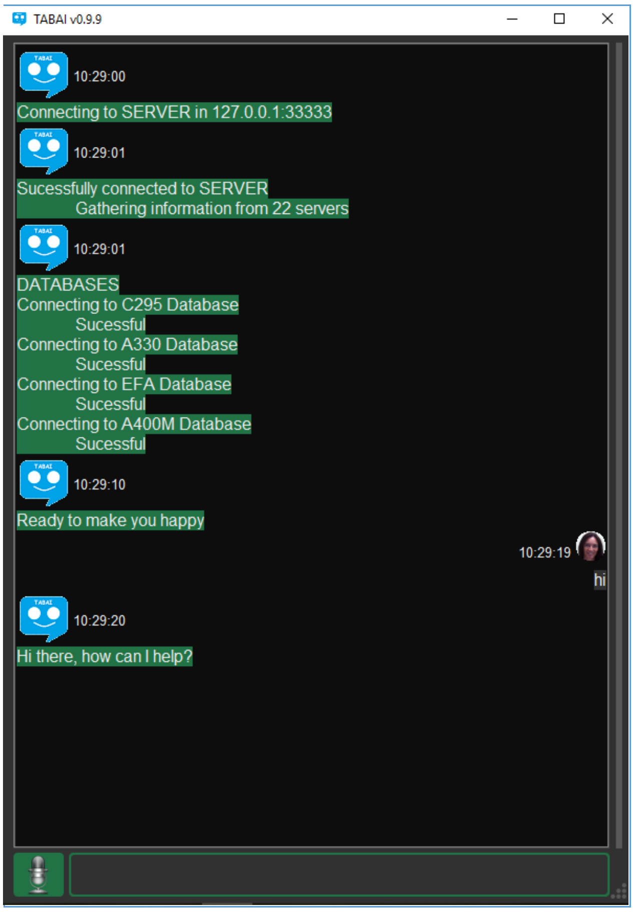

Figure 2. Interface

TABAI tool is composed by:

- **Intents.json** :JSON File that lists different tags that correspond to the different chat's inputs and the corresponding chat´s answers used in the Chatbot.
- **Chatbot_engine.py**: A python class in charge of interpreting user requests based on NLP and fuzzy string machine techniques [Ref.2]. That request is compared with the list contained in Intents.json and the most similar one is selected.
- **Chatbot_DB** . Python package to access to database.
- metaClient.py : Python package to access to file flight via server.

```
{"intents": [
        {"tag": "greeting",
         "patterns": ["Hi there", "Is anyone there?", "Hey", "Hello"],
         "responses": ["Hello, thanks for asking", "Good to see you ag
         "context": [""]
        },
        {"tag": "goodbye",
         "patterns": ["Bye", "See you later", "Goodbye", "Nice chattin
         "responses": ["See you!", "Have a nice day", "Bye Kica! Come
         "context": [""]
        },
        {"tag": "options",
         "patterns": ["How you could help me?", "What you can do?", "W
         "responses": ["I can give you link of FTnet, TEYVA confluence
         "context": [""]
        },
        {"tag": "noanswer",
         "patterns": [""],
         "responses": ["Please give me more information, try help, inf
         "context": [""]
        },
        {"tag": "FTnet",
         "patterns": ["FTnet", "link FTnet"],
         "responses": ["http://ftnet.intra.casa.corp/OneWebLogin/owl.a
         "context": [""]
                },
            {"tag": "email",
         "patterns": ["email","open email"],
         "responses": ["email"],
         "context": [""]
        },
```

Figure 3. Intents.json

- **TABAI_GUI.py** : Is the graphics interface that interacts with the user.
- **Metaserver** : A program written in C++ that serves to the client the user's requests via socket.
- **metaClient.py** : A python class that sends/receives the user's request to the Metaserver.
- **TABAI.py** : Main program in Python with the functions of user requirements interpretation using the chatbot_engine class ,execution of the corresponding actions using metaClient class and finally sending it in the TABAI_GUI.

2.2 Chatbot engine

A Chatbot is a computer program that simulates human conversation through text or text-to-speech.

A critical part of Chatbot implementation is selecting the right natural language processing engine (NLP).

DOI 10.5162/ettc2022/9.4

In the first version of TABAI, a Keras sequential neural network model was used as NLP. This model was trained using the list of sentences included in the Intents.json file.

Afterwards a Fuzzy String Comparison based on:

- Levenshtein distance
- Sort alphabetically words
- Removing blank spaces between words in sentences

was tested

Finally, it was decided to use **Fuzzy String Comparison** since it worked much better for this use case.

2.3 Access to links

This is the simplest function of **TABAI**, the links are directly included as a response in the Intents.json

In the Figure 4 you can see how are introduced the links in the json file and in the Figure 5 how use this feature in **TABAI** interface.

```
{"tag": "Experts confluence",
 "patterns": ["Experts confluence", "Experts space
 "responses": ["https://confluence.intra.airbusds.
 "context": [""]
},
{"tag": "TEYVA confluence",
 "patterns": ["TEYVA confluence","confluence","Sas
 "responses": ["https://confluence.intra.airbusds.
 "context": [""]
},
{"tag": "FTnet",
 "patterns": ["FTnet", "link FTnet"],
 "responses": ["http://ftnet.intra.casa.corp/OneWel
 "context": [""]
},
{"tag": "Weather",
 "patterns": ["weather", "weather today", "what wi
 "responses": ["https://weather.com"],
 "context": [""]
},
```

Figure 4. TABAI links

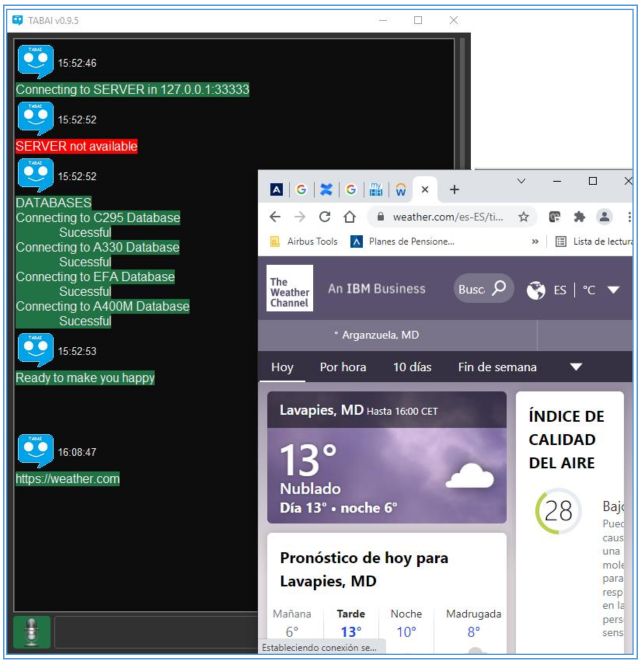

Figure 5. TABAI link

2.4 Access to Test Files information

During the last 30 years, several formats for storing Test Files have been used, depending on the current technology and the upcoming requirements. As an example, 30 years ago the number of available parameters were around hundreds and nowadays we manage hundreds of thousands, therefore the format to store these parameters has completely changed.

As we realized that the format of the Test Files change, and will change in the future, we decided to develop a network based unified protocol to access these data (FxS). In this approach, the final applications (plotting tools, analysis tools, any application that need Test Data) will remain unchanged, regardless the format we used.

For each format and new format, an FxS Server is developed that is able to serve data to any client compatible with this protocol.

DOI 10.5162/ettc2022/9.4

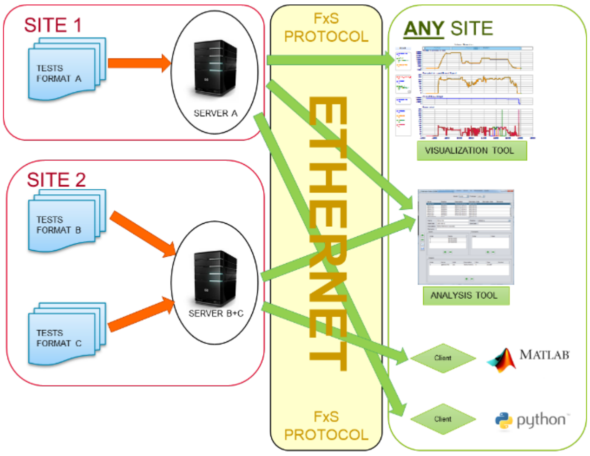

Figure 6. FxS Schematics

We used to handle tens of aircrafts across its lifecycle of testing, and even for a long program the format of the Test File could change.

In such complex scenery, sometimes is difficult to find out which FxS server is capable to give data for a specific aircraft/test. The solution is, the so called, **Metaserver**.

This Metaserver gathers the information of all the FxS running in our ecosystem (currently more than 40, and increasing…), basically gathers two main information:

- Aircrafts available in each server.
- Tests available per each aircraft.

This Metaserver uses a simple UDP network transactions based in XML for the queries and responses. Other ways of communication (json, REST API, and some other) will be evaluate in the future.

For each query, the matching is not an exact match, but a fuzzy string comparison based on the Levenshtein distance.

The Levenshtein distance is a string metric for measuring the difference between two sequences.

Currently, the queries available are:

- **AIRCRAFT**
  - **Query**: pattern of an aircraft.
  - **Response**: aircrafts available in any server that best *matches* the pattern.
- **TEST**
  - **Query:** pattern of an aircraft and pattern of a test.
  - **Response:** Tests available in any server that best *matches* the pattern. For each single test the Metaserver sends all the needed information to connect with the FxS server that really has the test file. If there are some, the Metaserver choose the less loaded.

2.5 Access to Data Base

Some of the information required by the user implies accessing the Test databases. Test have several oracle databases for the different aircraft models.

Each database contains tables with information of flights, programs, tests point, status of the program, etcetera.

Using **TABAI** you can ask for the programs of an aircraft model or even the status of a specific program.

3 User interaction with TABAI

The user can interact with the Chatbox using text or using the voice. **TABAI** interprets user's requirements using Natural Language Processing techniques and also, in the second case, using Speech Recognition Techniques.

In neither case the user is required to write or say a specific phrase and in a specific order, but rather **TABAI** will interpret what the user requires from a list of options.

Figure 7.User interface

3.1 Speech Recognition Technique

There are a lot of very good voice recognition applications in our devices, in mobile phones Siri, Alexa, in cars, in google meet etc. and it is clear that there is no intention to compete with them. But we decided to develop our own language model with a reduced dictionary in **TABAI** since the Google voice recognition library, apart from not being free, required an internet connection and this was a constraint for our application.

Three models are used in speech recognition to do the match between the audio and the combination of words: the acoustic model, phonetic dictionary and the language model.

CMUsphinx toolkit was used to create the three **TABAI** models. [Ref.3]

DOI 10.5162/ettc2022/9.4

The last step is to generate the acoustic model and to train it to enhance the accuracy of the speech recognition [Ref.5].

4 Uses cases

As mentioned in the abstract, the potential of **TABAI** is enormous, in this chapter, some of the use cases that are currently implemented in **TABAI** are described.

4.1 Programs info

The list of programs corresponding to an aircraft model can be obtained using text or the voice.

There are different options, for example writing or saying : programs C295, show C295, programs MRTT, programs efa, show programs C295....

Figure 12 shows the output of **TABAI** in the case that the user selects the C295 programs.

Figure 8. Programs C295

TABAI provides the total number of FTPRs corresponding to this program (in this example 32), the global TPKEY status of the program as a percentage of closed, performed, open and pending TPKEYS.

TABAI also shows the list of FTPR with theirs corresponding reference codes, descriptions and total number of TPKEYS. The colour indicates the status that predominates in the TPKEYS.

4.2 Program status

In a Flight Test Program, a list of requirements must be verified and validated. All these requirements are compiled in Flight Test Programs Requirements documents (FTPR).

The list of the requirements for each FTPR are translated into a list of Flight Test Points (TPKEY).

All this information is digitalized and stored in a table of a Flight Test database.

The status of each TPKEY can be OPEN (not flown), PERFORMED (flown but not analysed), CLOSED (flown and validated), and PENDING (flown but not validated).

A summary of the status of the program is obtained clicking on a program in **TABAI** interface.

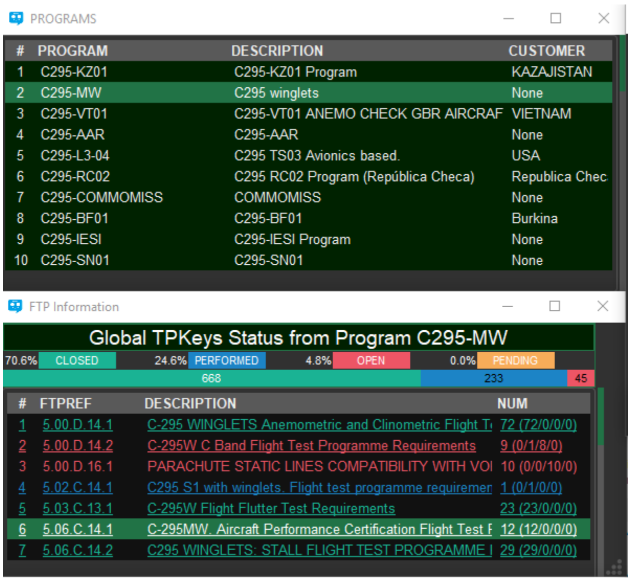

Figure 9. Status program C295 MW

This information could have been accessed directly by writing or saying: status program MW.

The correspondent pdf document can be accessed by double clicking on each FTPREF.

.

DOI 10.5162/ettc2022/9.4

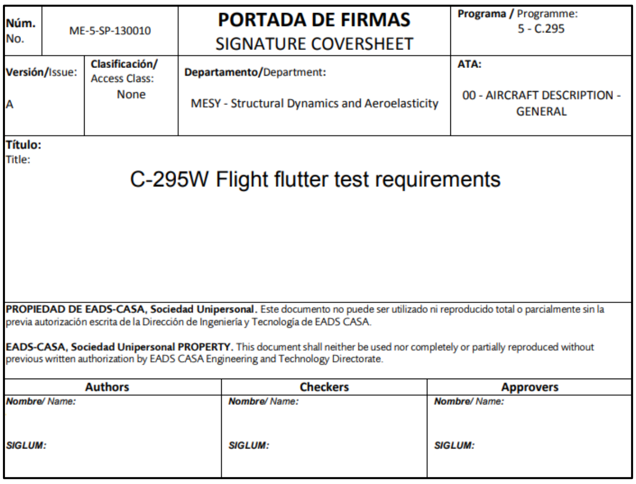
Núm. No. ME-5-SP-130010

PORTADA DE FIRMAS SIGNATURE COVERSHEET

Programa / Programme: 5 - C.295

Versión/Issue: A

Clasificación/ Access Class: None

Departamento/Department: MESY - Structural Dynamics and Aeroelasticity

ATA: 00 - AIRCRAFT DESCRIPTION - GENERAL

Título: Title: C-295W Flight flutter test requirements

PROPIEDAD DE EADS-CASA, Sociedad Unipersonal. Este documento no puede ser utilizado ni reproducido total o parcialmente sin la previa autorización escrita de la Dirección de Ingeniería y Tecnología de EADS CASA.

EADS-CASA, Sociedad Unipersonal PROPERTY. This document shall neither be used nor completely or partially reproduced without previous written authorization by EADS CASA Engineering and Technology Directorate.

Authors	Checkers	Approvers
Nombre/ Name:	Nombre/ Name:	Nombre/ Name:
SIGLUM:	SIGLUM:	SIGLUM:

Figure 10. FTPR document

By clicking on each FTPR, a new window appears containing the list of TPKEYS with its status.

By clicking a TPKEY a window appears showing the information about it.

In case the status of this TPKEY is performed or closed, a second window appears containing the flight and time slices that closed this TPKEY distributed in folders. At the bottom of the window, the list of flight files related to the TPKEY are also shown.

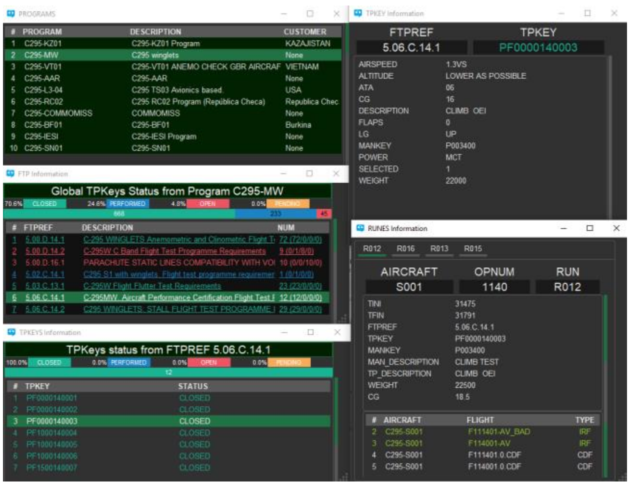

Figure 11. Info TPKEY

By selecting with a double click on one of the flight files, a plot tool appears containing the time histories of the characteristic flight parameters of the TPKEY manoeuvre.

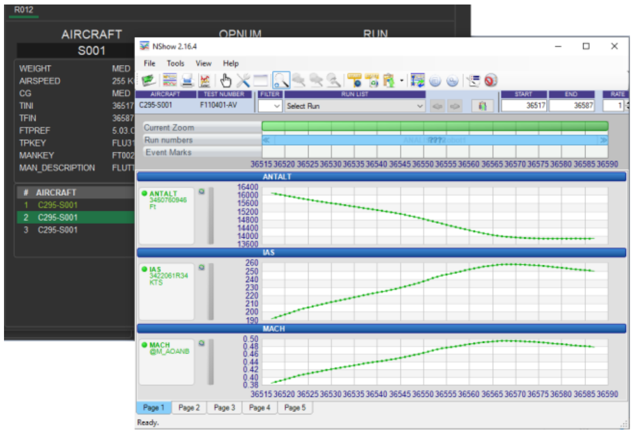

Figure 12.Plot flight parameters

4.3 Program Flights

Other functionality of TABAI is access to the flights information of a specific program.

This information can be obtained from the list of program by pressing the shift key and by clicking on the selected program.

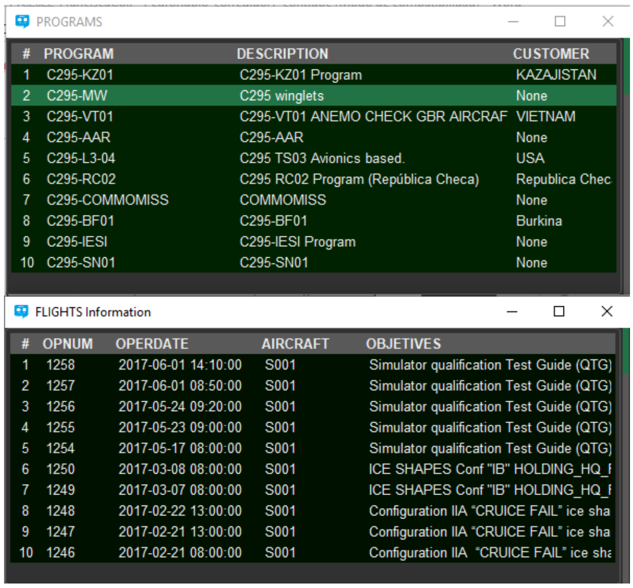

Figure 13. Program flights

This information could have been accessed directly by writing or saying: flights MW.

By double clicking on a flight, the list of flight files appears in a new window.

DOI 10.5162/ettc2022/9.4

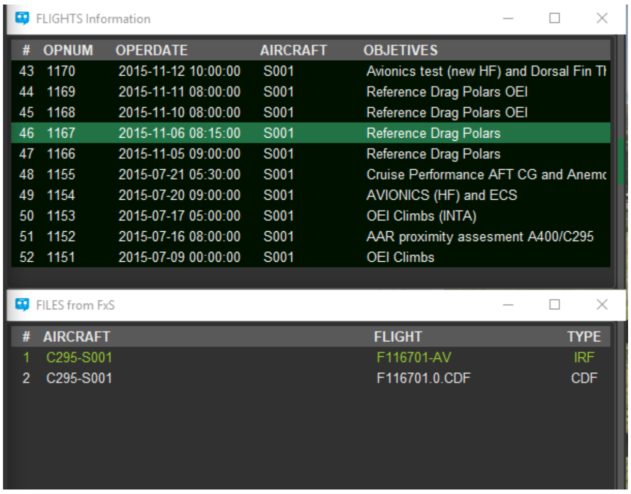

Figure 14. Flight files

By selecting with a double click on one of the flight files, a plot tool appears containing the time histories of the generic flight parameters of the complete flight.

5 Conclusion

TABAI is a Text Assistant based on Artificial Intelligence with the objective to be an aid to Test activities.

In the first TABAI version a group of interesting functions have been included in the tool, such as access to information on the status of programs, access to flight information or access to data files including their parameter visualization in a plot tool.

The potential of TABAI is enormous and it is easy to expand its functionalities by following the philosophy of the Chatbot.

TABAI may become a fundamental tool in testing by reducing the time required in those tasks where a machine can do instead using Artificial Intelligence techniques.

6 References

[1] Jere Xu https://towardsdatascience.com/how-to-create-a-chatbot-with-python-deep-learning-in-less-than-an-hour-56a063bdfc44

[2] Parthvi Shah. https://medium.com/mlearning-ai/all-about-rapidfuzz-string-similarity-and-matching-cd26fdc963d8

[3] CMUSphinx Documentation: https://cmusphinx.github.io/wiki/

[4] http://www.speech.cs.cmu.edu/tools/lmtool-new.html

[5] https://at.projects.genivi.org/wiki/display/PROJ/Using+CMUSphinx+and+Training+a+Model+to+Enhance+the+Accuracy+of+Speech+Recognition

[6] https://sourceforge.net/projects/cmusphinx/files/Acoustic%20and%20Language%20Models/

DOI 10.5162/ettc2022/10.1

Distributed Testing using VISTAS (ED-247 RevA)

Ramiro RODRIGUEZ-MARTINEZ[1], *Christian GAUREL*[1], *Marco GRUBER*[2]
[1] *Airbus Helicopters France, Aéroport International Marseille-Provence, 13725, Marignane, France,*
[2] *Airbus Helicopters Deutschland GmbH Industriestraße 4, 86609 Donauwörth, Deutschland*
ramiro.rodriguez-martinez@airbus.com, christian.gaurel@airbus.com, marco.gruber@airbus.com

Abstract:

Virtualization protocols, like EUROCAE VISTAS ED-247, provide new possibilities for designing future test benches architectures but also redefining test strategies. As the standard is more largely accepted and promoted, commercial off the shelf (COTS) equipment become available simplifying the setup and implementation of this technology for new or existing test rigs.

One of the possibilities brought by the signal virtualization is the possibility of interconnecting benches in different locations in a simple and non-intrusive way. This can lead to great benefits and cost reductions: more efficient use of available resources, limits the need of building additional benches and allows earlier system integration between suppliers and integrators.

Nevertheless these new possibilities come with their set of constraints: Transmission Latency, IT restrictions, Cybersecurity concerns, signals adaptation needs.

This paper will show the different possible setups for interconnecting benches in different rooms, buildings and even sites and the possible solutions to overcome the encountered problems.

Key words: VISTAS, ED-247, Distributed Testing, Signal Virtualization, Test Benches

Distributed Testing

The need of testing full complex systems as soon as possible in the development cycle is clear for all the stakeholders in the industry. Doing so is not so simple. Different partners located on different sites are often developing different parts (sub-systems) belonging to a complex system. Each partner uses its own benches for testing different subsystems and, when the time comes to test everything together, a full integration bench needs to be designed, developed and manufactured. A lot of the work in this stage goes to verifying interfaces and communication protocols between the different subsystems, limiting the time available for verifying functional and logical requirements.

Usually the historical tendency was to build integration benches on both sites, more or less centered in the subsystem under test. However, the cost is often a showstopper and the project milestones and the contract between parties usually don't allow for an efficient workshare.

A recurrent solution is building simple mobile benches that can easily be moved between locations, allowing to complete the missing part on the other side. But this comes with its own limitations: reduced representativeness, additional costs, logistics and export control constraints, remote maintenance and support, etc.

The ideal solution for anticipating integration activities would be interconnecting the different subsystem benches together, but avionic protocols are not often meant to cover long distances. This is where the signal virtualization enters the game. The main principle is: acquiring the avionic signals, transposing the avionic data into a long-distance compatible bus and rebuilding and synchronizing the avionic signal back to their physical state on the other site.

The VISTAS revolution

The use of virtualization buses allows the exchange of avionic data over long distances with reduced cost while letting a good flexibility to adapt to system evolutions.

The approach is nothing new. Field buses are extensively used in the industry to interconnect production tooling and Programmable Logic Controllers (PLCs) for exchanging measurement data. But none of these industrial field buses is meant to transport avionic data (A429, AFDX, MIL1553, etc.). Adapting them to

DOI 10.5162/ettc2022/10.1

that purpose would require developing specific drivers and boards.

Airbus has been doing this for several years now, between their own sites and with suppliers with very good results. Nevertheless, since no simple and open standard was available, implemented solutions where based on proprietary protocols and limited equipment.

With the arrival of EUROCAE ED-247 standard [1], the door was open for the use of a simple, open and shared avionic signals virtualization protocol. We took this opportunity inside Airbus Helicopters to implement some of the long-dated required interconnections between our different benches at minimal cost and with maximum flexibility.

Among a large portfolio of equipment compatible with ED-247, the choice considered that the developments should be reusable later, avoiding one-shot investments.

Technological choices

In order to setup our tests, the aim was to use COTS equipment, compatible with ED-247 and allowing the use of a large choice of input/output types. In the past Airbus Defense & Space has used NI CompactRio systems as described in [2]. In our case, UEI was the logical choice since it complied with all these criteria. In addition, it was already deployed on our test benches so we had all the required equipment already in site. On top of that UEI allows for very flexible network configurations and EAP/TLS authentication to connect them to IM infrastructure.

In order to overcome network infrastructure IM constraints Scalian Nodes were selected as network interfaces since they allowed stablishing secured VPNs internally and externally and their reliability had already been proven by Airbus Commercial Aircraft to establish permanent links between their sites.

Inter-Building benches connection use case

One of our first needs was to be able to connect our avionic integration benches with our mechanical vehicle rigs. Indeed, for safety, infrastructure and historical needs these benches are placed in different buildings. Until now mobile benches approach was in place, but we were looking for a solution that could be reusable and easier to implement and adapt.

The first application was the coupling of the Landing Gear (LDG) with the Helicopter Zero (HC0), a very high representativeness systems integration bench (see Fig.1).

The advantage was that the LDG could be installed on a mechanical rig, stimulating efforts on the system or climatic chamber, while the control computer could be in a full representative avionics environment with closed loop simulation of flight conditions. As a first trial it had the advantage of being relatively simple, only the power supplies and the control and monitoring discrete signals needed to be distributed.

The challenging part was the transmission latency. The control computer expected the system to acknowledge and react to control commands in a limited time. In parallel an additional constraint was that, while one of the LDGs was set apart in another building, the other two remained close by. These could lead, depending on the transmission latency, to discrepancies on the signal feedback from the three LDGs as seen by the control computer and leading to discrepancy failure modes.

The next difficulty to overcome was the network configuration. Indeed, the ED-247 standard encourages the use of UDP multicast for packet exchange, since it eases the distribution, monitoring and debugging while limiting the use bandwidth. Modern IM constraints usually forbid or limit the use of multicast in internal LANs. Although we could have configured the ED-247 to use only unicast UDP, we preferred using multicast since it allowed connecting monitoring tools to the setup without using mirroring switches or other tapping methods.

The last topic to cover was the signal adaptation on both sides of the setup. In

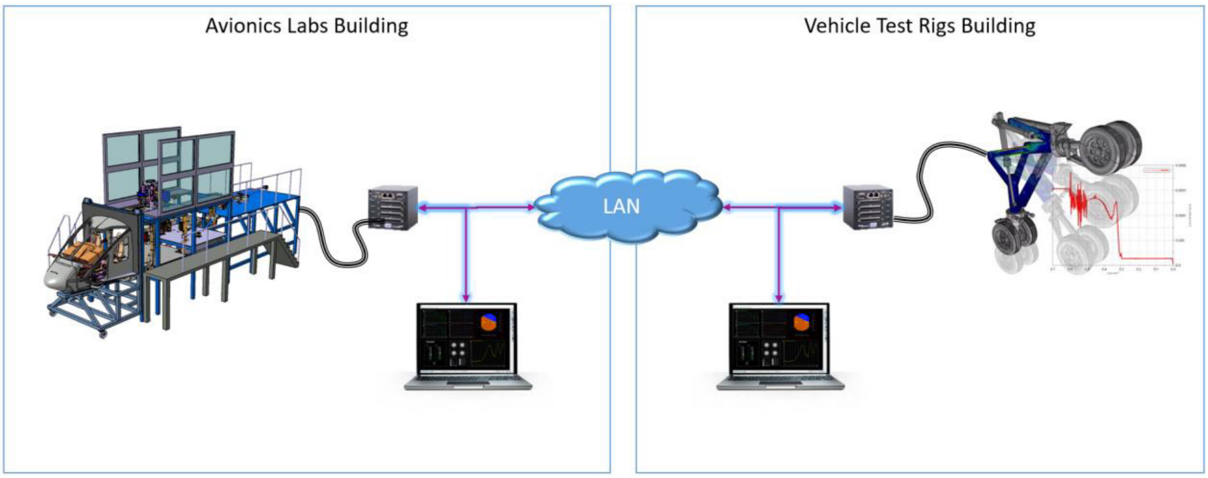

Fig. 1 Landing Gear Distributed Testing Setup

DOI 10.5162/ettc2022/10.1

particular for the discrete signal and power supplies, the introduction of a cut and visualization in the middle of the lines requires reviewing the signal polarization and the power lines reconstruction on the other side of the cut.

As an example, the typical setup for a 0V/Open line relies on the circuit shown on Fig 2.

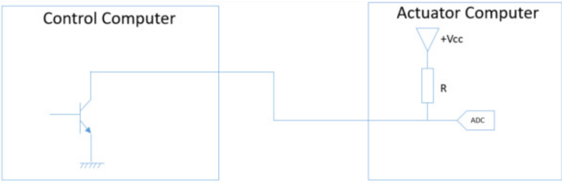

Fig. 2 Typical simplified 0V/Open discrete signal circuit

In the producer side, the control computer, usually uses an open collector design to set the line value to high impedance or ground. On the receiver side, the actuator computer, shall include a pullup resistor (R) that polarizes the producer transistor and brings the voltage to +Vcc for the receiver to be able to read the open state.

When the signal distribution is introduced (see Fig 3.), this mechanism cannot work anymore, and the pull up resistor has to be introduced on the producer side in order to keep the transistor polarization and allow the signal switching.

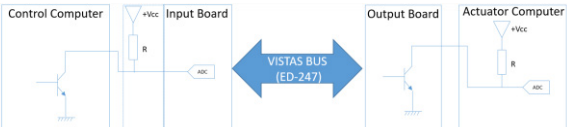

Fig. 3 Simplified 0V/Open discrete signal distributed circuit

For the power supply management, the difficulty comes from the impossibility to transfer the electrical power between both locations. It becomes necessary to use local power supplies on the receiver side driven by the power signal send by the producer. For this, there are several possibilities depending on the level of representativeness required:

- A first solution is acquiring the producer power output as a discrete and transmitting it to the receiver side where a relay commutes the local power supply. This solution has the advantage of being simple to setup, but has the inconvenience of poorly reproducing the power supply dynamic behavior.
- A second solution would be acquiring the producer output voltage as an analog signal and transmitting it to the actuator side. There the analog value is used to drive a programmable voltage supply connected to the receiver power input.

In both cases, if the controller computer monitors the outcoming current a resistor could be added to the power output to simulate the receiver consumption.

In our case, as a proof of concept, we chose the first simple solution (See Fig 4).

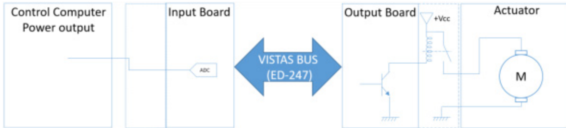

Fig. 4 Simple power output distribution

The results were very satisfactory. The distributed actuator was controlled in parallel to the local ones and the control computer raised no alert.

The average network transmission time was below 1ms. Due to the acquisition period of the input/output boards, running at 1 kHz, a maximum electrical transmission time of 3ms was measured.

Inter-site benches connection use case

The second trial was focused on the interconnection of benches between two different company sites. In this case we wanted to evaluate the feasibility of connecting our Marignane benches in France to our Donauwörth benches in Germany. It was also the opportunity to test the performance of the A429 lines distribution.

This time the goal was to be able to control the Automatic Flight Control System (AFCS), running in the German avionic bench in closed loop with a local flight simulation, from an Automatic Pilot Control Panel (APCP) located in France. At the same time we wanted to display the results in one of the Multifunction Displays (MFD) relocated in Marignane while the other two remained in Donauwörth (See Fig. 5)

From the signals point of view the setup require the bidirectional exchange of 20 A429 lines and 20 discrete lines.

The challenging part in this case was the network setup, since we needed to stablish a robust multicast exchange between to different countries with a much more important latency than the previous case.

DOI 10.5162/ettc2022/10.1

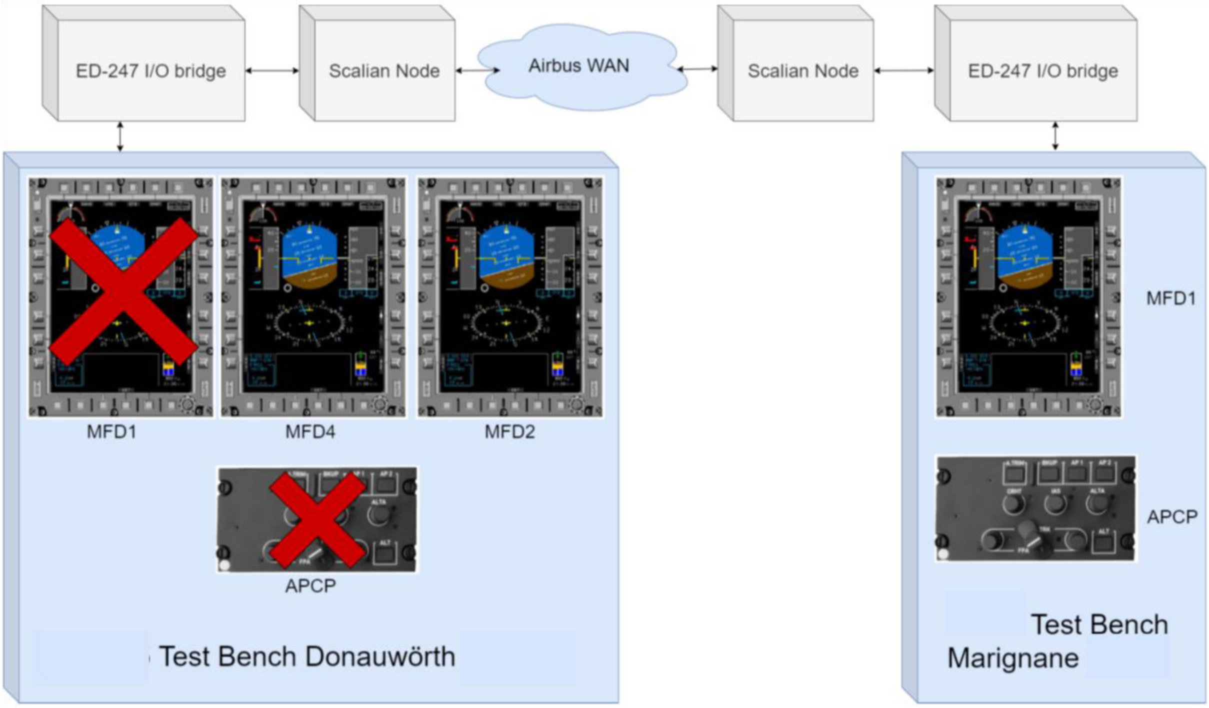

Fig. 5 Inter-site Distribution Test Setup

I was decided to introduce the Scalian Nodes in order to stablish a secure and robust VPN between the two locations. The Nodes allow the precise monitoring and synchronization of packages and implement a retrial mechanism in case of package lost. For that an additional but configurable latency is introduced. An additional advantage is that, once the VPN is stablished it becomes possible to transmit any kind of traffic, regardless IM restrictions.

In order to monitor the exchanged data we used Sandra, our Airbus Flight Analysis tool, that is ED-247 Rev A compatible and able to decode and display the data on the fly.

While setting up the system and doing the first tests we realized that, depending on the I/O racks CPU technology and the packetization strategy, the conversion of signals to the VISTAS bus could take a considerable amount of interruptions and thus overload the CPU on UEI devices. In our test setup, while using a packetization of 10 labels per ED-247 package, the maximum number of A429 lines per CPU was sixteen. We therefore had to use a second rack and CPU to manage the additional lines needed.

The results were promising. The user could control the Autopilot from its control panel 1000 km away seamlessly with an average latency of 17ms. While observing the remote and local MFDs the time gap between screens was almost unnoticed with a loop latency of 34ms.

Conclusion

The use of ED-247 for distributed testing has proved to be an efficient way of interconnecting test means. The advantages are numerous:

- Easy setup and configuration
- Large portfolio of compatible I/O boards from a large range of suppliers
- Very simple monitoring setup, either with open source or proprietary network analysis

Fig. 6 Donauwörth-Marignane Interconnection Setup

tools.

Nevertheless, several limitations or constraints need to be taken into account:

- Electrical and impedance adaptation of distributed signals.
- IM configuration and filtering constraints.
- Depending on the CPU technology, a limited amount of signals can be managed by a single CPU. In this case using dedicated computation technologies like FPGA could help overcome this limitation.

References

[1] EUROCAE ED-247A: Technical Standard of Virtual Interoperable Simulation for Tests of Aircraft Systems in Virtual or Hybrid Bench (March 2020)

[2] Santiago Rafael López Gordo, Emilio García García, Jose Luis Galindo Sanz, Vistas architecture implementation in a multi-system integration bench, ETTC 2020, DOI 10.5162/ettc2020/4.3

DOI 10.5162/ettc2022/10.2

How to get from MBSE to virtual product testing

Gregor Staudte
Airbus Defence and Space GmbH, Rechliner Str. 85077 Manching, Germany
gregor.staudte@airbus.com

Abstract:

Model-based system engineering (MBSE) is an important and useful approach to support very large system development. Especially within the defence aerospace industry. However, testing of system models is often performed only on a very static and abstract level. Its use often ends after a conceptual phase. Then the system models become detached from the real product.

The early and continuous verification and validation of the product against the MSBE models is a very important element to reduce program risks. The “Virtual Engineering” approach is our answer to enable testing of a virtual product as early as possible. A challenge is the relation to the MBSE world.

This paper outlines the recent experiences and the taken approach to couple the MBSE world with virtual testing. In fact, the environment is still in the setup phase were a special focus is put into this paper.

Key words: MBSE, virtual engineering, virtual product, virtual testing

Motivation

Most of the mistakes are made in the design phase. In contrast, errors, malfunctions and misbehaviour due to these mistakes are discovered very late. The later they are discovered, the higher the costs of removal. A mistake that was made early in the design phase, but is found very late, for example after the product has been delivered to the customer, can cost many times more compared to detection right after the mistake was made [1].

Therefore, a virtual product testing methodology shall be applied within our programmes. It shall discover design errors as early as possible and therefore reduce risks. In our context, it is not intended, at least not today, to use virtual testing as means of compliance. The desired benefit is, to gain a higher system maturity when entering the formal verification phase.

An additional beneficial side effect should be the higher efficiency of the actual formal verification activities on the real target product. This can be achieved through test preparation and its verification on virtualized means. Another expected beneficial side effect is the reuse of the virtual testing environment for later training operations.

Due to the agile nature of the programme, a virtual test bed may also act as environment to demonstrate the increments to its stakeholders, to validate the system and to act as foundation for reflection.

Now to focus again on the core objective for virtual testing “to discover errors early”, the following question arises: What kind of mistakes are usually made and why? Many things can go wrong: There can be wrong tests. The implementation of a functionality can be wrong. A device might by integrated in the wrong manner. Often this is due to a wrong design. For instance, the interface definition is wrong, or the requirements are interpreted differently, maybe are not consistent. Anyhow, the mistake is often made by miscommunication. Two individuals are misaligned which leads to errors.

MBSE intends to address this misalignment. It is “the formalized application of modeling to support system requirements, design, analysis, verification and validation beginning in the conceptual design phase, and continuing throughout development and later life cycle phases.” [2]

The outcome of the design phase are documents based on a complex MBSE model, which describes the entire system. The MBSE model acts then as input for further development activities such as implementation, integration, manufacturing and verification.

Consequently, a very important goal is on one hand to verify the consistency and applicability of the design, and on the other hand to verify the correct understanding and implementation within the preliminary work product. Since the first goal shall be covered by the MBSE framework itself, the second goal is the most important motivation for virtual product testing.

The focus of this paper is on the design and virtual product verification of avionics software. Mechanical or electrical engineering is out of scope.

Context

The systems addressed by this paper are in the field of military aircraft. Programmes that develop these systems tend to have an exponentially increasing complexity level. Both, on the system itself, and on the programme setup by multiple involved nations and companies in a partnership setup.

In order to meet customer needs better, and to stay on budget and on time, a semi-agile approach is used for our programme. The definition phase is split into several increments with a fixed duration, in which functional extensions are provided.

The design of such systems is structured into several layers, in which associated systems of layer n+1 act as subsystems of a system in layer n.

An illustrated, not to scale, timeline extract of our programme development phase is shown in the following Fig. 1. As remark, the design phase can be seen as phase spanning across concept & definition phase.

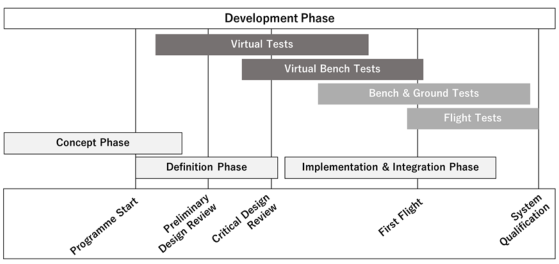

Fig. 1 Programme development phase timeline

MBSE approach

In the following, the focus is on how our programme applies MBSE. It should also be clarified whether the MBSE model is suitable for virtual product testing.

The MBSE approach relies on a framework, which provides the system engineering capability set to rely on common solutions from requirement, mission & operational analysis, architecture, safety and V&V, with a full digital continuity. As an overview, Fig. 2 visualizes our MBSE environment and how it is embedded into the overall engineering landscape.

The solution relies on the so-called R-MOFLT methodology [3]. It considers structural & behavioural views in both problem and solution space while keeping the focus on the system of interest and requirements along the entire development cycle:

- Mission analysis: Focuses on identifying the main purpose of the solution, characterizing the problem space, and determining possible solutions. Therefore, it describes what the problem is to be solved, and identifies potential solutions.
- Operational analysis: Focuses what the system does within missions. Therefore, it describes the system context and operation from user perspective.
- Functional analysis and architecture: Identifies the system functions to perform and their mutual relations to meet operational needs. Therefore, it describes how the system will work.
- Logical architecture: Describes logical system decomposition and clustering of functions into a logical structure in addition with their interfaces and corresponding behaviour.
- Technical architecture: Describes how to implement a logical architecture, by taking technological constraints into account, into a sufficient level of detail to support system implementation, integration and V&V.

The points listed are steps within the MBSE workflow, parts of the system model and perspectives to view the system model.

The MBSE solution contains a programme wide common visual modelling tool supporting SysML® [4] as the single modelling language for any MBSE activity. It also contains common access and data share for all programme partners. The integration, with respect to continuity and traceability with solutions outside MBSE scope, such as requirement, interface and test management, is ensured.

Within our programme execution, the actual MBSE practice is limited to static system modelling and interface, down to the system level of equipments & line replaceable units (LRU). The lower hardware / software level is in general not addressed by the MBSE model. Also not addressed are interface details, such as pin assignment or message formatting information of communication busses.

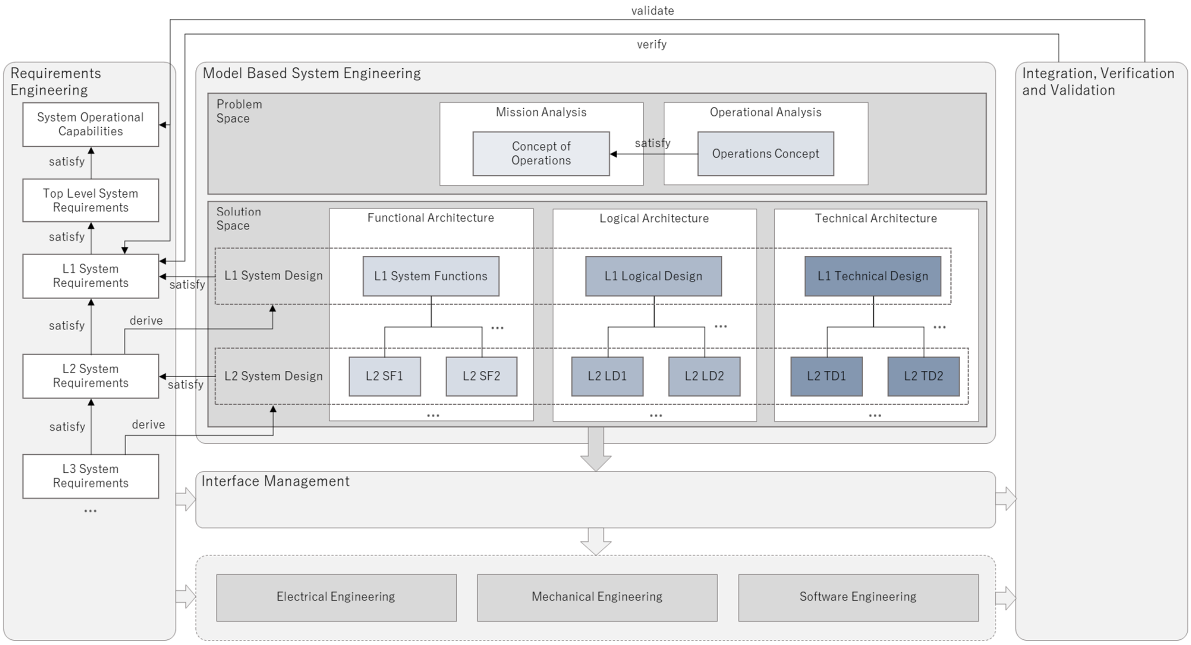

Fig. 2 Overview MBSE environment

Although the MBSE modelling tool offers capabilities for simulation, the MBSE model itself is not executable. The model is basically, a structured set of attributes and parameters. The fidelity level defines the possible simulation use-cases. Simulations based on our MBSE model are therefore limited to parameter evaluation. E.g. to calculate the overall system weight, out of weight parameters of subsystems.

These capabilities already offer some possibilities to verify the design. It can be checked automatically if the design complies with certain requirements, or whether certain parts are consistent. For the virtual product testing purpose, as addressed by this paper, these simulation capabilities are insufficient. There is the need for a simulated virtual product, which acts as the real target product.

Virtual Engineering

For that matter, our programme applies within the verification and validation (V&V) activities, the so-called Virtual Engineering (VE) principle. It is the structured and standardized end-to-end application of dynamic and functional / behavioural modelling and simulation of the entire system. Its purpose is mainly design verification and validation, but it also supports to product verification. Design verification aims to check whether a selected design results in a system implementation that meets the requirements. Product verification aims to verify the actual system implementation against the specification. Although formal certification and qualification activities are also a kind of product verification, those are not addressed by VE.

Its ambition is to have a virtualized product where testing can be performed as on a real product by a dynamic real-time simulation. The following two testing methodologies are addressed by VE:

- Model-in-the-Loop: Test setup within design verification, which uses simulation models as unit under test. Allows functional & logical verification of the unit functional chains and behaviour of the interfaces.
- Software-in-the-Loop: Test setup within product verification, which uses a re-targeted or re-hosted target software as unit under test. Allows verification of the unit implementation.

VE sets the focus on the avionics system. Computational mechanics simulations (e.g. computational fluid dynamics, computational structural mechanics) are out of scope for VE. However, simulation models based on such simulations may be integrated by simplification or connected by co-simulation. Goal is to achieve real-time execution capabilities of the simulation. Also not addressed by VE are tasks in context of high-level architecture exploration, operational analysis and parameter optimization.

The term “simulation” can be understood as the execution of simulation models over time. It is important to understand the difference of the term “simulation model” from the MBSE model. Both kinds of models represent a system by describing its key characteristics, behaviours and functions in a simplified version. The MBSE model is not executable. It is an abstract and formalized system description. In contrast, the simulation model is executable. It represents the system behaviour over time, acting and reacting on input data. The simulation model is not limited to the actual system in development. It also can represent an external system, a physical component or a phenomenon that interacts with the system. The simulation model is not limited to a simplified representation of a system component. In context of VE, it can also be the actual avionics target software, either re-targeted, or re-hosted. But the real physical target device does not fit anymore into the concept of a simulation model. Its integration with the simulation (hybrid configuration) is also not addressed by VE directly. It is driven by the product verification activities, which VE supports by providing the remaining system simulation around the unit under test in a hardware-in-the-loop test environment to ease its setup.

Since VE is located, similar to MBSE modelling, on the left side of the V-model, it needs to be tightly integrated within the overall system development process. In this phase, the actual system design has a low maturity. It is not fixed and incomplete. That means, VE needs continuously to respond on changes, and support quick fixes of definition gaps within the design. A certain degree of flexibility and adaptability within the processes and tools is necessary.

In order to setup the virtualized product and to make use of the opportunities described, a processes, methods and tools environment is established. Following building blocks are an essential in it:

- Simulation Breakdown Structure: Describes the hierarchy of simulation models required to develop and integrate a full system simulation. It is derived from the system equipment list. It describes the context and related equipment for each simulation model. Therefore it defines which equipment the simulation model represents, together with some meta-data. The simulation breakdown structure is complemented with physics, environment and simulation-specific models.
- Functional Increment / Artefact Roadmap: The Functional Increment Roadmap (FIR) describes which functions shall be realized by simulation models in which order, to which extent, in which fidelity at which point in time. The Artefact Roadmap (AR) describes which actual simulation provides a certain functionality at which point in time. Both together ensure that a certain functionality needed by one component is provided at the right time.
- Integration & Execution Environment: A set of software tools supporting the creation and integration of simulation models into an executable simulation. In addition, the simulation & test execution runtime and additional software tools are part. The toolset also provides the necessary connections to ensure exchange with the programme's interface management and test management solutions.
- Initial Simulation: Consist of an initial and generic simulation model set, integrated into an executable simulation. It initially describes a generic system of the same nature the programme intends to build, integrated with a natural and tactical environment. It intends to be used as starting point for the functional growth and helps to decouple the deliverables of different suppliers from each other.
- Environment for cooperation: Ensures that work can be coordinated and that information and assets are shared between all participants. It includes databases & repositories, together with a version control-, issue tracking-, and collaboration system. A special focus must be given to our programme setup, with accessibility by multiple companies, in different nations, with specific military and national regulations.
- Laboratories: Provides the physical integration and simulation & test execution environment accessible for all VE participants. Since VE addresses only virtualized avionics equipment, this environment can be identified as a virtual test bench. The actual laboratories are built on top of dedicated computers, or hosted within a cloud environment to ease accessibility and availability to the users.
- Joint Model Office: It is an organisation, including a set of roles, processes, standards and guidelines, to ensure the concurrent development of simulation models across all involved suppliers and their integration into a common simulation. It deploys the simulation back to all participants and laboratories. It provides all assets as described

before, and the necessary helpdesk and support.

The clear goal is to harmonize avionic simulation activities across various programme stakeholders.

The following example shall outline a typical use case, addressed by VE:

If supplier 'A' of component 'B' needs to have a simulation model of component 'Y', created by supplier 'X'. 'A' should get the simulation model of 'Y' from 'X'. 'A' must not do it by himself, since 'A' might have a different understanding of 'Y' than 'X'. Otherwise, 'A' creates a version of 'Y', which perfectly works with 'B', until it is integrated with the real component 'Y'.

Integration issues shall be detected as early as possible.

Interface Management

In between MBSE and the VE, lies the interface management. The main purpose is to detail the interfaces between subsystems, at all levels underneath the system, in context of their specific nature. Since this paper addresses avionics, the focus is on data nature, which includes logical interfaces (information flow between systems) & corresponding electrical interfaces (e.g. physical avionic network busses). Other natures, such as mechanical interfaces, are not addressed in here. Although those are also part of overall interface management.

The interface management tooling provides exporting capabilities for software coding and load analysis. However, the main result is the Interface Control Document (ICD). It captures the detailed data characteristic to ensure that interfacing equipment is compatible and can be integrated and operated as specified. It is the obligation of the equipment supplier to detail the information in negotiation with interfaced parties. The information is hereby stored within a common database, which also ensures the consistency to a certain degree.

The database is split into two interconnected sections. One section describes the interfaces of the actual system. This includes the subsystems, the logical interfaces in between. This includes the product structure with all equipments and their detailed logical and physical interfaces, and the relation to the system structure. The other section is specific to VE. It describes the Simulation Breakdown Structure with the entire set of simulation models and their relation to the system & equipment structure. By that, a simulation model inherits the interfaces of the component it references. In addition, simulation specific interfaces are described entirely in this part. This could be e.g. a physical parameter like the real outside temperature. It is provided by an environmental simulation model and consumed by a sensor model, which then outputs the sensed value to an avionic network interface it inherits from the referenced equipment. In addition, prototypic interfaces can be described in this section, which are so far not part of the systems interface model.

Since in our approach, both interface management tooling and the associated databases are separated from the MBSE environment, interface relevant MBSE model data has to be imported to the Interface Management environment. This separation leads to a break in the Single-Source-Of-Truth paradigm. In order to ensure digital continuity, automated export/import is used on one hand, and on the other a clear information ownership and change management process. As consequence, high-level changes such as a new interfaces or equipment must be made within the MBSE model, which is the owner of this information. These changes will then be reflected automatically within the interface management environment. Low-level changes such as the message formats are made directly within the interface management environment. This kind of information is not present within the MBSE model.

Workflow Description

In the following, the VE workflow will be described. The Fig 3 illustrates it.

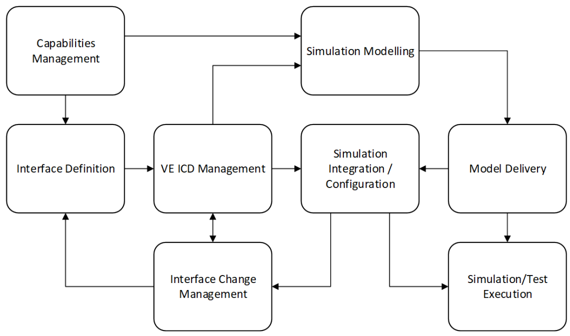

Fig. 3 VE Workflow Overview

First, as part of capabilities management the existence of the simulation model is defined, along with the avionic equipment's relationship, within the Simulation Breakdown Structure. In an iterative way, the Functional Increment & Artefact Roadmaps are defined based on the design and dependencies.

For each iteration, the avionic and simulation specific interfaces need to reflect the functional growth. The interfaces also need to be detailed enough to be usable within a simulation. This means that data types and formats need to be defined, so that S/W programs can access it.

Since the Simulation Breakdown Structure is located in the same database as the data interfaces, the interface management environment acts as the Single-Source-Of-Truth for a model interface specification. It is exported and provided to the simulation model supplier together with the functional specification.

The supplier creates the simulation model. It can be hand-written code, or also auto-generated by using a Model-Based Engineering approach [5], which might use specific exports or generated templates out of the MBSE or Interface Management environment. The actual quality of a simulation is the better the more a simulation model relies on the same source code as the target software does. Therefore, the usage of re-targeted avionics software is also aspired.

The initial integration is done by the supplier before it is delivered according to the standards and guidelines the VE Joint Model Office has defined. In an automated process, the delivery is verified against those rules and the basic executability, before it becomes part of the simulation.

It is important to consider also specification changes made during the simulation model development and simulation integration. These changes are a result of either immature design or design mistakes. These changes need to be made at the actual data source. This can be the MBSE or interface management environment, with dedicated change management processes. But it is also important not to wait for the next iteration until a working simulation exists, maybe with other changes then necessary. Therefore a trade-off is made to quickly introduce changes within the simulation and in parallel trigger the actual change management process. An important goal is to have a running simulation in each iteration cycle.

Every participant has access to the simulation and can execute it to perform tests. These are equipment & model suppliers to perform unit tests (although most of these can be performed before the simulation model is delivered). These are also system and subsystem testers, which perform specific non-formal integration tests on their level. The test can be the same used later for the formal product qualification, but also specifically adapted tests for the virtual environment. It is important to understand that the virtual product-testing environment if not feasible for all kinds of tests. E.g., timing constraints cannot be meaningfully tested, since the actual real target environment has different execution times & performance. The tests execution is linked with the test management solution. Tests can be directly triggered from there, as well are test results uploaded to further process them there. Some tests require a deeper analysis and post processing of the test data produced during the execution. For this reason, a solution for test data analysis is integrated into the pipeline. It is foreseen to apply the testing toolchain in a continuous integration pipeline. Automatable functional and regression test shall be triggered automatically once simulation models have been updated.

Our current reality is that almost all system level tests require manual interaction. Either during the test via virtualized human-machine-interfaces, or within the post processing / analysis step. It is our ambition to make tests more automatable.

Environment Setup

Now a brief overview shall follow of our experience to setup the environment. In our programme it was identified that the MBSE and VE approach would require preparation before the programme development begins, when the major contribution is within the definition phase. There the entire environment with processes, tools and infrastructure would need to be fully ready. By the time the preparation started, the MBSE approach was not defined, nor was the VE approach fully outlined. Unfortunately, in parallel the majority of contracts with partners and required deliveries were defined without knowing the MBSE and VE needs in detail. Since both, MBSE and VE require commitment and contribution by all stakeholders, many re-negotiation effort had to be performed.

In our industrial environment, testing is often seen as something to be done at the end of the classical development process. This lead to not adequate priorities inside programme management to support the MBSE and VE definition. Since VE is also a step towards test driven development, which changes traditional working methods, anxieties and resistances were created in various engineering teams. Therefore, it is important to have a clear and proven concept even before start of the programme concept phase. That the link between MBSE and VE is done only by interface management, and the limited usage of MBSE are consequences that both approaches were not defined then.

Summary

Virtual product testing is performed on the means provided by Virtual Engineering to support design & product verification. Our MBSE and Virtual Engineering environments and workflows are not directly linked with other. Implicitly both are connected through the interface management environment in a digital continuity. However, this is limited to structural and interface information. Although other aspects such as requirements and functional design are reflected in simulation models, the information does not have digital continuity. Manual lookup and transformation of design information during simulation model implementation is necessary. This is error prone. It can also lead to the decoupling of the MBSE model from the actual implemented reality. The more closely functional models are linked to target software, and the more the target software is based on auto-generation from MBSE, the more meaningful the virtual product testing.

Based on our experience, it is fundamental to define the detailed approach of "How to get from MBSE to virtual product testing" before the programme concept phase starts. Only then it is possible to involve all stakeholders appropriately and to steer the necessary change process. It may also lead to a deeper integration with a full digital continuity and a true single-source-of-truth paradigm.

References

[1] NIST Planning report 02-3, The Economic Impact of Inadequate Infrastructure for Software Testing, (May 2002)

[2] International Council on Systems Engineering (INCOSE), INCOSE Systems Engineering Vision 2020, INCOSE-TP-2004-004-02 (Sep 2007)

[3] F. Bouffaron, Airbus MBSE Framework: Model Execution of System Architectures (MOFLT), *MBSE Cyber Experience Symposium 2021 – Japan*

[4] Object Management Group, OMG System Modeling Language, *OMG SysML® home page (Apr 2022*), https://www.omg.org/spec/SysML/

[5] Model-Based Engineering Forum, *home page (Apr 2022)*, https://modelbasedengineering.com/